DEVELOPMENT OF A GIS-BASED INTEGRATED LANDSLIDE HAZARD MAPPING SYSTEM AND ITS APPLICATIONS

周, 蘇華

https://doi.org/10.15017/1785397

DEVELOPMENT OF A GIS-BASED INTEGRATED LANDSLIDE HAZARD MAPPING SYSTEM AND ITS APPLICATIONS

Suhua Zhou

2016

DEVELOPMENT OF A GIS-BASED INTEGRATED LANDSLIDE HAZARD MAPPING SYSTEM AND ITS APPLICATIONS

A Thesis Submitted

In Partial Fulfillment of the Requirements

For the Degree of

Doctor of Engineering

By

Suhua Zhou

to the

DEPARTMENT OF CIVIL AND STRUCTURAL ENGINEERING

GRADUATE SCHOOL OF ENGINEERING

KYUSHU UNIVERSITY

Fukuoka, Japan

August, 2016

DEPARTMENT OF CIVIL AND STRUCTURAL ENGINEERING
GRADUATE SCHOOL OF ENGINEERING
KYUSHU UNIVERSITY
Fukuoka, Japan

CERTIFICATE

The undersigned hereby certify that they have read and recommended to the Graduate School of Engineering for the acceptance of this thesis entitled, "***Development of a GIS-based integrated landslide hazard mapping system and its applications***" by **Suhua Zhou** in partial fulfillment of the requirements for the degree of **Doctor of Engineering**.

Dated: August, 2016

Thesis Supervisor:

_____

Prof. Guangqi CHEN, Dr. Sci.

Examining Committee

_____

Prof. Yasuhiro MITANI, Dr. Eng.

_____

Prof. Shinichiro YANO, Dr. Eng.

ABSTRACT

Landslide is one of the most serious natural hazards. It can be triggered by larger earthquakes or heavy rainfalls. For example, more than 700 landslides were triggered by the 2016 Kumamoto earthquake in Japan, they were responsible for 30% of total fatalities caused by the earthquake. Therefore, it is necessary to mitigate landslide disasters. Landslide hazard map can play an important role in decision-making of effective disaster prevention measures since it shows the landslide prone slopes and susceptible areas.

With the advancement of GIS (Geographic Information System), a variety of landslide hazard mapping (LHM) approaches have been proposed in the past decades, which can be classified into statistical approaches and physically-based approaches. Since a variety of LHM methods become available, there is an increasing awareness toward the need of an integrated landslide hazard mapping system so as to use these methods effectively and appropriately. And furthermore, there are the following 4 issues to be solved: (1) how to prepare the necessary landslide event data effectively; (2) how to improving the accuracy of landslide prone slope identification; (3) how to determine peak ground acceleration (PGA) in considering earthquake loading and (4) how to estimate the affected area of a landslide.

This study aims at (1) developing a GIS-based integrated landslide hazard mapping system (GeoILHMS) with three functional modules (GeoLHM-S, GeoLHM-P and GeoLHM-R), (2) solving the above mentioned issues by improving some existing methods and proposing some new methods, and (3) using GeoILHMS to analyze the 2016 Kumamoto earthquake induced landslides in Japan. The GeoLHM-S and the GeoLHM-P can be effectively used for LHM based on statistical approaches and a physically-based approach separately. The GeoLHM-R can be used for LHM by considering the affected area of a landslide based on the run-out simulation.

The thesis comprises the following chapters:

Chapter 1 introduces landslide disasters and mitigations, the problems in landslide hazard mapping, the scope and objectives of this study, and the organization of the thesis.

Chapter 2 reviews the existing LHM methods and clarifies the unresolved issues. The terminologies used in landslide hazard mapping are also described in this chapter.

Chapter 3 develops the functional module GeoLHM-S for effective landslide hazard mapping using statistical approach. At first, the issue of how to prepare the necessary landslide event data effectively is solved by proposing a method for landslide inventory mapping using online high-resolution images. The new method is incorporated into the functional module GeoLHM-Sb. And then, in order to solve the issue of how to improving the accuracy of landslide prone slope identification, (1) the four widely-used statistical methods: Information Value (IV), Weight of Evidence (WoE), Logistic Regression (LR), and Support Vector Machine (SVM), are incorporated into the functional module GeoLHM-S, which makes it possible to perform the LHM using different methods simultaneously, (2) a close comparison between the four methods, the merits, demerits and limitations of each method are clarified, which is very helpful for choosing the most suitable method based on the data availability and the characteristic of the study area, (3) four new methods are proposed by combining one of IV and WoE methods with one of the LR and SVM methods. Finally, the developed GeoLHM-S is used to make landslide hazard maps by using the four widely-used methods and the newly proposed combined method for the 2013 Lushan Earthquake event in China, and it has been shown that landslide hazard map by using the proposed technique is of the highest accuracy.

Chapter 4 develops the second functional module GeoLHM-P for effective landslide hazard mapping using a physically-based approach. Slope stability analysis is an effective and well-used method to identify the landslide prone slopes, since earthquakes loading can be considered directly in the limit equilibrium. However, how to determine PGA is still a very difficult problem in LHM. In this chapter, at first, a method is proposed to estimate the PGA value for each cell in the LHM area from a specified fault or the target fault based on the Next Generation of

Ground-Motion Attenuation Models for the western United States (NGA-West2). And then, the pseudo-static method based on an infinite slope stability model using PGA is incorporated into the functional module GeoLHM-P for calculating the factor of safety of each cell. Furthermore, the Monte Carlo simulation is applied for dealing with the uncertainties of geological parameters. Finally, the GeoLHM-P is used to make landslide hazard maps by considering expected earthquakes with different magnitudes from the Shuangshi-Dachuan fault in Lushan, China and its practicality has been verified.

Chapter 5 develops the third functional module GeoLHM-R for landslide hazard mapping by considering the affected area of a landslide based on the run-out simulation. Up to now, most of LHM methods only focus on the landslide prone slopes, and the affected areas are not included. Some LHM include the affected areas but they are estimated empirically based on slope heights. For example, the affected area is generally estimated based on the way given by Sediment Disaster Countermeasures for Sediment Disaster Prone Areas Act in Japan. It is a big challenge to estimate the affected area based on kinematics in LHM. In this chapter, a run-out simulation technique is developed based on modified multiple flow algorithm and the law of conservation of energy. The elevation difference between cells is taken into account for determining the possible directions towards which the landslide can move with a certain probability. The law of conservation of energy is used to determine the distance of sediment movement. When the mechanical energy from both the kinetic and potential energy becomes less than the friction-induced energy loss, the movement of landslide will stop so that the maximum affected area can be estimated. The method is incorporated into the functional module GeoLHM-R. A practical example is made by using the module and its practicality has been verified.

Chapter 6 presents a practical application of the GeoILHMS to analysis of the 2016 Kumamoto Earthquake in Japan. Firstly, an inventory map of 665 landslides induced by the earthquake is produced. Then, landslide hazard maps are produced by using each of statistical methods available in the GeoLHM-S. Also, landslide hazard maps with expected earthquakes of different magnitudes occurring along the

Futagawa fault and the Hinagu fault are produced by using the GeoLHM-P. Finally, the run-out analysis is carried out by using the GeoLHM-R and a landslide hazard map with the affected area is produced. The produced landslide hazard provides essential frameworks for the development planning and reconstruction of the study area as they present a spatial division of the study area of different levels of potential landslide threat, including the landslide prone areas and the potential affected areas.

Chapter 7 summarizes and concludes the results and achievements of the study. Problems are also highlighted for future studies.

ACKNOWLEDGMENTS

The three years I spent in Kyushu University at the Department of civil and structural engineering are amongst the most enjoyable years during my research career so far. The academic atmosphere here always made the search for wisdom full of fun right until now. I owe many thanks to many people. The thesis would have never been accomplished without their kind help.

Firstly, I would like to owe my sincere thanks to Prof. Dr. Guangqi Chen, my academic supervisor and life tutor. I am grateful to this esteemed senior for his excellent supervision, from which I benefit a lot. He always had an open ear for consultations and supplied invaluable thematic and methodical comments as well as a lot of organizational support. This thesis was completed thanks to his inputs and amazing ideas. Another special thanks to Prof. Dr. Baochen Liu and Prof. Ligang Fang. Their teaching at the Central South University, China, during my Master studies were immensely inspired for the completion of this thesis.

I would like to express my highest gratitude to members of my dissertation committee, Prof. Yasuhiro Mitani, and Prof. Shinichiro Yano for their invested time in review evaluation. A special thanks goes to the Department of civil and structural engineering, Kyushu University, and also to the education section of Consulate-general of the people's republic of China in Fukuoka. The division teams provided special help and support to the international students.

I am indebted to my parents for their love and encouragement for life. Finally, a great thanks to my wife, Yunwen Nie. She is my wife, my soul partner, and moreover my co-author of some papers. Thanks to her love, sacrifice, and support during these years. A preliminary thanks also to my daughter, Xiaowan Zhou, who is constantly my encouragement and inspiration. This thesis is dedicated to them.

This research was carried out thanks to the financial support of: -the China Scholarship Council (CSC) and National Program on Key Basic Research Project of China (973 Program) (No.2011CB710601). These financial supports are gratefully acknowledged.

TABLE OF CONTENTS

LIST OF FIGURES

LIST OF TABLES

CHAPTER 1

INTRODUCTION

1.1 BACKGROUND

Landslide is a geological terminology to describe the mass movement of rock, soils, debris or earth down from a slope, under the driving force of gravity (Varnes 1984; Cruden and Varnes 1996a; Cruden and Varnes 1996b; Hungr et al. 2014). Landslides can be triggered by different phenomenon, including the heavy rainfalls, large earthquakes, rapid snow melting and human activities, such as the excavation on slopes (Corominas and Moya 2008; Reid et al. 2008; Harp et al. 2011; McColl 2014). Types of landslides mainly involve the falling, toppling, sliding, flowing and a mixture of them (Cruden and Varnes 1996a; Cruden and Varnes 1996b; Ibsen and Casagli 2004; Reid et al. 2008; Piegari et al. 2009; McColl 2014).

The rapid urbanization associated with explosive population growth has brought great challenges to the environment and intensified pressures on land demand. During the process of land resource exploitation in mountainous terrain, fragile ecosystem and complex terrain conditions make these areas more susceptible to severe environmental disasters (Swenson and Franklin 2000; Bathrellos et al. 2012a; Bathrellos et al. 2012b). Landslides are especially prevalent in mountainous terrains (Lateltin et al. 2005; Cascini 2008; Fell et al. 2008a; Fell et al. 2008b), which always induce serious economic, human and environmental losses throughout the world. From 1900 to 2014, landslides accounted for nearly 40% of global natural hazards according to the International Disaster

Database(http://www.emdat.be).

1.1.1. CATASTROPHIC LANDSLIDES IN RECENT DECADES

It is widely accepted that landslide represents one of the most serious natural hazards globally, especially in mountainous regions, such as West China, Japan et al. This is particular in mountainous areas where earthquake activities are frequent and heavy. Landslides in these regions have posed severe dangers to the different components of mountainous societies. For example, in the May 12, 2008 Wenchuan earthquake with a magnitude of Ms8.0 in China. It was estimated that about 60,000 landslides were triggered by this earthquake and more than 10,000 people were killed by these landslides(Sato and Harp 2009; Yin et al. 2009; Gorum et al. 2011; Wang et al. 2014) .

In general, landslides masses travel down the slope and hit the buildings or humans down of the slope. Sometimes, landslides are capable of burying entire villages and killing thousands of people in a single event, and often endanger human lives and infrastructure facilities. For example, in the case of the 2010 Beichuan Middle School landslides triggered by the Wenchuan Earthquake in China (Figure 1-2a), 1600 residents were killed by the devastating landslides, and economic loss was up to 212 million RMB (Yuan et al. 2010; Tang et al. 2011a; Tang et al. 2011b). Another example is the Aso Bridge landslides triggered by the 2016 Kumamoto Earthquake in Japan (Figure 1-2b), at least 9 residents were reported dead in the event.

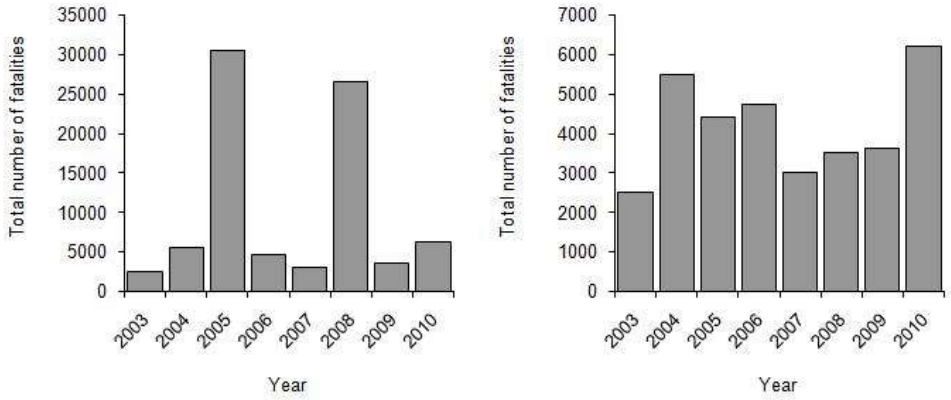

Figure 1-1 Number of landslides-induced fatalities. (a) the total fatalities that I have recorded from 2003 to 2010, including losses from landslides triggered by earthquakes. (b) the same data but with the two huge landslide-inducing earthquakes (2005 Kashmir and 2008 Wenchuan) (Source data from http://blogs.agu.org/landslideblog/2011/02/05/global-deaths-from-landslides-in-2010/)

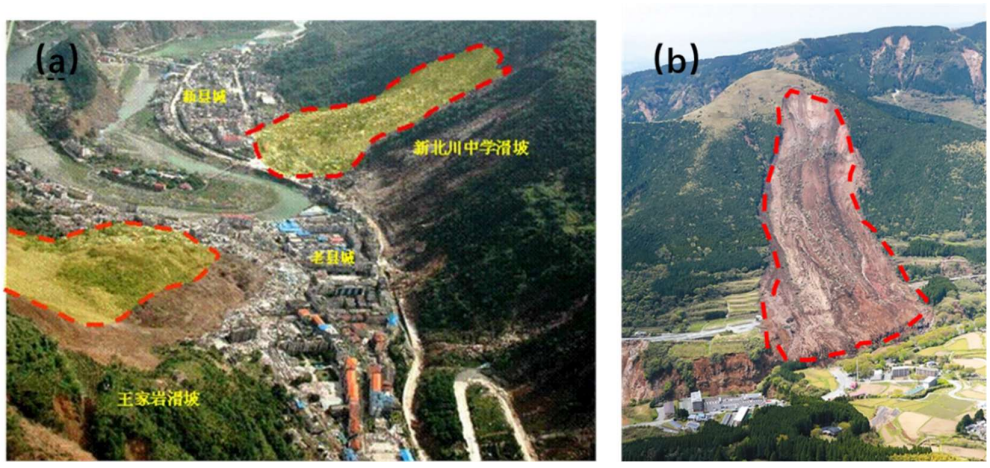

Figure 1-2 Catastrophic landslide disasters in this decade. (a). Image of the New Beichuan Middle School landslides triggered by the 2008 Wenchuan Earthquake in China. Source from NASA. (b). Image of the Aso Bridge landslide triggered by the 2016 Kumamoto Earthquake in Japan, data from www.ibtimes.com.

Table 1-1 Catastrophic landslides in recent decades

Event	Date /County	LN[#1]	LA(km^2)[#2]	Reference
New Zealand Rainfall	2004/02/16 New Zealand	60,000	16,000	www.niwa.co.nz
Typhoon Rainfall	2011/09 Japan	30	About 500	Hitoshi Saito (2012)
Wenchuan Earthquake	2008/05/12 China	Over 60,000	41,750	Dai et al., (2011)
Lushan Earthquake	2013/04/20 China	3,810	13,323	Tang et al.,(2015)
Tohoku Earthquake	2012/03/09 Japan	3,477	28,380	Joseph Wartman., et al. 2013
Kumamoto Earthquake	2016/04/16 Japan	Over 700	1,500	This study

[#1]LN: Landslide Number;

[#2]LA: Landslide distribution area

A recent study by Dave Petley (http://blogs.agu.org) has reviewed recent landslides

events with 70,000 fatalities on a global scale from 2003 to 2010. As shown in Figure 1-1, it comes to a conclusion that fatal landslide events are increasing year by year during the past decade. Also in the past decade, a lot of catastrophic landslides events were reported (Table 1.1).

1.1.2. FACTORS RELATED TO LANDSLIDES

Generally speaking, factors related to the occurrence of landslides can be grouped into two main categories: one is the controlling factors and the other is the triggering factors(Zhou et al. 2002; Khazai and Sitar 2004; Knapen et al. 2006; Masson et al. 2006; Chang et al. 2007; Shiels et al. 2008; Broothaerts et al. 2012; Sidle and Ochiai 2013). Geomorphic factors and local geology are classified as the controlling factors of landslides, while rainfall, earthquake, and human activities are considered as the triggering factors(Parise and Jibson 2000a; Wang et al. 2007; Qi et al. 2010; Zhou et al. 2015).

To find out the effects of factors on landslide occurrence, various statistical analysis of landslides with respect to these factors have been carried in the past few decades(Keefer 1984; Keefer 2002; Malamud et al. 2004). Most studies have concentrated on general correlations of landslides occurrence with slope gradient, distance to epicenter, to seismogenic fault, and to drainage and geology unit (Khazai and Sitar 2004). For example, Xu et al. 2013 examined distribution of landslides triggered by Ms7.1, Yushu, China earthquake and found strongly positive correlations between landslide occurrence and slope gradient, while Coe et al. 2003; Sassa et al. 2007 and Saez et al. 2013 show that the largest occurrence of landslides falls within an interval of slope angles ranging from 9 to 14°. More recently, coupling effect of controlling factors and triggers become popular. Topographic amplification effects of seismic force had been studied by many authors (Rodríguez et al. 1999; Bommer and Rodríguez 2002; Nishimura 2013),and typical example of them is as follows: Lenti and Martino (2013) studied the coupling effect of topography and seismic waves on landslide dynamics, revealing the fundamental role of topography in both amplifying and de-amplifying ground motion.

Landslides were also considered closely related to regional geology and

geomorphic evolution. Hovius and Stark (2006), Korup et al. (2010), Roering (2012) and Larsen and Montgomery (2012) thought hillslope evolution is adjusted to rapid uplift and bedrock incision through both an increase in the rate of relief-limiting landsliding and gradual slope steepening in tectonic-active areas. Besides, on the basis of understanding these correlations, the susceptibility of each analysis unit to landslides during an earthquake has also been calculated and ranked through assigning quantified weights to factors and then combining these factors (Parise and Jibson 2000b).

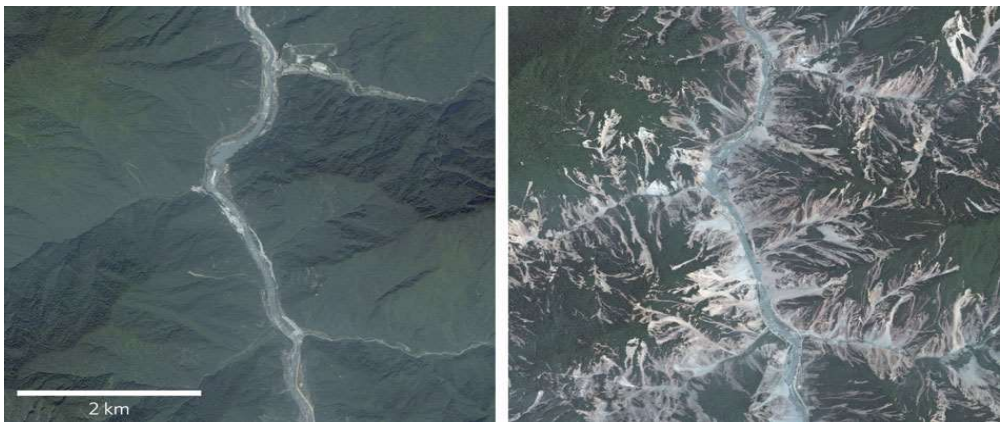

Figure 1-3 Pre- (Left) and Post-event (Right) Images showing the epicentral area of Wenchuan Earthquake (Tang et al., 2010)

Large earthquakes and heavy rainfall are two main triggers for landslides. These two main triggers, in general, showed a chain effects of the environment while triggering landslides(Wu and Chen 2009; Cepeda et al. 2010; Turner et al. 2010; Lee and Chi 2011; Berti et al. 2012). Heavy rainfall is one of the most common triggers for landslide occurrence. The pore pressures increases in the soil masses due to the rainfall infiltration during the raining periods will increase the driving force of the slope masses and reduce the resistance force of it. Such effects will result in instabilities of the slope mass. Additionally, a lot of previous studies had demonstrated that rainfall-induced landslides will turn to be debris flows under some favorable conditions(Glade 2000; Dahal and Hasegawa 2008; Minder et al. 2009).

Another main trigger for landslide is large earthquakes. Damages from

earthquake-induced landslides may sometimes exceed the ground shaking itself (Sato and Harp 2009; Schulz et al. 2009; Yin et al. 2009; Yuan et al. 2010; Gorum et al. 2011; Harp et al. 2011; Tang et al. 2011a; Tang et al. 2011b; Wang et al. 2014). Earthquake-induced landslides have recently drawn increasing attention from researchers in fields of tectonics, geomorphology, natural hazards, geographic information system (GIS) and remote sensing (RS). Damage from earthquake-induced landslides were documented from at least as early as 1789 B.C. in China and 373 or 372 B.C. in Greece (Li Zhongsheng 2003). Earthquake-induced landslides have been responsible for the deaths of tens of thousands of people and economic losses of billions of dollars. Particularly in mountainous areas, the damage caused by earthquake-induced landslides and slope collapses might be more severe than the damage caused by the earthquake itself (Keefer 1984; Keefer 2002). In the last decade, various studies of earthquake-induced landslides in mountainous areas have been carried out, including on the 2004 Niigata earthquake in Japan (Yin et al. 2009; Gorum et al. 2011) , the 2005 northern Pakistan earthquake (Saba et al. 2010), the 2008Wenchuan earthquake with a surface wave magnitude (Ms) of 8.0 in China (Yin et al. 2009; Gorum et al. 2011), 2011 Tohoku earthquake (Mw = 9.0) in Japan (Fraser et al. 2013; Chiaro et al. 2015) and 2013 Lushan earthquake (Ms = 7.0) in China (Zhou et al. 2015).

Studies on earthquake-induced landslides have a major significance for better understandings of regional distribution patterns. In the past few decades, various studies focused on relations between landslide distribution and triggering seismic factors, these were done by analysis of historic inventories of several earthquake events. Through analysis of 40 historical earthquake events between 1958 and 1977 around the world, Keefer (1984) firstly presented the general relations between the earthquake-induced landslides (such as spatial distribution, type and area coverage) and triggering seismic factors (such as distance to the epicenter, the distance to fault rupture earthquake magnitude and intensity). Rodríguez et al. (1999) made an extended Keefer (1984)'s study of the landslides triggered by 36 global earthquakes events from 1980-1997. As results of these studies, the minimum magnitude and intensity for triggering a landslide and the maximum area extent affected by

earthquake-induced landslides were estimated in Keefer (1984). Generally, a positive relation between landslide magnitude and seismic intensity and a negative relation between landslides concentration and distance to the epicenter and seismogenic fault were found Keefer (1984). Nevertheless, a few more recent studies found that earthquake-triggered landslides distribution was more related to the distance from the surface projection of the fault plane or the surface projection up-dip edge of the fault rather than the distance from the epicentre (Sassa et al. 2007; Sato and Harp 2009).

Seismogenic faults and their properties (such as geometry, focal mechanism and rupture process) strongly controlled the spatial distribution pattern of earthquake-induced landslides. A thrust fault earthquake released more energy than a strike-slip fault earthquake and subsequently caused large number of ground failures (Chen et al. 2011). Spatial distribution patterns of earthquake-induced landslides varied with different earthquake focal mechanisms. Negative relations between earthquake-induced landslide concentration and distance to seismogenic fault were found in many thrust-fault events, landslides triggered by which occurred most on its hanging wall and attenuated with the increasing distance to the seismogenic fault at a rate significantly lower than that on the footwall. Typical examples of thrust fault earthquakes are 1999 Chi-Chi earthquake (Hung 2000; Shin and Teng 2001), 2004 Chuetsu earthquakes(Wang et al. 2007; Chen et al. 2014) , the 2007 Niigata Chuetsu earthquake (Kayen et al. 2009; Collins et al. 2012) and the 2008 Wenchuan earthquake (Gorum et al. 2011) . As a comparison, landslides triggered by a strike-slip fault earthquake had similar distribution patterns on both sides of the seismogenic fault and were usually distributed close to the seismogenic fault, such as the 1973 Luhuo earthquake in Sichuan, China (Zhou et al. 1983; Nakanishi et al. 2004) and the 2010 Yushu earthquake (Xu et al. 2012).Seismic energy propagation and ground deformation differed with different fault geometry. Orientations of earthquake-induced landslides were related to the geometry of seismogenic fault, especially for thrust-fault earthquake events. Tibaldi et al. (1995) found that landslides preferentially occurred on slopes perpendicular to seismogenic fault plane and lying along its strike due to amplification of the ground

response, while slopes parallel to the seismogenic fault planes were almost unaffected by landsliding regardless of lithology and geological structure conditions. Distributions of landslides triggered by Wenchuan earthquake and Lushan earthquake also showed that the dominant orientations of landslides were in consistent with the movement direction of the seismogenic fault (Zhou et al. 2015). All these studies show that the distribution of the landslides triggered by the fault rupture was complicated phenomenon.

1.1.3. COMMONLY USED LANDSLIDE MITIGATION

Analysis of the factors that contributes to the occurrence of landslide had provided the kinds of ways for landslide hazard mitigation and prevention work. One is the hardware works, the other is the software works. Before the occurrence of the landslides, use the hardware works to control the drainages or reinforce the potential landslides. Another possible way for landslide hazard mitigation is to identify the potential landslides before it happens. Such measures usually were carried out by the landslide warning system or landslide hazard mapping. Besides, the software works is one of the most economic ways for landslide hazard mitigation.

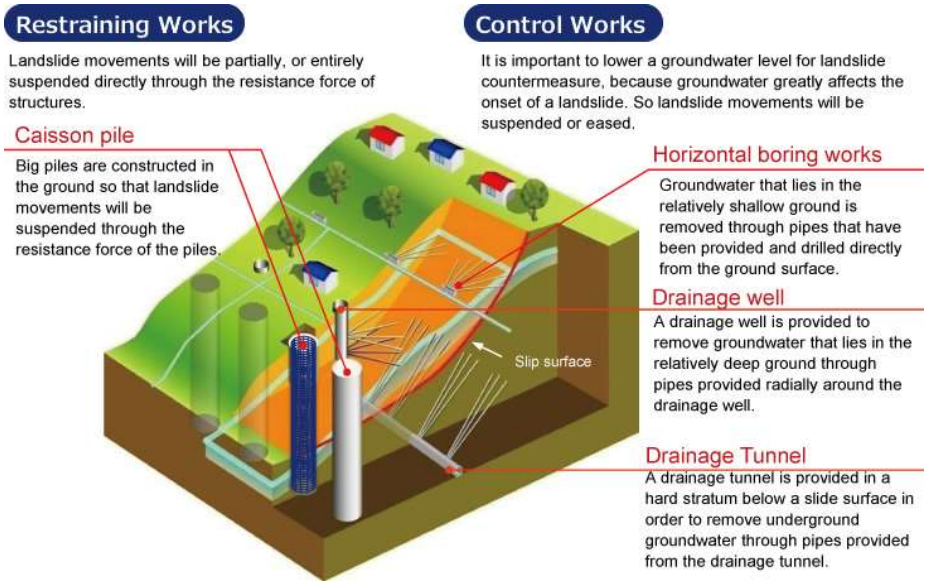

Figure 1-4 The commonly used structural mitigation methods against landslide disasters (Ministry of Land, Infrastructure and Transport Infrastructure Development Institute –

Japan. Guidelines for construction technology transfer, 2004)

As described above, the serious results of the landslides often pose great risks on human settlements and infrastructures in the mountainous regions, it is of great importance to do some countermeasure works to mitigate the landslide hazard (Figure 1-4). The commonly-used methods can be concluded as two categories, hardware ways and software ways (Fell 1994). Software ways usually include early warning systems, proper land-use strategy, and improvement of buildings. The purpose of software measures is to reduce the vulnerable to landslides, and consequently reduce the hazard risk. While hardware measures usually include constructing reinforcement in the landslide-prone slopes. The purpose of structural measures includes three aspects, (a) to prevent the start of landslide movement; (b) to prevent the landslide movement after its occurrence; (c) to control dissipation of landslide energy.

1.1.4. LANDSLIDE HAZARD MAPPING

Due to the serious consequences of landslides, numerous efforts have been done to mitigate the disasters. Of these efforts, the landslide hazard mapping is of the great significance(Lee et al. 2002; Lee et al. 2004; Yesilnacar and Topal 2005; Lee and Sambath 2006; Hong et al. 2007; Oh and Pradhan 2011; Bhandary et al. 2013; Lee et al. 2013; Feizizadeh et al. 2014). Although the time and location of landslide occurrence is hard to be predicted in advance, evaluation of a certain region's potential hazard to landslide is possible(Ayalew and Yamagishi 2005; Lee 2007; Kawabata and Bandibas 2009; Pradhan et al. 2010; Sezer et al. 2011). Identifying a region's susceptibility to landslides during an earthquake was an effective and most economical way to provide planners with foreknowledge of dangerous regions thereby helping with land management and infrastructure planning. For earthquake-induced landslide, landslide susceptibility assessment was to evaluate location of landslide susceptibility zones where landslides could be induced in future earthquake shaking (Zhou and Fang 2015).

1.2 PROBLEMS IN LANDSLIDE HAZARD MAPPING

Landslide hazard mapping involves several steps, i.e. scope definition, landslide hazard identification and consequence estimation. Scope definition addresses several issues including delineating the study area and methodology selection. Landslide hazard identification addresses several issues on understanding physical characteristic of study area regarding to landslide processes such as understanding geology, geomorphology, hydrogeology and climate. It also includes collecting landslide data, such as landslide classification, area, volume, travel distance, date occurrence, and elements at risk. Hazard identification activities are mostly related to landslide inventory.

Landslide inventory is very important in the landslide risk analysis because it gives information related to frequency of occurrences, landslide typology, landslide extents and damage of elements at risk. Estimation of spatial probability, temporal, probability and magnitude probability is not possible without landslide inventory containing sufficient data of past landslide events. Thus, producing landslide inventory maps for landslide hazard mapping are challenging task that this research focuses on. Given the variety of landslide hazard mapping methods, suitable selection of landslide hazard mapping methods is a central problem in the field of landslide hazard mapping. In addition, an ideal landslide hazard map should not only show the potential landslide prone slopes, but also show the affected area of landslides.

1.3 SCOPE AND OBJECTIVES

Thus, the main objective of this study is to develop a GIS-based integrated landslide hazard mapping system with three functional modules, in detail:

(1) To propose a method for effectively landslide inventory mapping using online high-resolution images;

(2) To compare the existing landslide hazard mapping methods using the landslide inventory and to propose a technique method to improve the accuracy of existing methods;

(3) To propose a physically-based landslide hazard mapping method, which can consider the ground motion parameters from a specified fault or the target fault.
(4) To develop a run-out simulation technique so as to consider the landslide affected areas in landslide hazard mapping.
(5) In addition, in order to verify the efficiency of the developed system, a case study of landslides triggered by the 2016 Kumamoto Earthquake was also carried out.

1.4 FRAMEWORK OF THE THESIS

The thesis comprises the following chapters:

Chapter 1 introduces landslide disasters and mitigations, the problems in landslide hazard mapping, the scope and objectives of this study, and the organization of the thesis.

Chapter 2 reviews the existing LHM methods and clarifies the unresolved issues. The terminologies used in landslide hazard mapping are also described in this chapter.

Chapter 3 develops the functional module GeoLHM-S for effective landslide hazard mapping using statistical approach. At first, the issue of how to prepare the necessary landslide event data effectively is solved by proposing a method for landslide inventory mapping using online high-resolution images. The new method is incorporated into the functional module GeoLHM-Sb. And then, in order to solve the issue of how to improving the accuracy of landslide prone slope identification, (1) the four widely-used statistical methods: Information Value (IV), Weight of Evidence (WoE), Logistic Regression (LR), and Support Vector Machine (SVM), are incorporated into the functional module GeoLHM-S, which makes it possible to perform the LHM using different methods simultaneously, (2) a close comparison between the four methods, the merits, demerits and limitations of each method are clarifed, which is very helpful for choosing the most suitable method based on the data availability and the characteristic of the study area, (3) four new methods are proposed by combining one of IV and WoE methods with one of the LR and SVM

methods. Finally, the developed GeoLHM-S is used to make landslide hazard maps by using the four widely-used methods and the newly proposed combined method for the 2013 Lushan Earthquake event in China, and it has been shown that landslide hazard map by using the proposed technique is of the highest accuracy.

Chapter 4 develops the second functional module GeoLHM-P for effective landslide hazard mapping using a physically-based approach. Slope stability analysis is an effective and well-used method to identify the landslide prone slopes, since earthquakes loading can be considered directly in the limit equilibrium. However, how to determine PGA is still a very difficult problem in LHM. In this chapter, at first, a method is proposed to estimate the PGA value for each cell in the LHM area from a specified fault or the target fault based on the Next Generation of Ground-Motion Attenuation Models for the western United States (NGA-West2). And then, the pseudo-static method based on an infinite slope stability model using PGA is incorporated into the functional module GeoLHM-P for calculating the factor of safety of each cell. Furthermore, the Monte Carlo simulation is applied for dealing with the uncertainties of geological parameters. Finally, the GeoLHM-P is used to make landslide hazard maps by considering expected earthquakes with different magnitudes from the Shuangshi-Dachuan fault in Lushan, China and its practicality has been verified.

Chapter 5 develops the third functional module GeoLHM-R for landslide hazard mapping by considering the affected area of a landslide based on the run-out simulation. Up to now, most of LHM methods only focus on the landslide prone slopes, and the affected areas are not included. Some LHM include the affected areas but they are estimated empirically based on slope heights. For example, the affected area is generally estimated based on the way given by Sediment Disaster Countermeasures for Sediment Disaster Prone Areas Act in Japan. It is a big challenge to estimate the affected area based on kinematics in LHM. In this chapter, a run-out simulation technique is developed based on modified multiple flow algorithm and the law of conservation of energy. The elevation difference between cells is taken into account for determining the possible directions towards which the landslide can move with a certain probability. The law of conservation of energy

is used to determine the distance of sediment movement. When the mechanical energy from both the kinetic and potential energy becomes less than the friction-induced energy loss, the movement of landslide will stop so that the maximum affected area can be estimated. The method is incorporated into the functional module GeoRALR. A practical example is made by using the module and its practicality has been verified.

Chapter 6 presents a practical application of the GeoILHMS to analysis of the 2016 Kumamoto Earthquake in Japan. Firstly, an inventory map of 665 landslides induced by the earthquake is produced. Then, landslide hazard maps are produced by using each of statistical methods available in the GeoLHM-S. Also, landslide hazard maps with expected earthquakes of different magnitudes occurring along the Futagawa fault and the Hinagu fault are produced by using the GeoLHM-P. Finally, the run-out analysis is carried out by using the GeoLHM-R and a landslide hazard map with the affected area is produced. The produced landslide hazard provides essential frameworks for the development planning and reconstruction of the study area as they present a spatial division of the study area of different levels of potential landslide threat, including the landslide prone areas and the potential affected areas.

Chapter 7 summarizes and concludes the results and achievements of the study. Problems are also highlighted for future studies.

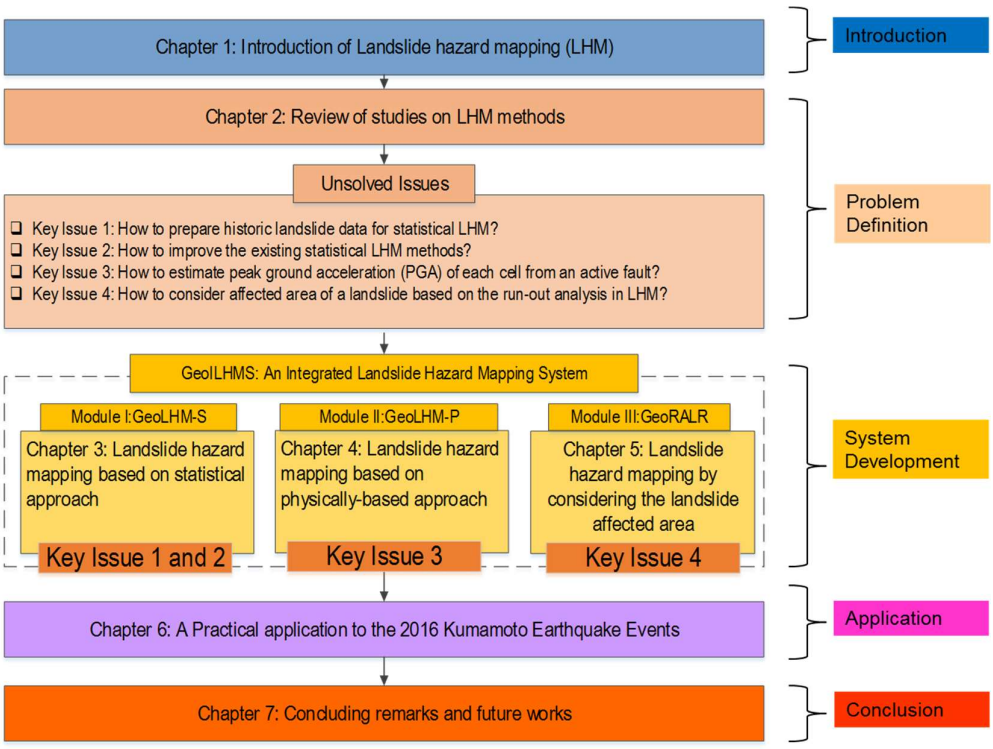

Figure 1-5 Framework of the thesis.

REFERENCES

Akkar S, Bommer JJ (2007) Empirical prediction equations for peak ground velocity derived from strong-motion records from Europe and the Middle East. Bull Seismol Soc Am 97:511–530. doi: 10.1785/0120060141

Atkinson GM (2010) Ground-motion prediction equations for Hawaii from a referenced empirical approach. Bull Seismol Soc Am 100:751–761. doi: 10.1785/0120090098

Atkinson GM, Boore DM (1997) Stochastic Point-Source Modeling of Ground Motions in the Cascadia Region. Seismol. Res. Lett. 68:74–85.

Atkinson GM, Boore DM (2006) Earthquake ground-motion prediction equations for eastern North America. Bull Seismol Soc Am 96:2181–2205. doi: 10.1785/0120050245

Atkinson GM, Silva W (2000) Stochastic modeling of California ground motions. Bull Seismol Soc Am 90:255–274. doi: 10.1785/0119990064

Ayalew L, Yamagishi H (2005) The application of GIS-based logistic regression for landslide susceptibility mapping in the Kakuda-Yahiko Mountains, Central Japan. Geomorphology 65:15–31. doi: 10.1016/j.geomorph.2004.06.010

Bathrellos GD, Gaki-Papanastassiou K, Skilodimou HD, et al (2012a) Potential suitability for urban planning and industry development using natural hazard maps and geological-geomorphological parameters. Environ Earth Sci 66:537–548. doi: DOI 10.1007/s12665-011-1263-x

Bathrellos GD, Gaki-Papanastassiou K, Skilodimou HD, et al (2012b) Potential suitability for urban planning and industry development using natural hazard maps and geological-geomorphological parameters. Environ Earth Sci 66:537–548. doi: 10.1007/s12665-011-1263-x

Berti M, Martina ML V, Franceschini S, et al (2012) Probabilistic rainfall thresholds for landslide occurrence using a Bayesian approach. J Geophys Res Earth Surf. doi: 10.1029/2012JF002367

Bhandary NP, Dahal RK, Timilsina M, Yatabe R (2013) Rainfall event-based landslide susceptibility zonation mapping. Nat Hazards 69:365–388. doi: 10.1007/s11069-013-0715-x

Bindi D, Parolai S, Grosser H, et al (2007) Empirical ground-motion prediction equations for northwestern Turkey using the aftershocks of the 1999 Kocaeli earthquake. Geophys Res Lett. doi: 10.1029/2007GL029222

Bommer JJ, Rodríguez CE (2002) Earthquake-induced landslides in Central America. Eng Geol 63:189–200. doi: 10.1016/S0013-7952(01)00081-3

Bommer JJ, Stafford PJ, Alarcón JE (2009) Empirical equations for the prediction of the significant, bracketed, and uniform duration of earthquake ground motion. Bull Seismol Soc Am 99:3217–3233. doi: 10.1785/0120080298

Boore DM (2003) Simulation of Ground Motion Using the Stochastic Method. Pure Appl. Geophys. 160:635–676.

Boore DM (2009) Comparing stochastic point-source and finite-source

ground-motion simulations: SMSIM and EXSIM. Bull Seismol Soc Am 99:3202–3216. doi: 10.1785/0120090056

Boore DM, Atkinson GM (2008) Ground-motion prediction equations for the average horizontal component of PGA, PGV, and 5%-damped PSA at spectral periods between 0.01 s and 10.0 s. Earthq Spectra 24:99–138. doi: 10.1193/1.2830434

Broothaerts N, Kissi E, Poesen J, et al (2012) Spatial patterns, causes and consequences of landslides in the Gilgel Gibe catchment, SW Ethiopia. Catena 97:127–136. doi: 10.1016/j.catena.2012.05.011

Caflisch RE (1998) Monte Carlo and quasi-Monte Carlo methods. Acta Numer. 7:1.

Campbell KW (2003) Prediction of Strong Ground Motion Using the Hybrid Empirical Method and Its Use in the Development of Ground-Motion (Attenuation) Relations in Eastern North America. Bull. Seismol. Soc. Am. 93:1012–1033.

Cascini L (2008) Applicability of landslide susceptibility and hazard zoning at different scales. Eng Geol 102:164–177. doi: 10.1016/j.enggeo.2008.03.016

Cepeda J, Hoeg K, Nadim F (2010) Landslide-triggering rainfall thresholds: A conceptual framework. Q J Eng Geol Hydrogeol 43:69–84. doi: 10.1144/1470-9236/08-066

Chang KT, Chiang SH, Hsu ML (2007) Modeling typhoon- and earthquake-induced landslides in a mountainous watershed using logistic regression. Geomorphology 89:335–347. doi: 10.1016/j.geomorph.2006.12.011

Chen H, Maki N, Hayashi H (2014) Disaster resilience and population ageing: The 1995 Kobe and 2004 Chuetsu earthquakes in Japan. Disasters 38:291–309. doi: 10.1111/disa.12048

Chiaro G, Kiyota T, Pokhrel RM, et al (2015) Reconnaissance report on geotechnical and structural damage caused by the 2015 Gorkha Earthquake, Nepal. Soils Found 55:1030–1043. doi: 10.1016/j.sandf.2015.09.006

Coe JA, Ellis WL, Godt JW, et al (2003) Seasonal movement of the Slumgullion landslide determined from global positioning system surveys and field instrumentation, July 1998-March 2002. Eng Geol 68:67–101. doi: 10.1016/S0013-7952(02)00199-0

Collins BD, Kayen R, Tanaka Y (2012) Spatial distribution of landslides triggered from the 2007 Niigata Chuetsu-Oki Japan Earthquake. Eng Geol 127:14–26. doi: 10.1016/j.enggeo.2011.12.010

Corominas J, Moya J (2008) A review of assessing landslide frequency for hazard zoning purposes. Eng Geol 102:193–213. doi: 10.1016/j.enggeo.2008.03.018

Cruden DM, Varnes DJ (1996a) Landslide types and processes. Turn. AK, Schuster, RL Landslides Investig. mitigation, Spec. Rep. 247. 36–75.

Cruden DM, Varnes DJ (1996b) Landslides: investigation and mitigation. Chapter 3-Landslide types and processes.

Dahal RK, Hasegawa S (2008) Representative rainfall thresholds for landslides in the Nepal Himalaya. Geomorphology 100:429–443. doi: 10.1016/j.geomorph.2008.01.014

Feizizadeh B, Shadman Roodposhti M, Jankowski P, Blaschke T (2014) A GIS-based extended fuzzy multi-criteria evaluation for landslide susceptibility mapping. Comput Geosci 73:208–221. doi: 10.1016/j.cageo.2014.08.001

Fell R (1994) Landslide risk assessment and acceptable risk. Can Geotech J 31:261–272. doi: 10.1139/t94-031

Fell R, Corominas J, Bonnard C, et al (2008a) Guidelines for landslide susceptibility, hazard and risk zoning for land use planning. Eng Geol 102:85–98. doi: 10.1016/j.enggeo.2008.03.022

Fell R, Corominas J, Bonnard C, et al (2008b) Guidelines for landslide susceptibility, hazard and risk zoning for land-use planning. Eng Geol 102:99–111. doi: 10.1016/j.enggeo.2008.03.014

Fraser S, Raby A, Pomonis A, et al (2013) Tsunami damage to coastal defences and buildings in the March 11th 2011 Mw9.0 Great East Japan

earthquake and tsunami. Bull Earthq Eng 11:205–239. doi: 10.1007/s10518-012-9348-9

Glade T (2000) Applying Probability Determination to Refine Landslide-triggering Rainfall Thresholds Using an Empirical “Antecedent Daily Rainfall Model” Pure Appl Geophys 157:1059–1079. doi: 10.1007/s000240050017

Gorum T, Fan X, van Westen CJ, et al (2011) Distribution pattern of earthquake-induced landslides triggered by the 12 May 2008 Wenchuan earthquake. Geomorphology 133:152–167. doi: 10.1016/j.geomorph.2010.12.030

Harp EL, Keefer DK, Sato HP, Yagi H (2011) Landslide inventories: The essential part of seismic landslide hazard analyses. Eng Geol 122:9–21. doi: 10.1016/j.enggeo.2010.06.013

Harrison RL (2010) Introduction To Monte Carlo Simulation. AIP Conf Proc 1204:17–21. doi: 10.1063/1.3295638

Hong Y, Adler R, Huffman G (2007) Use of satellite remote sensing data in the mapping of global landslide susceptibility. Nat Hazards 43:245–256. doi: 10.1007/s11069-006-9104-z

Hovius N, Stark CP (2006) Landslide-driven erosion and topographic evoution of active mountain belts. Landslides from massive Rock Slope Fail 573–590. doi: 10.1007/978-1-4020-4037-5

Hung J-J (2000) Chi-Chi Earthquake Induced Landslides in Taiwan. Earthq Eng Seismol 2:25–33.

Hungr O, Leroueil S, Picarelli L (2014) The Varnes classification of landslide types, an update. Landslides 11:167–194.

Hutchings L, Wu F (1990) Empirical Green's Functions from small earthquakes: A waveform study of locally recorded aftershocks of the 1971 San Fernando Earthquake. J. Geophys. Res. 95:1187.

Ibsen ML, Casagli N (2004) Rainfall patterns and related landslide incidence in the Porretta-Vergato region, Italy. Landslides 1:143–150. doi: 10.1007/s10346-004-0018-0

Kawabata D, Bandibas J (2009) Landslide susceptibility mapping using geological data, a DEM from ASTER images and an Artificial Neural Network (ANN). Geomorphology 113:97–109. doi: 10.1016/j.geomorph.2009.06.006

Kayen R, Brandenberg SJ, CoIlins BD, et al (2009) Geoengineering and seismological aspects of the Niigata-Ken Chuetsu-Oki earthquake of 16 July 2007. Earthq Spectra 25:777–802. doi: 10.1193/1.3240397

Keefer DK (1984) Landslides caused by earthquakes. Geol. Soc. Am. Bull. 95:406–421.

Keefer DK (2002) Investigating landslides caused by earthquakes - A historical review. Surv Geophys 23:473–510. doi: 10.1023/A:1021274710840

Khazai B, Sitar N (2004) Evaluation of factors controlling earthquake-induced landslides caused by Chi-Chi earthquake and comparison with the Northridge and Loma Prieta events. Eng Geol 71:79–95. doi: 10.1016/S0013-7952(03)00127-3

Knapen A, Kitutu MG, Poesen J, et al (2006) Landslides in a densely populated county at the footslopes of Mount Elgon (Uganda): Characteristics and causal factors. Geomorphology 73:149–165. doi: 10.1016/j.geomorph.2005.07.004

Korup O, Densmore AL, Schlunegger F (2010) The role of landslides in mountain range evolution. Geomorphology 120:77–90. doi: 10.1016/j.geomorph.2009.09.017

Kurahashi S, Irikura K (2010) Characterized source model for simulating strong ground motions during the 2008 Wenchuan earthquake. Bull Seismol Soc Am 100:2450–2475. doi: 10.1785/0120090308

Kwak YH, Ingall L (2007) Exploring Monte Carlo Simulation Applications for Project Management. Risk Manag 9:44–57. doi: 10.1057/palgrave.rm.8250017

Lateltin O, Haemmig C, Raetzo H, Bonnard C (2005) Landslide risk management in Switzerland. Landslides 2:313–320. doi: 10.1007/s10346-

005-0018-8

Lee S (2007) Application and verification of fuzzy algebraic operators to landslide susceptibility mapping. Environ Geol 52:615–623. doi: 10.1007/s00254-006-0491-y

Lee S, Chwae U, Min K (2002) Landslide susceptibility mapping by correlation between topography and geological structure: The Janghung area, Korea. Geomorphology 46:149–162. doi: 10.1016/S0169-555X(02)00057-0

Lee S, Hwang J, Park I (2013) Application of data-driven evidential belief functions to landslide susceptibility mapping in Jinbu, Korea. Catena 100:15–30. doi: 10.1016/j.catena.2012.07.014

Lee S, Ryu J-H, Won J-S, Park H-J (2004) Determination and application of the weights for landslide susceptibility mapping using an artificial neural network. Eng Geol 71:289–302. doi: 10.1016/S0013-7952(03)00142-X

Lee S, Sambath T (2006) Landslide susceptibility mapping in the Damrei Romel area, Cambodia using frequency ratio and logistic regression models. Environ Geol 50:847–855. doi: 10.1007/s00254-006-0256-7

Lee YF, Chi YY (2011) Rainfall-induced landslide risk at Lushan, Taiwan. Eng Geol 123:113–121. doi: 10.1016/j.enggeo.2011.03.006

Lenti L, Martino S (2013) A parametric numerical study of the interaction between seismic waves and landslides for the evaluation of the susceptibility to seismically induced displacements. Bull Seismol Soc Am 103:33–56. doi: 10.1785/0120120019

Li Zhongsheng (2003) The state of the art of the research on seismic landslide hazard at home and abroad. J Catastrophology 18:64–70. doi: 10.1139/t94-031

Malamud BD, Turcotte DL, Guzzetti F, Reichenbach P (2004) Landslides, earthquakes, and erosion. Earth Planet Sci Lett 229:45–59. doi: 10.1016/j.epsl.2004.10.018

Manousiouthakis VI, Deem MW (1999) Strict detailed balance is unnecessary in Monte Carlo simulation. J Chem Phys 110:2753. doi:

10.1063/1.477973

Masson DG, Harbitz CB, Wynn RB, et al (2006) Submarine landslides: processes, triggers and hazard prediction. Philos Trans A Math Phys Eng Sci 364:2009–2039. doi: 10.1098/rsta.2006.1810

McColl ST (2014) Landslide Causes and Triggers. In: Landslide Hazards, Risks, and Disasters. pp 17–42

Mena B, Martin Mai P, Olsen KB, et al (2010) Hybrid broadband ground-motion simulation using scattering green's functions: Application to large-magnitude events. Bull Seismol Soc Am 100:2143–2162. doi: 10.1785/0120080318

Mendoza C, Hartzell S (2009) Source analysis using regional empirical Green's functions: The 2008 Wells, Nevada, earthquake. Geophys Res Lett. doi: 10.1029/2009GL038073

METROPOLIS N, ULAM S (1949) The Monte Carlo method. J Am Stat Assoc 44:335–341. doi: 10.1080/01621459.1949.10483310

Minder JR, Roe GH, Montgomery DR (2009) Spatial patterns of rainfall and shallow landslide susceptibility. Water Resour Res. doi: 10.1029/2008WR007027

Nakanishi A, Smith AJ, Miura S, et al (2004) Structural factors controlling the coseismic rupture zone of the 1973 Nemuro-Oki earthquake, the southern Kuril Trench seismogenic zone. J Geophys Res Solid Earth. doi: 10.1029/2003JB002574

Nishimura T (2013) Earthquake-Induced Landslides.

Oh HJ, Pradhan B (2011) Application of a neuro-fuzzy model to landslide-susceptibility mapping for shallow landslides in a tropical hilly area. Comput Geosci 37:1264–1276. doi: 10.1016/j.cageo.2010.10.012

Parise M, Jibson RW (2000a) A seismic landslide susceptibility rating of geologic units based on analysis of characterstics of landslides triggered by the 17 January, 1994 Northridge, California earthquake. Eng Geol 58:251–270. doi: 10.1016/S0013-7952(00)00038-7

Parise M, Jibson RW (2000b) A seismic landslide susceptibility rating

of geologic units based on analysis of characteristics of landslides triggered by the 17 January, 1994 Northridge, California earthquake. Eng Geol 58:251–270. doi: 10.1016/S0013-7952(00)00038-7

Piegari E, Di Maio R, Milano L (2009) Characteristic scales in landslide modelling. Nonlinear Process Geophys 16:515–523. doi: 10.5194/npg-16-515-2009

Pitarka A, Somerville P, Fukushima Y, et al (2000) Simulation of near-fault strong-ground motion using hybrid Green's functions. Bull Seismol Soc Am 90:566–586. doi: 10.1785/0119990108

Pradhan B, Sezer EA, Gokceoglu C, Buchroithner MF (2010) Landslide susceptibility mapping by neuro-fuzzy approach in a landslide-prone area (Cameron Highlands, Malaysia). IEEE Trans Geosci Remote Sens 48:4164–4177. doi: 10.1109/TGRS.2010.2050328

Qi S, Xu Q, Lan H, et al (2010) Spatial distribution analysis of landslides triggered by 2008.5.12 Wenchuan Earthquake, China. Eng Geol 116:95–108. doi: 10.1016/j.enggeo.2010.07.011

Raychaudhuri S (2008) Introduction to monte carlo simulation. Simul Conf 2008 WSC 2008 91–100. doi: 10.1109/WSC.2008.4736059

Reid ME, Baum RL, LaHusen RG, Ellis WL (2008) Capturing landslide dynamics and hydrologic triggers using near-real-time monitoring. Landslides Eng Slopes From Past to Futur 179–191. doi: 10.1201/9780203885284-c10

Rodríguez CE, Bommer JJ, Chandler RJ (1999) Earthquake-induced landslides: 1980-1997. Soil Dyn Earthq Eng 18:325–346. doi: 10.1016/S0267-7261(99)00012-3

Roering J (2012) Tectonic geomorphology: Landslides limit mountain relief. Nat Geosci 5:446–447. doi: 10.1038/ngeo1511

Saba SB, van der Meijde M, van der Werff H (2010) Spatiotemporal landslide detection for the 2005 Kashmir earthquake region. Geomorphology 124:17–25. doi: 10.1016/j.geomorph.2010.07.026

Saez JL, Corona C, Berger F (2013) Probability maps of landslide

reactivation derived from tree-ring records. In: Landslide Science and Practice: Landslide Inventory and Susceptibility and Hazard Zoning. pp 409–416

Sassa K, Fukuoka H, Wang F, Wang G (2007) Progress in landslide science.

Sato HP, Harp EL (2009) Interpretation of earthquake-induced landslides triggered by the 12 May 2008, M7.9 Wenchuan earthquake in the Beichuan area, Sichuan Province, China using satellite imagery and Google Earth. Landslides 6:153–159. doi: 10.1007/s10346-009-0147-6

Scherbaum F (2006) The Estimation of Minimum-Misfit Stochastic Models from Empirical Ground-Motion Prediction Equations. Bull. Seismol. Soc. Am. 96:427–445.

Schulz WH, Kean JW, Wang G (2009) Landslide movement in southwest Colorado triggered by atmospheric tides. Nat Geosci 2:863–866. doi: 10.1038/ngeo659

Sezer EA, Pradhan B, Gokceoglu C (2011) Manifestation of an adaptive neuro-fuzzy model on landslide susceptibility mapping: Klang valley, Malaysia. Expert Syst Appl 38:8208–8219. doi: 10.1016/j.eswa.2010.12.167

Shiels AB, West CA, Weiss L, et al (2008) Soil factors predict initial plant colonization on Puerto Rican landslides. Plant Ecol 195:165–178. doi: 10.1007/s11258-007-9313-x

Shin TC, Teng TL (2001) An overview of the 1999 Chi-Chi, Taiwan, earthquake. Bull Seismol Soc Am 91:895–913. doi: 10.1785/0120000738

Sidle RC, Ochiai H (2013) Landslides: Processes, Prediction, and Land Use.

Sobol IM (2001) Global sensitivity indices for nonlinear mathematical models and their Monte Carlo estimates. Math Comput Simul 55:271–280. doi: 10.1016/S0378-4754(00)00270-6

Sobol IM (1998) On quasi-Monte Carlo integrations. Math Comput Simul 47:103–112. doi: 10.1016/S0378-4754(98)00096-2

Swendsen RH, Wang JS (1986) Replica Monte Carlo simulation of

spin-glasses. Phys Rev Lett 57:2607–2609. doi: 10.1103/PhysRevLett.57.2607

Swenson JJ, Franklin J (2000) The effects of future urban development on habitat fragmentation in the Santa Monica Mountains. Landsc Ecol 15:713–730. doi: 10.1023/A:1008153522122

Tang C, Zhu J, Qi X (2011a) Landslide hazard assessment of the 2008 Wenchuan earthquake: a case study in Beichuan area. Can Geotech J 48:128–145. doi: 10.1139/T10-059

Tang C, Zhu J, Qi X, Ding J (2011b) Landslides induced by the Wenchuan earthquake and the subsequent strong rainfall event: A case study in the Beichuan area of China. Eng Geol 122:22–33. doi: 10.1016/j.enggeo.2011.03.013

Tibaldi A, Ferrari L, Pasquar?? G (1995) Landslides triggered by earthquakes and their relations with faults and mountain slope geometry: an example from Ecuador. Geomorphology 11:215–226. doi: 10.1016/0169-555X(94)00060-5

Turner TR, Duke SD, Fransen BR, et al (2010) Landslide densities associated with rainfall, stand age, and topography on forested landscapes, southwestern Washington, USA. For Ecol Manage 259:2233–2247. doi: 10.1016/j.foreco.2010.01.051

Varnes DJ (1984) Landslide hazard zonation: a review of principles and practice. Nat. Hazards 5:63.

Wang G, Huang R, Lourenço SDN, Kamai T (2014) A large landslide triggered by the 2008 Wenchuan (M8.0) earthquake in Donghekou area: Phenomena and mechanisms. Eng Geol 182:148–157. doi: 10.1016/j.enggeo.2014.07.013

Wang HB, Sassa K, Xu WY (2007) Analysis of a spatial distribution of landslides triggered by the 2004 Chuetsu earthquakes of Niigata Prefecture, Japan. Nat Hazards 41:43–60. doi: 10.1007/s11069-006-9009-x

Wang Y (2011) Quantum Monte Carlo simulation. Ann Appl Stat 5:669–683. doi: 10.1214/10-AOAS406

Wu CH, Chen SC (2009) Determining landslide susceptibility in Central Taiwan from rainfall and six site factors using the analytical hierarchy process method. Geomorphology 112:190–204. doi: 10.1016/j.geomorph.2009.06.002

Xu C, Xu X, Lee YH, et al (2012) The 2010 Yushu earthquake triggered landslide hazard mapping using GIS and weight of evidence modeling. Environ Earth Sci 66:1603–1616. doi: 10.1007/s12665-012-1624-0

Xu C, Xu X, Yu G (2013) Landslides triggered by slipping-fault-generated earthquake on a plateau: an example of the 14 April 2010, Ms 7.1, Yushu, China earthquake. Landslides 10:421–431. doi: 10.1007/s10346-012-0340-x

Yao H, Campman X, de Hoop M V., van der Hilst RD (2009) Estimation of surface wave Green's functions from correlation of direct waves, coda waves, and ambient noise in SE Tibet. Phys Earth Planet Inter 177:1–11. doi: 10.1016/j.pepi.2009.07.002

Yesilnacar E, Topal T (2005) Landslide susceptibility mapping: A comparison of logistic regression and neural networks methods in a medium scale study, Hendek region (Turkey). Eng Geol 79:251–266. doi: 10.1016/j.enggeo.2005.02.002

Yin Y, Wang F, Sun P (2009) Landslide hazards triggered by the 2008 Wenchuan earthquake, Sichuan, China. Landslides 6:139–151. doi: 10.1007/s10346-009-0148-5

Yuan RM, Xu XW, Chen GH, et al (2010) Ejection landslide at northern terminus of beichuan rupture triggered by the 2008 Mw 7.9 Wenchuan earthquake. Bull Seismol Soc Am 100:2689–2699. doi: 10.1785/0120090256

Yue H, Lay T (2013) Source rupture models for the Mw 9.0 2011 Tohoku earthquake from joint inversions of high-rate geodetic and seismic data. Bull Seismol Soc Am 103:1242–1255. doi: 10.1785/0120120119

Zhou CH, Lee CF, Li J, Xu ZW (2002) On the spatial relationship between landslides and causative factors on Lantau Island, Hong Kong.

Geomorphology 43:197–207. doi: 10.1016/S0169-555X(01)00130-1

Zhou H-L, Allen CR, Kanamori H (1983) Rupture complexity of the 1970 Tonghai and 1973 Luhuo earthquakes, China, from P-wave inversion, and relationship to surface faulting. Bull Seismol Soc Am 73:1585–1597.

Zhou S, Fang L (2011) Support vector machine modeling of earthquake- induced landslides susceptibility in central part of Sichuan province, China. Zhou Fang Geoenvironmental Disasters. doi: 10.1186/s40677-014-0006-1

Zhou S, Fang L, Liu B (2015) Slope unit-based distribution analysis of landslides triggered by the April 20, 2013, Ms 7.0 Lushan earthquake. Arab J Geosci 8:7855–7868. doi: 10.1007/s12517-015-1835-2

CHAPTER 2

REVIEW OF STUDIES ON LANDSLIDE HAZARD MAPPING

2.1 INTRODUCTION

Landslides, representing one of the most serious natural hazards around the world, having considerable and destructive effects on human life, properties, infrastructures, and, of course, on the environment. Landslide hazard mapping to identify the areas within the landscape with the characteristics that could make them susceptible to landslides. Generally, landslide hazard mapping makes attempts not only to identify landslide prone slopes but also the potential area affected by the potential landslides.

Landslide hazard mapping is a common practice in many countries and regions around the world, principally used for aiding urban planning and as a first step to assessment of landslide hazards (Lee et al. 2002; Lee et al. 2004; Ayalew and Yamagishi 2005; Yesilnacar and Topal 2005; Bhandary et al. 2013; Lee et al. 2013; Feizizadeh et al. 2014). Therefore, many countries, particularly the developed ones, invest huge amount of money either in mitigation or in prevention of landslides. (Guzzetti et al. 2006; Lee and Sambath 2006; Hong et al. 2007; Lee 2007; Kawabata and Bandibas 2009; Pradhan et al. 2010; Oh and Pradhan 2011; Sezer et al. 2011). The most important step of landslide prevention efforts is to assess a certain region's hazard to landslides by obtaining data related to landslides, i.e. preparation of landslide inventory and database. If taken into consideration, results of these assessments, i.e. landslide hazard maps, will provide useful information and

economic benefits for urban planning, development plans, engineering applications, land use potential planning, and so on. When international scientific literature related to landslide assessments is examined, there has been an increasing interest in landslide hazard mapping studies in the last decades. Particularly, in recent years, with the development of computation technology, GIS (Geographic Information System), and RS (Remote Sensing) techniques (Santacana et al. 2003; Lee et al. 2004; Ayalew and Yamagishi 2005; Dahal et al. 2008; Bai et al. 2010; Mancini et al. 2010; Feizizadeh et al. 2014). This can be concluded as one of the most promising efforts with respect to combat with natural hazards since they opened wide range of opportunities for analyzing, evaluating, and assessing landslides. Thus, there are a multitude of studies carried out by different researchers in different parts of the world with the aid of these technological items.

The landslide hazard mapping studies can be dated back to 1950's, initiation of landslide hazard mapping was at the beginning of 1970's. The beginning of 1990's, with the exception of a very few cases, witnessed the GIS applications for mapping in landslide regions. In some cases, the majority of the analyses and map modeling were fully achieved through a given GIS package, but in other cases, the use of GIS was only partial. Since the1990's, with the rapid development and utilization of GIS technologies, which becomes a very important tool for mapping and evaluating landslides hazards, especially for studies at a regional scale.

In this study, it was aimed at reviewing the existing landslide hazard mapping methods by means of a detailed literature survey. By doing so, firstly, the terminologies related to landslide hazard mapping are described. Then, a historical development of the approaches in landslide hazard assessments were evaluated. Finally, it will summarize the unsolved issues landslide hazard mapping.

2.2 TERMINOLOGIES

The term landslide is defined as the movement of a mass of rock, debris or earth down a slope. Varnes (1984) landslide classification system is the most widely used one to explain the mechanisms of landslides and to provide communication among the researchers throughout the world, based on the type of movement and

material (Keefer 1984; Fell 1994; Keefer 2002; Malamud et al. 2004; Sassa et al. 2007; Alkhasawne et al. 2012; Feizizadeh et al. 2014). As for the terminology related to landslides and their mapping, there was a little bit conflict among the users for susceptibility, hazard, and risk.

2.2.1 LANDSLIDE SUSCEPTIBILITY

The susceptibility of landslide is a quantitative or qualitative assessment of the classification, volume (or area), and spatial distribution of landslides which exist or potentially may occur in an area (Cascini 2008; Fell et al. 2008a; Fell et al. 2008b). The landslide susceptibility may sometimes also contain a description of the velocity and intensity of the existing or potential landsliding. It is expected that landsliding will occur more frequently in the areas with the highest susceptibility, However, temporal frame is not taken into account in the susceptibility analysis. According to Fell et al. (2008a), the susceptibility of landslide includes landslides which have their source in the area, or may have their source outside the area but may travel onto or regress into the area.

2.2.2 LANDSLIDE HAZARD

The term of hazard can be defined as "a potential condition as an effect of an occurrence to have an undesirable consequences or damage" (Sassa 1997). According to Varnes (1984), the hazard of landslide hazard defined as the probability of occurrence within a specified period of time and within a given area of a potential landslide. The landslide hazard should not only include the spatial probability of landslide occurrence, but also the temporal probability of landslide events. It is characterized by statements of 'what', 'where', 'when', 'how strong' and 'how often', demanding knowledge of variation in both spatial conditions, temporal and magnitude behavior (Glade et al., 2005). The landslide hazard map is a tool used to portray the location of landslide, the predicted location of landslide, and can be used to divide the different level of risk areas (Van Westen et al. 1999; Guzzetti et al. 2000). Landslide hazard is expected to answer both spatial and temporal probability of landslide occurrence. The temporal probability is not taken

into account in landslide susceptibility mapping. Therefore, both the information about landslide susceptibility and landslide inventory containing the date of landslides events are needed in the landslide hazard analysis. Nevertheless, it is very difficult to include the detail information of the landslide events and area/volume in most of landslide hazard maps for the following reasons: first, the multi-temporal inventory of landslide is not always available; second it is difficult the get the detail information about the historical landslide information due to the heterogeneity of the subsurface conditions, and there is always some absences or insufficient length of historical records of landslide triggering events(Galli et al. 2008; Harp et al. 2011; Guzzetti et al. 2012). Thus, generating landslide inventory is a key issue remains to be solved in landslide hazard analysis.

2.2.3 LANDSLIDE RISK

Risk is a measure of the probability and severity of an adverse effect to health, property or the environment (Hong et al. 2007; Crozier and Glade 2012; Davies 2014). Risk is often estimated by the product of probability of a phenomenon of a given magnitude times the consequences. In landslides studies, quantitative risk assessment has been applied and developed since long time ago by geotechnical engineer on a site investigation scale, such as pipeline, road, dam, oil platform, and housing. The analysis will be more focused on the hazard analysis of a specific slope. It uses deterministic (factor of safety, numerical analyses) and/or probabilistic methods. landslide risk also involves hazard. Therefore, landslide risk zoning assesses the loss of life or property or environmental features accounting for temporal probability, spatial probability, magnitude probability and vulnerability. In practice, it would not be simple to achieve and need detailed investigation on each risk element, i.e. hazard, vulnerability and element at risk (Guzzetti et al. 1999; Fell et al. 2008a; Huggel et al. 2010; Vranken et al. 2014).

2.2.4 TERMINOLOGIES USED IN THIS STUDY

As can be seen from the definitions above, there was a little bit conflict among the users for landslide susceptibility, landslide hazard, and landslide risk. In the past,

a lot of definitions have been made with respect to their meanings and there were no global guidelines about selection of these terminologies in the field of engineering slopes. For this reason, in this study, we define the landslide hazard as the probability of failure of a slope and do not consider the temporal probability of landslides. Additionally, mapping refers to the division of the land surface into areas and the ranking of these areas according to the degree of potential hazard from landslides.

2.3 LANDSLIDE HAZARD MAPPING METHODS

Identifying the region's hazard to landslide is very important to avoid landslide damage or to reduce losses caused. It is difficult to accurately predict the time and location of landslides over a large region. However, it is possible to evaluate a certain region's potential hazard for landslides through landslide hazard mapping (LHM). In the past two decades, LSM has become a very important and effective way to assess landslide disasters. The results of LSM can be used for land management and landslide hazards mitigation.

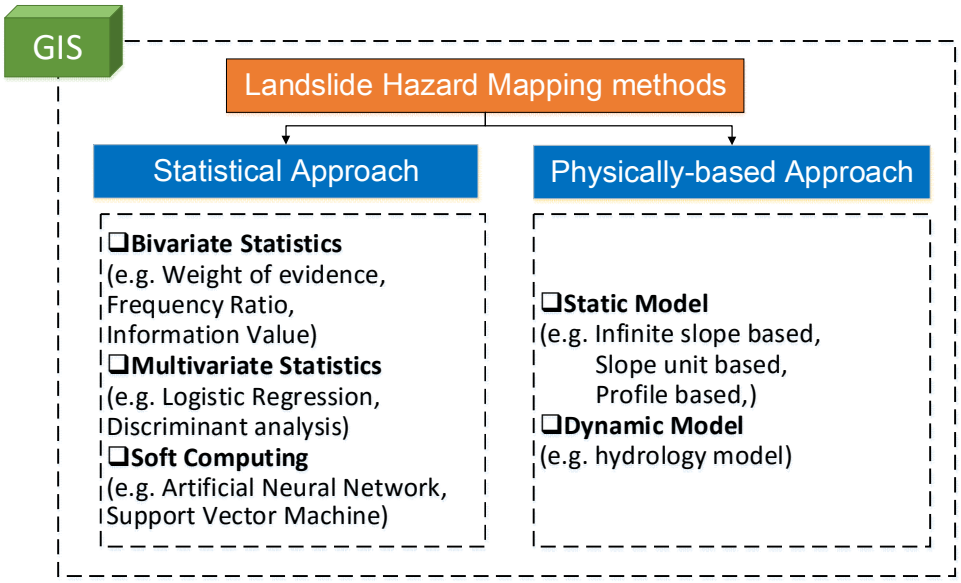

Figure 2-1 Approaches for landslide hazard mapping

During the past two decades, many studies on LHM were carried out on geographic information systems (GIS), which are efficient tools for integrating and

analyzing a large quantity of geographical data (Carrara et al. 2000; Wang et al. 2005). Generally speaking, methods of landslide hazard mapping based on GIS can be grouped into statistical methods and physically-based methods. General reviews of these landslide hazard mapping methods can be found in (Guzzetti et al. 1999; Carrara et al. 2000; Wang et al. 2005).

2.3.1 STATISTICAL APPROACH

The statistical approach is to give some numerical expressions of the relationship between controlling factors and landslide occurrence using statistical model. The statistical approaches are built on the basic assumption that areas with critical factors contributing to the past landslides will also be favorable to future landslides. Some of the quantitative methods are bivariate and some of them are multivariate methods.

2.3.1.1 Bi-variate statistical analysis

For the bi-variate statistical approaches of landslide hazard mapping, it compares each landslide predictive factors to the existing landslide information (Yalcin 2008; Nandi and Shakoor 2010). Weights of each landslide predictive factors are calculated according to the landslide density (Nandi and Shakoor 2010). Typical bi-variate statistical LHM approaches are the information value method, weight of evidence method and weighted overlay model, etc.

Information value method is based on the relationship between landslide occurrence and its predictive factors (Howard 1966). The information values for each subclass of landslide predictive factors are calculated according to the presence or absence of the landslide in a given mapping unit, such as a raster pixel or a slope unit (Howard 1966). In the past two decades, the information value method has been successfully used in several regions for landslide hazard mapping.

Sarkar et al. (2013) carried out a landslide hazard mapping in parts of the Darjeeling Himalayas using the information value method. He found that this method showed a good performance with a validation result value of 89% in accuracy. Zêzere (2002) applied the information value method for landslide hazard

mapping in the North Lisbon, Portugal. In his models, he considered the landslide typology and found the most important factors to predict the landslide hazards are the roads and the fluvial channels. Also mentioned by Zêzere (2002), the landslides magnitude depends largely upon the typologies. Lee and Sambath (2006) applied and compared the results of landslide hazard maps produced from the logistic regression method and the information value method in the Damrei Romel area, Cambodia and found that both of the two methods had high and similar prediction accuracy. Sharma et al. (2009) performed a GIS based landslide hazard mapping for Sikkim Himalayas areas using IVM and found the accuracy assessment of landslide hazard map confirmed the model with highest degree of accuracy for high susceptibility class. Therefore, it may be concluded that information value method has proved a useful method in quantifying the effect of individual landslide predictive factors, which are responsible for landslide occurrence (Wang et al. 2005; Kanungo et al. 2009).

The Weight of Evidence method is a log linear form of Bayesian probability model (Good 1985; Wing and Phelan 2005; Bacon and Aphramor (2011). This method uses landslide occurrence as training points to derive prediction outputs. By calculating both unconditional and conditional probability of landslide hazards. This method is based on calculation of positive and negative weights to quantify the spatial association degree between landslide occurrence and each classes within every landslide predictive factors (Guzzetti et al. 1999; Guzzetti et al. 2000).

The weight of evidence method had been used in landslide mapping within the GIS environment since the 1990's. Blahut et al. (2010) applied the weight of evidence method applied WoE model for accurate prediction of debris-flow source areas by analysis the inventory of landslides. To reduce the multitude of landslide-related conditions to a pattern of a few discrete predictive variables. Regmi et al. (2010) applied the weight of evidence method to produce the landslide hazard maps in Paonia–McClure Pass area of Colorado, USA with six different combination of landslide predictive factors representing topography, hydrology, geology, land cover, and human influences. The best result of Regmi et al. (2010)'s study showed an prediction accuracy of 78%. Armaş (2012) applied the weight of evidence

method to assess the landslide susceptibility of a hilly area in the Subcarpathian sector of the Prahova Valley. As a useful spatial data prediction model, the weight of evidence method has been successfully used in many regions according to the published literatures (Lee et al. 2002a; Van Westen et al. 2003; Lee et al. 2004; Lee and Choi 2004; Barbieri and Cambuli 2009; Pradhan et al. 2010a; Pradhan and Lee 2010; Pradhan et al. 2010b; Armaş 2012; Kayastha et al. 2012).

Other typical bi-variate statistical methods, such as the Fuzzy Logic method and Weighted overlay method are also frequently used in landslide hazard in the past decades and had proved to be useful statistical models in prediction landslide occurrence (Lee and Talib 2005; Wang et al. 2005; Guzzetti et al. 2006; Yoshimatsu and Abe 2006; Corominas and Moya 2008; Fell et al. 2008a; Guzzetti et al. 2012; Van Den Eeckhaut et al. 2012).

Generally, the Bi-variate statistical landslide hazard mapping methods is able to quantify the degree of effects of landslide predictive factors on landslide occurrence by comparing the factors with the landslide distribution. However, assigning weightage to the causative factors on the basis of this relationship may not always be appropriate since the interplays among the landslide predictive factors can't be assessed in these methods. Moreover, landslide occurrence is the general consequence of several landslide predictive factors at a time. Therefore, the degree of effects among the landslide predictive factors should also be quantified and such quantification can be performed by the multivariate statistical methods (Guzzetti et al. 2006; Yoshimatsu and Abe 2006; Corominas and Moya 2008; Fell et al. 2008a).

2.3.1.2 Multi-variate statistical analysis

Multi-variate statistical analysis for landslide hazard mapping considers relative contribution of each landslide predictive factor to the landslide occurrence (Nandi and Shakoor 2010). The multivariate methods calculate percentage of landslide occurrence for each mapping unit and the probability of landslide occurrence is produced followed by the application of multivariate statistical method for reclassification of hazard for the given area. Logistic regression model,

and support vector machine methods are commonly used methods for LHZ mapping (Santacana et al. 2003; Süzen and Doyuran 2004; Nandi and Shakoor 2010).

The Logistic Regression regress a dichotomous variable on a set of independent variables (Gortmaker et al. 1994; Davis and Offord 1997). In the landslide hazard mapping, the dichotomous variable is the presence or absence of the landslide occurrence, which the independent variables refer to the landslide predictive factors. Generally speaking, The Logistic Regression method can be of two types one is the Binary Logistic (when dependent variable is dichotomous and independent variable is of any type) and Multinomial Logistic Regression (dependent variable with more than two classes) (Gortmaker et al. 1994). For the landslide hazard mapping using the logistic regression model, the binary logistic model is usually incorporated. In case of landslide hazard mapping, the LR model find the best fitting model to describe the relationship between presence and absence of landslides and the set of independent variables such as slope angle, slope aspect, lithology and land use (Corominas and Moya 2008; Fell et al. 2008a). It generates the model statistics and coefficient of formulae useful in defining the landslide hazard indexes. If coefficient is positive, the landslide event is likely to occur. Logistic regression method is a statistical model of slope instability built on the assumption that factor which caused slope failure in a region are the same as those which will generate landslides in future (Wang et al. 2005; Guzzetti et al. 2006; Corominas and Moya 2008; Fell et al. 2008a).

Support vector machine (SVM), as the representative's kernel-based techniques, is a major development in machine learning algorithms. SVM is a group of supervised learning methods based on the statistical learning theory and the Vapnik-Chervonenkis (VC) dimension introduced by Vapnik (1995) and Vapnik (1999) that can be applied to pattern classification or non-linear regression. The SVM was originally developed by Vapnik (1995) as a new machine learning algorithm for pattern classification and non-linear regression. The main procedure involved in SVM modeling is a training phase with associated input and target output values. Recently, several authors have applied the SVM model successfully

on landslide susceptibility mapping. Wu and Chen (2009) and Intrieri et al. (2012) compared several classification approaches of SVM, Gaussian process, and LR modeling, with SVM having the best results. Xu et al. (2012) examined the use of SVM model for landslide susceptibility mapping in an earthquake zone with combination of 4 kernel functions and 3 different training sets and found that radial-basis and polynomial kernel functions were suitable for modeling with any input training data. Xu et al. (2012) applied 6 different models in susceptibility mapping of landslides induced by the 2008 Wenchuan earthquake with SVM having a second best results outranked only by logistic regression. Kavzoglu et al. (2013) also made a comparison of susceptibility results from multi-criteria decision analysis, SVM, and logistic regression and showed that multi-criteria decision analysis and SVM methods were better than logistic regression in shallow landslides susceptibility mapping. These applications proved that when used properly, SVM model in landslide susceptibility mapping might produce a good result. Two outstanding advantages of the SVM are: (a) Based on the principle of minimization structural risk; (b) Guarantee its performance by solving constrained quadratic form. Theoretically, it can achieve the optimal prediction result by using the SVM model. Its detailed mathematical formulas are introduced in Vapnik (1995) and Vapnik (1999).

Landslides are governed by several predictive and triggering factors which are complexly interrelated. The interrelationships between these factors and landslides are nonlinear in nature (Guzzetti et al. 1999; Guzzetti et al. 2006; Guzzetti et al. 2012). Recently, several GIS based landslide susceptibility analyses using raster pixel as mapping unit have been proposed. Several studies have applied multivariate statistical models for landslide hazard mapping with comparatively high success (Good 1985; Fell 1994; Ibsen and Casagli 2004; Guzzetti et al. 2006; Fell et al. 2008a; Galli et al. 2008; Fell et al. 2008b; Kawabata and Bandibas 2009; Kayen et al. 2009; Kayastha et al. 2012; Feizizadeh et al. 2014; Hungr et al. 2014).

2.3.2 PHYSICALLY-BASED APPROACH

Another popular landslide hazard mapping methods is the deterministic

approaches or the physically-based approaches. Physically-based landslide hazard mapping approaches describes physical processes leading to the slope instabilities based on a mechanical analysis (Menon and Bawa 1997; Kuriakose et al. 2008; Kuriakose et al. 2009a; Kuriakose et al. 2009b; Vijith et al. 2013). One of the biggest advantages of these models is that they do not need historical landslide data and therefore can also be applicable to the areas with no or incomplete landslide inventories. Another advantage of the physically-based approach over the statistical approach is that the triggering force can be directly considered in the mechanical analysis, such as the seismic force or the rainfall infiltration (Kuriakose et al. 2008).

The Transient Rainfall Infiltration and Grid based Slope Stability (TRIGRS) model (Baum et al. 2008) was applied in central Umbria region of central Italy by Salciarini et al. (2006) for modelling shallow landslides triggered by rainfall. In Salciarini et al. (2006)'s study, the known rainfall events and associated landslide records triggered by the rainfall were collected to calibrate the model and simulations were performed. Suggested by Salciarini et al. (2006) that to improve the accuracy of TRIGRS model, the digital elevation model (DEM) with high resolution is needed, also spatial distribution of geotechnical parameters of the surface should be considered in this model.

The TRIGRS (Transient Rainfall Infiltration and Grid based Slope Stability) models had also been successfully used in the real time prediction of shallow landslides by Chien-Yuan et al. (2005), HONG and ADLER (2008), Montrasio et al. (2011) and Park et al. (2013) in different regions. Of these research, Montrasio et al. (2011) also compared SLIP (shallow Landslide Instability Prediction) and TRIGRS models in prediction of shallow landslide occurrence in GIS environment. The results of the study indicate that both the models have similar predictive capability. Taking Western Ghats of Kerala, India as the study area, a detailed comparative study was carried out by Kuriakose (2010) using four physically-based models: Shallow Landsliding Stability (SHALSTAB) (Dietrich et al. 2001), TRIGRIS model (Baum et al. 2008), Stability Index Mapping (SINMAP) (Pack 2001), and Storage and Redistribution of Water on Agricultural and Revegetated Slope Probability of Stability (STARWAR+PROBSTAB) models (Dou et al. 2014).

According to Kuriakose (2010)'s study, STARWAR+PROBSTAB model is the most suitable model for assessment of spatial-temporal probabilities of shallow landslides.

2.4 CURRENT UNSOLVED ISSUES IN LANDSLIDE HAZARD MAPPING

In last few years the approach towards LHM has been proposed from statistical approach to physically-based approach to minimize subjectivity in weightage assignment procedure and produce more objective and reproducible results. Several issues in landslide hazard mapping include developing technique in inventory mapping, particularly in a data scarce environment, selecting methods for landslide hazard mapping, and improving the accuracy of current approaches for landslide hazard mapping. It varies depending on the availability of secondary data, geomorphological characteristic, and landslide typology. The availability of data input is very important prior to landslide risk analysis. It can affect the overall methodology or approaches applied in the landslide risk analysis. Despite the availability of landslide inventory, geomorphological characteristic of the study area should also be considered prior to selecting suitable landslide susceptibility and risk analysis. Some approaches in landslide hazard mapping was not sufficient in practical use. For example, in current landslide hazard mapping approaches, the area affected by the landslides was not considered.

2.4.1 INSUFFICIENT LANDSLIDE INVENTORY FOR STATISTICAL LHM APPROACH

Generating landslide analysis is difficult in some areas because the unavailability of the landslide inventory map. However, the recent technology developments such as the availability of the modern field instrument, high resolution DTMs, high resolution satellite imagery, recent development on GIS and remote sensing technology have made generating landslide map easier. But, the selection of this technique should be carefully reviewed based on the purpose, the extent of the study area, the scale of base maps and analysis, resolution and characteristics of the available imagery, and the skill and experience of the interpreter (Wang et al. 2005; Guzzetti et al. 2006; Guzzetti et al. 2006; Mancini et

al. 2010). Mapping landslide through field survey is the oldest technique for landslide inventory mapping and considered as the most accurate technique for mapping fresh landslide events. But it is difficult, by using field survey, to recognize old landslides in the field where the natural process (e.g. erosion, vegetation) and the anthropogenic activities (e.g. urbanization, road construction, ploughing) are exist. The use of aerial photograph interpretation is also difficult in Indonesia due to unavailability of multiple sets of aerial photograph in the same area and different time. In the other hand the use of recent technology such as very high resolution of DTMs and remote sensing imagery faces problems related to budget limitation and cloud problem in remote sensing images. Thus, combination techniques are needed to map landslide events either old or recent landslide events.

2.4.2 IMPROVING THE ACCURACY OF LHM METHODS

Generally, the Bi-variate statistical landslide hazard mapping methods is able to quantify the degree of effects of landslide predictive factors on landslide occurrence by comparing the factors with the landslide distribution. However, assigning weightage to the causative factors on the basis of this relationship may not always be appropriate since the interplays among the landslide predictive factors can't be assessed in these methods. Moreover, landslide occurrence is the general consequence of several landslide predictive factors at a time. Therefore, the degree of effects among the landslide predictive factors should also be quantified and such quantification can be performed by the multivariate statistical methods (Guzzetti et al. 2006; Yoshimatsu and Abe 2006; Corominas and Moya 2008; Fell et al. 2008a). Multi-variate statistical analysis for landslide hazard mapping considers relative contribution of each landslide predictive factor to the landslide occurrence (Nandi and Shakoor 2010). The multivariate methods calculate percentage of landslide occurrence for each mapping unit and the probability of landslide occurrence is produced followed by the application of multivariate statistical method for reclassification of hazard for the given area. Logistic regression model and support vector machine methods are commonly used methods for LHZ mapping (Santacana et al. 2003; Süzen and Doyuran 2004; Nandi and

Shakoor 2010). The relative contribution of different factors is not assessed in bivariate statistics. One the other hand, the interactions between the landslide predictive factors are encountered in multivariate analysis. The weights of the factors indicate the relative contribution of each of these factors to the degree of landslide occurrence. Therefore, the question arose that is it possible to improve the landslide hazard mapping using the statistical approaches and how to improve it.

2.4.3 CONSIDERING ASSUMED EARTHQUAKES IN LHM

Earthquake-induced landslides are one of the most damaging hazards in mountainous regions and these triggered landslides will cause serious damages to both human life and properties. Therefore, securing the seismic slope stability for by analysing considering the seismic force is one of the most important parts in earthquake-prone regions. Slope stability analysis is an effective and well-used method to identify the landslide prone slopes, since earthquakes loading can be considered directly in the limit equilibrium. However, how to determine PGA of each mapping unit, such as raster cells, over a large region is still a difficult problem in landslide hazard mapping. To date, most of the physically-based approaches for landslide hazard mapping only consider the effects of the rainfall and few of these approaches consider the earthquake scenarios.

2.4.4 CONSIDERING THE LANDSLIDES AFFECTED AREA IN LHM

As previous stated, landslide hazard mapping should not only identify the landslide-prone slopes, but also assess the potential affected area of the landslides. Estimation of the landslide affected area is a delicate task to since it is very difficult to predict the exact affected area of landslides based on its run out over a large region. Although several numerical simulation techniques existed for accurate landslide runout prediction (Crosta et al. 2003; Peng et al. 2009; Cepeda et al. 2010; Dahl et al. 2013). They are hard to be used at a regional scale due to the uncertainties of the geotechnical parameters and the computation efficiency of these numerical methods. Predicting the landslide runout distance and propagation areas, i.e. the areas potentially under the threat of landslide, is still a challenge. Another

possible way of prediction of landslide affected area is by the empirical or semi-empirical approaches. An empirical method were first developed for very large landslides (Legros 2002; McDougall and Hungr 2004; Rickenmann 2005; McDougall and Hungr 2006) by using the reach angle, which is defined between the line connoting the top of the landslide source and the tip of the final deposition of landslides. This reach angle statistically defined as a power law of the landslide volume. Such a model can be quickly applied to large areas for large or very large landslides. However, such analysis has ignored the topography of the terrains and movement behaviour of the landslide sources. Therefore, a more accurate method that can be used over a large region to simulate the landslide runout is needed.

2.5 CONCLUSIONS

Landslide hazard assessment comprises several terminologies which are used interchangeably and often generates confusion. It includes susceptibility, hazard, and risk. Understanding terminologies in the landslide hazard analysis is important in which allows scientists and engineer quantify landslide hazard in an objective way, reproducible and the result can be compared from one region to another region. There were no general guidelines about the use of these terminologies. In this chapter, we define the landslide hazard as the probability of failure of a slope and its consequence. Also, in this study, landslide hazard mapping refers to the dividing of the terrains into areas and the ranking of these areas according to the degree of potential hazard from landslides.

Landslide hazard mapping is a very important way for landslide hazard mitigation. Landslide is comprehension results of a variety of landslide predictive factors, including the controlling factors and triggering factors and these factors vary significantly from area to area. It is therefore difficult to determine weights for the landslide predictive factor. Determination weights of these factors based on relative importance of landslide causative factors is determined by several landslide hazard mapping methods differently. Statistical methods provide objective methods for determining weights for a given parameter based on their relationships with historical landslide occurrence. Physically-based models do not need long term

landslide data and therefore can also be applicable to the areas with incomplete landslide inventories.

Prepare the necessary landslide event data effectively, improving the accuracy of landslide prone slope identification; determining peak ground acceleration (PGA) in considering earthquake loading and estimating the affected area of a landslide in landslide hazard mapping are among the current issues that remain to be solved, which are also the key issues this research aims to solve.

REFERENCE

Alkhasawne MS, Ngah UKB, Tien TL, Isa NABM (2012) Landslide Susceptibility Hazard Mapping Techniques Review. J Appl Sci 12:802–808. doi: 10.3923/jas.2012.802.808

Armaş I (2012) Weights of evidence method for landslide susceptibility mapping. Prahova Subcarpathians, Romania. Nat Hazards 60:937–950. doi: 10.1007/s11069-011-9879-4

Ayalew L, Yamagishi H (2005) The application of GIS-based logistic regression for landslide susceptibility mapping in the Kakuda-Yahiko Mountains, Central Japan. Geomorphology 65:15–31. doi: 10.1016/j.geomorph.2004.06.010

Bacon L, Aphramor L (2011) Weight science: evaluating the evidence for a paradigm shift. Nutr J 10:9. doi: 10.1186/1475-2891-10-9

Bai SB, Wang J, L?? GN, et al (2010) GIS-based logistic regression for landslide susceptibility mapping of the Zhongxian segment in the Three Gorges area, China. Geomorphology 115:23–31. doi: 10.1016/j.geomorph.2009.09.025

Barbieri G, Cambuli P (2009) The weight of evidence statistical method in landslide susceptibility mapping of the Rio Pardu Valley (Sardinia, Italy). 18th World IMACS Congr. MODSIM09 Int. Congr. Model. Simul. Interfacing Model. Simul. with Math. Comput. Sci. Proc. 2658–2664.

Baum RL, Savage WZ, Godt JW (2008) TRIGRS — A Fortran Program for Transient Rainfall Infiltration and Grid-Based Regional Slope-Stability Analysis, Version 2.0. US Geol Surv Open-File Rep 75. doi: Open-File Report 2008–1159

Bhandary NP, Dahal RK, Timilsina M, Yatabe R (2013) Rainfall event-based

landslide susceptibility zonation mapping. Nat Hazards 69:365–388. doi: 10.1007/s11069-013-0715-x

Blahut J, van Westen CJ, Sterlacchini S (2010) Analysis of landslide inventories for accurate prediction of debris-flow source areas. Geomorphology 119:36–51. doi: 10.1016/j.geomorph.2010.02.017

Carrara a, Guzzetti F, Cardinali M, Reichenbach P (2000) Use of GIS Technology in the Prediction and Monitoring of Landslide Hazard. Nat Hazards 20:117–135. doi: 10.1023/A:1008097111310

Cascini L (2008) Applicability of landslide susceptibility and hazard zoning at different scales. Eng Geol 102:164–177. doi: 10.1016/j.enggeo.2008.03.016

Cepeda J, Chávez JA, Martínez CC (2010) Procedure for the selection of runout model parameters from landslide back-analyses: Application to the Metropolitan Area of San Salvador, El Salvador. Landslides 7:105–116. doi: 10.1007/s10346-010-0197-9

Chien-Yuan C, Tien-Chien C, Fan-Chieh Y, Sheng-Chi L (2005) Analysis of time-varying rainfall infiltration induced landslide. Environ Geol 48:466–479. doi: 10.1007/s00254-005-1289-z

Corominas J, Moya J (2008) A review of assessing landslide frequency for hazard zoning purposes. Eng Geol 102:193–213. doi: 10.1016/j.enggeo.2008.03.018

Crosta GB, Imposimato S, Roddeman DG (2003) Numerical modelling of large landslides stability and runout. Nat Hazards Earth Syst Sci 3:523–538. doi: 10.5194/nhess-3-523-2003

Crozier MJ, Glade T (2012) Landslide Hazard and Risk: Issues, Concepts and Approach. In: Landslide Hazard and Risk. pp 1–39

Dahal RK, Hasegawa S, Nonomura A, et al (2008) GIS-based weights-of-evidence modelling of rainfall-induced landslides in small catchments for landslide susceptibility mapping. Environ Geol 54:311–324. doi: 10.1007/s00254-007-0818-3

Dahl MPJ, Gauer P, Kalsnes BG, et al (2013) Numerical runout simulation of debris avalanches in the Faroe Islands, North Atlantic Ocean. Landslides 10:623–

631. doi: 10.1007/s10346-012-0355-3

Davies T (2014) Landslide Hazards, Risks, and Disasters: Introduction. In: Landslide Hazards, Risks, and Disasters. pp 1–16

Davis LJ, Offord KP (1997) Logistic regression. J Pers Assess 68:497–507. doi: 10.1207/s15327752jpa6803_3

Dietrich WE, Bellugi D, Asua RR de (2001) Validation of the Shallow Landslide Model, SHALSTAB, for forest management. Water Sci Appl 2:195–227. doi: 10.1029/WS002

Dou H qiang, Han T chun, Gong X nan, Zhang J (2014) Probabilistic slope stability analysis considering the variability of hydraulic conductivity under rainfall infiltration-redistribution conditions. Eng Geol 183:1–13. doi: 10.1016/j.enggeo.2014.09.005

Feizizadeh B, Shadman Roodposhti M, Jankowski P, Blaschke T (2014) A GIS-based extended fuzzy multi-criteria evaluation for landslide susceptibility mapping. Comput Geosci 73:208–221. doi: 10.1016/j.cageo.2014.08.001

Fell R (1994) Landslide risk assessment and acceptable risk. Can Geotech J 31:261–272. doi: 10.1139/t94-031

Fell R, Corominas J, Bonnard C, et al (2008a) Guidelines for landslide susceptibility, hazard and risk zoning for land use planning. Eng Geol 102:85–98. doi: 10.1016/j.enggeo.2008.03.022

Fell R, Corominas J, Bonnard C, et al (2008b) Guidelines for landslide susceptibility, hazard and risk zoning for land-use planning. Eng Geol 102:99–111. doi: 10.1016/j.enggeo.2008.03.014

Galli M, Ardizzone F, Cardinali M, et al (2008) Comparing landslide inventory maps. Geomorphology 94:268–289. doi: 10.1016/j.geomorph.2006.09.023

Good IJ (1985) Weight of evidence: A brief survey. Bayesian Stat 2 249–270.

Gortmaker SL, Hosmer DW, Lemeshow S (1994) Applied Logistic Regression. Contemp. Sociol. 23:159.

Guzzetti F, Cardinali M, Reichenbach P, Carrara A (2000) Comparing landslide maps: A case study in the upper Tiber River basin, central Italy. Environ Manage 25:247–263. doi: 10.1007/s002679910020

Guzzetti F, Carrara A, Cardinali M, Reichenbach P (1999) Landslide hazard evaluation: A review of current techniques and their application in a multi-scale study, Central Italy. In: Geomorphology. pp 181–216

Guzzetti F, Mondini AC, Cardinali M, et al (2012) Landslide inventory maps: New tools for an old problem. Earth-Science Rev. 112:42–66.

Guzzetti F, Reichenbach P, Ardizzone F, et al (2006) Estimating the quality of landslide susceptibility models. Geomorphology 81:166–184. doi: 10.1016/j.geomorph.2006.04.007

Harp EL, Keefer DK, Sato HP, Yagi H (2011) Landslide inventories: The essential part of seismic landslide hazard analyses. Eng Geol 122:9–21. doi: 10.1016/j.enggeo.2010.06.013

Hong Y, Adler R, Huffman G (2007) Use of satellite remote sensing data in the mapping of global landslide susceptibility. Nat Hazards 43:245–256. doi: 10.1007/s11069-006-9104-z

HONG Y, ADLER RF (2008) Predicting global landslide spatiotemporal distribution: Integrating landslide susceptibility zoning techniques and real-time satellite rainfall estimates. Int J Sediment Res 23:249–257. doi: 10.1016/S1001-6279(08)60022-0

Howard R a (1966) Information Value Theory. Syst Sci Cybern IEEE Trans 2:22–26. doi: 10.1109/TSSC.1966.300074

Huggel C, Khabarov N, Obersteiner M, Ram??rez JM (2010) Implementation and integrated numerical modeling of a landslide early warning system: A pilot study in Colombia. Nat Hazards 52:501–518. doi: 10.1007/s11069-009-9393-0

Hungr O, Leroueil S, Picarelli L (2014) The Varnes classification of landslide types, an update. Landslides 11:167–194.

Ibsen ML, Casagli N (2004) Rainfall patterns and related landslide incidence in the Porretta-Vergato region, Italy. Landslides 1:143–150. doi: 10.1007/s10346-004-0018-0

Intrieri E, Gigli G, Mugnai F, et al (2012) Design and implementation of a landslide early warning system. Eng Geol 147–148:124–136. doi: 10.1016/j.enggeo.2012.07.017

Kanungo DP, Arora MK, Sarkar S, Gupta RP (2009) Landslide sSusceptibility zonation (LSZ) mapping - a review. J South Asia Disaster Stud 2:81–106.

Kavzoglu T, Sahin EK, Colkesen I (2013) Landslide susceptibility mapping using GIS-based multi-criteria decision analysis, support vector machines, and logistic regression. Landslides 11:425–439. doi: 10.1007/s10346-013-0391-7

Kawabata D, Bandibas J (2009) Landslide susceptibility mapping using geological data, a DEM from ASTER images and an Artificial Neural Network (ANN). Geomorphology 113:97–109. doi: 10.1016/j.geomorph.2009.06.006

Kayastha P, Dhital MR, De Smedt F (2012) Landslide susceptibility mapping using the weight of evidence method in the Tinau watershed, Nepal. Nat Hazards 63:479–498. doi: 10.1007/s11069-012-0163-z

Kayen R, Brandenberg SJ, CoIlins BD, et al (2009) Geoengineering and seismological aspects of the Niigata-Ken Chuetsu-Oki earthquake of 16 July 2007. Earthq Spectra 25:777–802. doi: 10.1193/1.3240397

Keefer DK (1984) Landslides caused by earthquakes. Geol. Soc. Am. Bull. 95:406–421.

Keefer DK (2002) Investigating landslides caused by earthquakes - A historical review. Surv Geophys 23:473–510. doi: 10.1023/A:1021274710840

Kuriakose SL, Devkota S, Rossiter DG, Jetten VG (2009a) Prediction of soil depth using environmental variables in an anthropogenic landscape, a case study in the Western Ghats of Kerala, India. CATENA 79:27–38. doi: 10.1016/j.catena.2009.05.005

Kuriakose SL, Jetten VG, van Westen CJ, et al (2008) Pore Water Pressure as a Trigger of Shallow Landslides in the Western Ghats of Kerala, India: Some Preliminary Observations from an Experimental Catchment. Phys Geogr 29:374–386. doi: 10.2747/0272-3646.29.4.374

Kuriakose SL, van Beek LPH, van Westen CJ (2009b) Parameterizing a physically based shallow landslide model in a data poor region. Earth Surf Process Landforms 34:867–881. doi: 10.1002/esp.1794

Lee S (2007) Application and verification of fuzzy algebraic operators to landslide susceptibility mapping. Environ Geol 52:615–623. doi: 10.1007/s00254-

006-0491-y

Lee S, Choi J (2004) Landslide susceptibility mapping using GIS and the weight-of-evidence model. Int J Geogr Inf Sci 18:789–814. doi: 10.1080/13658810410001702003

Lee S, Choi J, Min K (2002a) Landslide susceptibility analysis and verification using the Bayesian probability model. Environ Geol 43:120–131. doi: 10.1007/s00254-002-0616-x

Lee S, Chwae U, Min K (2002b) Landslide susceptibility mapping by correlation between topography and geological structure: The Janghung area, Korea. Geomorphology 46:149–162. doi: 10.1016/S0169-555X(02)00057-0

Lee S, Hwang J, Park I (2013) Application of data-driven evidential belief functions to landslide susceptibility mapping in Jinbu, Korea. Catena 100:15–30. doi: 10.1016/j.catena.2012.07.014

Lee S, Ryu J-H, Won J-S, Park H-J (2004) Determination and application of the weights for landslide susceptibility mapping using an artificial neural network. Eng Geol 71:289–302. doi: 10.1016/S0013-7952(03)00142-X

Lee S, Sambath T (2006) Landslide susceptibility mapping in the Damrei Romel area, Cambodia using frequency ratio and logistic regression models. Environ Geol 50:847–855. doi: 10.1007/s00254-006-0256-7

Lee S, Talib JA (2005) Probabilistic landslide susceptibility and factor effect analysis. Environ Geol 47:982–990. doi: 10.1007/s00254-005-1228-z

Legros F (2002) The mobility of long-runout landslides. Eng Geol 63:301–331. doi: 10.1016/S0013-7952(01)00090-4

Malamud BD, Turcotte DL, Guzzetti F, Reichenbach P (2004) Landslides, earthquakes, and erosion. Earth Planet Sci Lett 229:45–59. doi: 10.1016/j.epsl.2004.10.018

Mancini F, Ceppi C, Ritrovato G (2010) GIS and statistical analysis for landslide susceptibility mapping in the Daunia area, Italy. Nat Hazards Earth Syst Sci 10:1851–1864. doi: 10.5194/nhess-10-1851-2010

McDougall S, Hungr O (2006) Towards landslide runout prediction using the dynamic model DAN3D. In: European Geoscience Union.

McDougall S, Hungr O (2004) A model for the analysis of rapid landslide motion across three-dimensional terrain. Can Geotech J 41:1084–1097. doi: 10.1139/t04-052

Menon S, Bawa KS (1997) Applications of geographic information systems, remote-sensing, and a landscape ecology approach to biodiversity conservation in the Western Ghats. Curr Sci 73:134–145. doi: 10.1017/CBO9781107415324.004

Montrasio L, Valentino R, Losi GL (2011) Towards a real-time susceptibility assessment of rainfall-induced shallow landslides on a regional scale. Nat Hazards Earth Syst Sci 11:1927–1947. doi: 10.5194/nhess-11-1927-2011

Nandi A, Shakoor A (2010) A GIS-based landslide susceptibility evaluation using bivariate and multivariate statistical analyses. Eng Geol 110:11–20. doi: 10.1016/j.enggeo.2009.10.001

Oh HJ, Pradhan B (2011) Application of a neuro-fuzzy model to landslide-susceptibility mapping for shallow landslides in a tropical hilly area. Comput Geosci 37:1264–1276. doi: 10.1016/j.cageo.2010.10.012

Pack RT (2001) Assessing Terrain Stability in a GIS using SINMAP. 15th Annu GIS Conf GIS 2001 9.

Park DW, Nikhil N V., Lee SR (2013) Landslide and debris flow susceptibility zonation using TRIGRS for the 2011 Seoul landslide event. Nat Hazards Earth Syst Sci 13:2833–2849. doi: 10.5194/nhess-13-2833-2013

Peng WF, Wang CL, Chen ST, Lee ST (2009) Incorporating the effects of topographic amplification and sliding areas in the modeling of earthquake-induced landslide hazards, using the cumulative displacement method. Comput Geosci 35:946–966. doi: 10.1016/j.cageo.2008.09.007

Pradhan B, Lee S (2010) Landslide susceptibility assessment and factor effect analysis: backpropagation artificial neural networks and their comparison with frequency ratio and bivariate logistic regression modelling. Environ Model Softw 25:747–759. doi: 10.1016/j.envsoft.2009.10.016

Pradhan B, Lee S, Buchroithner MF (2010a) A GIS-based back-propagation neural network model and its cross-application and validation for landslide susceptibility analyses. Comput Environ Urban Syst 34:216–235. doi:

10.1016/j.compenvurbsys.2009.12.004

Pradhan B, Oh H-J, Buchroithner M (2010b) Weights-of-evidence model applied to landslide susceptibility mapping in a tropical hilly area. Geomatics, Nat Hazards Risk 1:199–223. doi: 10.1080/19475705.2010.498151

Pradhan B, Sezer EA, Gokceoglu C, Buchroithner MF (2010c) Landslide susceptibility mapping by neuro-fuzzy approach in a landslide-prone area (Cameron Highlands, Malaysia). IEEE Trans Geosci Remote Sens 48:4164–4177. doi: 10.1109/TGRS.2010.2050328

Regmi NR, Giardino JR, Vitek JD (2010) Modeling susceptibility to landslides using the weight of evidence approach: Western Colorado, USA. Geomorphology 115:172–187. doi: 10.1016/j.geomorph.2009.10.002

Rickenmann D (2005) Runout prediction methods. Debris-flow hazards Relat Phenom 305–324.

Salciarini D, Godt JW, Savage WZ, et al (2006) Modeling regional initiation of rainfall-induced shallow landslides in the eastern Umbria Region of central Italy. Landslides 3:181–194. doi: 10.1007/s10346-006-0037-0

Santacana N, Baeza B, Corominas J, et al (2003) A GIS-based multivariate statistical analysis for shallow landslide susceptibility mapping in La Pobla de Lillet Area (Eastern Pyrenees, Spain). Nat Hazards 30:281–295. doi: 10.1023/B:NHAZ.0000007169.28860.80

Sarkar S, Roy AK, Martha TR (2013) Landslide susceptibility assessment using Information Value Method in parts of the Darjeeling Himalayas. J Geol Soc India 82:351–362. doi: 10.1007/s12594-013-0162-z

Sassa K, Fukuoka H, Wang F, Wang G (2007) Progress in landslide science.

Sassa K, 佐々恭二 (1997) International Symposium on Landslide Hazard Assessment, Xian, China 13-16 July 1997. WGL/RLM

Sezer EA, Pradhan B, Gokceoglu C (2011) Manifestation of an adaptive neuro-fuzzy model on landslide susceptibility mapping: Klang valley, Malaysia. Expert Syst Appl 38:8208–8219. doi: 10.1016/j.eswa.2010.12.167

Süzen ML, Doyuran V (2004) A comparison of the GIS based landslide susceptibility assessment methods: Multivariate versus bivariate. Environ Geol

45:665–679. doi: 10.1007/s00254-003-0917-8

Van Den Eeckhaut M, Hervás J, Jaedicke C, et al (2012) Statistical modelling of Europe-wide landslide susceptibility using limited landslide inventory data. Landslides 9:357–369. doi: 10.1007/s10346-011-0299-z

Van Westen CJ, Rengers N, Soeters R (2003) Use of geomorphological information in indirect landslide susceptibility assessment. Nat Hazards 30:399–419. doi: 10.1023/B:NHAZ.0000007097.42735.9e

Van Westen CJ, Seijmonsbergen AC, Mantovani F (1999) Comparing Landslide Hazard Maps. Nat Hazards 20:137–158. doi: 10.1023/A:1008036810401

Vapnik VN (1995) The Nature of Statistical Learning Theory.

Vapnik VN (1999) An overview of statistical learning theory. IEEE Trans Neural Netw 10:988–99. doi: 10.1109/72.788640

Varnes DJ (1984) Landslide hazard zonation: a review of principles and practice. Nat. Hazards 5:63.

Vijith H, Krishnakumar KN, Pradeep GS, et al (2013) Shallow landslide initiation susceptibility mapping by GIS-based weights-of-evidence analysis of multi-class spatial data-sets: a case study from the natural sloping terrain of Western Ghats, India. Georisk Assess Manag Risk Eng Syst Geohazards 8:48–62. doi: 10.1080/17499518.2013.843437

Vranken L, Vantilt G, Van Den Eeckhaut M, et al (2014) Landslide risk assessment in a densely populated hilly area. Landslides 12:787–798. doi: 10.1007/s10346-014-0506-9

Wang HB, Liu GJ, Xu WY, Wang GH (2005) GIS-based landslide hazard assessment: an overview. Prog Phys Geogr 29:548–567. doi: 10.1191/0309133305pp462ra

Wing RR, Phelan S (2005) Long-term weight loss maintenance. Am. J. Clin. Nutr. 82:

Wu CH, Chen SC (2009) Determining landslide susceptibility in Central Taiwan from rainfall and six site factors using the analytical hierarchy process method. Geomorphology 112:190–204. doi: 10.1016/j.geomorph.2009.06.002

Xu C, Dai F, Xu X, Lee YH (2012) GIS-based support vector machine

modeling of earthquake-triggered landslide susceptibility in the Jianjiang River watershed, China. Geomorphology 145–146:70–80. doi: 10.1016/j.geomorph.2011.12.040

Yalcin A (2008) GIS-based landslide susceptibility mapping using analytical hierarchy process and bivariate statistics in Ardesen (Turkey): Comparisons of results and confirmations. Catena 72:1–12. doi: 10.1016/j.catena.2007.01.003

Yesilnacar E, Topal T (2005) Landslide susceptibility mapping: A comparison of logistic regression and neural networks methods in a medium scale study, Hendek region (Turkey). Eng Geol 79:251–266. doi: 10.1016/j.enggeo.2005.02.002

Yoshimatsu H, Abe S (2006) A review of landslide hazards in Japan and assessment of their susceptibility using an analytical hierarchic process (AHP) method. Landslides 3:149–158.

Zêzere JL (2002) Landslide susceptibility assessment considering landslide typology. A case study in the area north of Lisbon (Portugal). Nat Hazards Earth Syst Sci 2:73–82. doi: 10.5194/nhess-2-73-2002

Zhou S, Fang L (2015) Support vector machine modeling of earthquake-induced landslides susceptibility in central part of Sichuan province, China. Geoenvironmental Disasters 2:1–12. doi: 10.1186/s40677-014-0006-1

Zhou S, Fang L, Liu B (2015) Slope unit-based distribution analysis of landslides triggered by the April 20, 2013, Ms 7.0 Lushan earthquake. Arab J Geosci 8:7855–7868. doi: 10.1007/s12517-015-1835-2

Zhou, S., Chen, G., & Fang, L. (2016). Distribution Pattern of Landslides Triggered by the 2014 Ludian Earthquake of China: Implications for Regional Threshold Topography and the Seismogenic Fault Identification. ISPRS International Journal of Geo-Information, 5(4), 46.

Zhou, S., Chen, G., Fang, L., & Nie, Y. (2016). GIS-Based Integration of Subjective and Objective Weighting Methods for Regional Landslides Susceptibility Mapping. Sustainability, 8(4), 334.

Zhou, S., Chen, G., Liu B., & Fang, L. (2016). A Combined Weight of Evidence and Logistic Regression Method for Susceptibility Mapping of

Earthquake‐induced Landslides: A Case Study of the April 20, 2013 Lushan Earthquake, China. Acta Geologica Sinica (English Edition), 90(2), 511-524.

CHAPTER 3

3 DEVELOPMENT OF GEOLHM-S FOR LANDSLIDE HAZARD MAPPING USING FOUR STATISTICAL METHODS AND FOUR COMBINED METHODS

3.1 INTRODUCTION

Landslides are considered to be the most widely geological disasters, causing deaths and damage to the properties. As previous stated in Chapter 2, during the last decades, the implementation of statistical methods in GIS has been widely applied in landslide hazard mapping. Although the statistical LHM methods have been widely used and successfully validated in many areas as mentioned in the published research literatures, there is no such a tool for effectively perform LHM using statistical approaches. Therefore, in this chapter, we aim to develop a functional module GeoLHM-S. At first, a method for landslide inventory mapping using online high-resolution images is proposed. The new method is incorporated into the functional module GeoLHM-S. And then, the four widely-used statistical methods: Information Value(IV), Weight of Evidence(WoE), Logistic Regression(LR), and Support Vector Machine(SVM), are incorporated into the functional module GeoLHM-S, which makes it possible to perform the LHM using different methods simultaneously. After that, four new methods are proposed by combining one of IV and WoE methods with one of the LR and SVM methods to increase the landslide hazard mapping performance. Finally, the developed GeoLHM-S is used to make landslide hazard maps by using the four widely-used methods and the newly

proposed combined method for the 2013 Lushan Earthquake event in China.

3.2 STUDY AREA

On April 20, 2013, a series of powerful earthquakes hit the central part of Sichuan province, China, especially Lushan County, about 116 km from Chengdu along the Longmenshan fault in the same province heavily impacted by the 2008 Sichuan earthquake. The main shock of this earthquake was Ms=7.0 according to China Earthquake Data Center (CEDC) or Mw=6.6 as measured by the United States Geological Survey (USGS). The epicenter of the main shock was monitored at 30.3°N, 103.0°E near Lushan County at a depth of 13 km along the south segment of Longmenshan thrust belt. Many aftershocks including some Ms=6.0 class event included. This earthquake was another destructive earthquake in Sichuan Province 5 years after the 2008 Wenchuan earthquake (Figure 3-1).

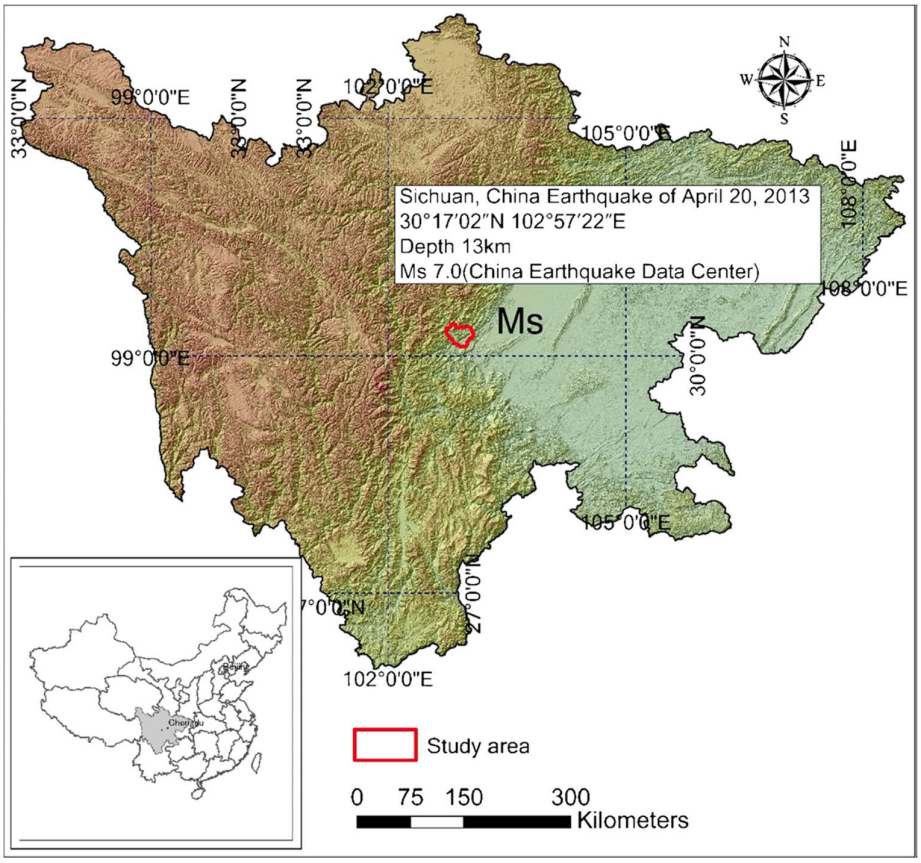

Figure 3-1 Hillshade image showing the location of the study area in red polygons. (Zhou and Fang, 2015)

The study area is celebrated for its active tectonization with many folds and active faults. Main faults affected by the earthquake in the area, as shown in Figure 3-2, are thrust faults, such as Shuangshi–Dachuan fault (SDF), Dayi fault (DF), and Western Shangli fault (WSF) (Xu et al. 2013b). Despite the shallow activity of the present earthquake, no obvious surface rupture had been recognized in the aftershock area (Chen et al.2013a). With the understanding of the aftershocks distribution, focal mechanism solution, and surface structural geology, Xu et al. (2013b) pointed that the Lushan earthquake is a typical blind reverse fault event.

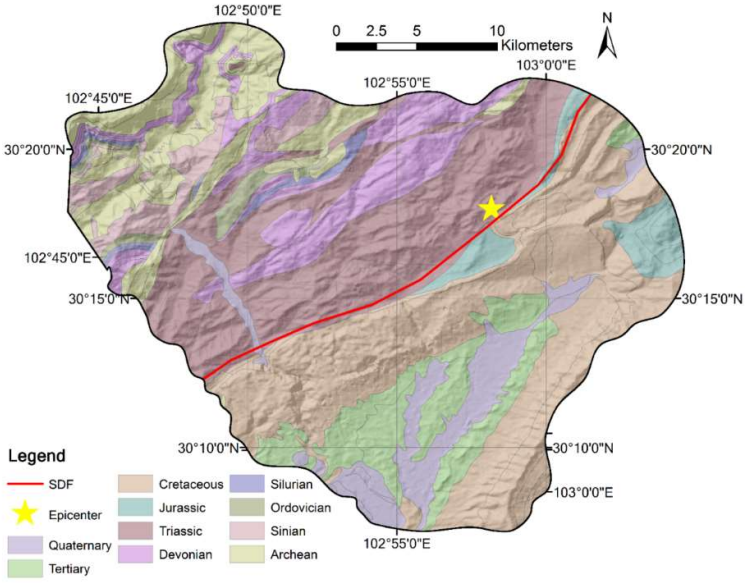

Figure 3-2 Geological map of the study area (Zhou and Fang, 2015)

The exposure of the strata unit in the area ranged from the pre-Paleozoic to Quaternary periods and was dominated by Cretaceous and Triassic (Figure 3-2). Sandstone, mudstone, and shale were main rock types in the study area. As a result of the abundant supply of rainfall and the local rich groundwater, almost all bedrocks found in the study area had undergone a certain degree of weathering and deforming. In many slopes, weathering has penetrated deep into rock masses through joints and bedding planes. Topographically, as located in the north-eastern

boundary of the Tibet plateau, the study area ranged from plain in the east to hilly and mountainous with steep and rugged slopes in the west. Land use types include mainly cropland distributed on the ridges and slope wasteland on side slopes and gullies and town in flat river valleys. Most of the study area has gradients between 10 and 30°, with an average gradient of 5°in the eastern part of the study area and valleys and a much higher average gradient of more than 30° in the west. The study area had suffered serious shallow landslides during this earthquake, since the steep slopes and jagged ridges are susceptible to landslide while suffering heavy ground shaking.

Table 3-1 Geology unit and main rock types in the study area (Zhou and Fang, 2015)

Age	Lithology
Quaternary	Alluvium, clay, loose deposit
Tertiary	Marl, sometimes intercalated with mudstone
Cretaceous	Marl, siltstone, conglomerate, sandstone
Jurassic	Sandy slate, mudstone, sandy stone intercalated with mudstone
Triassic	Sandy stone, limestone, slate
Devonian	mudstone, sandstone, carbonatite
Silurian	Sandstone, phyllite intercalated with limestone
Ordovician	Limestone, marble and phyllite
Sinian	Metamorphic sandstone, dolomite
Archean	Granite, diorite, gabbro

3.3 LANDSLIDE INVENTORY MAPPING

A landslide inventory map usually portrays the location and the date of occurrence and the type of landslides, as well as the surface geometry of landslides. Landslide inventory maps can be produced using different techniques with a dependence of the aims, the extent of the study area, the availability, resolution, and characteristics of imagery (e.g., satellite image, aerial photograph). A landslide event inventory map may show all the slope failures as the result of a single trigger, such as an earthquake, a rainstorm, or a rapid snowmelt (inventories), or they can show the cumulative effects of many landslide events over a long period (historical inventories).

Compiling of a detail and comprehensive landslide inventory is the prerequisite for subsequent studies, such as distribution analysis, hazard assessment,

and regional topographic evolution research. Landslide inventory maps can be produced using different techniques such as field investigation, digitalization of historic landslide inventory, visual interpretation of aerial photos, computer-aided supervised or unsupervised interpretation of remote sensing images. Although field investigation provides more detailed and intuitive information of landslides, the significant shortcoming of this method is that landslides occurred in the inaccessible areas will be missed, especially in some mountainous areas. In contrast, the photo interpretation method greatly enhanced the efficiency of landslide inventory preparation and had become popular since the 1970s. In the last two decades, with the increasing availability of high and very-high resolution sensors, development of computer hardware and remote sensing (RS) technologies, use of satellite images and RS technologies for landslide investigations had increased significantly. Many detailed and comprehensive inventories of earthquake-induced landslides have been reported, which had provided a good basis for landslide hazard evaluation and mitigation. Currently, studies on automatic extraction of landslides through remote-sensing images became important topics in engineering, geology and other related fields. This method depended heavily on image resolution and models and was very suitable for large-scale landslides mapping. However, it might cause errors when applied for small landslides. Hence, visual-interpretation by well-trained personnel is still believed to be more accurate and reliable than computers, although it is more time-consuming. Results' quality of such visual interpretation method largely depended upon the experience of the interpreters. A better way to minimize the subjectivity of visual interpretation is to carry out some field investigations for validation.

3.3.1 DATA SOURCE

Colour airborne images with a high resolution of 0.16 m and pre-earthquake SPOT-4 satellite images with a median resolution of 12.5 m covering the study area were proposed by the National Administration of Surveying, Mapping and Geo-information of China. Locations of landslides triggered by the devastating earthquake were manually interpreted by Sichuan Geomantic Center, and an

inventory map of landslides was proposed on Geo-Information Platform of Lushan Earthquake (http://www.scgis.net/LSXEarthquake/) based on Tianditu, a WebGIS service (Chen et al. 2013b). Due to a critical use for rescue after the earthquake, only location data of suspected landslides were available, and some of landslides that did not cause damage to humans, constructions, or transportations were missed on the platform. This given landslide inventory map only pointed out the location of landslide without any other information, which is essential for our research, and it was impossible to carry out detailed field investigations on every landslide.

3.3.2 PROPOSED METHODS FOR LANDSLIDE INVENTORY MAPPING

In this paper, we proposed a detailed landslide inventory map, which shows the geometry of landslides, with the help of ArcGIS servers. Since ArcGIS 10.0 is capable of using any ArcGIS server cached map service as a base map, we firstly specified the high-resolution image as our base map using ArcGIS server with the endpoint URL (http://www.scgis.net.cn/imap/iMapServer/defaultRest/services/) provided by Tianditu as the address for invoking image service. Then, an empty vector layer named 'Landslide' with the same coordinate system as the base map was created as a mask to store the landslide information, and imaginary layers of Tianditu Polymerized DOM Tile Map service were selected and added below the landslide layer. After that, high-resolution pre-earthquake satellite images of SPOT-4 and Radarsat-2 of the study area were added in to ArcGIS and geometrically rectified and matched as a contrast. Finally, experts on earthquakes and geo-hazards were called upon to visually interpret the base map and delineated the landslide scars on aerial photograph according to vegetation variations between pre- and post-earthquake, experts' knowledge and experience (Zhou and Fang, 2015).

3.3.3 CRITERIA USED IN LANDSLIDE VISUAL INTERPRETATION

In this study, we followed several principles for the landslide visual interpretation: (i) all landslides that can be recognized in the images should be mapped; (ii) Both landslide boundaries and the positions of landslide source area should be mapped; (iii) Landslide complexes should be divided into individual ones;

and (iv) Landslides happened before the earthquake should be excluded. Based on principles above, following criteria were used during the landslide visual interpretation processes:(i) If a landslide did not exist on the pre-earthquake image but exists on post-earthquake images, it is considered as a co-seismic landslide; (ii) If a landslide exists on both pre- and post-earthquake images and shows the same morphology and texture, it is considered a pre-earthquake landslide not triggered by the earthquake.

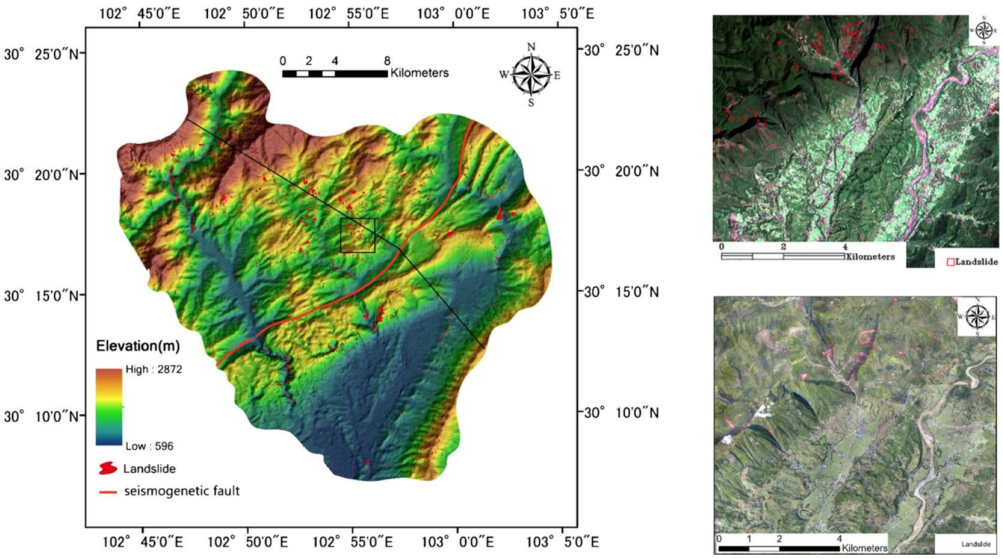

Figure 3-3 Distribution of interpreted landslides in the study area. a Landslides were indicated using red polygons on shaded relief map. Sample area of b pre-earthquake SPOT-4 image and c post-earthquake aerial photographs were indicated in black rectangle in a . (Zhou and Fang, 2015)

3.3.4 RESULTS AND DISCUSSIONS

By using the proposed method, an inventory of 1289 landslides triggered by the 2013 Lushan earthquake were visually mapped. This landslide inventory is intended to provide users with a first-hand information regarding earthquake-induced landslides within the study area and can be used to a series of studies, such as evaluation of landslide disasters and regional hazard mitigations in this area.

The proposed landslide inventory is not regulatory, and revisions can happen when new information regarding landslides is found or future (new) landslides

occur. Therefore, it is possible that landslides within the mapping area were not identified or occurred after the map was produced. Therefore, a continuous update of the landslide inventory is suggested with the increasing availability of data sources both in area and time scale.

Another limitation of the proposed method is that few information about the landslide type is included in the proposed landslide inventory. Landslide is a general term used to describe the downslope movement of soil, rock under the effects of gravity and can be classified according to types of movement (fall, topple, slide spread or flow) and materials involved (soil, rock or both). Landslide may also form a complex failure encompassing more than one type of movement. On the basis of type of material involved, type of movement, degree of internal disruption of the landslide mass, and geologic environment, Keefer (1984) classified earthquake-induced landslides into three categories and described them as: (I) Disrupted slides and falls: rock falls, rock slides, rock avalanches, soil falls, disrupted soil slides, and soil avalanches; (II) coherent slides: rock slumps, rock block slides, soil slumps, soil block slides, and slow earth flows; and (III) lateral spreads and flows: soil lateral spreads, rapid soil flows, and subaqueous landslides. Following previous classification criterion and in combination of our analysis results and field investigations, landslides triggered by the Ludian earthquake can be categorized as: (I) rock and soil falls; (II) rock avalanches and (III) shallow landslides. For simplicity's sake, we use landslide as a general term for all types of material downslope movement. It is difficult to distinguish the landslide types accurately on the images, since it only shows the 2D information of the landslide information. In recent years, with the increasing availability of images of more accuracy, such as the Lidar and SAR images, a more detailed landslide inventory mapping can be obtained

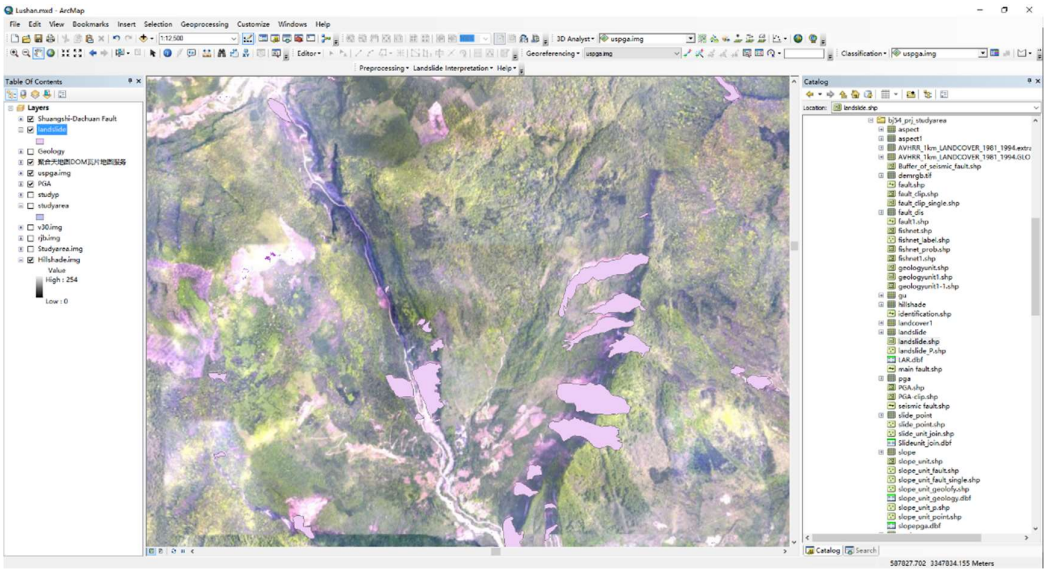

Figure 3-4 Screenshot show the ArcGIS plugin tool for landslide inventory mapping using online high-resolution image (landslides are shown in red polygons)

The interpretation procedures including the following 5 steps: (I) Acquisition and pre-process of images of the study area, including system calibration, ortho-rectification, geometric correction, and image fusion; (II) The geometrically corrected fusion images were then imported into ArcGIS 9.3 software and were specified as the based map; (III) An empty vector layer with the same coordinate system as the base map was created for the storage of landslides; (IV) High-resolution pre-event satellite images of the study area were geometrically rectified and matched as a contrast showing the pre-earthquake conditions; (V) Experts in earthquakes and geo-hazards were called upon to visually interpret the base map according to their experiences and knowledge. Because it was right time for vegetation, earthquake-induced landslides could be easily recognized according to landslide scars and vegetation change; (VI) The boundaries of landslides were interpreted on the base map and transformed into vector format.

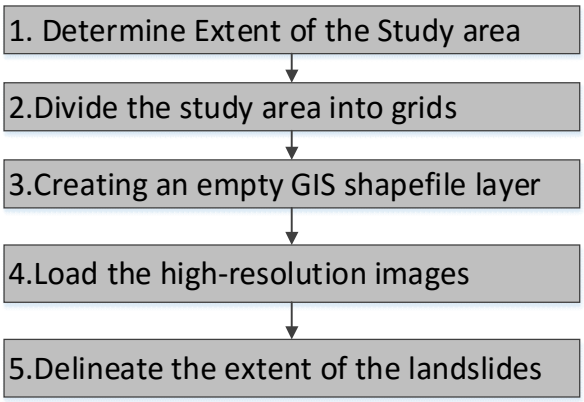

Figure 3-5 Flowchart of the proposed landslide inventory mapping methods

Due to long-term human activity, many parts of the natural vegetation have been replaced by farming. Because it is right time for plantation, earthquake-induced landslides are easy to be recognized according to landslide scars on aerial photos (Figure 3-3 b and c).

3.4 COMPARISON STUDY OF FOUR STATISTICAL METHODS

3.4.1 INFORMATION VALUE METHOD (IV)

The Information value (IV) method is based on the assumptions that landslide occurrences are determined by causal factors and that future landslides will occur under the same condition as those contributing to past landslides. The IV model requires the selection of landslide predictive factors and the categorization of these factors. The information value of area where landslides occurred in the total study area, and also is the probability of a landslide occurrence to a non-occurrence for a given attribute. Based on that, the landslide inventory is overlaid with each predictive factor map, and frequency ratio values of each class get calculated. In this study, the frequency ratio is calculated in the following three steps: Firstly, the information value for each class of factor was calculated using Eq.(3-1). Then information values were summed to calculate the landslide hazard index. The weight value for each class of factor can be defined as the information values and then they were summed to produce the landslide hazard index (LHI) map Eq.(3-2).

The calculated values of LHI for each pixel in the LHI indicate the relative susceptibility to landslide occurrence.

$$w_i^j = ln \frac{N_{pix}(s_i)/N_{pix}(N_i)}{\sum N_{pix}(s_i) / \sum N_{pix}(N_i)} \quad (3\text{-}1)$$

$$LHI^{(x,y)} = \sum_{j=1}^{n} w_{i(x,y)}^j \quad (3\text{-}2)$$

Where $N_{pix}(S_i)$ is the number of pixels containing landslide in class j of factor i; $N_{pix}(N_i)$ is the total number of pixels of class j in factor i. x and y indicates the spatial location of the cells.

The results obtained by the IV are easy to understand. A positive value of w_i^j indicates a favourable effects of the subclasses with a certain factor, and a negative value indicates an unfavourable effect. The higher the final LHI is, the higher the possibility of the landslide occurrence is.

3.4.2 WEIGHT OF EVIDENCE METHOD (WOE)

Weights of Evidence (WoE) is based on the log-linear from of Bayesian probabilities modeling to calculate the strength of the spatial association between a training set (e.g., known landslides) and predictor maps (e.g., predictive factors) and to assign predictive factors weights. This method was originally introduced for mineral potential mapping(Bonham-Carter et al., 1989;Agterberg et al., 1993), and many approaches have been proposed on landslide susceptibility mapping (Xu et al., 2012b;Rezaei Moghaddam et al., 2007;Pradhan et al., 2010;Dahal et al., 2008). A detailed description of the mathematical formulation of this modeling is available in (Van Westen et al., 2003) and more recently in (Dahal et al., 2008).

In WoE modelling, weight is calculated for each class of landslide predictive factors (B_j^i) based on the presence or absence of landslides (L) within the area, assuming that future landslides will happen under the same conditions as those contributing to the past landslides. As indicated in (Bonham-Carter et al., 1989):

$$\begin{cases} w_j^{i+} = \ln(P\{B_j^i|L\}/P\{B_j^i|\overline{L}\}) \\ w_j^{i-} = \ln(P\left\{\overline{B_j^i}\middle|L\right\}/P\left\{\overline{B_j^i}\middle|\overline{L}\right\}) \end{cases} \quad (3\text{-}3)$$

Where P is the probability, B_j^i is the presence of class i of landslide causal factor j, while $\overline{B_j^i}$ is the absence of class i of landslide causal factor i. Similarly, L and $\overline{\text{L}}$ represent the presence and absence of landslides respectively. w_j^{i+} and w_j^{i-} are the weight of evidence when the class i of predictive factor j is present and absent respectively. A positive weight w_j^{i+} indicates the presence of positive spatial association between B_j^i and L while the magnitude of this weight indicates the positive correlation between the presence of the predictive factor and the landslides. A negative weight w_j^{i-} indicates an absence of the spatial association between B_j^i and L, and the magnitude shows the level of negative correlation.

The contrast between the two weights is defined, as the final weights of factor B_j^i can be expressed as follows:

$$w_j^i = w_j^{i+} - w_j^{i-} \quad (3\text{-}4)$$

Where a positive w_j^i indicates the predictive class is favourable for the landslides, and a negative w_j^i means the class is unfavourable for the landslides. The magnitude of the contrast indicates an overall of spatial association between the causative factor and landslides; whereas w_j^i is equal to zero when a class has no spatial relationship with landslides occurrence.

The total value of cell at spatial location of x and y in weight of evidence map is determined by the total of weight contrast of landslide predictive factor j in class i as follows:

$$P_{total}^{(x,y)} = \sum_{j=1}^{n} w_j^i\,(x,y) \quad (3\text{-}5)$$

Where n is the total number of landslide predictive factors.

For weight of evidence modeling, landslide training data layers were compared with every thematic layer respectively for the calculation of positive weights and negative weights. For this purpose, Eq. 3 was rewritten according to the number of cells Dahal et al. (2008) (see Eq.5) and the final results were given in Table3.

$$\begin{cases} w_j^{i+} = ln\dfrac{N_j^{i1}/(N_j^{i1}+N_j^{i2})}{N_j^{i3}/(N_j^{i3}+N_j^{i4})} \\ w_j^{i-} = ln\dfrac{N_j^{i2}/(N_j^{i1}+N_j^{i2})}{N_j^{i4}/(N_j^{i3}+N_j^{i4})} \end{cases} \tag{3-6}$$

Where N_j^{i1} is the number of pixels representing the presence of both class i of predictive factor j and landslides; N_j^{i2} is the number of pixels representing the presence of landslides and absence of class i of predictive factor j; N_j^{i3} is the number of pixels representing the presence of class i of predictive factor j and absence of landslides; N_j^{i4} is the number of pixels representing the absence of both class i and landslides.

3.4.3 LOGISTIC REGRESSION METHOD (LR)

Logistic regression (LR) model regresses a dichotomous variable on a set of independent, continuous or categorical variables. The association between the dependent variables (e.g., causal factors) and the independent variable (e.g., presence/ absence of landslides) was tested by using the maximum likelihood model. The LR model has no requirement for the distribution pattern of the independent variables and most of landslide causal factors don't follow normal distribution. The output values of LR model ranging from 0 to 1 can be defined as landslide susceptibility index, with 0 indicating a 0% possibility of landslide occurrence and 1 indicating a 100% possibility of landslide. Therefore, a logistic regression model is applied to create landslide hazard map. The main formula in the logistic regression can be expressed as follows:

$$\mathrm{z} = b_0 + b_1x_1 + b_2x_2 + \cdots + b_nx_n \tag{3-7}$$

$$P = e^z/(1 + e^z) \quad (3\text{-}8)$$

Where P is the probability of landslide occurrence, z is the linear logistic model, b_0 is the intercept of the model, n is the number of landslide predictive factors, b is the weight of each factor, $x_1, x_2, \dots, x_n$ represent the landslide predictive factors.

3.4.4 SUPPORT VECTOR MACHINE METHOD (SVM)

Support vector machine (SVM), as the representative's kernel-based techniques, is a major development in machine learning algorithms. SVM is a group of supervised learning methods based on the statistical learning theory and the Vapnik-Chervonenkis (VC) dimension introduced by V Vapnik and Cortes, (1995) and Chervonenkis, (2013) that can be applied to pattern classification or non-linear regression. For the linear separable condition, consider a set of training vectors with two classes as follows:

$$D = \{(x_1, y_1), (x_2, y_2), \dots, (x_n, y_n)\} \quad (3\text{-}9)$$

Where $x_i \in X \subset R^m, y_i \in \{1, -1\}, i = 1,2, \dots, n$ that can be separated the two classes [1, -1] by a hyper-plane:

$$(w \cdot x) + b = 0, w \in R^N, b \in R \quad (3\text{-}10)$$

Where w is the normal of the hyper-plane, b is a scalar base, and (·) denotes the scalar product operation.

After normalization, the geometrical margin between the two groups can be expressed as $\frac{2}{||w||}$, The operation of the SVM algorithm is to find the hyper-plane that gives the largest geometrical margin to the training examples. The maximum $\frac{2}{||w||}$ can be expressed as:

$$Minimize \ \frac{1}{2}||w||^2 \quad (3\text{-}11)$$

Subjecting to constrains:

$$y_i = (w^T x_i + b) \geq 1, \quad i = 1,2,\dots,n \tag{3-12}$$

Introducing the Lagrangian multiplier, the cost function can be defined as:

$$\phi(w,b,\alpha) = \frac{1}{2}||w||^2 - \sum_{i=1}^{n} \alpha_i (y_i[w \cdot x_i + b] - 1) \tag{3-13}$$

Where $\alpha = (\alpha_1, \alpha_2, \dots, \alpha_n)^T \in R^n$ is the Lagrangian multiplier, and the problem can be solved by dual minimization of Eq.(3-13), with respect to w and b through standard procedures (Eq.(3-14)). More detail of SVM was discussed in[V N Vapnik, 1995].

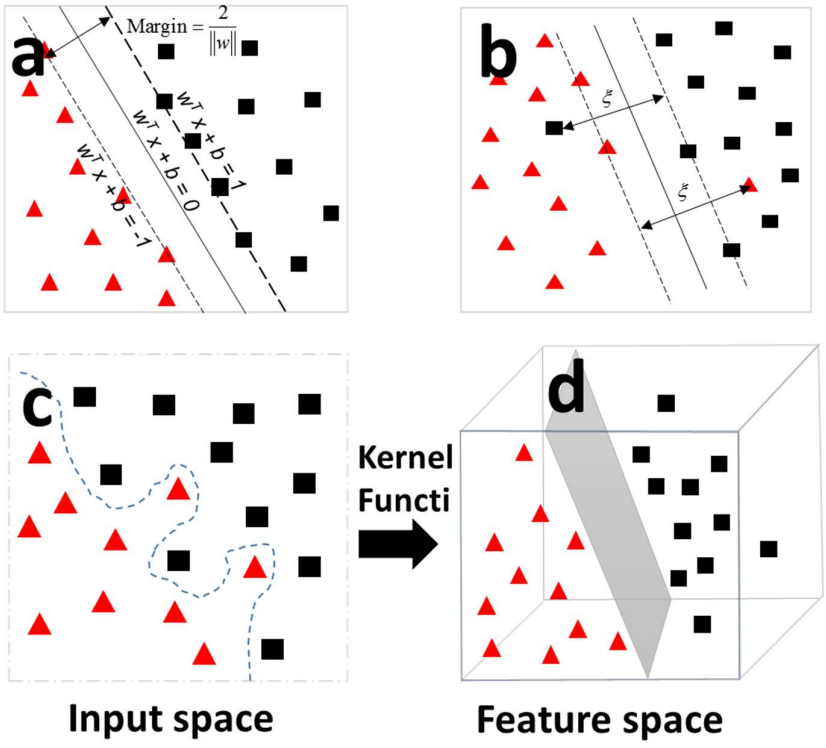

Figure 3-6 Illustration of the support vector machine

$$\begin{cases} \nabla_b \phi(w,b;\alpha) = 0 \\ \nabla_w \phi(w,b;\alpha) = 0 \end{cases} \tag{3-14}$$

Mostly, however, the training vectors are non-separable,[V N Vapnik, 1995]

introduced an slack variables ζ_i modified the constraints as follows:

$$y_i = \big((\mathrm{w} \cdot \mathrm{x}) + \mathrm{b}\big) \geq 1 - \zeta_i, i = 1,2, \dots, n, \zeta_i \geq 0 \qquad (3\text{-}15)$$

To avoid a high value of ζ_i, some kind of penalty term C was introduced into the original optimization Equation 3.16, which can be modified as:

$$Minimize \ \ \frac{1}{2}||w||^2 + C\sum_{i=1}^{n}\zeta_i \qquad (3\text{-}16)$$

Where $\mathrm{C} > 0$ is the penalty factor to control the trade-off between the maximum margin and the minimum error. Additionally, a kernel function $\mathrm{k}(x_i, x_j)$ is introduced by V N Vapnik (1995) to transform the originally non-linear data pattern to a linear one in higher dimensional feature space.

In reality, the unstable slope cases (with landslides) are recognized as positive pattern, while stable slope cases (without landslides) are recognized as negative pattern. Note that we often commonly have only a one-class dataset without negative data. One-class SVM models also have been developed, but their theories are not reach perfection and they produce poor prediction efficiency than two-class SVM (Guo et al., 2005; Yao et al., 2008). Hence, a two-class SVM modelling is utilized in this study.

To carry out the two-class SVM modelling, we established a spatial database containing all the landslides triggered by the earthquake and their controlling parameters. Then all the data layers were classified and rasterized in Arcgis. The landslides as well as the same amount of selected stable slopes were randomly divided into two groups for training and validation purpose, respectively. We use the training dataset as input to train the SVM model, then the testing dataset were used to examine the model. Finally, all the cells in the study area were input into the established model for possibility prediction of landslide occurrence.

3.5 INCREASING LANDSLIDE HAZARD MAPPING PERFORMANCE BY

3.5.1 DATA PREPARATION OF LANDSLIDE PREDICTIVE FACTORS

3.5.1.1 Landslide Predictive factors

The occurrence of landslides is considered to be related to a series of geological, hydrological, topographic factors, which reflects natural settings in the study area. All the factors mentioned above is so called the landslide predictive factors in this study. Collecting and preparation of the landslide predictive factors at a suitable scale is an intriguing task, requires a comprehensive understanding of the importance of each predictive factor. Generally speaking, there is no general rules for selecting the landslide predictive factors, and the factors used in landslide hazard mapping is generally determined by the data availability and the knowledge of the person who perform the landslide hazard mapping. In this study, a topographic-related dataset, a hydrology-related dataset, a geology dataset, a land use dataset and a triggering factor dataset were constructed for landslide hazard mapping (Table 3-2). Based on these datasets, 11 landslide predictive factors were used in this study. Each controlling factor of landslide was mapped and converted to raster map with 30- meter cell size.

Table 3-2 Sources and significance of the landslide controlling factors

Data Type	Factors	Source	Significance	Type
Topographic	1. Elevation	Topographic Map	Climate, potential energy	Scale
	2. Slope	Topographic Map	Gravity, flow velocity	Scale
	3. Aspect	Topographic Map	Solar insolation, evapotranspiration	Categorical
	4. Curvature	Topographic Map	Converging, diverging flow	Scale
Hydrology	5. SPI (Stream Power Index)	Topographic Map	Potential erosive power	Scale

	6. TWI (Topographic Wetness Index)	Topographic Map	Soil water content	Scale
	7. Distance to river	Topographic Map	River undercutting	Scale
Landuse	8. Landuse	Topographic Map	Landslide triggering by slope cutting, trees effect on landslide	Categorical
Geology	9. Geology Unit	Geology Map	Rock strength	Categorical
	10.Distance to fault	Geology Map	Ground deformation	Scale
Trigger	11. PGA	Seismic Hazard Map	External triggering force	Scale

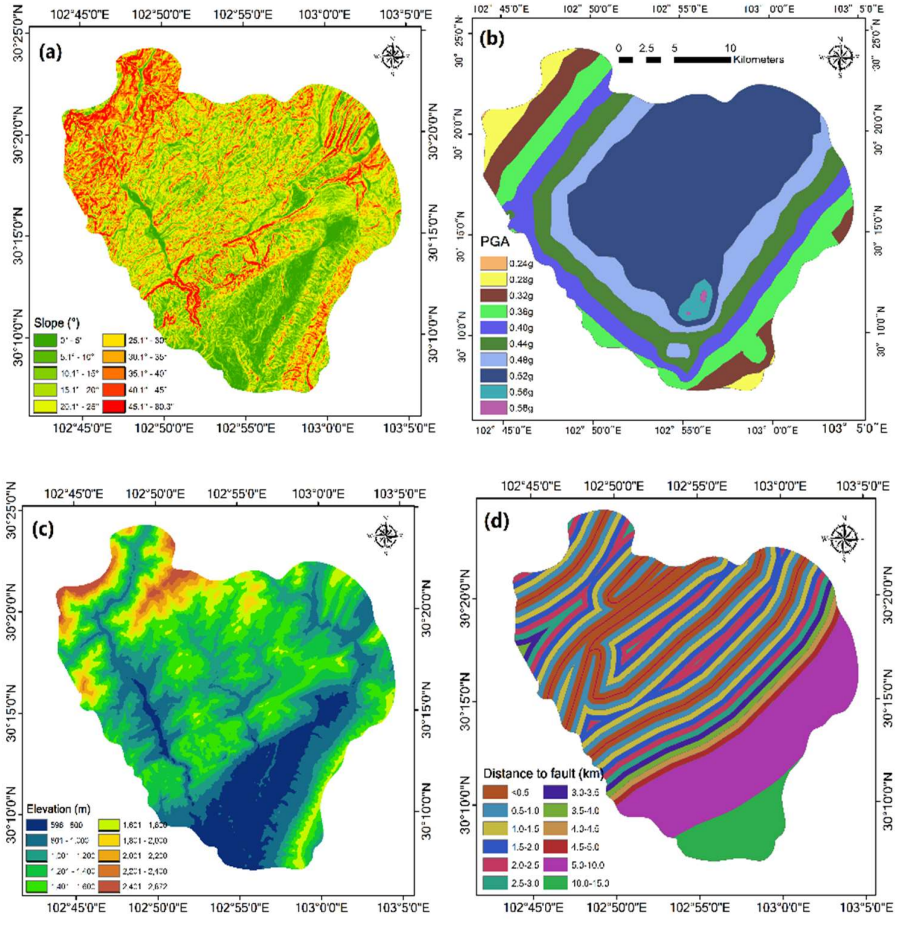

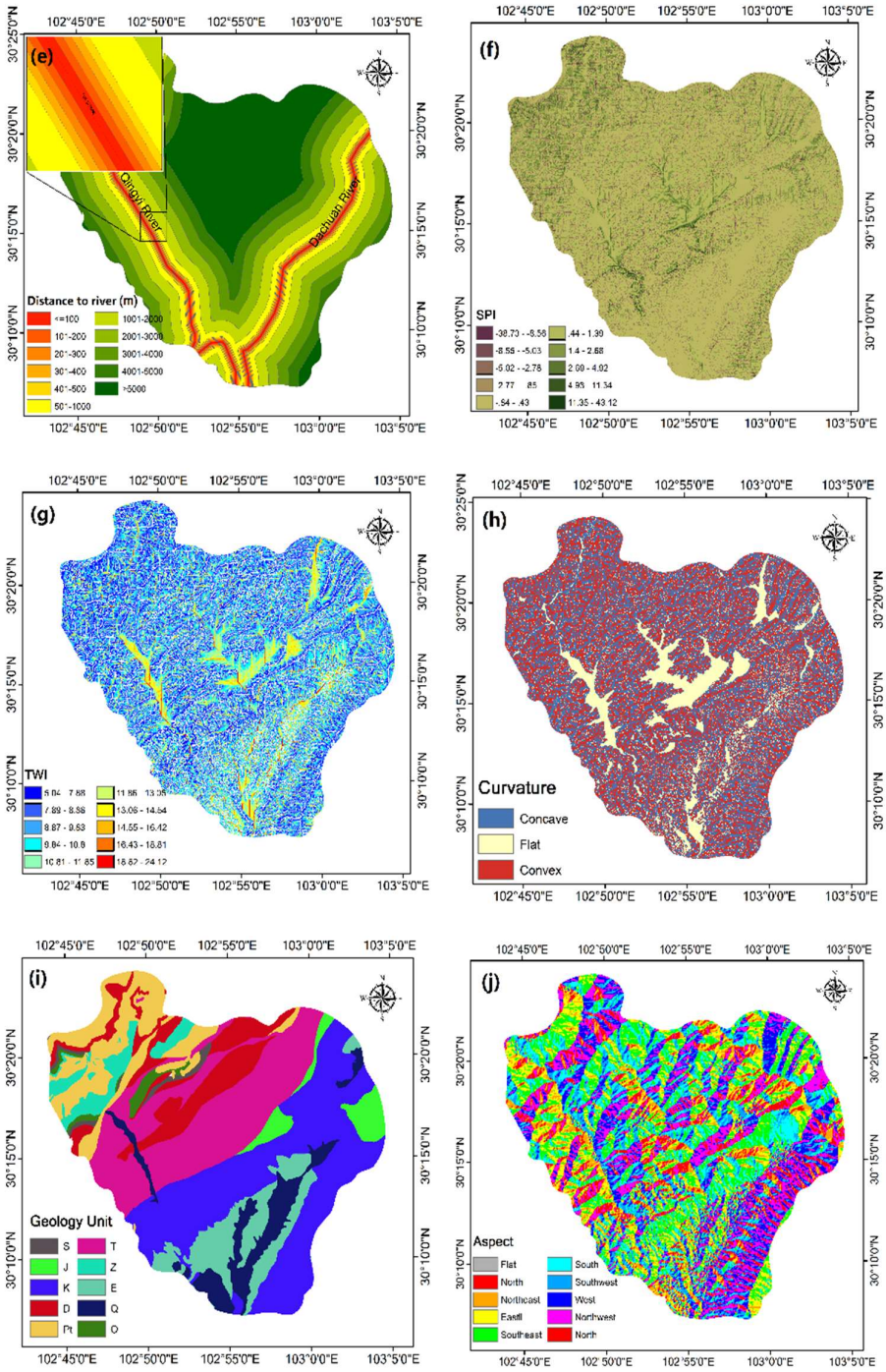
(e)
Distance to river (m)
<=100
101-200
201-300
301-400
401-500
501-1000
1001-2000
2001-3000
3001-4000
4001-5000
>5000
Chinyi River
Dechuan River
(f)
SPI
-38.73 - -8.56
-8.55 - -5.03
-5.02 - -2.78
-2.77 - .85
-.84 - .43
.44 - 1.39
1.4 - 2.88
2.89 - 4.92
4.93 - 11.34
11.35 - 43.12
(g)
TWI
5.04 - 7.88
7.89 - 8.86
8.87 - 9.63
9.64 - 10.8
10.81 - 11.85
11.86 - 13.05
13.06 - 14.54
14.55 - 16.42
16.43 - 18.81
18.82 - 24.12
(h)
Curvature
Concave
Flat
Convex
(i)
Geology Unit
S
J
K
D
Pt
T
Z
E
Q
O
(j)
Aspect
Flat
North
Northeast
East
Southeast
South
Southwest
West
Northwest
North
102°45'0"E
102°50'0"E
102°55'0"E
103°0'0"E
103°5'0"E
30°25'0"N
30°20'0"N
30°15'0"N
30°10'0"N

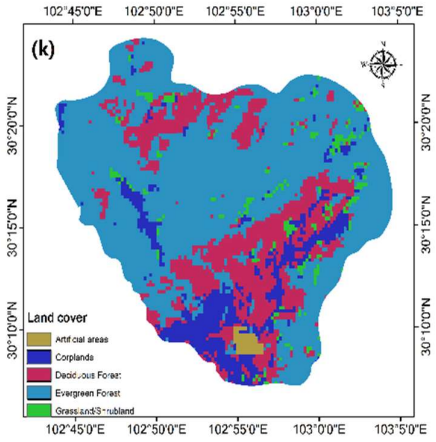

Figure 3-7 List of all the predictive factors: (a) Slope gradient, (b) PGA, (c) Elevation, (d) Distance to fault, (e) Distance to river, (f) SPI, (g) TWI, (h) Curvature, (i) Geology unit, (j) Aspect and (k) Land cover.

Topography makes great contributions in landslide occurrence through controlling surface flowing, sedimentation source and soil moisture concentration et al. Digital Elevation Model (DEM) used in this study in GeoTIFF format with geographic coordinates and 1 arc-second (30 m resolution) grid of elevation postings comes from NASA's Land Processes Distributed Active Archive Centre (LP-DAAC) (https://wist.echo.nasa.gov/~wist/api/imswelcome/). The DEM model is used to generate the various topographic parameters such as elevation, slope, aspect, curvature, stream power index (SPI), topographic wetness index (TWI).

The occurrence of the landslide was related to the elevation very much. For instance, during an earthquake, ground shaking was amplified as elevation increased (Sepúlveda et al., 2005;Shafique et al., 2009). Therefore, elevation was chosen as a predictive factor in earthquake-triggered landslides and the elevation of the study area was classified into 10 classes using 200m intervals as shown in Figure 3-7. Usually, topography was associated with landslides as a result of other topographic factors such as slope, aspect and curvature. The possibility of slope instability was expected to increase as the rise of slope gradients. The slope gradient of the study area varied from 0° to 81° and a total of 10 classes were used to make the slope layers (see Figure 3-7). Aspect, defined as the maximum slope of the terrain surface, played a fundamental role in slope stability due to variance in

temperature, vegetation and directional PGA. For example, in the northern hemisphere, slopes facing south were more open to sunshine and warm wind than those facing north. Aspect was classified into 9 classes as flat (-1); north (0°-22.5° and 337.5°-360°); northeast (22.5°-67.5°); east (67.5°-112.5°); southeast (112.5°-157.5°); south (157.5°-202.5°); southwest (202.5°-247.5°); west (247.5°-292.5°) and northwest (292.5°-337.5°) (see Figure 3-7). The flat covered less than 0.5% of the study area, so it was merged into the north class (see Figure 3-7). The factor of curvature represented the morphology of the topography, and a positive curvature indicated that a surface was upwardly convex in that grid, while a negative one meant an upwardly concave surface. A zero value represented a flat surface (see Figure 3-7). Other DEM-derived factors such as the topographic wetness index (TWI) and the stream power index (SPI) were derived based on specific catchment areas (As) and slope maps. The topographic wetness index (TWI) has been extensively used to describe the effect of topography on the location and size of saturated source areas of runoff generation. Moore et al. (1991) proposed Eq.(3-17) for the calculation of TWI under the assumption of steady state conditions and uniform soil properties (i.e., transitivity is constant throughout the catchments and equal to unity). The stream power index (SPI) is a measure of the erosive power of water flow based on the assumption that discharge (q) is proportional to a specific area of a catchment (As)(see Eq.(3-18))

$$TWI = \ln(A_S/tan\beta) \tag{3-17}$$

$$SPI = A_S \times tan\beta \tag{3-18}$$

where A_S is the catchment area and β is the slope gradient.

Land cover was one of the main factors for slope stability analysis. Land cover performed as a shelter and reduced the susceptibility of soil erosion. The variation in the surface vegetation cover in an area was a dominant factor that seriously affected the slope failure. Vegetation benefitted the increase of soil strength by root reinforcement and ground surface with less vegetation cover was more susceptible to landslide(Shahabi et al., 2012). In this study, the land cover dataset was extracted

from International Geosphere-Biosphere Program Data and Information System (IGBP Land cover) (Friedl et al., 2010). Six categories of land cover were determined and compared to landslides (i.e., artificial areas, croplands, deciduous forest, evergreen forest, and grassland/shrub land).

Peak ground acceleration (PGA) was considered as the leading indicator of an earthquake, as well as a major measurement of triggering force for earthquake-induced landslide mapping. PGA map of the study area was extracted from the U.S.G.S. ShakeMap (http://comcat.cr.usgs.gov/). To verify and compare the landslide occurrence with PGA, the ShakeMap was categorized into 10 classes.

Geology condition also played a decisive role regarding the landslide manifestation. Faults formed a highly fractured line or zones of unstable slopes and the degree of fracturing and shearing played an important role in determining slope stability(Chau and Chan, 2005;Chen et al., 2014). As mentioned before by Xu et al. (2013), there was no obvious surface rupture produced by this earthquake, so the main active faults (e.g., Shuangshi-Dachuan fault) was chosen near the epicenter as the predictive factors in this study. The distance from the fault was calculated at 2 kilometres via using the buffer functions and 10 classes were generated. Strata unit was an indispensable factor in landslide occurrence for its lithology formation, and its varied structures could lead to a variation in rock strength and soil texture. The strata unit of this study area is very complex. They are classified into 10 classes according to geological age.

3.5.1.2 Generation of training and validation dataset

There is no universal rule for the selection of training and testing data. In this study, 1289 landslides (with 4754 grid cells) are randomly divided into two subsets: A training dataset, which contains 900 (70%) landslides (3297 grid cells), is used for building the prediction models; and a testing dataset containing the rest 30% of landslides (1457 grid cells) is used for testing the model efficiencies (Figure 3-8 a). In the FR and the WoE model, only the landsliding dataset (positive sample) is enough. But it is necessary to obtain satisfactory sample data representing the absence of landslide occurrences (negative sample) to match the LR and SVM

requirements. Since 4754 grid cells are used to represent the presence of landslide occurrence, similarly 4754 grid cells are randomly selected from the stable region in the studied area. In order to make the selection of negative sample more reasonable, the pixels within a distance of 60 meters (2 pixels) are excluded (Figure 3-8 b and c), because the pixel approximates to the landslides display similar conditions as the landslide pixel and it might cause problems in building the prediction model. Therefore, the training dataset for WoE model contains 3297 grid cells with landslide occurrence, and in five other models, the training dataset contains 6594 grid cells, half of which represents landslide occurrence and the other half are considered to be stable). 1457 grid cells of the landslides source area and 1457 randomly selected stable cells are used for the testing dataset.

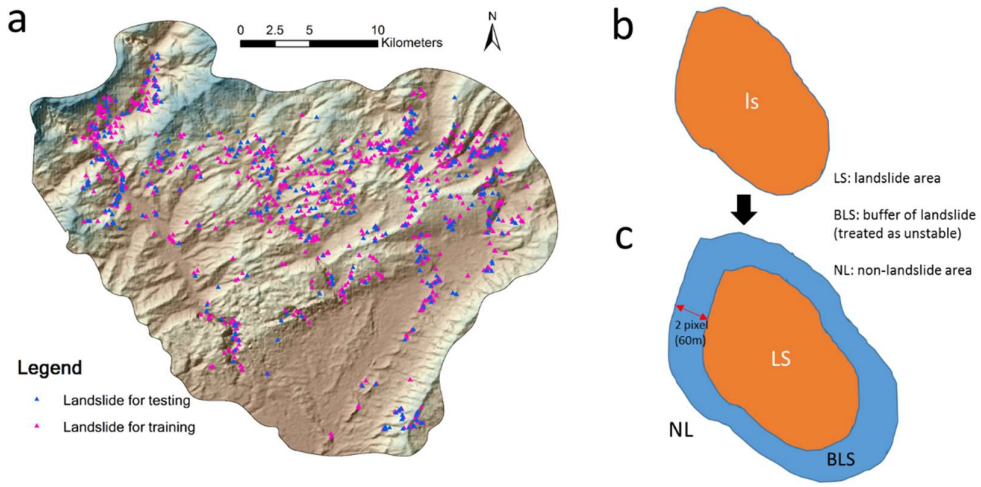

Figure 3-8 (a) Result of random separation of landslides for training and testing; (b) and (c) Diagram showing the method of generating stable points

3.5.1.3 Conditional independence of the factors

Tests for conditional independence, i.e. Cramer's V and Multicollinearity diagnostic statistics were also carried out. Cramer's V coefficient (Kendall and Stuart, 1979) ranged between 0 and 1 was used to test the spatial association between parameters. It was derived from a chi-square ($\chi 2$) test using contingency tables in order to identify any interrelationships within the landslide controlling factors that may effect on statistical analysis as follows Eq.(3-19):

$$V = \sqrt{\frac{\chi^2}{N \min(R-1, C-1)}} \quad (3\text{-}19)$$

where N is the sample size, R is the number of rows in the contingency table, and C is the number of the columns. Cramer's V coefficient is undertaken just on areas with landslides (Bonham-Carter, 1994).

The result of the chi-squares tests in terms of the calculated Cramer's V value for each variable is presented in Table 3-3. The value ranges from 0 to 1 indicating that higher values reflect a stronger association. Cramer's V value >0.5 indicates a high association, 0.3 to 0.5 indicates a moderate association, 0.1 and 0.3 indicates a low association and 0 to 0.1 indicates little if any association. Table 3-3 shows that the association of all the factors can be categorized as low to little association.

Table 3-3 Cramer's V Values for Comparison of Multi-class Chi-square Contingency Tables

	Elev	**Slo**	**Asp**	**Cur**	**SPI**	**TWI**	**DtR**	**LU**	**GU**	**DtF**	**PGA**
	(1)	(2)	(3)	(4)	(5)	(6)	(7)	(8)	(9)	(10)	(11)
(1)											
(2)	0.19										
(3)	0.13	0.20									
(4)	0.09	0.25	0.17								
(5)	0.27	0.13	0.08	0.05							
(6)	0.18	0.17	0.23	0.08	0.27						
(7)	0.09	0.10	0.14	0.21	0.06	0.19					
(8)	0.13	0.08	0.06	0.14	0.08	0.17	0.20				
(9)	0.24	0.19	0.18	0.16	0.15	0.23	0.10	0.13			
(10)	0.26	0.11	0.20	0.15	0.12	0.21	0.08	0.21	0.07		
(11)	0.24	0.15	0.19	0.07	0.19	0.25	0.17	0.14	0.18	0.28	

Elev: Elevation; Slo: Slope; Asp: Aspect; Cur: Curvature; DtR: Distance to river; LU: Landuse; GU: Geology Unit; DtoF: Distance to fault;

3.5.2 COMBINATION OF IV AND LR

The classified conditioning factors are illustrated in Table 3-2 and Figure 3-7. The information value method and the Weight of evidence method was produced using the weights for each class of each conditioning factor. Through analysing the relationship between 11 conditioning factors and landslide occurrence, the information value was calculated (Table 3-4).

Table 3-4 represents the relationship between landslide event and the classes of each conditioning factor. Results of the information value method showed that in the case of the relationship between landslide occurrence and elevation, landslide mostly occurred in the elevation range of 1200–1400 m. It showed that the probability of landslide occurrence is very low in low elevation areas. It also can be seen that, the higher the slope gradient is, the more favourable the slope is to landslide occurrence. In the case of the aspect, the ratio was high for the class of south and southwest facing slopes, having ratios of 0.194 and 0.148, respectively. For the curvature, higher curvature values were more favourable in predicting landslides. For SPI, the information value was highest (1.502) for the class of <-30.17, and it was lowest (-0.375) for the class of -1.92—1.27. The highest value for PGA classes as main contributors of landslide belonged to the category of 0.48-0.52 g with a value of 0.445. As for the factor of distance to stream and fault, it shows that, the further the distance is, the low effects of the stream and fault on landslide occurrence is. Also, as the terrain become rougher, it becomes more favourable to landslide occurrence.

Table 3-4 Information values of landslide predictive factors

Classes of Factor	Class Pixels	Landslides Pixels	%Factor	%Landslide	IV
Slope aspect					
Flat and N	72827	300	9.718987838	9.099181074	-0.066
NE	63749	257	8.507500731	7.79496512	-0.087
E	93653	432	12.49828179	13.10282075	0.047
SE	136942	504	18.2753324	15.2866242	-0.179
S	96575	516	12.88823171	15.65059145	0.194
SW	75693	386	10.10146438	11.70761298	0.148

W	97583	482	13.02275242	14.61935093	0.116
NW	112305	420	14.98744874	12.7388535	-0.163
Slope gradient (degree)					
0-5	50879	30	6.789959524	0.909918107	-2.010
5-10	73742	119	9.841097411	3.609341826	-1.003
10-15	95101	195	12.69152186	5.914467698	-0.764
15-20	114723	444	15.3101383	13.46678799	-0.128
20-25	114454	499	15.27423942	15.13497119	-0.009
25-30	100290	451	13.38400992	13.67910221	0.022
30-35	79310	453	10.58416419	13.73976342	0.261
35-40	55042	355	7.345524718	10.76736427	0.382
40-45	33308	256	4.445055363	7.764634516	0.558
45-81	32478	495	4.334289302	15.01364877	1.242
Elevation (m)					
596-800	92155	65	12.29836907	1.971489233	-1.831
800-1000	115695	480	15.4398547	14.55868972	-0.059
1000-1200	138950	662	18.54330619	20.07885957	0.080
1200-1400	174886	1208	23.33907626	36.63936912	0.451
1400-1600	124420	763	16.60423286	23.14225053	0.332
1600-1800	50598	114	6.752459207	3.457688808	-0.669
1800-2000	22509	4	3.003895496	0.121322414	-3.209
2000-2200	14378	1	1.91878846	0.030330604	-4.147
2200-2400	8376	0	1.117803042	0	0.000
2400-2872	7360	0	0.982214707	0	0.000
Distance to river (m)					
<100	15265	127	2.037161346	3.851986655	0.637
100-200	15278	118	2.038896236	3.579011222	0.563
200-300	15257	124	2.036093721	3.760994844	0.614
300-400	15247	134	2.034759191	4.06430088	0.692
400-500	15167	50	2.024082944	1.516530179	-0.289
500-1000	71629	261	9.559111042	7.916287534	-0.189
1000-2000	132130	256	17.63315615	7.764634516	-0.820
2000-3000	118652	341	15.83447547	10.34273582	-0.426
3000-4000	104937	314	14.00416641	9.523809524	-0.386
4000-5000	71288	183	9.51360354	5.550500455	-0.539
>5000	174548	1389	23.29396912	42.12920837	0.593
Distance to fault (m)					
<500	129448	668	17.27523498	20.26084319	0.159
500-1000	103165	448	13.76768754	13.5881104	-0.013
1000-1500	90048	344	12.01718342	10.43372763	-0.141
1500-2000	80100	591	10.68959213	17.92538672	0.517

2000-2500	51237	378	6.837735728	11.46496815	0.517
2500-3000	24409	160	3.257456358	4.852896573	0.399
3000-3500	19249	164	2.568838438	4.974218987	0.661
3500-4000	17218	180	2.297795222	5.459508644	0.865
4000-4500	16076	60	2.145391798	1.819836215	-0.165
4500-5000	15777	87	2.105489326	2.638762511	0.226
5000-10000	152859	127	20.39950516	3.851986655	-1.667
10000-15000	49806	90	6.646764363	2.729754322	-0.890
Land cover					
Artificial areas	5757	0	0.768289412	0	0.000
Croplands	81530	119	10.88043004	3.609341826	-1.103
Deciduous Forest	167509	545	22.35459285	16.53017895	-0.302
Evergreen Forest	470372	2558	62.77259461	77.58568396	0.212
Grassland/Shrub land	24226	75	3.233034443	2.274795268	-0.352
Geology unit					
S	7780	46	1.038265003	1.395207765	0.295
J	27526	46	3.673429624	1.395207765	-0.968
K	217638	1084	29.04446256	32.87837428	0.124
D	79888	589	10.66130007	17.86472551	0.516
Pt	87020	416	11.61308748	12.61753109	0.083
T	169483	860	22.61802924	26.08431908	0.143
Z	29151	120	3.890290888	3.639672429	-0.067
E	66550	72	8.881302822	2.183803458	-1.403
Q	54419	30	7.262383445	0.909918107	-2.077
O	9907	34	1.322119715	1.031240522	-0.248
TWI					
<-3.46	100037	498	13.35024629	15.10464058	0.123
-3.46--3.44	36702	76	4.897995134	2.305125872	-0.754
-3.44-1.73	60	0	0.008007185	0	0.000
1.73-5.17	2	0	0.000266906	0	0.000
5.18-8.63	188236	1159	25.12067495	35.15316955	0.336
8.64-12.08	348221	1409	46.47116679	42.73582044	-0.084
12.09-15.53	61992	120	8.27302366	3.639672429	-0.821
15.54-18.99	11622	32	1.550991757	0.970579315	-0.469
19.00-22.44	2348	3	0.313347844	0.090991811	-1.237
22.45-25.89	107	0	0.01427948	0	0.000
SPI					
<-30.17	1519	30	0.202715236	0.909918107	1.502
30.17- -3.52	11087	92	1.479594356	2.790415529	0.634
-3.52--2.27	37490	195	5.003156165	5.914467698	0.167

-2.27--1.92	62903	213	8.394599421	6.460418562	-0.262
-1.92--1.27	249614	755	33.31175842	22.8996057	-0.375
0.44-1.39	274573	1242	36.64261397	37.67060965	0.028
1.40-2.68	91107	550	12.15851024	16.68183197	0.316
2.69-4.92	18168	157	2.424575653	4.761904762	0.675
4.93-11.34	2684	57	0.358188081	1.728844404	1.574
11.35-43.12	182	6	0.024288462	0.181983621	2.014
Curvature					
Concave	320099	1503	42.71819913	45.58689718	0.065
Flat	120711	353	16.10925537	10.70670306	-0.409
Convex	308517	1441	41.1725455	43.70639976	0.060
PGA (g)					
<0.24	133	0	0.01774926	0	0.000
0.24-0.28	21648	0	2.888992389	0	0.000
0.24-0.32	49698	234	6.63235143	7.097361237	0.068
0.32-0.36	84456	277	11.27091377	8.401577191	-0.294
0.36-0.4	86065	86	11.48563978	2.608431908	-1.482
0.4-0.44	95368	232	12.72715383	7.03670003	-0.593
0.44-0.48	95248	350	12.71113946	10.61571125	-0.180
0.48-0.52	308381	2118	41.15439588	64.24021838	0.445
0.52-0.56	7738	0	1.032659974	0	0.000
0.56-0.58	659	0	0.087945583	0	0.000

After analysis of effects of each subclasses within each factor, the next step to perform the landslide hazard mapping using the proposed combined methods is the perform the multivariate analysis using the logistic regression and support vector machine method. As stated in chapter 3, in the combined method, the value of the independent landslide predictive factors was replaced by the obtained weights (information values) according to the classes it belongs to (Figure 3-9).

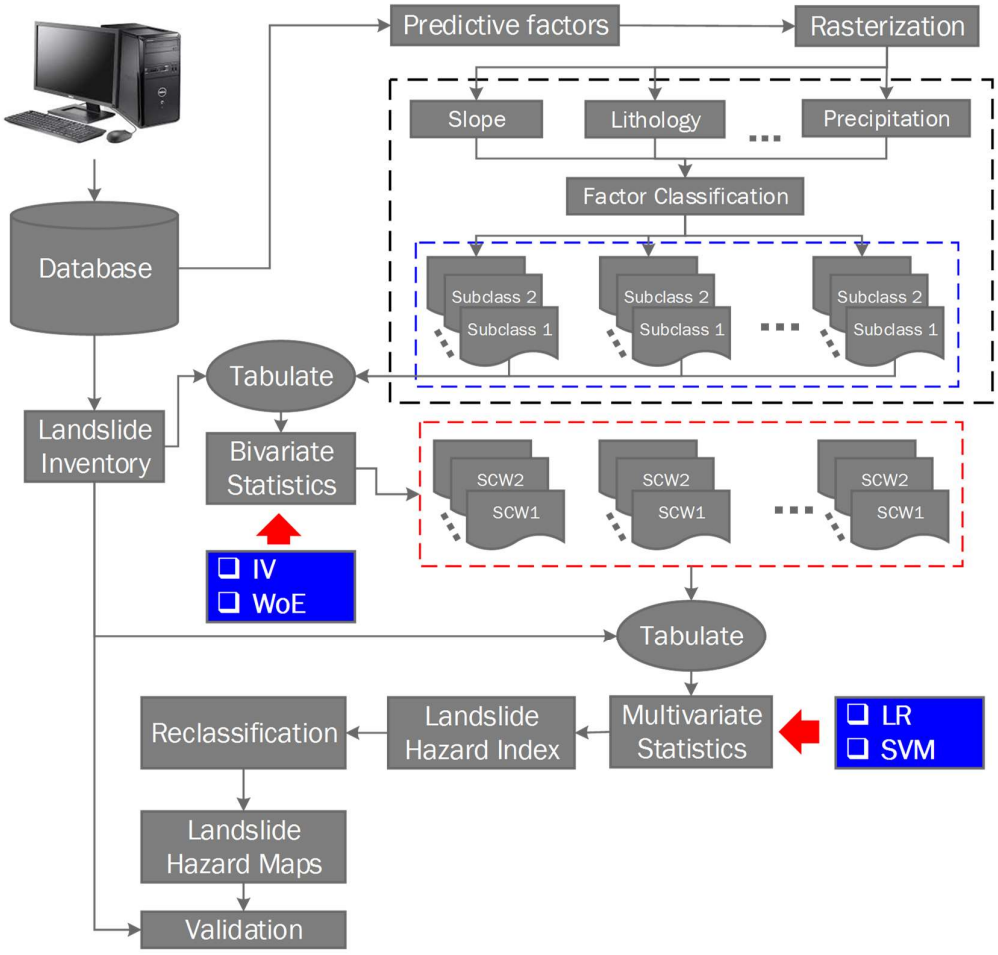

Figure 3-9 Flow chart of the proposed combined methods

The LR coefficients for the three methods are listed in Table 3-5. One is for the LR single method, in which the categorical factors of aspect, land cover and geology unit were excluded. For the combined method of LR-IV. The calculated information value or the weight were used to replace the factor values. As can be seen in Table 3-5, slope gradient and curvature showed the high and positive correlation with landslide occurrence as it could acquire the highest LR coefficient of 0.28 and 0.27. Similarly, SPI and PGA are the other effective conditioning factors, by the LR coefficient of 0.215 and 0.167 respectively.

Table 3-5 LR Coefficients for the LR method and LR-IV method

No.	Factor	LR Coefficient

		LR	LR-IV
1	Elevation	-0.556	-0.122
2	Slope	0.28	0.241
3	Aspect	--	0.062
4	Curvature	0.27	0.248
5	SPI (Stream Power Index)	0.215	0.198
6	TWI (Topographic Wetness Index)	-0.352	-0.315
7	Distance to river	-0.034	-0.218
8	Landuse	--	0.126
9	Geology Unit	--	0.088
10	Distance to fault	-0.020	-0.013
11	PGA	0.167	0.182
12	Constant	-1.31	-4.67

As for the combined method of LR-IV, curvature and slope gradient also showed the high and positive correlation with landslide occurrence as it could acquire the highest LR coefficient of 0.248 and 0.241. And the factors of SPI, PGA and Landuse are the other effective conditioning factors, by the LR coefficient of 0.198, 0.182 and 0.126 respectively.

3.5.3 COMBINATION OF IV AND SVM

Similarities, by combining the methods of IV with the SVM method, we can also obtain the probability maps of landslide occurrence. As stated previous in chapter3, the SVM gives the implicit expressions of the correlations between landslide occurrence and its predictive factors, it is impossible to tell which predictive factor is more important in landslide occurrence. By exchanging the value of the independent variables from X1 to Xn representing the value of cells of class layer with the Weights obtained from the IV (Figure 3-9).

3.5.4 COMBINATION OF WOE AND LR

As for the weight of evidence method (WoE), generally, it showed the same trends with the information value method. The highest value of weights occurred in the class of 1400-1600 meters in elevation, greater than 50° and east facing slopes. The lithology map is one of the predictive factors that have direct impacts on landslide occurrence. For the slope aspect, the highest weights of 0.227 was obtained in the class of south. In terms of the triggering factors, the class of 0.48-

0.52g gave the highest weights of 0.948. The result showed that for a terrain with higher slope gradient, it is more susceptible to landslides. For the stream power index and terrain wetness index, the high weights occurred in the area with higher values, both in negative and positive. The results also indicated that areas where it is concave or convex were more susceptible to landslides. For the factors produced from buffering of distance to the fault, it also a decreasing tendency of possibilities of landslide occurring with the increase of the distances.

Table 3-6 Results of weight of evidence for classes of each predictive factor

Classes of Factor	Class Pixels	Landslides Pixels	W^+	W^-	W_{Final}
Slope aspect					
Flat and N	72827	300	-0.06618	0.00687	-0.07305
NE	63749	257	-0.08784	0.00779	-0.09563
E	93653	432	0.04745	-0.00696	0.05441
SE	136942	504	-0.17930	0.03608	-0.21538
S	96575	516	0.19514	-0.03236	0.22751
SW	75693	386	0.14826	-0.01811	0.16637
W	97583	482	0.11619	-0.01861	0.13480
NW	112305	420	-0.16322	0.02622	-0.18944
Slope gradient (degree)					
0-5	50879	30	-2.01367	0.06145	-2.07512
5-10	73742	119	-1.00584	0.06714	-1.07298
10-15	95101	195	-0.76589	0.07510	-0.84099
15-20	114723	444	-0.12882	0.02163	-0.15045
20-25	114454	499	-0.00920	0.00165	-0.01085
25-30	100290	451	0.02191	-0.00343	0.02533
30-35	79310	453	0.26225	-0.03609	0.29834
35-40	55042	355	0.38449	-0.03779	0.42228
40-45	33308	256	0.56109	-0.03551	0.59660
45-81	32478	495	1.25335	-0.11886	1.37221
Elevation (m)					
596-800	92155	65	-1.83438	0.11184	-1.94622
800-1000	115695	480	-0.05902	0.01041	-0.06943
1000-1200	138950	662	0.07992	-0.01911	0.09904
1200-1400	174886	1208	0.45352	-0.19132	0.64483
1400-1600	124420	763	0.33374	-0.08199	0.41573
1600-1800	50598	114	-0.67146	0.03488	-0.70634
1800-2000	22509	4	-3.21345	0.02942	-3.24286
2000-2200	14378	1	-4.15163	0.01916	-4.17079
2200-2400	8376	0	0	0.01129	0
2400-2872	7360	0	0	0.00991	0
Distance to river (m)					
<100	15265	127	0.64107	-0.01878	0.65985
100-200	15278	118	0.56612	-0.01592	0.58204
200-300	15257	124	0.61750	-0.01784	0.63534
300-400	15247	134	0.69638	-0.02103	0.71741
400-500	15167	50	-0.28970	0.00519	-0.29489
500-1000	71629	261	-0.18924	0.01807	-0.20731
1000-2000	132130	256	-0.82258	0.11367	-0.93625
2000-3000	118652	341	-0.42734	0.06348	-0.49082
3000-4000	104937	314	-0.38688	0.05100	-0.43788
4000-5000	71288	183	-0.54058	0.04305	-0.58363

>5000	174548	1389	0.59622	-0.28288	0.87910
Distance to fault (m)					
<500	129448	668	0.16027	-0.03694	0.19720
500-1000	103165	448	-0.01310	0.00208	-0.01518
1000-1500	90048	344	-0.14179	0.01790	-0.15969
1500-2000	80100	591	0.52003	-0.08486	0.60489
2000-2500	51237	378	0.51992	-0.05117	0.57109
2500-3000	24409	160	0.40088	-0.01670	0.41759
3000-3500	19249	164	0.66505	-0.02511	0.69016
3500-4000	17218	180	0.87160	-0.03304	0.90464
4000-4500	16076	60	-0.16516	0.00333	-0.16849
4500-5000	15777	87	0.22697	-0.00549	0.23246
5000-10000	152859	127	-1.67041	0.18977	-1.86018
10000-15000	49806	90	-0.89243	0.04128	-0.93371
Land cover					
Artificial areas	5757	0	0	0.00775	0
Croplands	81530	119	-1.10630	0.07878	-1.18508
Deciduous Forest	167509	545	-0.30291	0.07264	-0.37554
Evergreen Forest	470372	2558	0.21300	-0.50925	-0.72225
Grassland/Shrub land	24226	75	-0.35275	0.00989	0.36264
Geology unit					
S	7780	46	0.29706	-0.00363	0.30069
J	27526	46	-0.97077	0.02348	-0.99425
K	217638	1084	0.12462	-0.05581	0.18042
D	79888	589	0.51925	-0.08443	0.60367
Pt	87020	416	0.08338	-0.01149	0.09487
T	169483	860	0.14331	-0.04604	0.18935
Z	29151	120	-0.06683	0.00261	-0.06944
E	66550	72	-1.40616	0.07125	-1.47741
Q	54419	30	-2.08092	0.06655	-2.14747
O	9907	34	-0.24940	0.00296	-0.25235
TWI					
-8.64--5.18	100037	498	0.12405	-0.02054	0.14459
-5.17--1.73	36702	76	-0.75603	0.02702	-0.78305
-1.72-1.72	60	0	0	0.00008	0
1.73-5.17	2	0	0	0.00000	0
5.18-8.63	188236	1159	0.33779	-0.14444	0.48223
8.64-12.08	348221	1409	-0.08415	0.06776	-0.15191
12.09-15.53	61992	120	-0.82358	0.04950	-0.87308
15.54-18.99	11622	32	-0.47041	0.00590	-0.47631
19.00-22.44	2348	3	-1.23968	0.00224	-1.24191
22.45-25.89	107	0	0	0.00014	0
SPI					
-38.73--8.56	1519	30	1.51709	-0.00714	1.52423
-8.55--5.03	11087	92	0.63835	-0.01345	0.65180
-5.05--2.78	37490	195	0.16814	-0.00968	0.17782
-2.77--0.85	62903	213	-0.26291	0.02099	-0.28390
-0.84-0.43	249614	755	-0.37617	0.14577	-0.52194
0.44-1.39	274573	1242	0.02779	-0.01643	0.04422
1.40-2.68	91107	550	0.31794	-0.05309	0.37103
2.69-4.92	18168	157	0.67926	-0.02435	0.70361
4.93-11.34	2684	57	1.59121	-0.01391	1.60512
11.35-43.12	182	6	2.04303	-0.00159	2.04461
Curvature					
Concave	320099	1503	0.06529	-0.05160	0.11689
Flat	120711	353	-0.41001	0.06270	-0.47270
Convex	308517	1441	0.05999	-0.04422	0.10421
PGA (g)					
<0.24	133	0	0	0.00018	0
0.24-0.28	21648	0	0	0.02945	0

0.24-0.32	49698	234	0.06807	-0.00501	0.07309
0.32-0.36	84456	277	-0.29493	0.03197	-0.32690
0.36-0.4	86065	86	-1.48576	0.09602	-1.58178
0.4-0.44	95368	232	-0.59457	0.06345	-0.65803
0.44-0.48	95248	350	-0.18087	0.02383	-0.20470
0.48-0.52	308381	2118	0.44778	-0.49983	0.94761
0.52-0.56	7738	0	0	0.01043	0
0.56-0.58	659	0	0	0.00088	0

As for the method of LR-WoE, the factor of aspect and slope gradient showed that highest positive correlation with landslide occurrence with the coefficient of 1.157 and 0.828, other factors with positive correlation of landslide are curvature, distance to river, and elevation. Finally, the landslide probability map can be calculated using Eq. (3-6) and Eq. (3-7).

Table 3-7 Results of weight of evidence for classes of each predictive factor

No.	Factor	LR Coefficient	
		LR	LR-WoE
1	Elevation	-0.556	0.554
2	Slope	0.28	0.828
3	Aspect	--	1.157
4	Curvature	0.27	0.748
5	SPI (Stream Power Index)	0.215	0.157
6	TWI (Topographic Wetness Index)	-0.352	0.183
7	Distance to river	-0.034	0.820
8	Landuse	--	-0.054
9	Geology Unit	--	-0.156
10	Distance to fault	-0.020	0.501
11	PGA	0.167	0.225
12	Constant	-1.31	-0.186

3.5.5 COMBINATION OF WOE AND SVM

Similarities, by combining the methods of IV with the SVM method, we can also obtain the probability maps of landslide occurrence. As stated previous in chapter3, the SVM gives the implicit expressions of the correlations between landslide occurrence and its predictive factors, it is impossible to tell which predictive factor is more important in landslide occurrence. By exchanging the value of the independent variables from X1 to Xn representing the value of cells of

class layer with the Weights obtained from the WoE (Figure 3-9).

3.6 RESULTS

The results of statistical LHM methods were calculated probabilities which can be represented as a landslide hazard map. It is common that landslide hazard maps show the degree of hazard by qualitative way by dividing calculated probabilities in some classes. In this research, the calculated probabilities were split as very low, low, moderate, high and very high. Low and very low indicate that this classified area is a stable zone. Whereas, vary high and high indicates the unstable zone. Medium classification might be classified as grey zone where stable or unstable cannot be clearly defined.

There is no strict rule to classify calculated probability into some classes and usually determined based on expert opinion. Several trials based on associated histogram using automated classification methods available were applied to find the classification that suits the scale of the calculated probability. A few classification methods, such as natural breaks, equal intervals and defined interval, were used to distinguish the hazard classes for trial. Equal intervals classification was found not to be useful for its emphasis on the amount of one class value relative to other classes. Natural breaks are identified that best group similar values and that maximize the differences between classes and not useful for comparing multiple maps built from different underlying information. A series of specified interval sizes can be used to define the classes with different ranges in defined interval methods based on a comprehensive consideration of the data distribution.

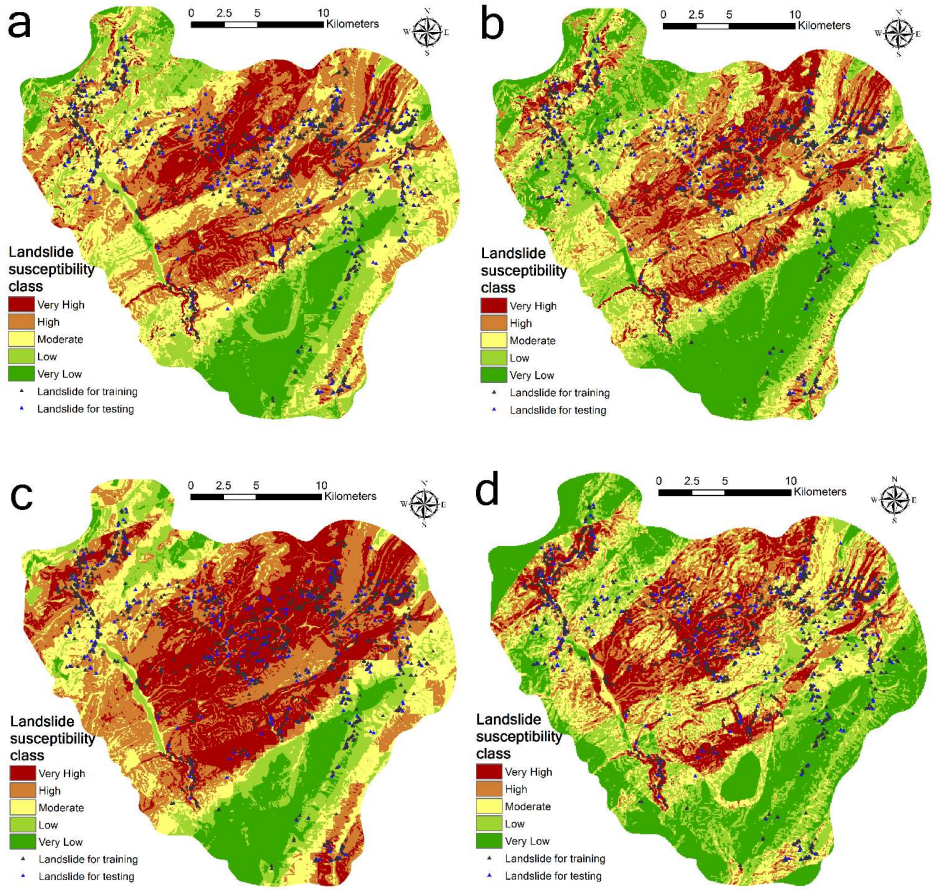

Figure 3-10 Landslide hazard map generated using: (a) Information value; (b) Logistic regression; (c) Weight of evidence; (d) Support vector machine (with linear kernel function)

The calculate weight of the information value method ranges from -3.19 to 6.93. Using natural breaks, the very low, low, medium, high and very high hazard zone has a value ranging from -3.19 to 1.10, -1.10 to 1.93, 1.93 to 2.73, 2.73 to 3.68 and 3.68 to 6.93 respectively (Figure 3-10a).

Table 3-8 Validation Matrix of IV based on the Number of Pixels

		Predicted (model)	
		Unstable	Stable
Landslide	Landslide (1)	2638(73%)	976 (27%)

Inventory	No landslide (0)	1359(37%)	2324(63%)

Table 3-8 shows that 63% stable and 73% unstable cells are correctly classified. Whereas, 27% stable and 37% unstable cells of the randomly sampled cells are incorrectly classified. IV has better capability to classify stable zone (80%) than unstable zone (65%).

The weight of WoE method has a value ranging from -13.81 to 7.26. Using natural breaks, the very low, low, medium, high and very high hazard zone has a value ranging from -13.81 to -3.00, -4.00 to 0.00, 0.00 to 1.00, 1.00 to 4.00 and 4.00 to 7.26 respectively (Figure 3-10b). On the susceptibility map, 29.01%, 30.49%, 18.46%, 11.62% and 10.43% area are shown as very low, low, medium, high and very high susceptibility respectively.

Table 3-9 Validation Matrix of WoE based on the Number of Pixels

		Predicted (model)	
		Unstable	Stable
Landslide Inventory	Landslide (1)	2464(71%)	1006(29%)
	No landslide (0)	1327(35%)	2490(65%)

Table 3-9 shows that 65% stable and 71% unstable cells in the sample are correctly classified. Whereas, 35% stable and 29% unstable cells of the randomly sampled cells are incorrectly classified.

The calculated probabilities of logistic regression method, ranging from0.03 to 0.99, were splitted by a geometrical interval because the data value indicated negative skewness. It was classified into 0.03-0.53, 0.53-0.64, 0.64-0.75, 0.75-0.92, and 0.92-0.99 for the very low, low, medium and high susceptibility zone respectively (Figure 3-10c). The very low, low, medium and high susceptibility zone covers 13.18%, 21.84%, 21.96%, 20.96% and 22.05% area respectively.

Table 3-10 Validation Matrix of LR based on the Number of cells

	Predicted (model)

		Unstable	Stable
Landslide Inventory	Landslide (1)	2362(62%)	1061(38%)
	No landslide (0)	1448(43%)	1910(57%)

Table 3-10 shows that 57% stable and 62% unstable cells are correctly classified. Whereas, 43% stable and 38% unstable cells of the randomly sampled cells are incorrectly classified.

The calculated probabilities of SVM method ranging from 0.021 to 0.986, were split by natural breaks. The very low, low, moderate, high and very high hazard zone has a value ranging from 0.021 to 0.310, 0.310 to 0.462, 0.462 to 0.580, 0.580 to 0.730 and 0.732 to 0.986 respectively (Figure 3-10d). On the susceptibility map, 8.29%, 19.21%, 14.93%, 24.89% and 32.68% area are shown as very low, low, medium and high susceptibility respectively.

Table 3-11 Validation Matrix of SVM based on the Number of Pixels

		Predicted (model)	
		Unstable	Stable
Landslide Inventory	Landslide (1)	2511(74%)	928(26%)
	No landslide (0)	882(25%)	2640(75%)

Table 3-11 shows that 75% stable and 74% unstable cells are correctly classified. Whereas, 25% stable and 26% unstable cells of the randomly sampled cells are incorrectly classified.

3.7 VALIDATION AND COMPARISONS

The validation can be carried by comparing the all the datasets including the landslide and non-occurrence with the calculated indexes. We can obtain a contingency table according to the results.

		Predicted	
	Total	Unstable	Stable
Actual	Landslide	Success (A)	Miss-alarm (B)
	No landslide	False-alarm (C)	Success (D)

Figure 3-11 Contigency Table used to validate the result of the classification

According to the contingency table, we employ the three indexes to validate the efficiency of the models, (1) success rate (SR)= (A+D)/(A+B+C+D); (2) miss-alarm rate(MAR) =B/(A+B) and (3) false-alarm rate(FAR)= C/(A+C).

Table 3-12 Comparison of performance of landslide hazard maps

	Methods	Success Rate	False-Alarm Rate	Miss-Alarm Rate
1	IV	68%	34%	27%
2	WoE	66%	35%	29%
3	LR	63%	38%	31%
4	SVM	74%	26%	27%
5	LR-IV	83%	9%	8%
6	LR-WoE	76%	11%	13%
7	SVM-IV	78%	8%	14%
8	SVM-WoE	81%	9%	10%

Success rate is to express the percentage of the cells in the total datasets that are correctly classified, including the cells with landslide ouccurrence and the cells without landslide occurrences. Although the success rate shows an overall performance of a classification model, it is not widely used in landslide hazard maps, because sometimes cells with landslide occurrence only covers a very little percentage of the total study area. From the success rate it is hard to tell the actual percentage of the landslides that are correctly classified.

Miss-alarm rate shows the percentage of the cells that was with landslide occurrence but it was predicted as stable, this rate was very important, a higher miss-alarm rate indicates more landslides were not classified by the classifier, which may cause serious consequence due to miss classification. On the other hand,

the false-alarm rate shows the percentage of cells that was incorrectly classified as landslides in the total unstable cells. A higher false-alarm rate will provide the false information in landslide hazard prevention. Among the three indexes, both success rate and false-alarm rate largely depended on the sample size. A great sample size will give a higher success rate as well as the false-alarm rate. Therefore, in this study we choose the miss-alarm rate to compare the performance of the landslide hazard maps.

Indicated by Table 3-12, we can see, all of the four single methods gives the acceptable results. Based on the validation results using the randomly sampled datasets, the SVM and IV methods give the minimum miss-alarm rate (27%), followed by the WoE method (29%) and the LR method shows the highest miss-alarm rate (31%). By comparing with the combined methods, the SVM-IV methods gives the lowest false-alarm rate of 8%, followed by the methods of LR-IV and SVM-WoE. On the other hand, according to the miss-alarm rate, the method of LR-IV gives the lowest miss-alarm-rate of 8%, while the SVM-IV method gives the highest value of 14%. Therefore, all the combined methods have improved the performance of landslide hazard maps. Of all the 8 methods used in this study, the SVM-IV gives the best performance according to the false-alarm rate, while the LR-IV and the SVM-WoE methods show the best performance according to the Miss-alarm rate.

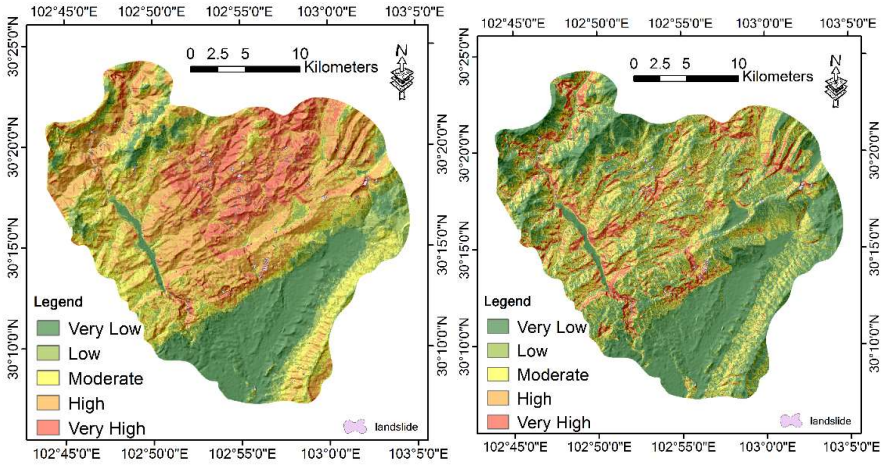

(a) (b)

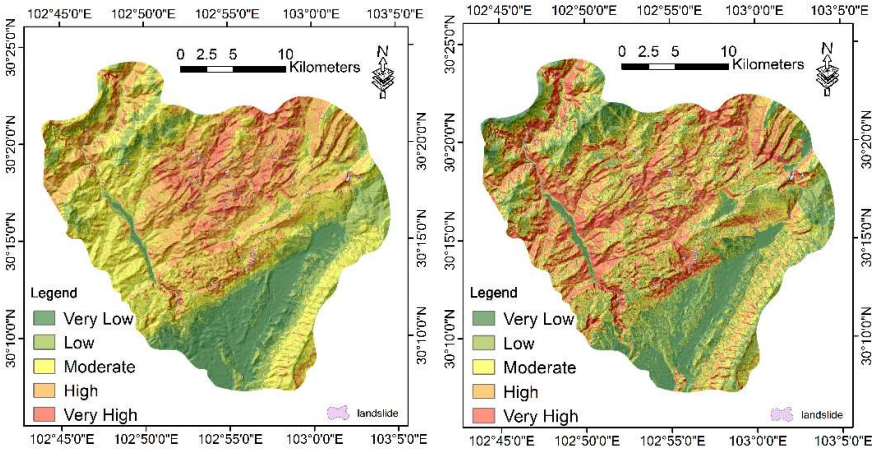

(c) (d)

Figure 3-12 Landslide hazard maps from combine methods (a) LR-IV;(b) SVM-IV; (c)LR-WoE; (d)SVM-WoE

Based on the results, there are pros-and-cons of each method in predicting landslide susceptibility zones. The IV and WoE method has advantages as follows:1) they can indicate identify influence of each class within a factor on landslides; 2) they can indicate the linear relationship between landslides and its controlling factor individually; 3) sampling is not necessary; 4) Both scale and categorical factors can be used. The disadvantages are 1) weight value may underestimates or overestimates if landslides are very small and not evenly distributed; 2) the weight cannot be compared for different area.

Some advantages of logistic regression are: 1) LR has ability to explicitly identify the relationship between landslides and its controlling factors simultaneously; 2) value represents meaningful probability and can be compared for different area; 3) LR also provides a technique to detect a linear relationship of landslide controlling factors. Whereas, the disadvantages are 1) LR requires formal statistical training; 2) undersampled may significantly impact the result; 3. the final susceptibility map may be over or underestimated.

SVM has advantages as follows: 1) It requires less formal statistical training; 2) SVM can implicitly identify the complex nonlinear relationship between landslides and its controlling factors. However, the disadvantages are 1) SVM has

limited ability to explicitly identify possible causal relationship; 2) SVM requires greater computational resources; 3) SVM is prone to overfitting.

3.8 DISCUSSIONS

Since the past landslide inventory plays a very important role in landslide hazard mapping using the statistical approaches, thus, the preparation of the landslide inventory is very important issue in landslide hazard mapping. In practical of generation the landslide inventory, how to determine whether a cell is a landslide cell or not in a cell-by-cell analysis will affect the samples used in following statistical analysis. In the past studies, there was no general rules about how to determine whether a cell should be regarded as a landslide. Therefore, to test the effects of the landslide cells on the landslide hazard maps, it is necessary to test the sensibility of the landslide.

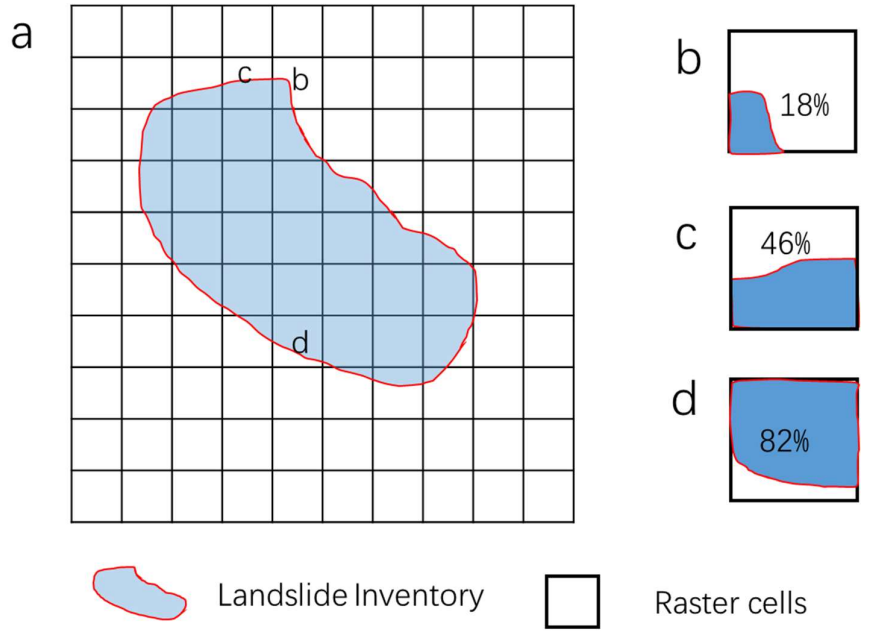

Figure 3-13 (a) Rasterize of landslide inventory polygon;(b) sample cell with less landslide coverage (18%); (c) sample cell with landslide 46% of landslide coverage; (d) sample cell with landslide 82% of landslide coverage

To determine the threshold percentage of coverage over which the cell should be regarded as landslide. We choose two methods of the four methods used as a

test, one is the information value method, which is bivariate, another is the logistic regression method, which is multivariate. We set different threshold values of landslide coverage in our analysis as 10%, 20%, 30%, 40% and 50%. (Figure 3-13)

Table 3-13 No. of landslide cells from the landslide inventory from different thresholds

Threshold Coverage	10%	20%	30%	40%	50%
No. of landslide cells	4754	4421	4153	3826	3755
Percentage	100%	93%	87.4%	80.1%	78.9%

Indicate by Table 3-13, as the threshold coverage increases, the total landslide pixels decreased from 4754 to 3755, with a total of 21.1% reduction.

Using the different landslide inventory rasters, we repeated the data preparation process described in the section 3.5.1 and landslide hazard mapping process described in the section 3.5 to produce the landslide hazard maps. Finally, the validation results were given in Table 3-14 and Figure 3-14.

Table 3-14 Validation result of landslide hazard maps using different landslide datasets

	Information Value			Logistic Regression		
Index	SR	FAR	MAR	SR	FAR	MAR
10%	68%	34%	27%	63%	38%	31%
20%	66%	35%	26%	62%	39%	32%
30%	65%	35%	28%	64%	41%	31%
40%	66%	32%	31%	63%	40%	30%
50%	67%	36%	30%	61%	42%	31%

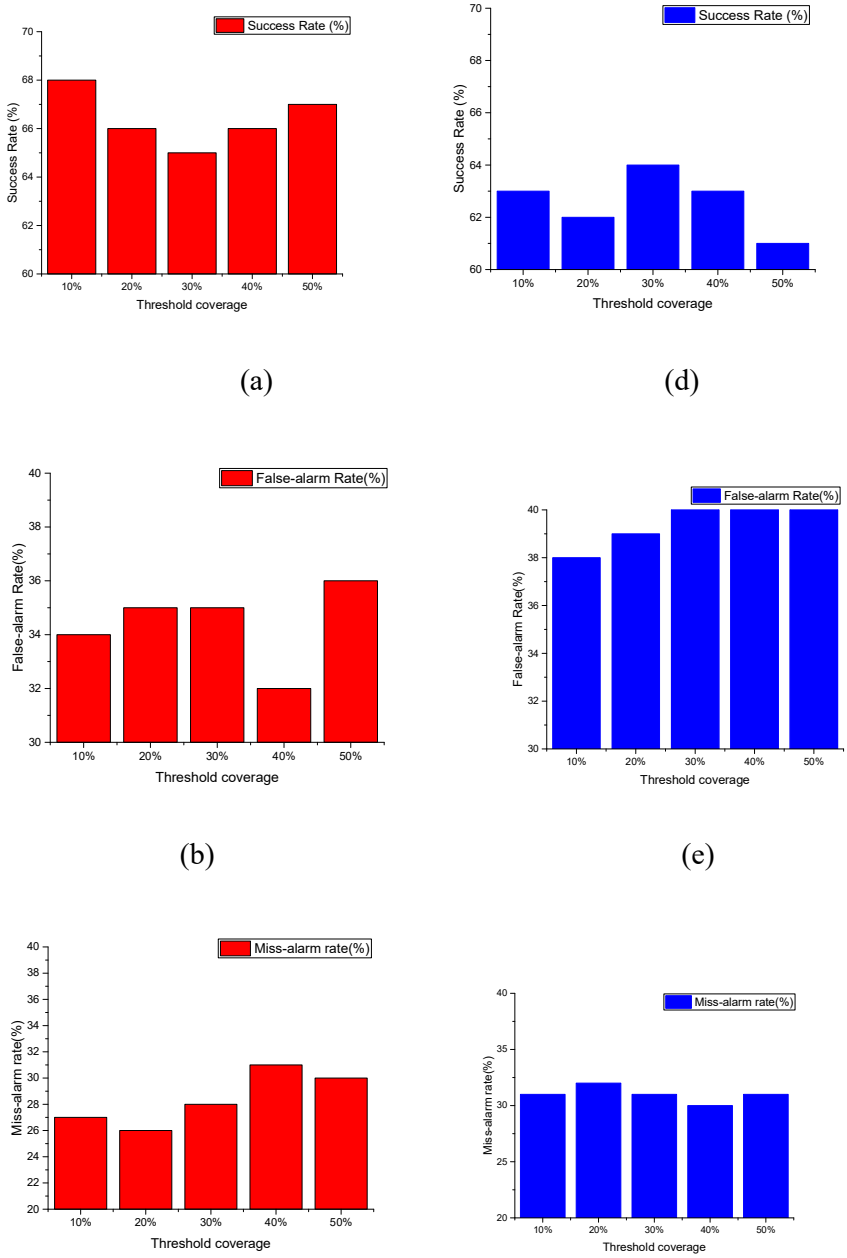

Figure 3-14 Validation result of landslide hazard maps using different landslide datasets (a-c) for IV method and (d-f) for LR method

Indicated by the results, generally, with the increase of threshold of landslide coverage, the landslide count will decrease, Using the different landslide datasets,

no obvious effects were observed on success rate of the models. However, as the threshold landslide coverage increase, the false alarm rate slightly increases using the logistic regression methods, while the miss-alarm rate slight decreases. As for the information value method, there was no obvious effects on the false-alarm rate, while the miss-alarm rate increases as the threshold landslide coverage become large. Therefore, based on a general consideration, a threshold of 10% of the landslide coverage threshold used in this study is appropriate. If a higher value was set to identify the landslide cells, some necessary information will be lost in the pseudo-unstable cells, which is very close to the landslide cells.

3.9 CONCLUSIONS

There are different approaches and techniques for evaluating landslide susceptibility and no agreement has been reached both in the procedure and the use of specific controlling factors employed in the landslide hazard mapping. Each approach has its own assumption and the result may differ from place to place. The different result may also be affected by different landslides controlling factors and the completeness of landslide inventory. Landslide susceptibility approaches need to be compared in order to identify the most realistic landslide susceptibility approach applied typically in the Lushan County by using complete landslide inventory. The conclusions can be drawn as follows:

(1) A method for effectively mapping of landslide inventory is proposed by using on-line high-resolution online images. In the proposed method, some Criteria should be pre-defined before visual interpretation of landslides;

(2) Four widely-used statistical landslide hazard mapping methods Information Value (IV), Weight of Evidence (WoE), Logistic Regression (LR), and Support Vector Machine (SVM) are used to produce the landslide hazard maps, the merits, demerits and limitations of each method are clarifed based on a close comparison between the four methods. Generally, all of the four methods shows an acceptable accuracy according to the test results on the landslides triggered by the 2013 Lushan

earthquake in China.

(3) Although several validation methods exist, in this chapter, a validation method based on the cross-table of the landslide inventory and its predicted status was employed, since it can give a clear engineering sense. To compare different landslide hazard maps, the miss-alarm rate and false-alarm rate are suggested as the main index to evaluate the performance or he landslide hazard maps.

(4) Accurate determination of the landslide cells in statistical LHM is very important, a sensitive analysis was carried out to test the effects of threshold landslide coverage on the landslide hazard maps. The result shows that, as the threshold values increase, no obvious effect found on the success rate, however both the miss-alarm rate and miss-alarm rate will increase. Generally, a 10% of the threshold percentage is recommended in this study.

(5) The advantages and disadvantages of the models have been used to evaluate the models and to propose a technique to improve the accuracy of the model. four new methods are proposed by combining one of IV and WoE methods with one of the LR and SVM methods. The validation results show that the combined method could improve the accuracy of the landside hazard maps.

REFERENCE

Carrara, A., Guzzetti, F., Cardinali, M. and Reichenbach, P. (1999) Use of GIS technology in the prediction and monitoring of landslide hazard. Natural hazards 20(2-3), 117-135.

Carrara, A., Cardinali, M., Detti, R., Guzzetti, F., Pasqui, V. and Reichenbach, P. (1991) GIS techniques and statistical models in evaluating landslide hazard. Earth surface processes and landforms 16(5), 427-445.

Clerici, A., Perego, S., Tellini, C. and Vescovi, P. (2002) A procedure for landslide susceptibility zonation by the conditional analysis method.

Geomorphology 48(4), 349-364.

Baeza, C. and Corominas, J. (2001) Assessment of shallow landslide susceptibility by means of multivariate statistical techniques. Earth surface processes and landforms 26(12), 1251-1263.

Kelarestaghi, A. and Ahmadi, H. (2009) Landslide susceptibility analysis with a bivariate approach and GIS in Northern Iran. Arabian Journal of Geosciences 2(1), 95-101.

Ayalew, L. and Yamagishi, H. (2005) The application of GIS-based logistic regression for landslide susceptibility mapping in the Kakuda-Yahiko Mountains, Central Japan. Geomorphology 65(1), 15-31.

Lee, S. and Pradhan, B. (2007) Landslide hazard mapping at Selangor, Malaysia using frequency ratio and logistic regression models. Landslides 4(1), 33-41.

Pradhan, B. and Lee, S. (2010a) Delineation of landslide hazard areas on Penang Island, Malaysia, by using frequency ratio, logistic regression, and artificial neural network models. Environmental Earth Sciences 60(5), 1037-1054.

Solaimani, K., Mousavi, S.Z. and Kavian, A. (2013) Landslide susceptibility mapping based on frequency ratio and logistic regression models. Arabian Journal of Geosciences 6(7), 2557-2569.

Regmi, A.D., Devkota, K.C., Yoshida, K., Pradhan, B., Pourghasemi, H.R., Kumamoto, T. and Akgun, A. (2014) Application of frequency ratio, statistical index, and weights-of-evidence models and their comparison in landslide susceptibility mapping in Central Nepal Himalaya. Arabian Journal of Geosciences 7(2), 725-742.

Pourghasemi, H.R., Pradhan, B., Gokceoglu, C., Mohammadi, M. and Moradi, H.R. (2013) Application of weights-of-evidence and certainty factor models and their comparison in landslide susceptibility mapping at Haraz watershed, Iran. Arabian Journal of Geosciences 6(7), 2351-2365.

Montgomery, D.R. and Dietrich, W.E. (1994) A physically based model for the topographic control on shallow landsliding. Water resources research 30(4), 1153-1171.

Terlien, M.T., Van Westen, C.J. and van Asch, T.W. (1995) Geographical information systems in assessing natural hazards, pp. 57-77, Springer.

Salciarini, D., Godt, J.W., Savage, W.Z., Conversini, P., Baum, R.L. and Michael, J.A. (2006) Modeling regional initiation of rainfall-induced shallow landslides in the eastern Umbria Region of central Italy. Landslides 3(3), 181-194.

Pradhan, B. (2011) Use of GIS-based fuzzy logic relations and its cross application to produce landslide susceptibility maps in three test areas in Malaysia. Environmental Earth Sciences 63(2), 329-349.

Pourghasemi, H.R., Pradhan, B. and Gokceoglu, C. (2012) Application of fuzzy logic and analytical hierarchy process (AHP) to landslide susceptibility mapping at Haraz watershed, Iran. Natural hazards 63(2), 965-996.

Pradhan, B. and Lee, S. (2010b) Regional landslide susceptibility analysis using back-propagation neural network model at Cameron Highland, Malaysia. Landslides 7(1), 13-30.

Zare, M., Pourghasemi, H.R., Vafakhah, M. and Pradhan, B. (2013) Landslide susceptibility mapping at Vaz Watershed (Iran) using an artificial neural network model: a comparison between multilayer perceptron (MLP) and radial basic function (RBF) algorithms. Arabian Journal of Geosciences 6(8), 2873-2888.

Yao, X., Tham, L. and Dai, F. (2008) Landslide susceptibility mapping based on support vector machine: a case study on natural slopes of Hong Kong, China. Geomorphology 101(4), 572-582.

Pradhan, B. (2013) A comparative study on the predictive ability of the decision tree, support vector machine and neuro-fuzzy models in landslide susceptibility mapping using GIS. Computers & Geosciences 51, 350-365.

Xu, C., Dai, F., Xu, X. and Lee, Y.H. (2012a) GIS-based support vector machine modeling of earthquake-triggered landslide susceptibility in the Jianjiang River watershed, China. Geomorphology 145, 70-80.

Wei-Min, W., Jin-Lai, H. and Zhen-Xing, Y. (2013) Preliminary result for rupture process of Apr. 20, 2013, Lushan Earthquake, Sichuan, China. CHINESE JOURNAL OF GEOPHYSICS-CHINESE EDITION 56(4), 1412-1417.

Xu, X., Wen, X., Han, Z., Chen, G., Li, C., Zheng, W., Zhnag, S., Ren, Z., Xu,

C. and Tan, X. (2013) Lushan M S7. 0 earthquake: a blind reserve-fault event. Chinese Science Bulletin 58(28-29), 3437-3443.

Chen, W., Li, W., Hou, E., Bai, H., Chai, H., Wang, D., Cui, X. and Wang, Q. (2014) Application of frequency ratio, statistical index, and index of entropy models and their comparison in landslide susceptibility mapping for the Baozhong Region of Baoji, China. Arabian Journal of Geosciences, 1-13.

Varnes, D.J. (1978) Slope movement types and processes. Transportation Research Board Special Report (176).

Sepúlveda, S.A., Murphy, W., Jibson, R.W. and Petley, D.N. (2005) Seismically induced rock slope failures resulting from topographic amplification of strong ground motions: The case of Pacoima Canyon, California. Engineering geology 80(3), 336-348.

Shafique, M., van der Meijde, M., Kerle, N. and van der Meer, F. (2009) Impact of topographic parameters on seismic amplification applying Geospatial tools, p. 386, IOS Press.

Shahabi, H., Ahmad, B.B. and Khezri, S. (2012) Application of Satellite remote sensing for detailed landslide inventories using Frequency ratio model and GIS. International Journal of Computer Science Issues (IJCSI) 9(4).

Friedl, M.A., Sulla-Menashe, D., Tan, B., Schneider, A., Ramankutty, N., Sibley, A. and Huang, X. (2010) MODIS Collection 5 global land cover: Algorithm refinements and characterization of new datasets. Remote Sensing of Environment 114(1), 168-182.

Chau, K. and Chan, J. (2005) Regional bias of landslide data in generating susceptibility maps using logistic regression: case of Hong Kong Island. Landslides 2(4), 280-290.

Bonham-Carter, G., Agterberg, F. and Wright, D. (1989) Weights of evidence modelling: a new approach to mapping mineral potential. Statistical Applications in Earth Sciences 89(9), 171-183.

Agterberg, F., Bonham-Carter, G., Cheng, Q. and Wright, D. (1993) Weights of evidence modeling and weighted logistic regression for mineral potential mapping. Computers in geology 25, 13-32.

Xu, C., Xu, X., Lee, Y.H., Tan, X., Yu, G. and Dai, F. (2012b) The 2010 Yushu earthquake triggered landslide hazard mapping using GIS and weight of evidence modeling. Environmental Earth Sciences 66(6), 1603-1616.

Rezaei Moghaddam, M., Khayyam, M., Ahmadi, M. and Farajzadeh, M. (2007) Mapping susceptibility landslide by using the weight-of-evidence model: a case study in Merek Valley, Iran. Journal of Applied Sciences 7, 3342-3355.

Pradhan, B., Oh, H.-J. and Buchroithner, M. (2010) Weights-of-evidence model applied to landslide susceptibility mapping in a tropical hilly area. Geomatics, Natural Hazards and Risk 1(3), 199-223.

Dahal, R.K., Hasegawa, S., Nonomura, A., Yamanaka, M., Masuda, T. and Nishino, K. (2008) GIS-based weights-of-evidence modelling of rainfall-induced landslides in small catchments for landslide susceptibility mapping. Environmental Geology 54(2), 311-324.

Van Westen, C., Rengers, N. and Soeters, R. (2003) Use of geomorphological information in indirect landslide susceptibility assessment. Natural hazards 30(3), 399-419.

Vapnik, V. and Cortes, C. (1995) Support-vector networks. Machine learning 20(3), 273-297.

Chervonenkis, A.Y. (2013) Early History of Support Vector Machines. Empirical Inference: Festschrift in Honor of Vladimir N. Vapnik, 13-20.

Guo, Q., Kelly, M. and Graham, C.H. (2005) Support vector machines for predicting distribution of Sudden Oak Death in California. Ecological Modelling 182(1), 75-90.

Vapnik, V.N. (1995) The nature of statistical learning theory, Springer-Verlag New York, Inc.

Lepore, C., Kamal, S.A., Shanahan, P. and Bras, R.L. (2012) Rainfall-induced landslide susceptibility zonation of Puerto Rico. Environmental Earth Sciences 66(6), 1667-1681.

Chen, Z. and Wang, J. (2007) Landslide hazard mapping using logistic regression model in Mackenzie Valley, Canada. Natural hazards 42(1), 75-89.

Chang, C.-C. and Lin, C.-J. (2011) LIBSVM: a library for support vector

machines. ACM Transactions on Intelligent Systems and Technology (TIST) 2(3), 27.

Joachims, T. (1999) Svmlight: Support vector machine. SVM-Light Support Vector Machine http://svmlight. joachims. org/, University of Dortmund 19(4).

Berrar, D.P., Dubitzky, W. and Granzow, M. (2003) A practical approach to microarray data analysis, Springer.

Lee, S., Hwang, J. and Park, I. (2013) Application of data-driven evidential belief functions to landslide susceptibility mapping in Jinbu, Korea. Catena 100, 15-30.

Yesilnacar, E. and Topal, T. (2005) Landslide susceptibility mapping: a comparison of logistic regression and neural networks methods in a medium scale study, Hendek region (Turkey). Engineering Geology 79(3), 251-266

Yin, Y., Wang, F. and Sun, P. (2009) Landslide hazards triggered by the 2008 Wenchuan earthquake, Sichuan, China. Landslides 6(2), 139-152.

Yin, Y., Zhang, Y., Ma, Y., Hu, D. and Zhang, Z. (2010) Research on major characteristics of geohazards induced by the Yushu Ms7. 1 earthquake. J Eng Geol 18(3), 289-296.

Zhou S, Fang L (2015) Support vector machine modeling of earthquake-induced landslides susceptibility in central part of Sichuan province, China. Geoenvironmental Disasters 2:1–12. doi: 10.1186/s40677-014-0006-1

Zhou S, Fang L, Liu B (2015) Slope unit-based distribution analysis of landslides triggered by the April 20, 2013, Ms 7.0 Lushan earthquake. Arab J Geosci 8:7855–7868. doi: 10.1007/s12517-015-1835-2

Zhou, S., Chen, G., & Fang, L. (2016). Distribution Pattern of Landslides Triggered by the 2014 Ludian Earthquake of China: Implications for Regional Threshold Topography and the Seismogenic Fault Identification. ISPRS International Journal of Geo-Information, 5(4), 46.

Zhou, S., Chen, G., Fang, L., & Nie, Y. (2016). GIS-Based Integration of Subjective and Objective Weighting Methods for Regional Landslides Susceptibility Mapping. Sustainability, 8(4), 334.

Zhou, S., Chen, G., Liu B., & Fang, L. (2016). A Combined Weight of

Evidence and Logistic Regression Method for Susceptibility Mapping of Earthquake‐induced Landslides: A Case Study of the April 20, 2013 Lushan Earthquake, China. Acta Geologica Sinica (English Edition), 90(2), 511-524.

Yin, Y., Wang, F. and Sun, P. (2009) Landslide hazards triggered by the 2008 Wenchuan earthquake, Sichuan, China. Landslides 6(2), 139-152.

Yin, Y., Zhang, Y., Ma, Y., Hu, D. and Zhang, Z. (2010) Research on major characteristics of geohazards induced by the Yushu Ms7. 1 earthquake. J Eng Geol 18(3), 289-296.

Guzzetti, F., Carrara, A., Cardinali, M. and Reichenbach, P. (1999) Landslide hazard evaluation: a review of current techniques and their application in a multi-scale study, Central Italy. Geomorphology 31(1), 181-216.

Carrara, A., Guzzetti, F., Cardinali, M. and Reichenbach, P. (1999) Use of GIS technology in the prediction and monitoring of landslide hazard. Natural hazards 20(2-3), 117-135.

van Westen, C.J., Castellanos, E. and Kuriakose, S.L. (2008) Spatial data for landslide susceptibility, hazard, and vulnerability assessment: an overview. Engineering geology 102(3), 112-131.

Carrara, A., Cardinali, M., Detti, R., Guzzetti, F., Pasqui, V. and Reichenbach, P. (1991) GIS techniques and statistical models in evaluating landslide hazard. Earth surface processes and landforms 16(5), 427-445.

Clerici, A., Perego, S., Tellini, C. and Vescovi, P. (2002) A procedure for landslide susceptibility zonation by the conditional analysis method. Geomorphology 48(4), 349-364.

Baeza, C. and Corominas, J. (2001) Assessment of shallow landslide susceptibility by means of multivariate statistical techniques. Earth surface processes and landforms 26(12), 1251-1263.

Kelarestaghi, A. and Ahmadi, H. (2009) Landslide susceptibility analysis with a bivariate approach and GIS in Northern Iran. Arabian Journal of Geosciences 2(1), 95-101.

Ayalew, L. and Yamagishi, H. (2005) The application of GIS-based logistic regression for landslide susceptibility mapping in the Kakuda-Yahiko Mountains, Central Japan. Geomorphology 65(1), 15-31.

Lee, S. and Pradhan, B. (2007) Landslide hazard mapping at Selangor, Malaysia using frequency ratio and logistic regression models. Landslides 4(1), 33-

41.

Pradhan, B. and Lee, S. (2010a) Delineation of landslide hazard areas on Penang Island, Malaysia, by using frequency ratio, logistic regression, and artificial neural network models. Environmental Earth Sciences 60(5), 1037-1054.

Solaimani, K., Mousavi, S.Z. and Kavian, A. (2013) Landslide susceptibility mapping based on frequency ratio and logistic regression models. Arabian Journal of Geosciences 6(7), 2557-2569.

Regmi, A.D., Devkota, K.C., Yoshida, K., Pradhan, B., Pourghasemi, H.R., Kumamoto, T. and Akgun, A. (2014) Application of frequency ratio, statistical index, and weights-of-evidence models and their comparison in landslide susceptibility mapping in Central Nepal Himalaya. Arabian Journal of Geosciences 7(2), 725-742.

Pourghasemi, H.R., Pradhan, B., Gokceoglu, C., Mohammadi, M. and Moradi, H.R. (2013) Application of weights-of-evidence and certainty factor models and their comparison in landslide susceptibility mapping at Haraz watershed, Iran. Arabian Journal of Geosciences 6(7), 2351-2365.

Montgomery, D.R. and Dietrich, W.E. (1994) A physically based model for the topographic control on shallow landsliding. Water resources research 30(4), 1153-1171.

Terlien, M.T., Van Westen, C.J. and van Asch, T.W. (1995) Geographical information systems in assessing natural hazards, pp. 57-77, Springer.

Salciarini, D., Godt, J.W., Savage, W.Z., Conversini, P., Baum, R.L. and Michael, J.A. (2006) Modeling regional initiation of rainfall-induced shallow landslides in the eastern Umbria Region of central Italy. Landslides 3(3), 181-194.

Pradhan, B. (2011) Use of GIS-based fuzzy logic relations and its cross application to produce landslide susceptibility maps in three test areas in Malaysia. Environmental Earth Sciences 63(2), 329-349.

Pourghasemi, H.R., Pradhan, B. and Gokceoglu, C. (2012) Application of fuzzy logic and analytical hierarchy process (AHP) to landslide susceptibility mapping at Haraz watershed, Iran. Natural hazards 63(2), 965-996.

Pradhan, B. and Lee, S. (2010b) Regional landslide susceptibility analysis

using back-propagation neural network model at Cameron Highland, Malaysia. Landslides 7(1), 13-30.

Zare, M., Pourghasemi, H.R., Vafakhah, M. and Pradhan, B. (2013) Landslide susceptibility mapping at Vaz Watershed (Iran) using an artificial neural network model: a comparison between multilayer perceptron (MLP) and radial basic function (RBF) algorithms. Arabian Journal of Geosciences 6(8), 2873-2888.

Yao, X., Tham, L. and Dai, F. (2008) Landslide susceptibility mapping based on support vector machine: a case study on natural slopes of Hong Kong, China. Geomorphology 101(4), 572-582.

Pradhan, B. (2013) A comparative study on the predictive ability of the decision tree, support vector machine and neuro-fuzzy models in landslide susceptibility mapping using GIS. Computers & Geosciences 51, 350-365.

Xu, C., Dai, F., Xu, X. and Lee, Y.H. (2012a) GIS-based support vector machine modeling of earthquake-triggered landslide susceptibility in the Jianjiang River watershed, China. Geomorphology 145, 70-80.

Wei-Min, W., Jin-Lai, H. and Zhen-Xing, Y. (2013) Preliminary result for rupture process of Apr. 20, 2013, Lushan Earthquake, Sichuan, China. CHINESE JOURNAL OF GEOPHYSICS-CHINESE EDITION 56(4), 1412-1417.

Xu, X., Wen, X., Han, Z., Chen, G., Li, C., Zheng, W., Zhnag, S., Ren, Z., Xu, C. and Tan, X. (2013) Lushan M S7. 0 earthquake: a blind reserve-fault event. Chinese Science Bulletin 58(28-29), 3437-3443.

Chen, W., Li, W., Hou, E., Bai, H., Chai, H., Wang, D., Cui, X. and Wang, Q. (2014) Application of frequency ratio, statistical index, and index of entropy models and their comparison in landslide susceptibility mapping for the Baozhong Region of Baoji, China. Arabian Journal of Geosciences, 1-13.

Varnes, D.J. (1978) Slope movement types and processes. Transportation Research Board Special Report (176).

Sepúlveda, S.A., Murphy, W., Jibson, R.W. and Petley, D.N. (2005) Seismically induced rock slope failures resulting from topographic amplification of strong ground motions: The case of Pacoima Canyon, California. Engineering geology 80(3), 336-348.

Shafique, M., van der Meijde, M., Kerle, N. and van der Meer, F. (2009) Impact of topographic parameters on seismic amplification applying Geospatial tools, p. 386, IOS Press.

Shahabi, H., Ahmad, B.B. and Khezri, S. (2012) Application of Satellite remote sensing for detailed landslide inventories using Frequency ratio model and GIS. International Journal of Computer Science Issues (IJCSI) 9(4).

Friedl, M.A., Sulla-Menashe, D., Tan, B., Schneider, A., Ramankutty, N., Sibley, A. and Huang, X. (2010) MODIS Collection 5 global land cover: Algorithm refinements and characterization of new datasets. Remote Sensing of Environment 114(1), 168-182.

Chau, K. and Chan, J. (2005) Regional bias of landslide data in generating susceptibility maps using logistic regression: case of Hong Kong Island. Landslides 2(4), 280-290.

Bonham-Carter, G., Agterberg, F. and Wright, D. (1989) Weights of evidence modelling: a new approach to mapping mineral potential. Statistical Applications in Earth Sciences 89(9), 171-183.

Agterberg, F., Bonham-Carter, G., Cheng, Q. and Wright, D. (1993) Weights of evidence modeling and weighted logistic regression for mineral potential mapping. Computers in geology 25, 13-32.

Xu, C., Xu, X., Lee, Y.H., Tan, X., Yu, G. and Dai, F. (2012b) The 2010 Yushu earthquake triggered landslide hazard mapping using GIS and weight of evidence modeling. Environmental Earth Sciences 66(6), 1603-1616.

Rezaei Moghaddam, M., Khayyam, M., Ahmadi, M. and Farajzadeh, M. (2007) Mapping susceptibility landslide by using the weight-of-evidence model: a case study in Merek Valley, Iran. Journal of Applied Sciences 7, 3342-3355.

Pradhan, B., Oh, H.-J. and Buchroithner, M. (2010) Weights-of-evidence model applied to landslide susceptibility mapping in a tropical hilly area. Geomatics, Natural Hazards and Risk 1(3), 199-223.

Dahal, R.K., Hasegawa, S., Nonomura, A., Yamanaka, M., Masuda, T. and Nishino, K. (2008) GIS-based weights-of-evidence modelling of rainfall-induced landslides in small catchments for landslide susceptibility mapping. Environmental

Geology 54(2), 311-324.

Van Westen, C., Rengers, N. and Soeters, R. (2003) Use of geomorphological information in indirect landslide susceptibility assessment. Natural hazards 30(3), 399-419.

Vapnik, V. and Cortes, C. (1995) Support-vector networks. Machine learning 20(3), 273-297.

Chervonenkis, A.Y. (2013) Early History of Support Vector Machines. Empirical Inference: Festschrift in Honor of Vladimir N. Vapnik, 13-20.

Guo, Q., Kelly, M. and Graham, C.H. (2005) Support vector machines for predicting distribution of Sudden Oak Death in California. Ecological Modelling 182(1), 75-90.

Vapnik, V.N. (1995) The nature of statistical learning theory, Springer-Verlag New York, Inc.

Lepore, C., Kamal, S.A., Shanahan, P. and Bras, R.L. (2012) Rainfall-induced landslide susceptibility zonation of Puerto Rico. Environmental Earth Sciences 66(6), 1667-1681.

Chen, Z. and Wang, J. (2007) Landslide hazard mapping using logistic regression model in Mackenzie Valley, Canada. Natural hazards 42(1), 75-89.

Chang, C.-C. and Lin, C.-J. (2011) LIBSVM: a library for support vector machines. ACM Transactions on Intelligent Systems and Technology (TIST) 2(3), 27.

Joachims, T. (1999) Svmlight: Support vector machine. SVM-Light Support Vector Machine http://svmlight. joachims. org/, University of Dortmund 19(4).

Berrar, D.P., Dubitzky, W. and Granzow, M. (2003) A practical approach to microarray data analysis, Springer.

Lee, S., Hwang, J. and Park, I. (2013) Application of data-driven evidential belief functions to landslide susceptibility mapping in Jinbu, Korea. Catena 100, 15-30.

Yesilnacar, E. and Topal, T. (2005) Landslide susceptibility mapping: a comparison of logistic regression and neural networks methods in a medium scale study, Hendek region (Turkey). Engineering Geology 79(3), 251-266.

CHAPTER 4

4 DEVELOPMENT OF GEOLHM-P FOR LANDSLIDE HAZARD MAPPING USING A PHYSICALLY-BASED APPROACH

4.1 INTRODUCTION

Landslide is one of the most severe natural hazards usually associated with an intense rainfall, an earthquake and other triggers. Damages from triggered landslides had sometimes exceeded damage directly related to earthquake itself in mountainous regions (Jibson et al. 2000). For example, about 200,000 landslides triggered by the 2008 Wenchuan earthquake distributed within an area of 44,000 km2 had directly caused about 20,000 deaths (Xu et al. 2015, Yin et al. 2009). It is, therefore, necessary to assess and manage earthquake-prone areas' susceptibility to landslides in advance. Estimation of where and in what conditions landslides are likely to be triggered by earthquakes is a vital element of regional seismic hazard assessment and the most economical way to reduce the damage of earthquake-induced landslides.

The stability of slope subject to seismic shaking at a specific site is a very complex process. In the past three decades, modelling of earthquake-induced landslide susceptibility can be accomplished using a variety of methodologies ranging from bivariate, multivariate or neural-network based statistical analysis, geotechnical analysis to deterministic or semi-deterministic physically-based approaches (Berti et al. 2012, Pourghasemi et al. 2012, Wang et al. 2012, Kayastha et al. 2013, Rajabi et al. 2013, Tien Bui et al. 2013, Chen et al. 2014, Zhou & Fang

2015). Statistical methods are successfully and most frequently used in combination with geographic information system (GIS) at the regional scale. These approaches are built on a basic assumption that landslide will occur in the future because of the same conditions that produced them in the past (Guzzetti et al. 1999; Crozier & Glade 2012). In these statistical approaches, mostly used earthquake-related parameters are the distance to the seismic source (epicenter or seismogenic fault), the recorded ground motions and the seismic intensities. However,

On the other hand, deterministic or semi-deterministic physically-based methods are often employed at basin scales (Westen et al. 2006) due to the complexities. The seismic stability of a slope is often assessed using the limit equilibrium method based on the assumptions that slope consists of rigid materials and that the failure mass slides along a single failure surface, on which the shear stress acting exceeds the resistance force. The most popular ways to assess seismic force are: pseudo-static method (PSM) and Newmark's Sliding Block method (NSBM). The PSM consider the earthquake force as an inertial force, expressed a product of a so-called seismic coefficient and the weight of the sliding mass (Baker et al. 2006, Choudhury & Savoikar 2011, Yang et al. 2014). While the NSBM estimates the expected co-seismic displacement of a sliding block for a given recorded acceleration time-history (Rajabi et al. 2013; Chousianitis et al. 2014; Chen et al. 2014). A major drawback of these applications is the important probabilistic features of earthquakes such as potential source, magnitude and ground motion variabilities were ignored.

The ground-motion parameters, such as peak ground acceleration (PGA) are prerequisites in deterministic landslide susceptibility assessment. Generally speaking, approaches for ground motion prediction can be classified as: empirical seismological and stochastic. Empirical approaches usually use a few empirical equations, derived from regression analyses of past recorded ground-motion data, to predict ground motion parameters (Scherbaum 2006, Akkar & Bommer 2007, Bindi et al. 2007, Boore & Atkinson 2008, Bommer et al. 2009, Atkinson 2010). The general forms of these empirical ground motion prediction equations (GMPEs) are usually specified so that the various terms of the equations have some physical

significance, such as source, path and site terms. However, the quality and confidence of these GMPEs largely dependent upon the quality of the dataset used for the regression. As a comparison, seismological approaches, such as the use of empirical Green's functions (EGFs)(Hutchings & Wu 1990, Yao et al. 2009, Mendoza & Hartzell 2009, Kurahashi & Irikura 2010, Yue & Lay 2013) and hybrid Green's functions (Pitarka et al. 2000, Mena et al. 2010, Campbell 2003) and the stochastic method (Atkinson & Boore 1997, Atkinson & Silva 2000, Boore 2003, Boore 2009,Atkinson & Boore 2006) require the complex specification of many parameters associated with source, path and site effects on the ground motion being modelled. Hence, the seismological approaches are generally used to study earthquake processes following the occurrence of an earthquake. The major advantage of the empirical approaches over the seismological approaches and stochastic is due to its simplicity in engineering practice use. The GMPEs are the overwhelming favorited and been successfully used in fields of seismic design, hazard mitigation. Therefore, there is a need to develop a methodology that is able with yet maintains the simplicity of the index approach.

Therefore, in this chapter, we describe the development and application of a functional module, called GeoLHM-P (Landslide hazard mapping using physically-based approach), to facilitate the landslide hazard mapping at a regional scale. The developed module of GeoLHM-P is embedded in the GeoILHMS system.

4.2 METHODOLOGY

4.2.1 INFINITE SLOPE MODEL

The stability of slopes is often assessed using the limit equilibrium method based on the assumptions that slope consists of rigid materials and that the failure mass slides along a single failure surface, on which the shear stress acting exceeds the resistance force. The fraction of the contrasting force acting on the failure surface is expressed as the factor of safety (FS). In this study, the stability analysis of slope was built on the infinite slope model, which assumes that landslides are infinitely long but have small depth compared to its length and width. The failure

surface was assumed to be the soil-bedrock interface parallel to the lope pf the ground. The infinite slope model is the most appropriate method for the analysis of shallow landslide with planar surface. Since shallow slope failures always take a large account of earthquake-induced landslides, the infinite slope model has been used in many physically-based landslide hazard mapping tools. The easy adoption of GIS enables the use of this simple physical model for analysis and modeling of slope conditions over broad areas.

An infinite slope model is shown in Figure 4-1. For this model, the weight of the sliding mass (for a unit dimension into the page) under static loading condition is:

$$G = \gamma HL \tag{4-1}$$

Where G is the weight of the sliding mass, γ is the unit weight of sliding mass, H is the slope normal thickness of the failure surface, L is the length of the sliding mass. As indicated by Figure 4-1b, the total normal force T_n and the shear force T_s acting on the sliding mass are related to the weight of soil mass using:

$$T_n = G \times sin\alpha = \gamma HL sin\alpha \tag{4-2}$$

$$T_s = G \times cos\alpha = \gamma HL cos\alpha \tag{4-3}$$

Where α is the slope gradient.

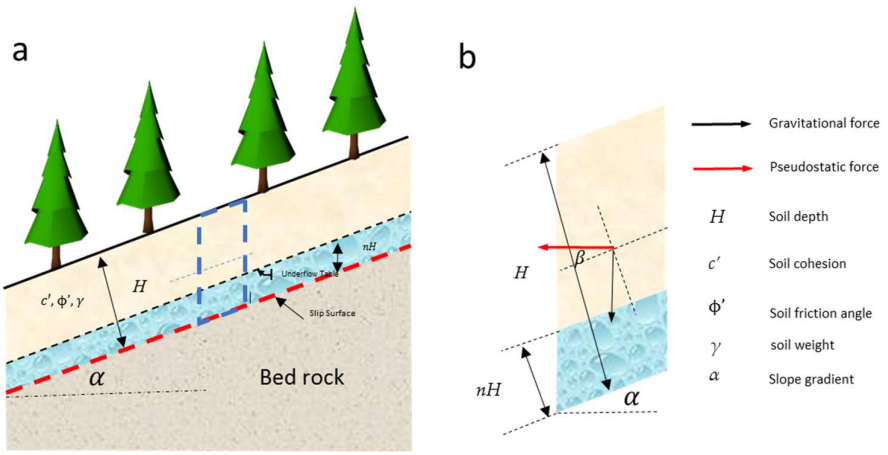

Figure 4-1 (a) Limit equilibrium analysis for infinite slope considering seismic forces; (b) Force analysis of unit soil slice (dash rectangle in a).

For a unit dimension into the page, the effective normal stress and the shear stress are defined as:

$$\sigma' = \frac{T_n}{L} - \gamma_w n H cos\alpha = (\gamma - n\gamma_w)\mathrm{H}\cos\alpha \tag{4-4}$$

$$\tau = \frac{T_s}{L} = \gamma H sin\alpha \tag{4-5}$$

Where γ_w the unit weight of water, n is the percentage of saturated failure thickness.

Thus, the static factor of safety can be expressed as:

$$F_s = \frac{c' + \sigma' tan\phi'}{\tau} = \frac{c' + [(\gamma - n\gamma_w)\mathrm{H}\cos\alpha]tan\phi'}{\gamma H sin\alpha} \tag{4-6}$$

4.2.2 PSEUDOSTATIC STABILITY ANALYSIS

Generally, there are three kinds of approaches are proposed to evaluate the seismic stability of natural slopes with soil dominant: (1) the pseudo-static method; (2) the sliding block method (Newmark,1965) and the Ishihara's method (Ishihara,1985). Based on the three methods, various modifications have been made to assess the seismic stability of natural slope. The pseudostatic method for seismic slope stability analysis is based on assumptions of the limit equilibrium and is still the most popular method among practicing engineers. The sliding block method (Newmark, 1965) has been universally applied in dam engineering.

In the pseudostatic method, a seismic force is added to the sliding force except the weight of sliding mass, which can be expressed as a product of a so-called seismic coefficient k and mass weight. In order to use the infinite slope model, a few additional assumptions need to be introduced as follow:

(1) The sliding surface is a straight plane parallel to the surface;

(2) Inter-slide force on each side of every vertical cross section are equal and parallel to the ground surface;

(3) The seepage force is considered to be steady and the direction of the seepage force is parallel to the ground surface

(4) The magnitude of the seismic force is constant in the soil mass above the sliding surface;

(5) There is no pore pressure increase in the sliding mass during seismic loading.

Supposing the angle between the incident direction of the pseudostatic force and the ground surface is β, and the pseudostatic force can be divided into the normal-slope S_N and the parallel-slope force S_P as:

$$S_N = \frac{k_s}{g}\gamma H sin\beta \tag{4-7}$$

$$S_P = \frac{k_s}{g}\gamma H cos\beta \tag{4-8}$$

Where k_s is the seismic coefficient, g is the acceleration of gravity.

By substituting the (4-7) and (4-8) in to (4-6), we get the seismic slope stability as:

$$F_s = \frac{c' + \sigma' tan\phi'}{\tau} = \frac{c' + [(\gamma - n\gamma_w)\mathrm{H}\cos\alpha - \frac{k_s}{g}\gamma H sin\beta]tan\phi'}{\gamma H sin\alpha + \frac{k_s}{g}\gamma H cos\beta} \tag{4-9}$$

For a pseudostatic slope stability analysis, a static force representing the effects of earthquake shaking is applied to the limit equilibrium analysis. This pseudostatic force is then taken as the product of the seismic coefficient (k_s) and the total weight of the sliding mass. The pseudostatic FS includes the destabilizing effects of this force. The biggest challenges for the pseudostatic procedure are the selection of a proper seismic coefficient and the value of an acceptable factor of safety. A summary of the horizontal seismic coefficients and acceptable factor of safety values in Table 4-1. The horizontal seismic coefficients range from 0.1 to 0.15 and

minimum factor of safety range from 1.0 to 1.5. In the America, the seismic coefficients have ranged from 0.05 to 0.15, whereas in Japan the coefficients have been less than about 0.2 (Seed 1979).

The Corps of Engineers Manual (EM-1110-2-1902), published in 1982, suggested a seismic coefficient value of 0.1 or 0.15 for where earthquake threat is major and great, respectively, and a minimum factor of safety of 1.0 for all magnitude earthquakes. At issue with all of these values of seismic coefficient is that they were arbitrarily selected and do not rigorously account for the level of expected shaking.

Marcuson and Franklin (1983) and Hynes-Griffin and Franklin (1984) related the seismic coefficient value for a dam to the expected peak ground acceleration (PGA) at a site. Marcuson and Franklin (1983) recommended a seismic coefficient of 1/3 or 1/2 at the crest of dam, whereas Hynes-Griffin and Franklin (1984) recommend a seismic coefficient of 1/2 of the PGA of bedrock with a minimum factor of safety of1.0 and a 20% reduction in shear strength. Bray et al. (1998) also suggested the seismic coefficient as 75% of the PGA of bedrock. This value is appropriate for seismic stability evaluations of solid-waste landfills, where the allowable levels of deformation are relatively small. Stewart et al (2013) use the data of Bray and Rathje (1998) to develop an expression for the seismic coefficient in terms of ground motion (PGA, duration) and earthquake (magnitude) parameters. Theses seismic coefficients values generally range from 25% to 75% of the PGA of bedrocks.

Table 4-1 Pseudostatic coefficients used in landslide stability analysis from various analysis

Investigator	Seismic coefficient	Threshold factor of safety (Fs)
Terzhagi (1950)	0.1 (R-F = IX) 0.2 (R-F = X) 0.5 (R-F > X)	> 1.0
Seed (1979)	0.10 (M = 6.50) 0.15 (M = 8.25)	>1.15
Marcuson (1981)	0.33-0.50 × PGA/*g*	> 1.0
Hynes-Griffin and Franklin (1984)	0.50 × PGA/*g*	> 1.0
California Division of Mines and	0.15	>1.1

Geology (1997)		

4.2.3 GROUND MOTION PREDICTION EQUATIONS (GMPE)

The ground-motion parameters, such as peak ground acceleration (PGA) are prerequisites in deterministic landslide hazard assessment. Generally speaking, approaches for ground motion prediction can be classified as: empirical seismological and stochastic. Empirical approaches usually use a few empirical equations, derived from regression analyses of past recorded ground-motion data, to predict ground motion parameters (Scherbaum 2006, Akkar & Bommer 2007, Bindi et al. 2007, Boore & Atkinson 2008, Bommer et al. 2009, Atkinson 2010). The general forms of these empirical ground motion prediction equations (GMPEs) are usually specified so that the various terms of the equations have some physical significance, such as source, path and site terms. However, the quality and confidence of these GMPEs largely dependent upon the quality of the dataset used for the regression. As a comparison, seismological approaches, such as the use of empirical Green's functions (EGFs) (Hutchings & Wu 1990, Yao *et al.* 2009, Mendoza & Hartzell 2009, Kurahashi & Irikura 2010, Yue & Lay 2013) and hybrid Green's functions (Pitarka *et al.* 2000, Mena *et al.* 2010, Campbell 2003) and the stochastic method (Atkinson & Boore 1997, Atkinson & Silva 2000, Boore 2003, Boore 2009,Atkinson & Boore 2006) require the complex specification of many parameters associated with source, path and site effects on the ground motion being modelled. Hence, the seismological approaches are generally used to study earthquake processes following the occurrence of an earthquake. The major advantage of the empirical approaches over the seismological approaches and stochastic is due to its simplicity in engineering practice use. The GMPEs are the overwhelming favourite and been successfully used in fields of seismic design, hazard mitigation. Therefore, in the GeoLHM-P, we choose to employ GMPEs to assess the regional ground motion parameter prediction under specified seismic scenarios, such as an assumed earthquake from a specified active fault with an assumed magnitude or assumed earthquake mechanism, such as strike-slip or

reverse fault et al.

In the developed GeoLHM-P, the Next Generation Attenuation Relationships for Western US (NGA-West2) (Boore et al. ,2014) proposed by the Pacific Earthquake Engineering Research Centre (PEER) was adopted. These equations were derived from a global database from 1989-2013 for a moment magnitude range of 3.0-7.9. In the NGA-West2 ground motion prediction equations, the ground motions are taken as the average horizontal component and the intensity measures (IMs) consist of peak ground acceleration and velocity (PGA, PGV) as well as 5% damped pseudo-spectral acceleration (PSA) for periods ranging from 0.01s to 10s. The ability of NGA-West2 GMPEs to successfully characterize the ground motion has been thoroughly demonstrated in Figure 4-2 a and b.

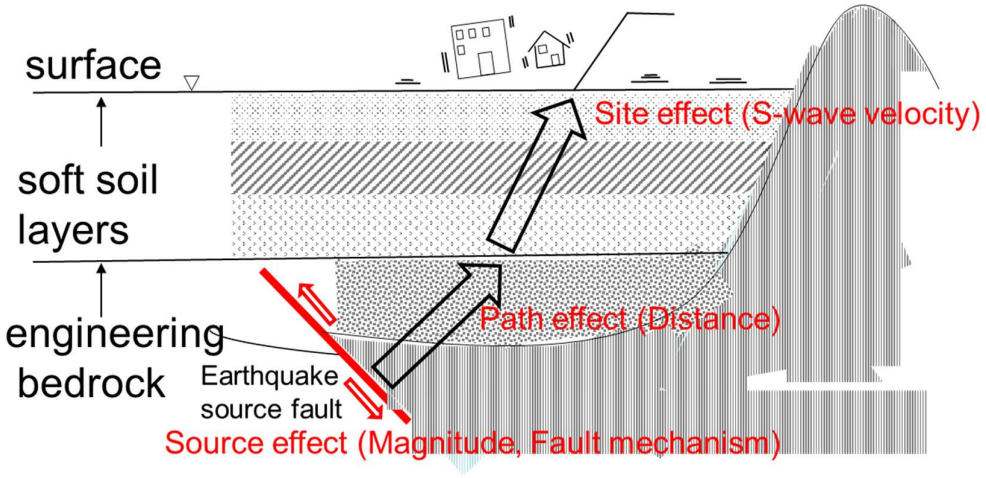

Figure 4-2 Schematic illustration of seismic wave propagation

The general forms of the NGA-West2 GMPEs constitutes of three parts as (Boore et al. ,2014):

$$\ln Y = F_E(M, mech) + F_p(R_{JB}, M, region) + F_s(V_{s30}, R_{JB}, M, region, z_1) + \varepsilon_n \sigma(M, V_{s30}, R_{JB}) \quad (4\text{-}10)$$

where $\ln Y$ represents the natural logarithm of the ground motion parameters (PGA, PGV and PSA); F_E represent the source effects, F_p shows the effects of the path of seismic waves and F_s describes the effects of the ground sites where the parameters is to be predicted. ε_n is the fractional number of standard devastations

of single predicted value of lnY away from the mean and σ is the total standard deviation of the model; M is the moment magnitude of the earthquake; M is the moment magnitude of the earthquake; $R_{JB}$is the distance in kilometres of the site location to the seismic fault plane; V_{s30} is a soil property, which is defined as the average speed of seismic wave in the 30m depth from the ground surface; Parameter $mech = 0, 1, 2$ and 3 is to describe the earthquake mechanism of unspecified, strike-slip, normal and reverse faulting, respectively. The output of PGA and PSA are g, while the output PGV are in $\mathrm{cm/s}$. Parameters $region = 0$ means no regional correction, 1 for California, New Zealand and Taiwan, 2 for China and Turkey and 3 for Italy and Japan.

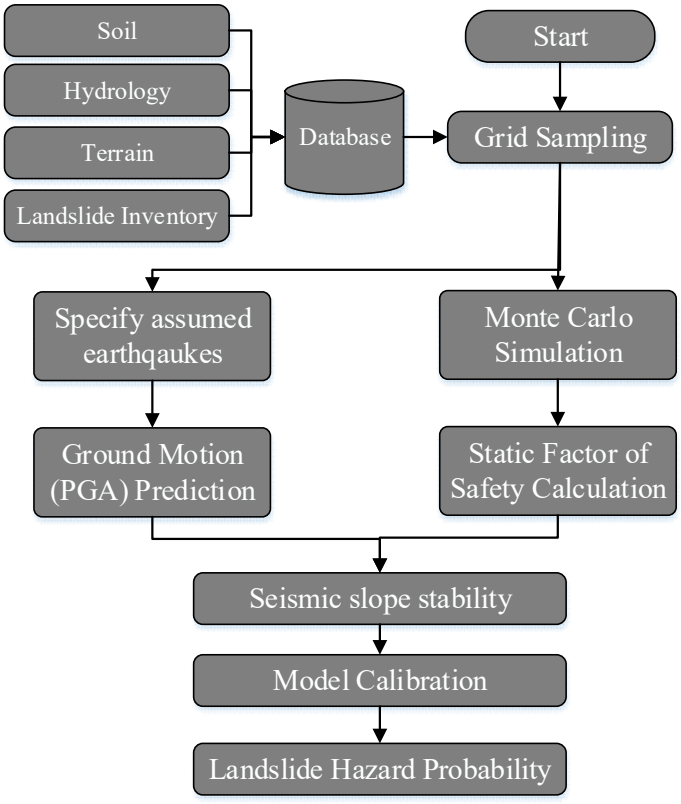

Figure 4-3 Flow Chart of the GeoLHM-P

4.2.4 ASSESSMENT OF UNCERTAINTIES USING MONTE CARLO SIMULATIONS

Uncertainties and variabilities were involved in the analysis of landslide

hazard over large areas using a deterministic model because of the complex geological conditions, the intrinsic variability of slope mass, and the limited number of data. Thus, applying a deterministic model to an extensive study area can be particularly difficult. However, uncertainties and variabilities mentioned can be quantitatively assessed the application of probabilistic analysis.

In probabilistic analysis, with a physically based slope model, string parameters should be considered as random variables to account for the uncertainties involved in their determination. To evaluate the slope stability and to calculate the probability of slope instability from theses random parameters, the random properties (such as distribution patterns and its related parameters) are determined from the available data and are then used in the analysis. Probabilistic analysis methods include the point estimate method (PEM), the first order second moment method (FOSM), and the Monte Carlo simulations. PEM and FOSM offer the advantage of allowing estimation of the probability of failure using probabilistic distribution patterns even without additional information. However, the calculation become impossible when the performance functions are complex. Moreover, because the PEM and FOSM can only be used to obtain approximate values for the probability of failure.

Monte Carlo simulations (METROPOLIS and ULAM 1949; Swendsen and Wang 1986; Caflisch 1998), on the other hand, are one of the most widely used methods of probabilistic analysis, which can be applied to all models where deterministic analysis is possible. Monte Carlo simulations are considered to be the most complete probabilistic analysis method because all random parameters and the probability of failure that results from the reliability analysis are represented by their probability density functions through repeated calculations. Another outstanding advantage of the Monte Carlo simulations is that this method is relatively easy to be implemented in a computer program can accommodate a wide range of functions, including those that cannot be expresses conveniently in an explicit form (Sobol 2001; Kwak and Ingall 2007; Raychaudhuri 2008). Therefore, the Monte Carlo simulation is utilized in the GeoLHM-P to obtain the probability of failure by considering a series of parameters related to the slope stability as

random parameters (such as the cohesion, friction angle of slope mass, ground water level, soil thickness et al.) (Manousiouthakis and Deem 1999; Sobol 2001; Kwak and Ingall 2007; Raychaudhuri 2008; Harrison 2010; Wang 2011).

4.3 CASE STUDY

4.3.1 GENERAL SETTINGS OF THE STUDY AREA

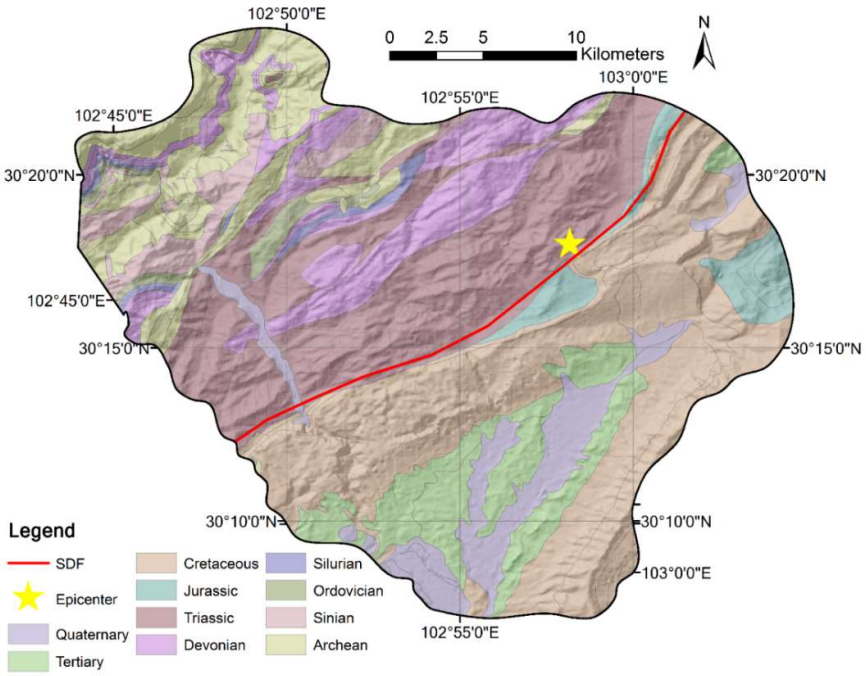

Figure 4-4 Geologic settings of the study area (Zhou and Fang, 2015)

We take the April20 ,2013 Lushan earthquake as an example to verify the GeoLHM-P module. This area is very tectonic-active with many folds and active faults trending NW–SE (Figure 4-4). Mesozoic volcanic rocks and Mesozoic group dominate the bedrock exposure in the area. The volcanic rocks comprise tuffs and lavas with intercalated sedimentary rocks. Intrusive rocks mainly consist of granites, sandstone and dykes of various compositions. As a result of the abundant supply of rainfall and the local rich groundwater, almost all rocks in the study area have undergone a certain degree of weathering(Xu et al., 2013; Zhou, et al, 2015). In

many slopes, weathering has penetrated deep into rock masses through joints and bedding planes (Zhou, et al, 2015).

Table 4-2 Description of the lithology in the study area (Zhou and Fang, 2015)

Age	Symbol	Lithology
Quaternary	Q	Alluvium, clay, loose deposit
Tertiary	E	Marl, sometimes intercalated with mudstone
Cretaceous	K	Marl, siltstone, conglomerate, sandstone
Jurassic	J	Sandy slate, mudstone, sandy stone intercalated with mudstone
Triassic	T	Sandy stone, limestone, slate
Devonian	D	mudstone, sandstone, carbonatite
Silurian	S	Sandstone, phyllite intercalated with limestone
Ordovician	O	Limestone, marble and phyllite
Sinian	Z	Metamorphic sandstone, dolomite
Archean	Pt	Granite, diorite, gabbro

4.3.2 PGA VALUES ESTIMATED FROM DIFFERENT EARTHQUAKES FROM AT THE SHUANGSHI-DACHUAN FAULT

Table 4-3 Parameters used in the GeoLHM-P to predict the PGA values

Input Parameter	**Value or code**
Region	China
Magnitude	Mw5.0, Mw6.0 and Mw6.6 (Real Case)
Mechanism	Reverse-Fault
Miu-Vs30	California
Vs30 data	Estimated according to the rocks
Fault Plane	Shuangshi-Dachuan Fault

There was no obvious surfaces rupture found during the earthquake according to after-event field investigations and many studies of focal mechanism inversions had suggested that the 2013 Lushan earthquake was caused by a reverse fault striking in NE direction. However, the NE-trending Shuangshi-Dachuan fault (SDF) also have induced movements based on some field phenomena found along this fault(Xu et al., 2013; Zhou, et al, 2015). In this chapter, we take the NE-trending Shuangshi-Dachuan fault and assumed the different earthquakes on these two fault

to estimate the PGA values (Table 4-3). for the Vs30 data, it was downloaded from the Japan seismic hazard information station(JSHIS) (http://www.j-shis.bosai.go.jp/). The result of the PGA estimation is illustrated in Figure 4-5, Figure 4-6 and Figure 4-7 for the assumed earthquakes happened on the Shuangshi-Dachuan fault with the moment magnitude of Mw5.0, Mw6.0 and Mw6.6, respectively.

Table 4-4 Site asses in NEHRP Provisions (Martin 1994)

NEHRP Category	**Description**	**Mean Shear Wave Velocity to 30m**	**Characteristics**
A	Hard rock	>1500 m/s	
B	Firm to hard rock	760-1500m/s	760, 1070m/s
C	Dense soil, soft rock	360-760m/s	620, 520m/s
D	Stiff soil	180-360m/s	310, 255m/s
E	Soft clays	<180 m/s	
F	Special study soils, e.g. liquefiable soils, sensitive clays, organic soils, soft clays >36m thick		

NEHRP: National Earthquake Hazard Reduction Program

One of the biggest challenges in using the NGA-West2 GMPEs at a regional scale is to determine the Vs30 (average speed of seismic wave in the 30m depth from the ground surface). For some developed countries such as Japan, there is an online source available, which can be downloaded directly. However, for China, there is no such source available, so this Vs30 parameters used in this study was estimated from U. S. National Earthquake Hazard Reduction Program (NEHRP: www.nehrp.gov/). According to the NEHRP, the Vs30 of the site can be estimated from the general rock compositions as indicated in Table 4-4.

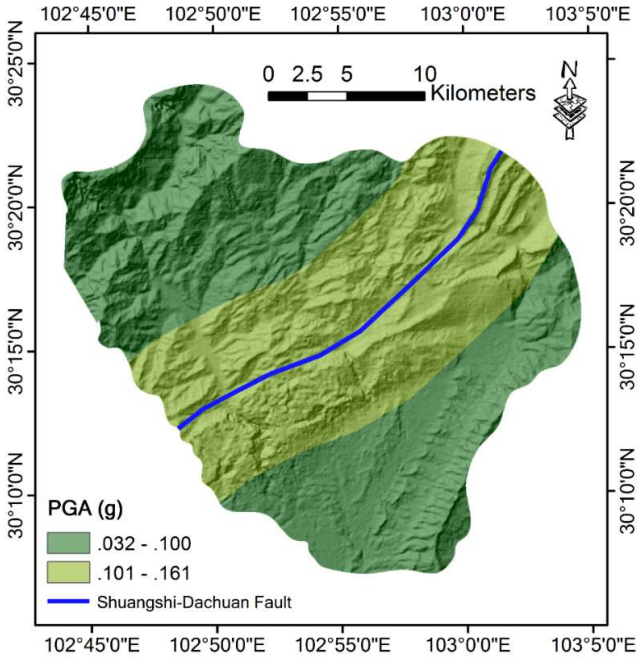

Figure 4-5 PGA map (Mw5.0) estimated from the Shuangshi-Dachuan fault

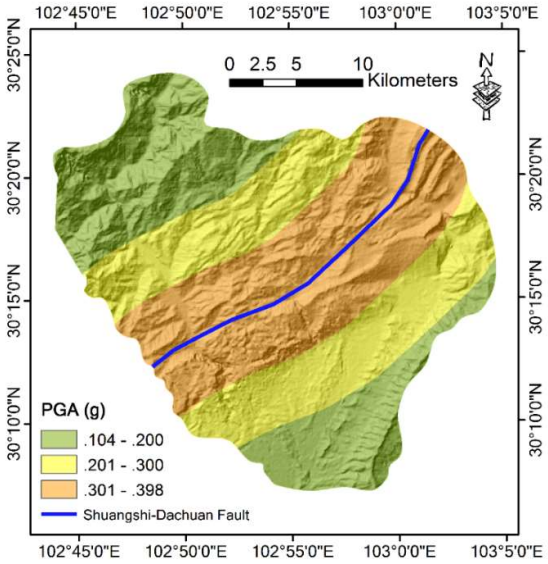

Figure 4-6 PGA map (Mw6.0) estimated from the Shuangshi-Dachuan

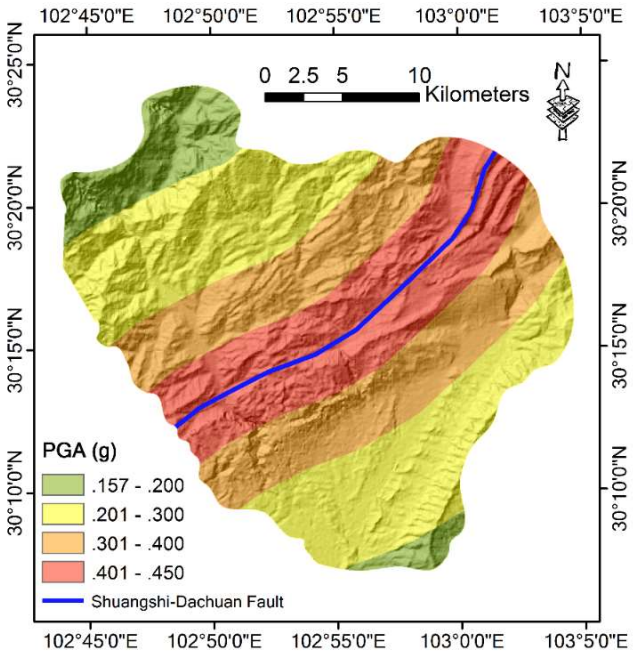

Figure 4-7 PGA map (Mw6.6) estimated from the Shuangshi-Dachuan

4.3.3 LANDSLIDE HAZARD MAPS CONSIDERING ASSUMED EARTHQUAKES

Geotechnical parameters, such as the strength parameters (friction angle and cohesion) typically has large spatial variabilities over the study area even within the same geologic units. To model such variability, Monte Carlo simulations are computationally simple way of probabilistically assessing such uncertainties. For the already mentioned geotechnical problems, homogeneous lithological units were considered, of which, shear strength parameters were given probability distribution functions. However, in practical engineering, the distribution of these geotechnical parameters around the expected mean value was not always symmetrical. The distribution of soil cohesion was in a clear lower bound such as zero, and generally, a few extreme large values also existed. This distribution seems to be better approximated by the asymmetrical function; however, it was accepted that many soil properties were reasonably well modelled by the lognormal distribution (Fenton and Griffiths 2004). In this study, while cohesion parameters were assumed to be β general distributions skewed to the right and friction angles to be log-

normally distributed. Due to sampling insufficiency, distribution functions of geotechnical parameters could not be realistically explored, and these uncertainties will thus lead to misclassifications of areas prone to landsliding after the shaking occurred. Meanwhile, as similarly discussed in Chigira and Yagi (2006), apparently mobile landslides and new landslides triggered by the Chuetsu event had rather larger apparent friction angles than previous seismic landslides in Japan due to the difference in the materials and the extent to saturation. As one of disadvantages for Monte Carlo simulations, the distribution obtained for the performance function is only accurate to the extent; hence, uncertainties from the above assumptions influenced the reliability of assessing seismic landslide hazards. In the method proposed, random numbers were generated to obtain the variables, mainly being geotechnical parameters; these variables were entered in the calculation of displacement.

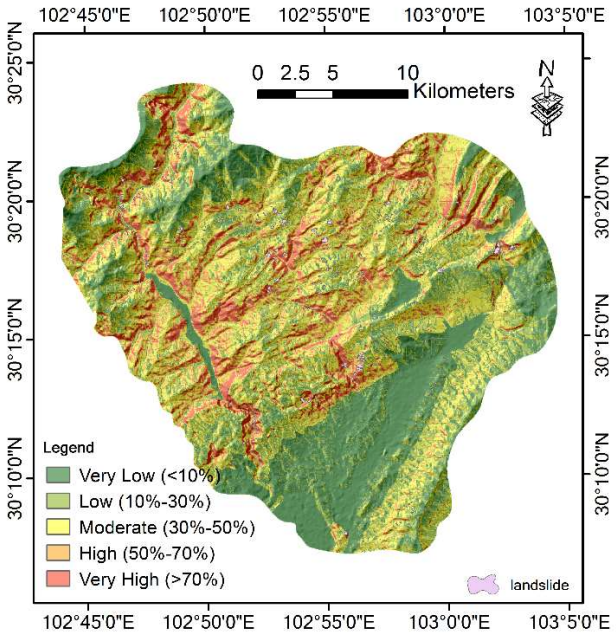

Figure 4-8 Landslide hazard maps by considering the PGA (Mw5.0)

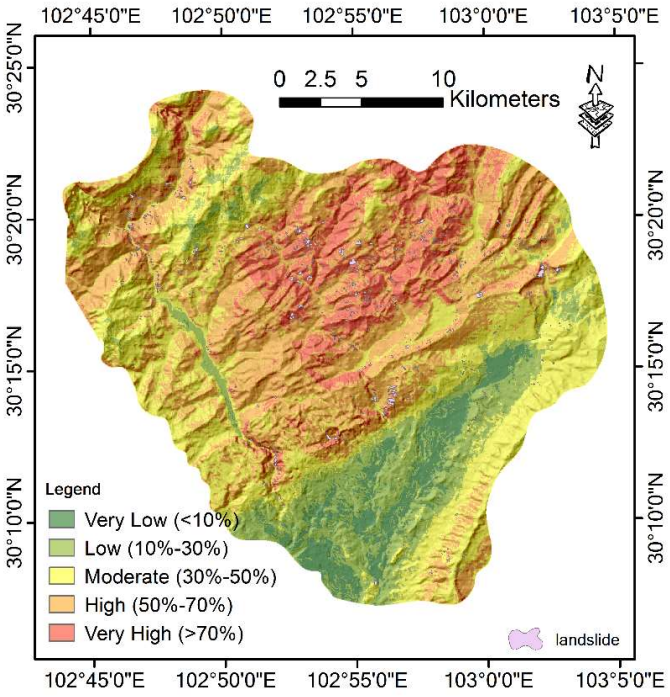

Figure 4-9 Landslide hazard maps by considering the PGA (Mw6.0)

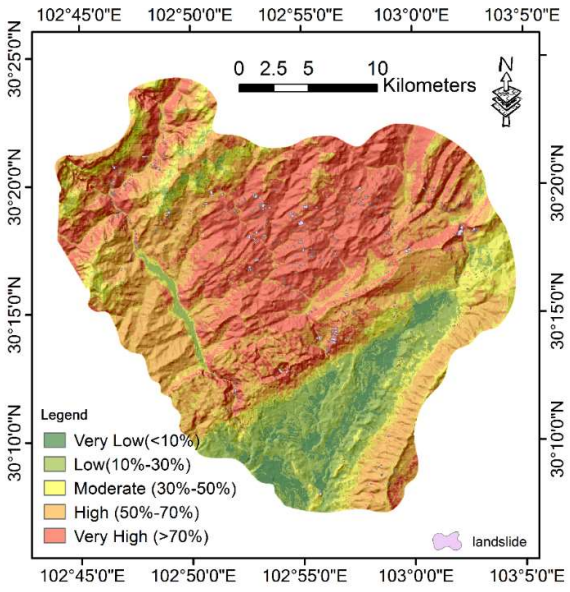

Figure 4-10 Landslide hazard maps by considering the PGA (Mw6.6)

In this study, the seismic force is set to the 25% of the PGA values, and the

factor of safety is set as 1.0. The Monte Carlo simulations ran 2,000 times and calculated 2,000 Fs values for each grid cell. The percentage of Fs, which is greater than 1.2, is calculated. The percentage were then shown as a map of seismic landslide hazard. In the study area, many shallow landslides occurred on steep slopes in the Lushan event. The final landslide hazard maps of this study area was classified into five categories: very low (<10%), low (10%-30%), moderate (30%–50%), high (50%-70%) and very high (>70%).

For the landslide hazard maps produced from the earthquake with the Mw6.6, which is real case. It can be seen that 41% of the total area was classified as having very low susceptibility, and the low-susceptibility zones were predicted to include 17.1% of the area. In the resulting map, it was also shown that about 38% of areas with landslide occurrence were classified as medium-high levels of landslide hazards. Compared with the actual landslides, moreover, it was demonstrated that several locations were misclassified to be areas not prone to landsliding after the earthquake occurrence. Using the same dataset in the Chapter 3, the validation result was shown in Table 4-5.

Table 4-5 Validation and comparison of the physically-based approach

No.	Method	Success rate	False-alarm rate	Miss-alarm rate
1	IV	68%	34%	27%
2	WoE	66%	35%	29%
3	LR	63%	38%	31%
4	SVM	74%	26%	27%
5	IV+LR	83%	9%	8%
6	WoE + LR	76%	11%	13%
7	IV+SVM	78%	8%	14%
8	WoE + SVM	81%	9%	10%
9	Physically	71%	42%	28%

From the comparison result, we can see the physically-based method can provide an acceptable result. It gives an overall success rate of 71%, However, comparing with the statistical methods mentioned before, the physically-based methods lower accuracy than some of statistical methods since it gives the highest false-alarm rate of 42% and a third highest miss-alarm rate of 28%. The biggest

advantages of the physically-based approaches over the statistical method is that it doesn't dependent on the historical landslide data and can consider the specified triggering event. As for the landslide hazard maps produced from the assumed earthquake scenarios (Figure 4-8 and Figure 4-9), it is hard to validate the results. However, these landslide hazard maps can serve as a reference for earthquake resistance design and urban planning in this regions.

4.4 CONCLUSIONS

In this chapter, functional module GeoLHM-P for effective landslide hazard mapping using a physically-based approach was developed and tested in the area affected by 2013 Lushan earthquake in China. In this chapter, the following conclusions can be drawn:

(1) A method was presented to evaluate the probability of slope failures on a pixel-by-pixel basis. A pseudo-static model, was adopted to calculate the slope stability in case of earthquake shaking.

(2) Under consideration of the variability of geotechnical parameters, the Monte Carlo simulations were used to evaluate probabilities of slope failures given a threshold of factor of safety. After deriving the factor of safety values from related inputs, the simulations ran 2000 times and yielded 2000 factor of safety values for each grid cell. Finally, the probabilities of values exceeding minimum factor of safety were shown as a map of seismic landslide hazards.

(3) Uncertainties arose from the variability of parameters used and the model itself; in other words, the impact of this sensitivity should be clarified in further research. Despite these limitations, it was found that GIS, as a powerful tool of spatial analyses, can facilitate the integration of pseudo-static modelling and Monte Carlo simulations over a regional seismic landslide hazard assessment.

(4) To consider the assumed earthquake from a specified fault or the target fault, the Next Generation of Ground-Motion Attenuation Models for the western United States (NGA-West2) was used to predict the PGA values

of each cell in the study area from different assumed earthquakes from the Shuangshi-Dachuan fault.

(5) Landslide hazard maps considering different PGA values from assumed earthquakes was produced. These landslide hazard maps can be used for future landslide mitigation, urban planning in this area.

(6) Comparing with the statistical methods mentioned before, the physically-based methods lower accuracy than some of statistical methods since it gives the highest false-alarm rate of 42% and a third highest miss-alarm rate of 28%. The biggest advantages of the physically-based approaches over the statistical method is that it doesn't dependent on the historical landslide data and can consider the specified triggering event.

REFERENCE

AKKAR, S. & BOMMER, J.J. 2007. Empirical prediction equations for peak ground velocity derived from strong-motion records from Europe and the Middle East. Bulletin of the Seismological Society of America, 97, 511–530, doi: 10.1785/0120060141.

ATKINSON, G.M. 2010. Ground-motion prediction equations for Hawaii from a referenced empirical approach. Bulletin of the Seismological Society of America, 100, 751–761, doi: 10.1785/0120090098.

ATKINSON, G.M. & BOORE, D.M. 1997. Stochastic Point-Source Modeling of Ground Motions in the Cascadia Region. Seismological Research Letters, 68, 74–85, doi: 10.1785/gssrl.68.1.74.

ATKINSON, G.M. & BOORE, D.M. 2006. Earthquake ground-motion prediction equations for eastern North America. Bulletin of the Seismological Society of America, 96, 2181–2205, doi: 10.1785/0120050245.

ATKINSON, G.M. & SILVA, W. 2000. Stochastic modeling of California ground motions. Bulletin of the Seismological Society of America, 90, 255–274, doi: 10.1785/0119990064.

BAKER, R., SHUKHA, R., OPERSTEIN, V. & FRYDMAN, S. 2006. Stability charts for pseudo-static slope stability analysis. Soil Dynamics and

Earthquake Engineering, 26, 813–823, doi: 10.1016/j.soildyn.2006.01.023.

BERTI, M., MARTINA, M.L. V, FRANCESCHINI, S., PIGNONE, S., SIMONI, A. & PIZZIOLO, M. 2012. Probabilistic rainfall thresholds for landslide occurrence using a Bayesian approach. Journal of Geophysical Research: Earth Surface, 117, doi: 10.1029/2012JF002367.

BINDI, D., PAROLAI, S., GROSSER, H., MILKEREIT, C. & DURUKAL, E. 2007. Empirical ground-motion prediction equations for northwestern Turkey using the aftershocks of the 1999 Kocaeli earthquake. Geophysical Research Letters, 34, doi: 10.1029/2007GL029222.

BOMMER, J.J., STAFFORD, P.J. & ALARCÓN, J.E. 2009. Empirical equations for the prediction of the significant, bracketed, and uniform duration of earthquake ground motion. Bulletin of the Seismological Society of America, 99, 3217–3233, doi: 10.1785/0120080298.

BOORE, D.M. 2003. Simulation of Ground Motion Using the Stochastic Method. Pure and Applied Geophysics, 160, 635–676, doi: 10.1007/PL00012553.

BOORE, D.M. 2009. Comparing stochastic point-source and finite-source ground-motion simulations: SMSIM and EXSIM. Bulletin of the Seismological Society of America, 99, 3202–3216, doi: 10.1785/0120090056.

BOORE, D.M. & ATKINSON, G.M. 2008. Ground-motion prediction equations for the average horizontal component of PGA, PGV, and 5%-damped PSA at spectral periods between 0.01 s and 10.0 s. Earthquake Spectra, 24, 99–138, doi: 10.1193/1.2830434.

Caflisch RE (1998) Monte Carlo and quasi-Monte Carlo methods. Acta Numer. 7:1.

CAMPBELL, K.W. 2003. Prediction of Strong Ground Motion Using the Hybrid Empirical Method and Its Use in the Development of Ground-Motion (Attenuation) Relations in Eastern North America. Bulletin of the Seismological Society of America, 93, 1012–1033, doi: 10.1785/0120020002.

CHEN, X.-L., LIU, C.-G., YU, L. & LIN, C.-X. 2014. Critical acceleration as a criterion in seismic landslide susceptibility assessment. Geomorphology, 217, 15–

22, doi: 10.1016/j.geomorph.2014.04.011.

CHOUDHURY, D. & SAVOIKAR, P. 2011. Seismic stability analysis of expanded MSW landfills using pseudo-static limit equilibrium method. Waste management & research : the journal of the International Solid Wastes and Public Cleansing Association, ISWA, 29, 135–145, doi: 10.1177/0734242X10375333.

CHOUSIANITIS, K., DEL GAUDIO, V., KALOGERAS, I. & GANAS, A. 2014. Predictive model of Arias intensity and Newmark displacement for regional scale evaluation of earthquake-induced landslide hazard in Greece. Soil Dynamics and Earthquake Engineering, 65, 11–29, doi: 10.1016/j.soildyn.2014.05.009.

CROZIER, M.J. & GLADE, T. 2012. Landslide Hazard and Risk: Issues, Concepts and Approach. In: Landslide Hazard and Risk. 1–39., doi: 10.1002/9780470012659.ch1.

GUZZETTI, F., CARRARA, A., CARDINALI, M. & REICHENBACH, P. 1999. Landslide hazard evaluation: A review of current techniques and their application in a multi-scale study, Central Italy. In: Geomorphology. 181–216., doi: 10.1016/S0169-555X(99)00078-1.

Harrison RL (2010) Introduction To Monte Carlo Simulation. AIP Conf Proc 1204:17–21. doi: 10.1063/1.3295638

HUTCHINGS, L. & WU, F. 1990. Empirical Green's Functions from small earthquakes: A waveform study of locally recorded aftershocks of the 1971 San Fernando Earthquake. Journal of Geophysical Research, 95, 1187, doi: 10.1029/JB095iB02p01187.

JIBSON, R.W., HARP, E.L. & MICHAEL, J.A. 2000. A method for producing digital probabilistic seismic landslide hazard maps. Engineering Geology, 58, 271–289, doi: 10.1016/S0013-7952(00)00039-9.

KAYASTHA, P., DHITAL, M.R. & DE SMEDT, F. 2013. Application of the analytical hierarchy process (AHP) for landslide susceptibility mapping: A case study from the Tinau watershed, west Nepal. Computers & Geosciences, 52, 398–408, doi: 10.1016/j.cageo.2012.11.003.

KURAHASHI, S. & IRIKURA, K. 2010. Characterized source model for simulating strong ground motions during the 2008 Wenchuan earthquake. Bulletin

of the Seismological Society of America, 100, 2450–2475, doi: 10.1785/0120090308.

Kwak YH, Ingall L (2007) Exploring Monte Carlo Simulation Applications for Project Management. Risk Manag 9:44–57. doi: 10.1057/palgrave.rm.8250017

Manousiouthakis VI, Deem MW (1999) Strict detailed balance is unnecessary in Monte Carlo simulation. J Chem Phys 110:2753. doi: 10.1063/1.477973

METROPOLIS N, ULAM S (1949) The Monte Carlo method. J Am Stat Assoc 44:335–341. doi: 10.1080/01621459.1949.10483310

MENA, B., MARTIN MAI, P., OLSEN, K.B., PURVANCE, M.D. & BRUNE, J.N. 2010. Hybrid broadband ground-motion simulation using scattering green's functions: Application to large-magnitude events. Bulletin of the Seismological Society of America, 100, 2143–2162, doi: 10.1785/0120080318.

MENDOZA, C. & HARTZELL, S. 2009. Source analysis using regional empirical Green's functions: The 2008 Wells, Nevada, earthquake. Geophysical Research Letters, 36, doi: 10.1029/2009GL038073.

PITARKA, A., SOMERVILLE, P., FUKUSHIMA, Y., UETAKE, T. & IRIKURA, K. 2000. Simulation of near-fault strong-ground motion using hybrid Green's functions. Bulletin of the Seismological Society of America, 90, 566–586, doi: 10.1785/0119990108.

POURGHASEMI, H.R., MOHAMMADY, M. & PRADHAN, B. 2012. Landslide susceptibility mapping using index of entropy and conditional probability models in GIS: Safarood Basin, Iran. Catena, 97, 71–84, doi: 10.1016/j.catena.2012.05.005.

RAJABI, A.M., KHAMEHCHIYAN, M., MAHDAVIFAR, M.R., DEL GAUDIO, V. & CAPOLONGO, D. 2013. A time probabilistic approach to seismic landslide hazard estimates in Iran. Soil Dynamics and Earthquake Engineering, 48, 25–34, doi: 10.1016/j.soildyn.2012.09.005.

Raychaudhuri S (2008) Introduction to monte carlo simulation. Simul Conf 2008 WSC 2008 91–100. doi: 10.1109/WSC.2008.4736059

Sobol IM (2001) Global sensitivity indices for nonlinear mathematical models and their Monte Carlo estimates. Math Comput Simul 55:271–280. doi:

10.1016/S0378-4754(00)00270-6

Sobol IM (1998) On quasi-Monte Carlo integrations. Math Comput Simul 47:103–112. doi: 10.1016/S0378-4754(98)00096-2

Swendsen RH, Wang JS (1986) Replica Monte Carlo simulation of spin-glasses. Phys Rev Lett 57:2607–2609. doi: 10.1103/PhysRevLett.57.2607

SCHERBAUM, F. 2006. The Estimation of Minimum-Misfit Stochastic Models from Empirical Ground-Motion Prediction Equations. Bulletin of the Seismological Society of America, 96, 427–445, doi: 10.1785/0120050015.

TIEN BUI, D., PRADHAN, B., LOFMAN, O., REVHAUG, I. & DICK, Ø.B. 2013. Regional prediction of landslide hazard using probability analysis of intense rainfall in the Hoa Binh province, Vietnam. Natural Hazards, 66, 707–730, doi: 10.1007/s11069-012-0510-0.

WANG, W.D., GUO, J., FANG, L.G. & CHANG, X.S. 2012. A subjective and objective integrated weighting method for landslides susceptibility mapping based on GIS. Environmental Earth Sciences, 65, 1705–1714, doi: 10.1007/s12665-011-1148-z.

Wang Y (2011) Quantum Monte Carlo simulation. Ann Appl Stat 5:669–683. doi: 10.1214/10-AOAS406

WESTEN, C.J., ASCH, T.W.J. & SOETERS, R. 2006. Landslide hazard and risk zonation—why is it still so difficult? Bulletin of Engineering Geology and the Environment, 65, 167–184, doi: 10.1007/s10064-005-0023-0.

XU, C., XU, X., SHYU, J.B.H., GAO, M., TAN, X., RAN, Y. & ZHENG, W. 2015. Landslides triggered by the 20 April 2013 Lushan, China, Mw 6.6 earthquake from field investigations and preliminary analyses. Landslides, 12, 365–385, doi: 10.1007/s10346-014-0546-1.

YANG, C. WEI, ZHANG, J. JING, FU, X., ZHU, C. BIN & BI, J. WEI. 2014. Improvement of pseudo-static method for slope stability analysis. Journal of Mountain Science, 11, 625–633, doi: 10.1007/s11629-013-2756-8.

YAO, H., CAMPMAN, X., DE HOOP, M. V. & VAN DER HILST, R.D. 2009. Estimation of surface wave Green's functions from correlation of direct waves,

coda waves, and ambient noise in SE Tibet. Physics of the Earth and Planetary Interiors, 177, 1–11, doi: 10.1016/j.pepi.2009.07.002.

YIN, Y., WANG, F. & SUN, P. 2009. Landslide hazards triggered by the 2008 Wenchuan earthquake, Sichuan, China. Landslides, 6, 139–152, doi: 10.1007/s10346-009-0148-5.

YUE, H. & LAY, T. 2013. Source rupture models for the Mw 9.0 2011 Tohoku earthquake from joint inversions of high-rate geodetic and seismic data. Bulletin of the Seismological Society of America, 103, 1242–1255, doi: 10.1785/0120120119.

ZHOU, S. & FANG, L. 2015. Support vector machine modeling of earthquake-induced landslides susceptibility in central part of Sichuan province, China. Geoenvironmental Disasters, 2, 2, doi: 10.1186/s40677-014-0006-1.

CHAPTER 5

5 DEVELOPMENT OF GEOLHM-R FOR LANDSLIDE HAZARD MAPPING CONSIDERING THE LANDSLIDE AFFECTED AREA

5.1 INTRODUCTION

According to the United States Geology Survey (U.S.G.S.), an ideal landslide hazard map shows not only the chances that a landslide may form at a particular place, but also the chance that it may travel downslope a given distance. To assess whether an area is potentially hit by a landslide is thus one of the most essential part of landslide hazard assessment. Up to now, most of LHM methods only focus on the landslide prone slopes, and the affected areas are not included. Some LHM include the affected areas but they are estimated empirically based on slope heights. For example, the affected area is generally estimated based on the way given by Sediment Disaster Countermeasures for Sediment Disaster Prone Areas Act in Japan. It is a big challenge to estimate the affected area based on kinematics in LHM. In this chapter, a run-out simulation technique is developed based on modified multiple flow algorithm and the law of conservation of energy. The elevation difference between cells is taken into account for determining the possible directions towards which the landslide can move with a certain probability. The law of conservation of energy is used to determine the distance of sediment movement. When the mechanical energy from both the kinetic and potential energy becomes less than the friction-induced energy loss, the movement of landslide will stop so that the maximum affected area can be estimated. The method is incorporated into

the functional module GeoLHM-R. A practical example of the Aso Ohashi Bridge landslide triggered during the 2016 Kumamoto earthquake is made by using the module and its practicality has been verified.

5.2 METHODOLOGY

To simulate the runout of the landslide source, a run-out simulation technique is developed based on modified multiple flow algorithm and the law of conservation of energy. Generally, the proposed method contains two parts: Firstly, the multiple flow direction algorithm in the GIS is used to determine the possible path of the landslide sources; and to determine the runout extent of the landslide source, the energy conservation law is incorporated. The movement directions is controlled by flow direction and persistence functions.

5.2.1 FLOW DIRECTION

Terrain surfaces are usually modelled with raster datasets. A raster is a matrix of cells organized in rows and columns. Each cell in the matrix represents a square unit of area and contains a numeric value that is a measurement or estimate of elevation for that location.

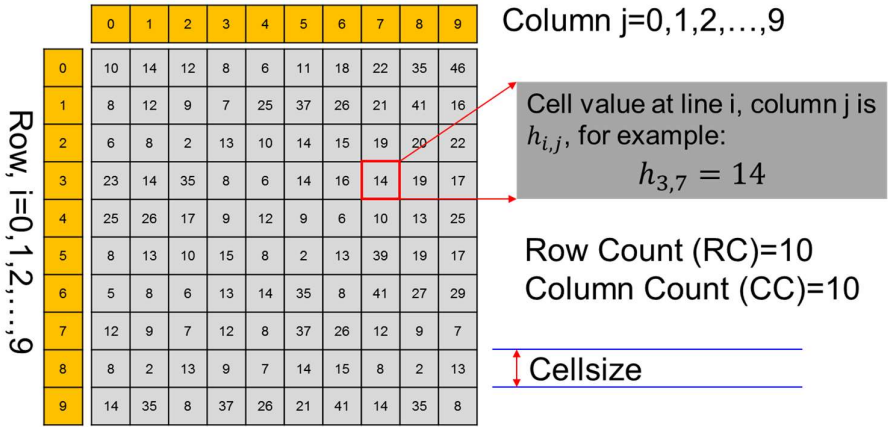

	0	1	2	3	4	5	6	7	8	9
0	10	14	12	8	6	11	18	22	35	46
1	8	12	9	7	25	37	26	21	41	16
2	6	8	2	13	10	14	15	19	20	22
3	23	14	35	8	6	14	16	14	19	17
4	25	26	17	9	12	9	6	10	13	25
5	8	13	10	15	8	2	13	39	19	17
6	5	8	6	13	14	35	8	41	27	29
7	12	9	7	12	8	37	26	12	9	7
8	8	2	13	9	7	14	15	8	2	13
9	14	35	8	37	26	21	41	14	35	8

Figure 5-1 A terrain surface

For each cell $h_{i,j}$,we can obtain 3×3table, with $h_{i,j}$ cantered.

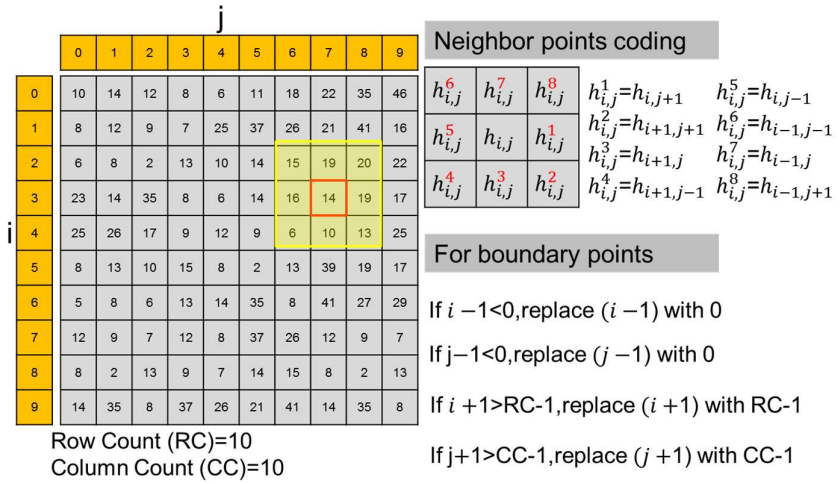

Figure 5-2 Cell coding in calculation of the flow direction

Flow Direction Algorithms in Geographic information system is one of the useful methods to simulate downslope movement of masses on the terrain surface. Although the flow direction algorithm is often used to model hydrology and the physical movement of water on a terrain surface, some applications of the flow direction algorithm were also found as a means of searching paths with least costs. A common approach to describing these downslope movements is to assume that materials moving downslope exclusively follow the path of steepest descent.

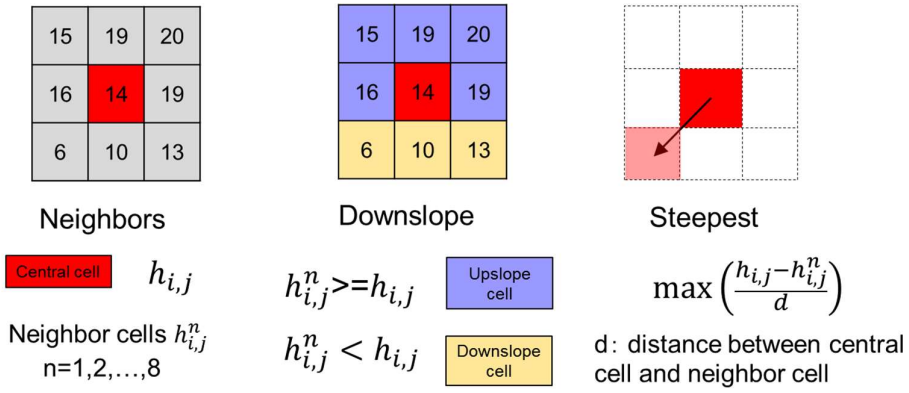

Figure 5-3 Single flow direction in GIS

In the GIS environment, single flow direction of each source cell is derived from central cell to its steepest downslope neighbours and can be used to describe the mass movement path with maximum likelihood as indicated in Figure 5-3. As

an improvement, the Multi-Flow Direction algorithms is similar to that of the single direction algorithm above in that direction of flow is a function of steepness between the source cell and its neighbours, the difference being that Multi-Flow Direction algorithm calculates the flow to multiple downslope cells in proportion to the steepness between them as indicated in Figure 5-4. The likelihoods of all possible paths is in proportion to the steepness between the centrals and the neighbours.

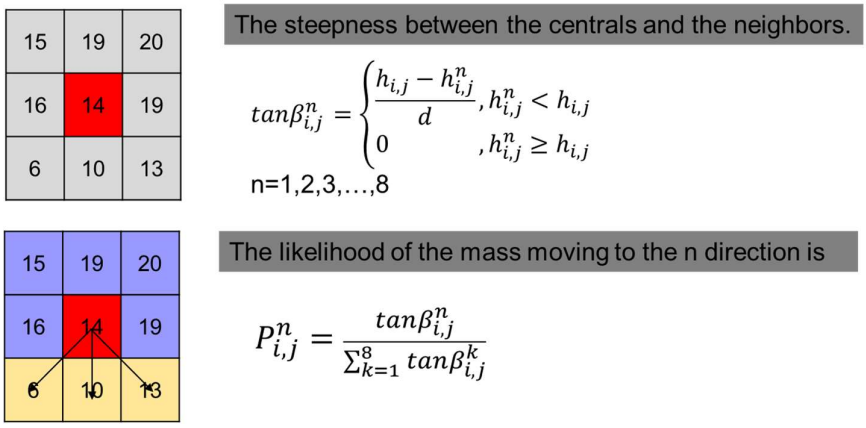

Figure 5-4Multiple flow direction in GIS

To optimize this algorithm, Freeman (1991) gave the slopes power weights, and tested the performance of a number of values to control the divergence of the multiple flow algorithm. This model is given formally given by:

$$P_{i,j}^{n} = \frac{(tan\beta_{i,j}^{n})^{\alpha}}{\sum_{k=1}^{8} (tan\beta_{i,j}^{n})^{\alpha}} \tag{5.1}$$

where i, j are the spatial location of the source cell, $P_{i,j}^{n}$ the likelihood that the source cell will go to the neighbour cell in direction n, $tan\beta_{i,j}^{n}$ is a tangent of the slope gradient to describe the steepness between the source cell and the neighbour cell in direction n, and α the divergence exponent. For α = 1 the algorithm becomes the original MFD. When α increases to the infinite, the algorithm turns to be the single flow direction. This divergence exponent is used to control the movement spreading and to reproduce a wide range of other flow accumulations. Based on the field, laboratory measurements and back analysis of real cases,

Horton et al. (2011) and Horton et al. (2013) suggested the exponent value of 4 for debris flows and shallow landslides.

5.2.2 INERTIAL FORCE

During the movement of the landslide source, the inertial force should also be considered. The Inertial force function (Eq. 2) is used to describe the behaviour of inertia force inherited from the original movement of landslide sources, and it is calculated based on the change between the original direction and the new direction (see Fig. 5.4).

$$R_{i,j}^{n} = w_{\alpha(i)} \tag{5.2}$$

where $R_{i,j}^{n}$ is the likelihood of the movement from the source cell to the direction i according to the inertial resistance, and $\alpha(i)$ is the difference of the directions between the original direction and the new direction from the source. Three implementations of the persistence were chosen (Table 5.1). In every Inertial force function, the neighbour cell opposed to the original direction is set to null to avoid backward movement of the landslide source.

Table 5-1 Persistence function in the assessment of the spreading (Horton et al. 2013)

$\Delta\alpha$	0	45	90	135	180
Proportion	1	0.8	0.4	0	0
Cosines	1	0.707	0	0	0
Gamma (2000)	1.5	1	1	1	0

5.2.3 OVERALL LIKELIHOOD OF MOVEMENT

Finally, the overall likelihood of mass movement from the source cell to it 8 neighbour cells can be calculated by a weighted combination of the likelihood from the flow movement and the inertial resistance and can be shown in Eq. (5.3)

$$L_{i,j}^{n} = \frac{R_{i,j}^{n} \times P_{i,j}^{n}}{\sum_{n=1}^{n=8} R_{i,j}^{n} \times P_{i,j}^{n}} L_{i,j} \tag{5.3}$$

where i, j are the location of the central cells, $L_{i,j}^{n}$ is final calculated likelihood of source movement from the central cell to its neighbour cell in direction n, and $L_{i,j}$ the previously inherited possibility of the landslide occurrence in the central cell.

The result of Eq. (5.3) is a 3×3 matrix with assigned likelihood of mass movement from the central cell to its neighbours. After obtaining of such an matrix, the additional step is to check whether the mass can move from the central cell to its neighbours according to energy conservation.

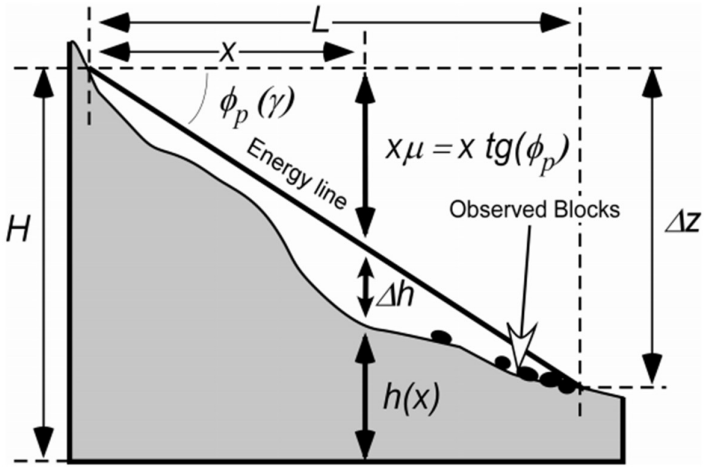

Figure 5-5 Energy conservation (Loye et al. 2008a and Loye et al. 2008b)

5.2.4 ENERGY CONSERVATION

In order to check the energy conservation during the mass movement from the central cell to its neighbours, the simple friction laws is used to calculated the energy loss during the mass movement; During the mass movement from the central cell to any neighbour cell, the energy conservation can be expressed as the follows:

$$E_{i,j}^{n} = E_{i,j} + E_{dh}^{n} - E_{f}^{n} \tag{5.4}$$

Where $E_{i,j}$:kinetic energy at the central cell, E_{dh}^{n}:increase in potential energy due to elevation difference from the central cell to the n direction neighbor cell (Equation 5.5). E_{f}^{n}:energy lost due to friction, during the path from the central cell to the n

direction neighbour cell (Equation 5.6). μ: friction coefficient g: gravitational acceleration; d: distance between central cell and neighbor cell.

$$E_{dh}^{n}=\mathrm{g}^{*}(h_{i,j}-h_{i,j}^{n}),\ n\epsilon\{1,2,3,\ldots.,8\} \tag{5.5}$$

$$E_{f}^{n}=\mu*g*d\ ,\ n\epsilon\{1,2,3,\ldots.,8\} \tag{5.6}$$

During the process of mass movement:

$$\begin{cases} E_{i,j}^{n}\geq 0, popagation\ \ to\ \ the\ \ n\ \ direction\ \ is\ \ possible \\ E_{i,j}^{n}<0, popagationto\ \ the\ \ n\ \ direction\ \ is\ \ impossible \end{cases} \tag{5.7}$$

Judged by the energy conservation, When the mechanical energy from both the kinetic and potential energy becomes less than the friction-induced energy loss, the movement of landslide will stop so that the maximum affected area can be estimated.

5.2.5 FLOWCHART OF GEOLHM-R

The process of the computation involved in the GeoLHM-R for estimation of landslide affected area is illustrated in Fig.5 7. The runout simulation considers the whole landslide source cells in the study area at the same time, which is usually a binary raster in the GIS with landslide cell indicated as “1” and non-landslide cells indicated as “0”.

Then each landslide cell in landslide rasters is transferred into the current active cells list (see Fig. 6). From active cells list, each landslide cell is calculated one by one according to the multiple flow direction algorithm. During each step of each landslide cell simulation, a likelihood of movement is calculated using the proposed method. At the end of each simulation step, the neighbour cells with a positive likelihood of will be added to the end of the active cell list as a new active cell. The process is repeated until the current active cell list is empty. For each cell in the landslide rasters, just repeat the calculation one by one. The output of the simulation is a raster, in which all the cells with positive value represent the potential area that can potentially be reached by landslides.

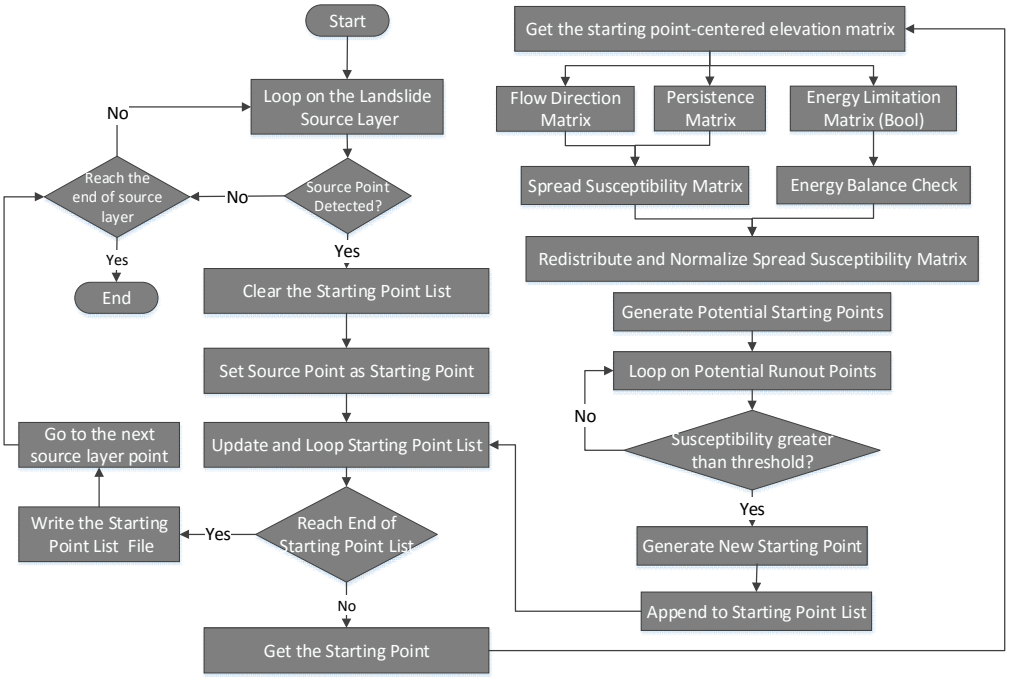

Figure 5-6 Flow Chart of the main process within GeoLHM-R

5.3 CASE STUDY

5.3.1 ASO OHASHI LANDSLIDE

On May 4,2016, an site investigation found that cracks had also formed on the upper part of the slope, posing a continuing danger of another major slide. The JR Hohi Line and National Route 57 run by the bottom of the slope, and private houses are scattered about nearby. Officials say, however, that none of the residents are at home as an evacuation order is already in effect. According to the regional development bureau, there was about 500,000 cubic meters of earth and other materials in the some 700-metre-long, 200-meter-wide landslide that wiped away the Aso Ohashi bridge.

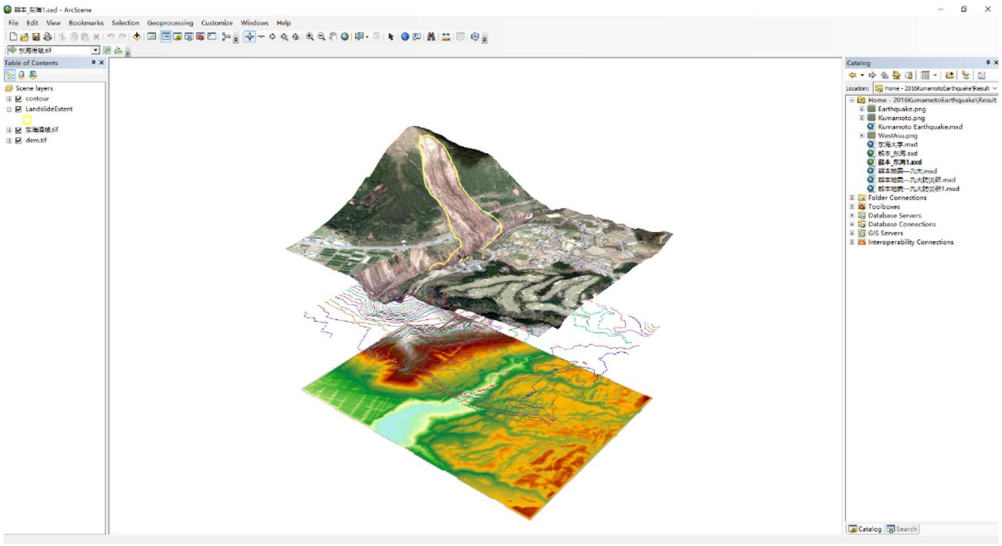

Figure 5-7Interpretation of the Aso Ohashi Bridge landslide

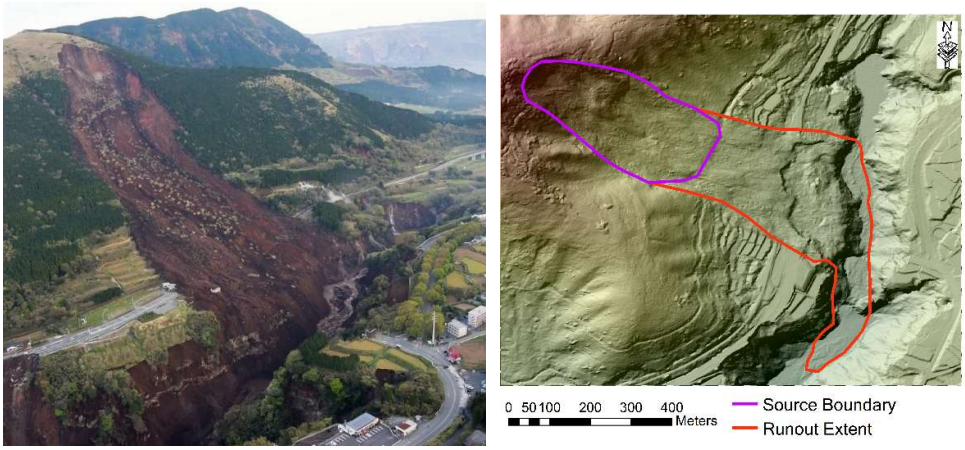

Figure 5-8 Image showing the Aso Ohashi Bridge landslide

5.3.2 BACK ANALYSIS OF THE FRICTION COEFFICIENT

In the proposed method, maximum runout distance and extent of the landslide movement is determined by the frictional coefficient, a field survey is sometimes difficult to be conducted because the unavailability of track to reach the landslide sources. Also, it is not realistic to identify the frictional coefficient for every landslide, since the original purpose of this approach is to facilitate a regional scale analysis of a large number of landslides. Thus, the frictional coefficient can be

identified by reduction of lithology strength.

In practical, firstly, lithological composition of potential landslide sources was identified from the lithological maps, then the friction coefficient μ can be approximately estimated at $\mu = \tan\phi$, where ϕ is the inner friction angle of the landslide masses.

For the study case, the main composition of the landslides was deposits and volcanic ashes and weathered volcanic rocks. The friction angle of the lithology is estimated from a collection of previous literatures of landslides with similar composition (Inoue et al. 1970; Miyagi 2004; Mikami and Sawada 2005; Sassa et al. 2005). Generally, the inner friction angle of the masses ranges from 14° -20° , thus ,an estimated frictional coefficient ranging from 0.25-0.36.

Further, we carried out a back analysis of the coefficient with input value of 0.25, 0.30, 035. (Figure5.9)

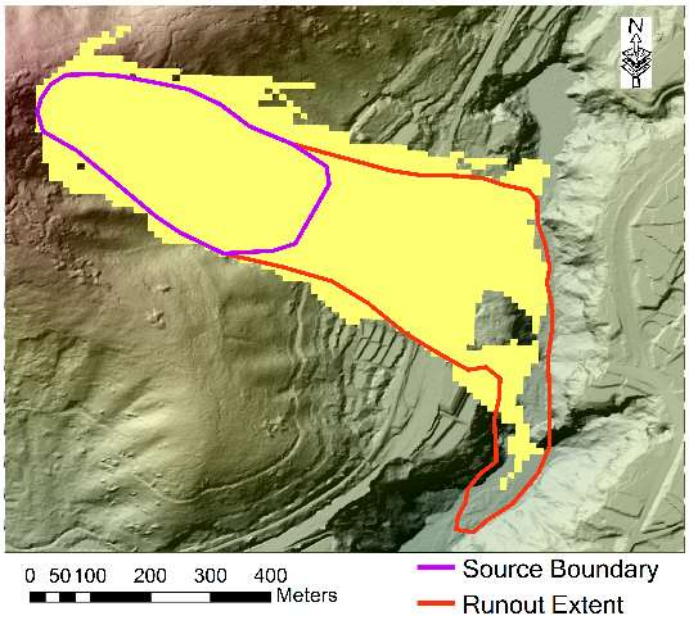

(a) $\mu = 0.25$

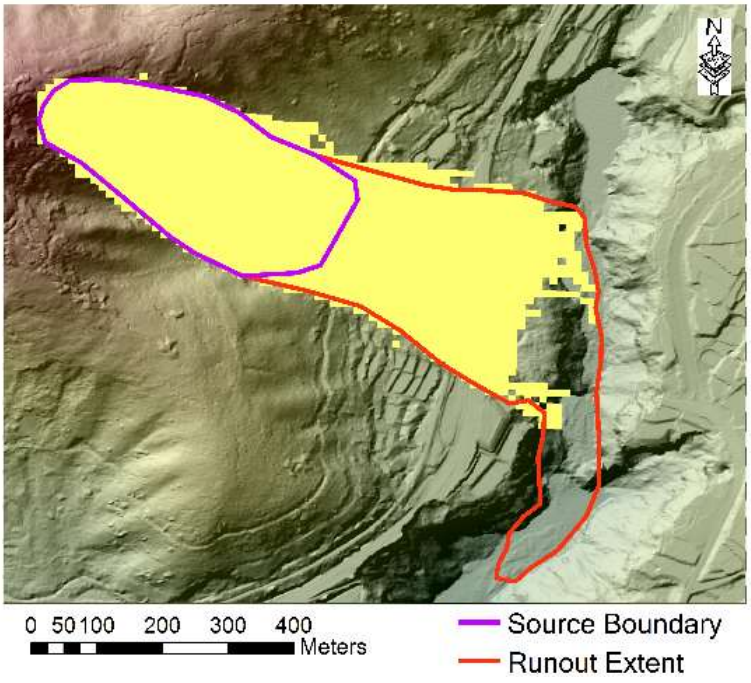

(b) μ = 0.30

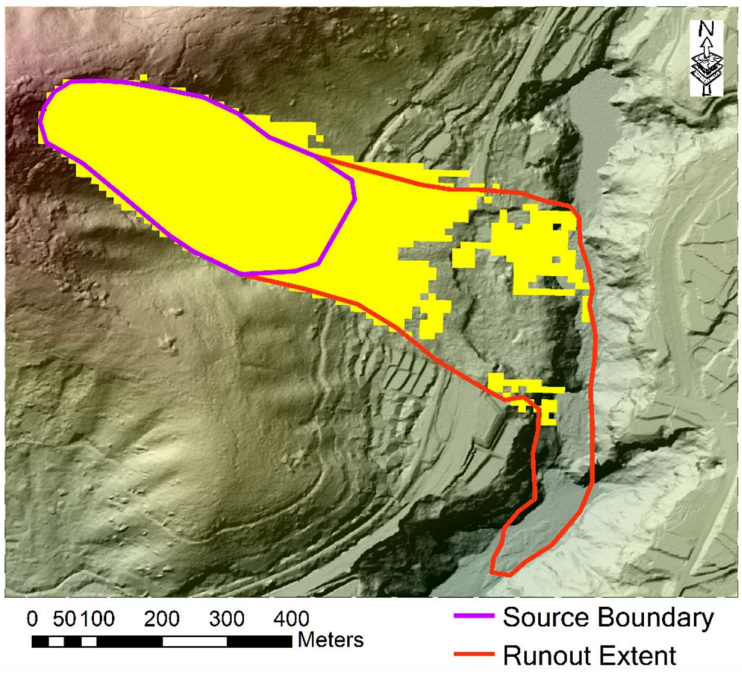

(c) μ = 0.35

Figure 5-9 Runout simulation results of the landslide μ = 0.30

As indicated by the back analysis result ,the frictional coefficient showed the

best fitting result to describe the estimated affected area of a landslide.

5.4 CONCLUSION

Estimation of landslide affected area plays an important role in landslide hazard mapping. Up to now, most of LHM methods only focus on the landslide prone slopes, and the affected areas are not included. Some LHM include the affected areas but they are estimated empirically based on slope heights. A functional module of GeoLHM-R for landslide hazard mapping considering the affected area of a landslide based on the runout simulation is proposed and tested in this chapter. The following conclusions can be drawn:

(1) A run-out simulation technique is developed based on modified multiple flow algorithm and the law of conservation of energy. In the proposed technique, the elevation difference between cells is taken into account for determining the possible directions towards which the landslide can move with a certain probability. The law of conservation of energy is used to determine the distance of sediment movement.

(2) A practical examples of the Aso Ohashi Bridge landslides triggered during the 2016 Kumamoto earthquake was carried out and test the efficiency of the module.

(3) One of its main advantages of the proposed module lies in its low data requirement, only the DEM data and potential landslide source are needed for runout prediction. This makes is possible to be applied to predict the landslide affected area at the regional scale. The proposed technique and the developed module had provided a solution to fill the gap exists in landslide prone slope identification and affected area estimation.

(4) The practical example shows that the maximum runout distance and extent were largely depended on the surface friction coefficient. It is suggested that frictional coefficient can be obtained either by inferred from the lithology map or by back-analysis of existing landslide cases.

(5) Once the potential landslide source is identified and proper frictional coefficient values is determined, reliable landslide effected area can be

mapped.

REFERENCE

Ayalew, L. and Yamagishi, H. (2005) The application of GIS-based logistic regression for landslide susceptibility mapping in the Kakuda-Yahiko Mountains, Central Japan. Geomorphology 65(1), 15-31.

Carrara, A., Guzzetti, F., Cardinali, M. and Reichenbach, P. (1999) Use of GIS technology in the prediction and monitoring of landslide hazard. Natural hazards 20(2-3), 117-135.

Carrara, A., Cardinali, M., Detti, R., Guzzetti, F., Pasqui, V. and Reichenbach, P. (1991) GIS techniques and statistical models in evaluating landslide hazard. Earth surface processes and landforms 16(5), 427-445.

Clerici, A., Perego, S., Tellini, C. and Vescovi, P. (2002) A procedure for landslide susceptibility zonation by the conditional analysis method. Geomorphology 48(4), 349-364.

Baeza, C. and Corominas, J. (2001) Assessment of shallow landslide susceptibility by means of multivariate statistical techniques. Earth surface processes and landforms 26(12), 1251-1263.

Kelarestaghi, A. and Ahmadi, H. (2009) Landslide susceptibility analysis with a bivariate approach and GIS in Northern Iran. Arabian Journal of Geosciences 2(1), 95-101.

Lee, S. and Pradhan, B. (2007) Landslide hazard mapping at Selangor, Malaysia using frequency ratio and logistic regression models. Landslides 4(1), 33-41.

Pradhan, B. and Lee, S. (2010a) Delineation of landslide hazard areas on Penang Island, Malaysia, by using frequency ratio, logistic regression, and artificial neural network models. Environmental Earth Sciences 60(5), 1037-1054.

Solaimani, K., Mousavi, S.Z. and Kavian, A. (2013) Landslide susceptibility mapping based on frequency ratio and logistic regression models. Arabian Journal of Geosciences 6(7), 2557-2569.

Regmi, A.D., Devkota, K.C., Yoshida, K., Pradhan, B., Pourghasemi, H.R.,

Kumamoto, T. and Akgun, A. (2014) Application of frequency ratio, statistical index, and weights-of-evidence models and their comparison in landslide susceptibility mapping in Central Nepal Himalaya. Arabian Journal of Geosciences 7(2), 725-742.

Pourghasemi, H.R., Pradhan, B., Gokceoglu, C., Mohammadi, M. and Moradi, H.R. (2013) Application of weights-of-evidence and certainty factor models and their comparison in landslide susceptibility mapping at Haraz watershed, Iran. Arabian Journal of Geosciences 6(7), 2351-2365.

Montgomery, D.R. and Dietrich, W.E. (1994) A physically based model for the topographic control on shallow landsliding. Water resources research 30(4), 1153-1171.

Terlien, M.T., Van Westen, C.J. and van Asch, T.W. (1995) Geographical information systems in assessing natural hazards, pp. 57-77, Springer.

Salciarini, D., Godt, J.W., Savage, W.Z., Conversini, P., Baum, R.L. and Michael, J.A. (2006) Modeling regional initiation of rainfall-induced shallow landslides in the eastern Umbria Region of central Italy. Landslides 3(3), 181-194.

Pradhan, B. (2011) Use of GIS-based fuzzy logic relations and its cross application to produce landslide susceptibility maps in three test areas in Malaysia. Environmental Earth Sciences 63(2), 329-349.

Pourghasemi, H.R., Pradhan, B. and Gokceoglu, C. (2012) Application of fuzzy logic and analytical hierarchy process (AHP) to landslide susceptibility mapping at Haraz watershed, Iran. Natural hazards 63(2), 965-996.

Pradhan, B. and Lee, S. (2010b) Regional landslide susceptibility analysis using back-propagation neural network model at Cameron Highland, Malaysia. Landslides 7(1), 13-30.

Zare, M., Pourghasemi, H.R., Vafakhah, M. and Pradhan, B. (2013) Landslide susceptibility mapping at Vaz Watershed (Iran) using an artificial neural network model: a comparison between multilayer perceptron (MLP) and radial basic function (RBF) algorithms. Arabian Journal of Geosciences 6(8), 2873-2888.

Yao, X., Tham, L. and Dai, F. (2008) Landslide susceptibility mapping based on support vector machine: a case study on natural slopes of Hong Kong, China.

Geomorphology 101(4), 572-582.

Pradhan, B. (2013) A comparative study on the predictive ability of the decision tree, support vector machine and neuro-fuzzy models in landslide susceptibility mapping using GIS. Computers & Geosciences 51, 350-365.

Xu, C., Dai, F., Xu, X. and Lee, Y.H. (2012a) GIS-based support vector machine modeling of earthquake-triggered landslide susceptibility in the Jianjiang River watershed, China. Geomorphology 145, 70-80.

Wei-Min, W., Jin-Lai, H. and Zhen-Xing, Y. (2013) Preliminary result for rupture process of Apr. 20, 2013, Lushan Earthquake, Sichuan, China. CHINESE JOURNAL OF GEOPHYSICS-CHINESE EDITION 56(4), 1412-1417.

Freeman TG (1991) Calculating catchment area with divergent flow based on a regular grid. Comput Geosci 17:413–422. doi: 10.1016/0098-3004(91)90048-I

Horton P, Jaboyedoff M, Rudaz B, Zimmermann M (2013) Flow-R, a model for susceptibility mapping of debris flows and other gravitational hazards at a regional scale. Nat Hazards Earth Syst Sci 13:869–885. doi: 10.5194/nhess-13-869-2013

Horton P, Jaboyedoff M, Zimmermann M, et al (2011) Flow-R, a model for debris flow susceptibility mapping at a regional scale - some case studies. Proc 5th Int Conf Debris-Flow Hazards Mitig Mech Predict Assess 875–884. doi: 10.4408/IJEGE.2011-03.B-095

Inoue Y, Honsho S, Matsushima M, Esashi Y (1970) Geological and soil mechanical studies on the slides occurred during the 1968 Toakachioki earthquake in southeastern area of Aomori Prefecture. Report, vol. 69086. Central Research Institute of Electric Power Industry, pp 1–27

Jaboyedoff M, Labiouse V (2011) Technical note: Preliminary estimation of rockfall runout zones. Nat Hazards Earth Syst Sci 11:819–828. doi: 10.5194/nhess-11-819-2011

Loye A, Pedrazzini A, Jaboyedoff M (2008a) Preliminary regional rockfall hazard mapping using LiDAR-based slope frequency distribution and CONEFALL modelling. 4th Can Conf Geohazards From Causes to Manag 445–452.

Loye A, Pedrazzini A, Jaboyedoff M (2008b) Regional indicactive rockfall

map using Lidar-based slope slope frequency histogram and confall modelling. In: Interdisciplinary Rockfall Workshop. pp 64–66

CHAPTER 6

6 A PRACTICAL APPLITION TO ANALYZING THE 2016 KUMAMOTO EARTHQUAKE-INDUCED LANDSLIDES IN JAPAN

6.1 INTRODUCTION

In previous chapters, we have developed an integrated GIS-based landslide hazard mapping system. In addition, a series of cases were carried out to test the efficiency of the three functional modules, separately. Although significant developments have been achieved, there are still some problems in practical engineering cases. Therefore, in this chapter, we aimed to apply the developed system to analysing the 2016 Kumamoto Earthquake-induced landslides in Japan as a full case study to verify the efficiency of the developed system.

The 2016 Kumamoto earthquake consists of a series of powerful shocks, including a foreshock on April 14th, 2016, with a moment magnitude of Mw 6.2 (at local time 21:26) and a Mw 7.0 main shock on April 16th, 2016 (at local time 01:25). The epicenter of the foreshock (32.740°N,130.800°E) at a depth of 10 km and the epicenter of the main shock (32.800°N,130.800°E) at a depth of 11 km located beneath the Kumamoto City of the Kumamoto Prefecture in Japan. An intense aftershock sequence followed the earthquake. On 9th October 2005, highest numbers of aftershocks (122) were recorded and as of April 20, 2016, a total of 1,778 aftershocks were recorded. The Kumamoto earthquake represents the most catastrophic event in Japan since the 2011 Tohoku Earthquake and had caused a large number of landslides, which had caused serious damages.

Right after the Kumamoto earthquake, several institutions had provided unprecedented amount of data for studying the landslides triggered by the Kumamoto earthquake. Especially, the Geospatial Information Authority of Japan had published a large quantity of high-resolution images for post-earthquake rescue. These images had provided a value information for our study.

In this chapter, we focus on the need for evaluating and assessing the landslides hazards triggered by the Kumamoto Earthquake. The structure of this chapter is organized as follows: We firstly mapped the location and extent of landslides associated with the earthquake using the high-resolution satellite images and aerial photography taken next days following the main shocks. Then, we produce a hazard map using the proposed two combined methods, one is the combined method of information value and the logistic regression and another is the combined method of information value and the support vector machine. After that, we performed the landslide hazard mapping using the GeoLHM-P module, one of the biggest difference of this method is that it can consider the future assumed earthquakes. Finally, the affected area of landslides triggered by during the Kumamoto Earthquake were simulated using the GeoLHM-R. All the landslide hazard maps produced in of this chapter were compare with the landslide hazard maps made using the traditional empirical method suggested by the Act on Sediment Disaster Countermeasures for Sediment Disaster Prone Areas of Japan.

6.2 BACKGROUND OF 2016 KUMAMOTO EARTHQUAKE

The 2016 Kumamoto earthquakes are a series of earthquakes, including a magnitude 7.0 main shock which struck at 01:25 JST on April 16, 2016 (16:25 UTC on April 15) beneath Kumamoto City of Kumamoto Prefecture in Kyushu Region,Japan, at a depth of about 10 kilometres and a foreshock earthquake with a magnitude 6.2 at 21:26 JST (12:26 UTC) on April 14, 2016, at a depth of about 11 kilometres. The two earthquakes killed at least 29 people and injured about 3,000 others in total. Severe damage occurred in Kumamoto and Oita Prefectures, with numerous structures collapsing and catching fire. More than 44,000 people have been evacuated from their homes due to the disaster.

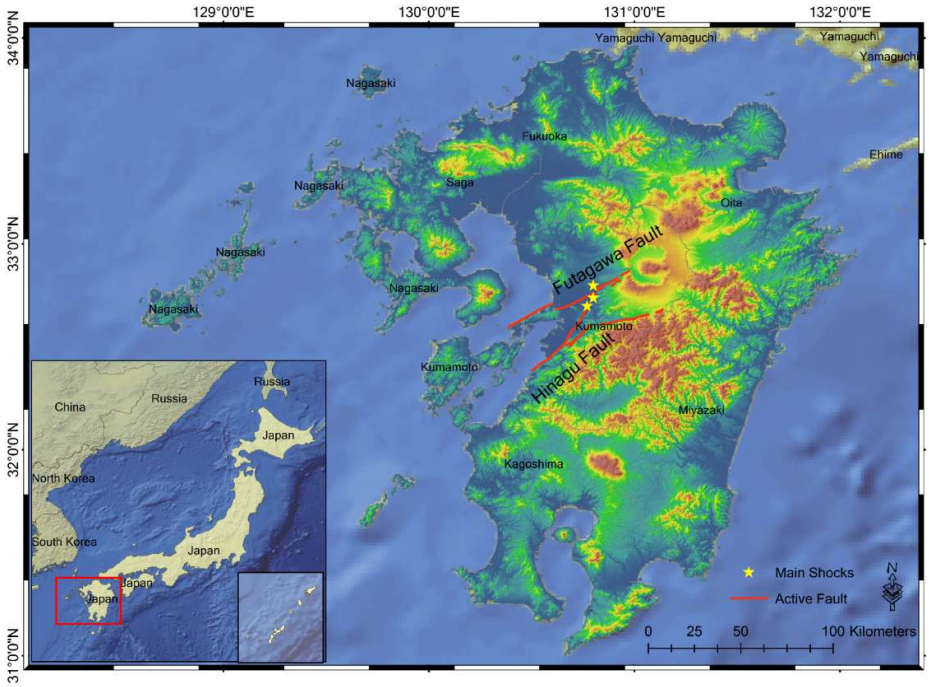

Figure 6-1 Brief introduction of the 2016 Kumamoto earthquake

6.3 STUDY AREA

According to the right-after damage estimation report published by the National Research Institute for Earth Science and Disaster Resilience (NIED), the most severely damaged zones of the Kumamoto earthquake was the northeast part of Kumamoto Prefecture, and several high-resolution images were published covering this area. Therefore, the study area, shown by the red rectangle in Fig. 6.2, including: Aso-shi, Ozu-machi, Takamori-machi, Nishihara-mura, Minamiaso-mura and Mashiki-machi. An enlarged view of the study area is also shown in Fig. 6.1 with elevation data from the Ecoris Inc. (©1995-2016) with a cellsize of 10m. Total relief within the study area approximately ranges from 3 meters to 1591 meters above the sea level. Geographically the study area is located between latitude 32°40′–33°10′ South and longitude 130° 45′–131°20′East, encompassing 931 km^2 (Fig. 1). In total, the land area is equivalent to 12.57% of the land area of the Kumamoto Prefecture. Mount Aso (1592 m), an extensive active volcano, located in the centre of the study area.

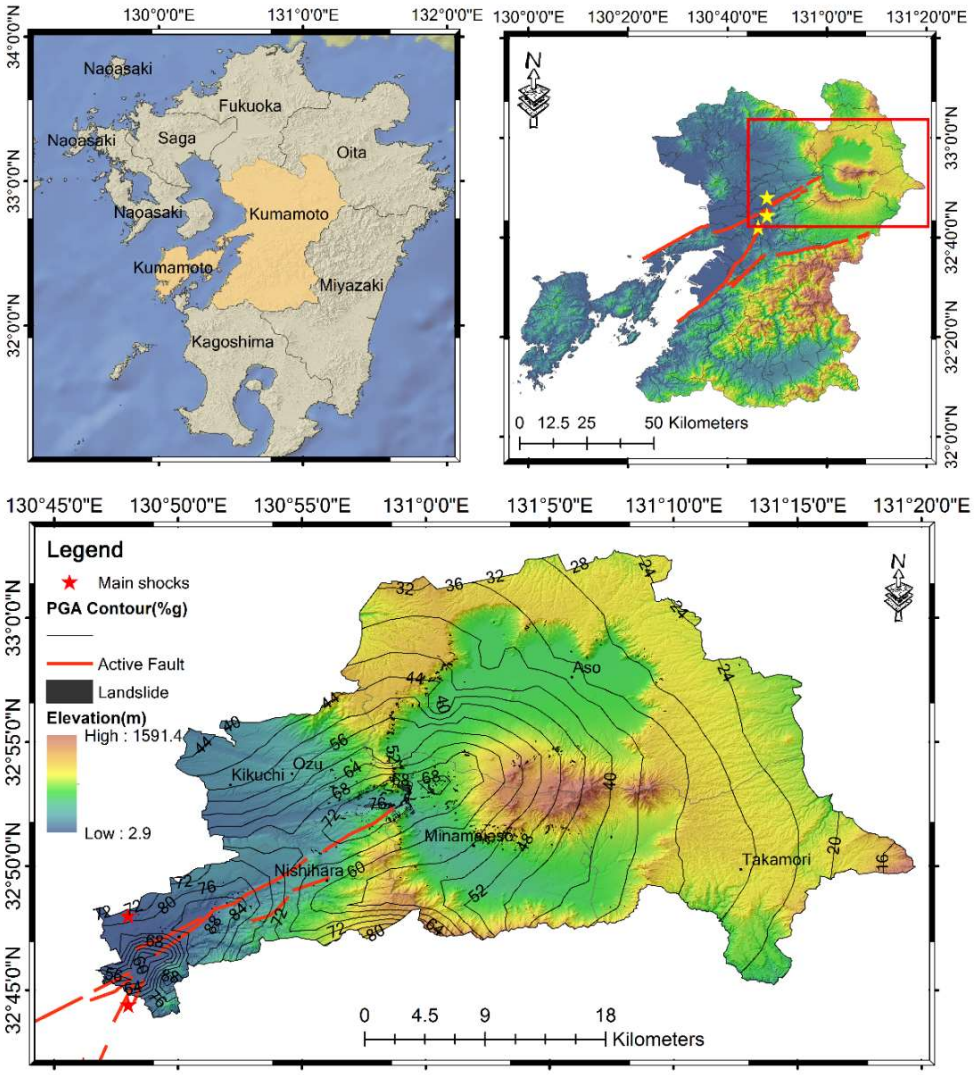

Figure 6-2 Overview of the study area showing the extent of the study area

Geological formations in the study area generally can be grouped into the following categories: deposits and terrace; sedimentary; metamorphic; ultramafic; volcanic and plutonic. Since the Mountain Aso is an active volcanic, the volcanic rocks including the felsic, mafic and pyroclastic volcanic rocks takes a large percentage of the study area. The study area lies at the southern end of the Japan Median Tectonic Line, Japan's longest, where a system of active faults forks in two directions at the Beppu-Haneyama Fault Zone. Specifically, the series of quakes ruptured the 81-km-long Hinagu Fault and 64-km-long Futagawa Fault to its north,

as well as lesser but discernable interaction with the farther flung Beppu-Haneyama Fault Zone. A 27-km section of the Futagawa Fault Zone slid 3.5 meters. The earthquakes are occurring along the Beppu–Shimabara graben, with epicentres moving from west to east over time.

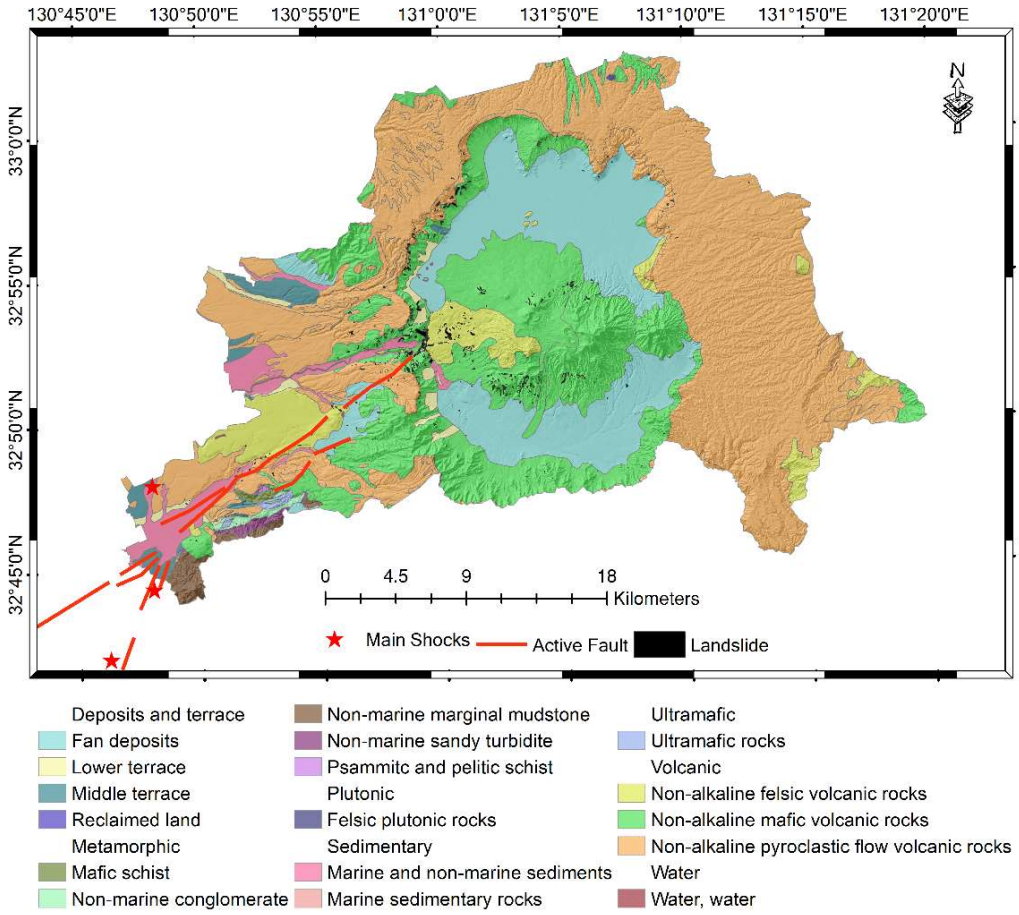

Figure 6-3 Geology map of the study area

6.4 LANDSLIDE INVENTORY MAPPING

Interpretation of remote sensing photographs (including satellite image and aerial photos) has been considered to be the most efficient and realistic way for identifying landslide in wide area. Currently, studies on automatic extraction of landslides through remote sensing images become important topics in engineering, geology and other related fields. However, visual-interpretation by well-trained

personnel is still believed to be more accurate and reliable than computers. Visual interpretation needs high skills and the results largely depended on the experience of the interpreters.

In this study, inventory of co-seismic landslides was produced through visual interpretation of online high-resolution images The interpretation procedures including the following 5 steps: (1) Define the extent of the study area;(2) Divide the study area in to several grids; (3) Create an empty GIS shapefile to store the landslide information; (4) Load the high-resolution images; (5) Visual interpretation of landslides. Experts in earthquakes and geo-hazards were called upon to visually interpret the base map according to their experiences and knowledge. Because it was right time for vegetation, earthquake-induced landslides could be easily recognized according to landslide scars. The boundaries of landslides were interpreted on the base map and transformed into vector format. The resultant landslide inventory was shown in Figure 6.5.

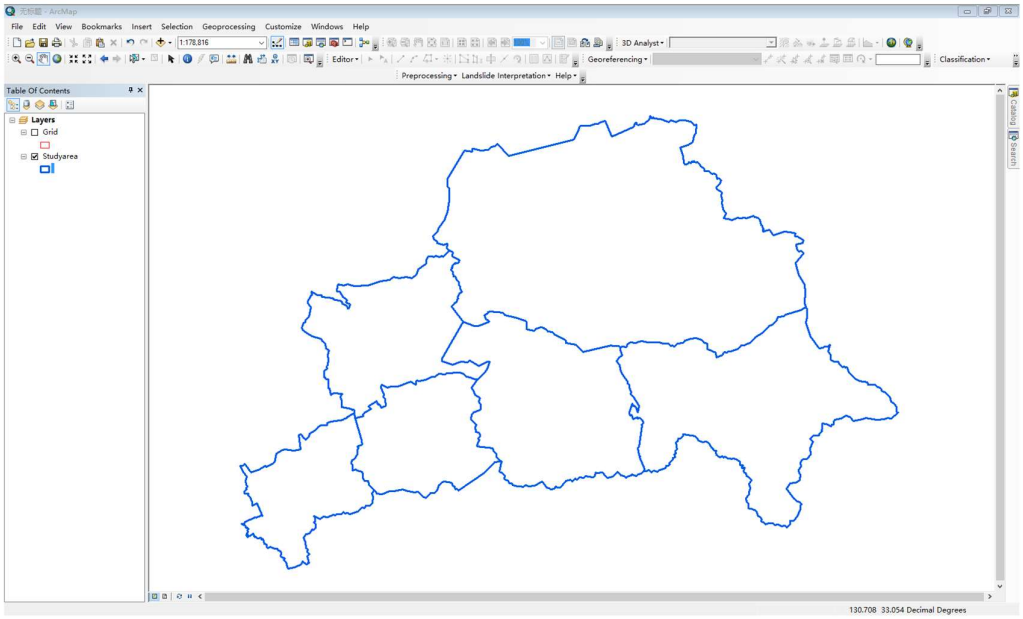

(a)

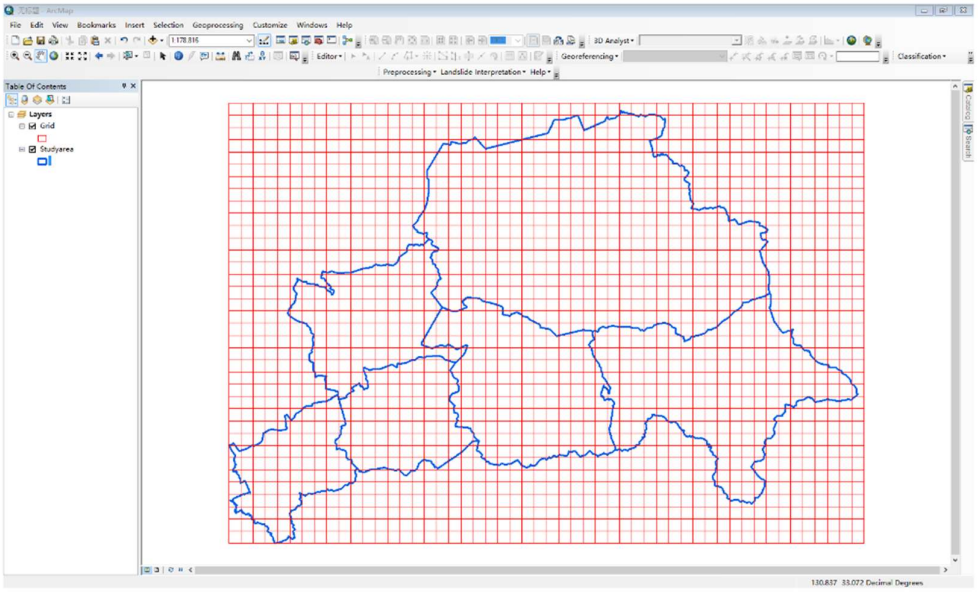

(b)

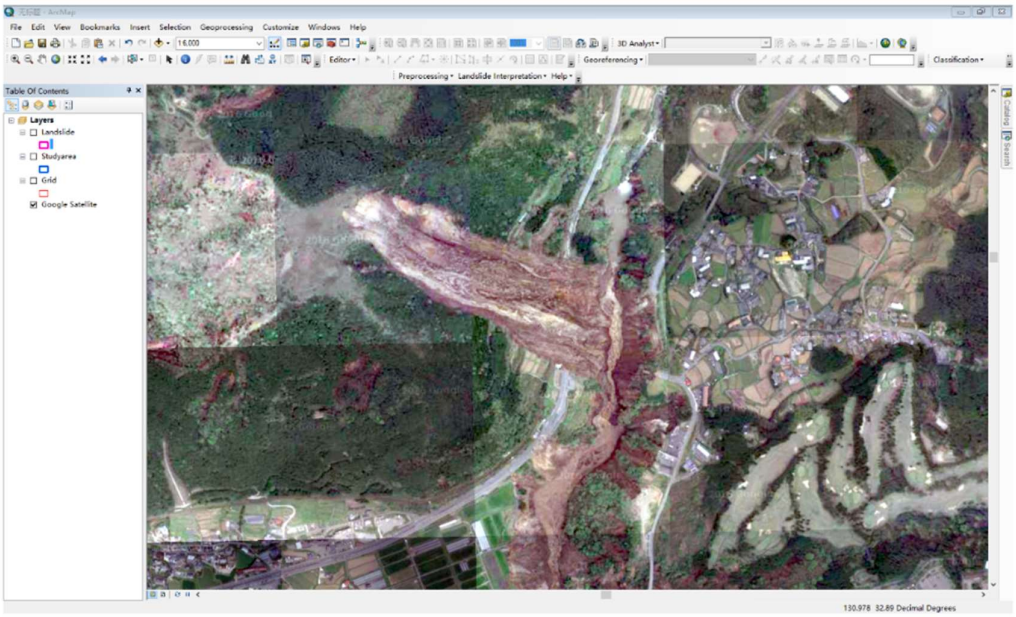

(c)

Figure 6-4 Main steps for mapping of landslides triggered by the 2016 Kumamoto Earthquake

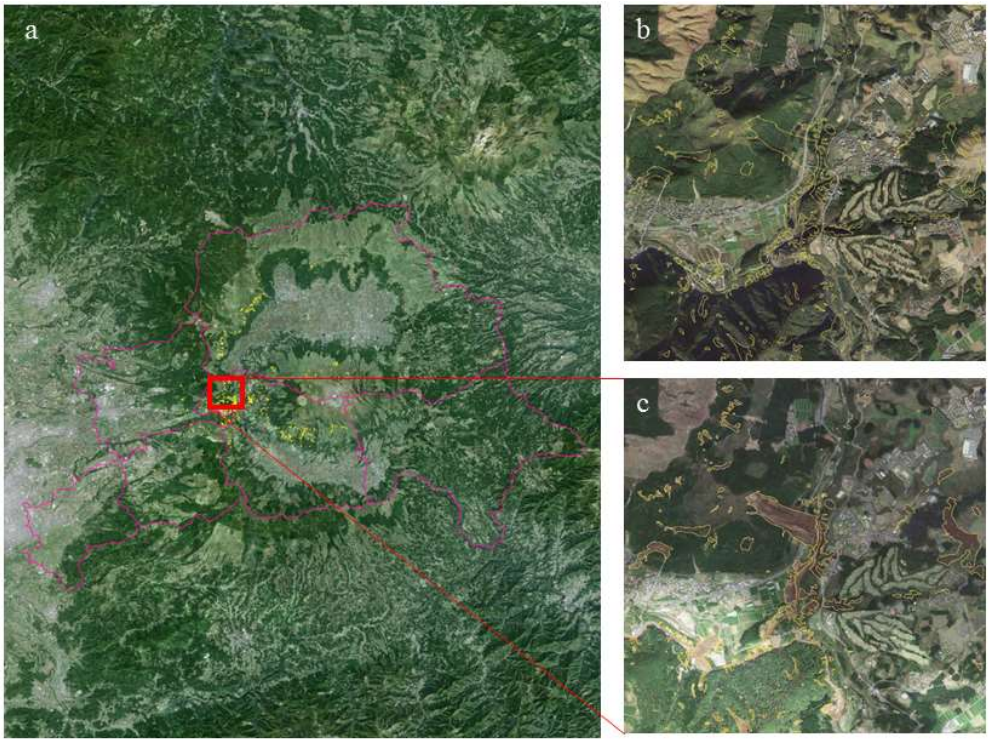

Figure 6-5 Results of landslides based on high-resolution images published on Google Earth. (a) Overview of study area (pink lines) and landslides (yellow polygons) overlaid on the google earth. (b) Pre-earthquake (December 18, 2015) and Post-earthquake (April 16,2016) image of the sample area showing the location and extent of landslides triggered by the Kumamoto earthquake. The sample area extent was indicated in (a) as red polygon.

6.5 LANDSLIDE HAZARD MAPPING USING GEOLHM-S

6.5.1 LANDSLIDE PREDICTIVE FACTORS

Generally speaking, the conditioning factors are responsible for the occurrence of landslide in specific region. These factors are needed to be used in landslide hazard mapping (Liu and De Smedt, 2005), which can be in nominal, ordinal, or scale format (Park et al., 2013). For current research the conditioning factors are: slope, aspect, elevation, distance to stream, topographic wetness index (TWI), drainage density, distance to fault, geology, landform, normalized difference vegetation index (NDVI), peak ground acceleration (PGA), terrain roughness, stream power index (SPI), plan curvature, profile curvature. The list of the

conditioning factors and their characteristics is shown in Table 6.1. Each factor was resized to 10 × 10 m grid and the grid of the study area was constructed by 2795 columns and 2850 rows. For FR analysis, manual defined method was used to classify each conditioning factor and the list of all the data layers is illustrated in Fig. 6.6.

Elevation is one of the topographic factors that directly affect slope instability (Wan et al., 2012). Other parameters such as precipitation and weathering variations are considered as indirect factors. In this study, the elevation map was obtained from the altitude which was generated using survey of Japan topographic map sheets of the Kumamoto area (1984, 1995 and 2011). The elevation of the study area ranges from 3m to 1591m. This factor of elevation was manually classified into 8 classes (<200m; 200-400m; 400-600m; 600-800m; 800-1000m; 1000-1200m; 1200-1400m; >1400m). One of the most important conditioning factors in the slope stability analysis is the slope angle. For this reason, the slope map of the study area was prepared from the elevation map, and it was divided into 11 slope categories by an increment of 5° from 5-° 50°, less than 5° and greater than 50°. In landslide hazard mapping studies, slope aspect is also considered to be an important conditioning factor (Baeza and Corominas, 2001), since aspect-related parameters such as exposure to sunlight and drying winds, control the concentration of the soil moisture which is directly related to the landslide occurrence (Magliulo et al., 2008). In the case of the aspect map, ten classes have been made (flat, North, Northeast, East, Southeast, South, Southwest, West and Northwest).

Generally, plan curvature is considered to be geometry of the earth surface, and it describes a slope changes in the inclination or aspect (Nefeslioglu et al. 2008). The convergence or divergence of water during downhill flow is affected by plan curvature (Yilmaz et al. 2012). In this study, the plan curvature was extracted from the DEM and classified into four classes: −3.17–0.40, −0.40–0.00, −0.00–0.43, and 0.43–3.22. Profile curvature is defined as the curvature in the vertical plane parallel to the slope direction (Yilmaz et al. 2012). It describes the rate of change of slope and can be used as an influencing factor for landslide in the study area. For

this reason, in the same way as for plan curvature was also derived from the DEM with the aid of ArcGIS 10.0 and classified into four classes: −3.79–0.48, −0.48–0.02, −0.02–0.43, and 0.43–4.49, respectively.

Several active geological faults exist in the study area, so we should take distance to faults into account for landslides susceptibility analysis. In general, geological faults are responsible for triggering a large number of landslides, because the tectonic breaks usually decrease the surrounding rock strength. In the study area, the faults buffer categories were defined as <1000, 1000–2000, 2000–3000, 3000–4000, and >4000 m. In the study area, there are a widely distributed large number of small rivers and its branches. Water is considered to be the basic factor for triggering landslide mechanisms. In many areas all over the world, rivers play an important role in the occurrence of landslides (Park et al. 2013). In view of the current study, distance to rivers was considered. thirteen buffer classes (50 m, 100 m, 150 m, 200 m, 250 m, 300 m, 350 m, 400 m, 450 m, 500 m, 1000m, 1500m and 2000m) were made using the buffer tool. In the SPI (-36.0-29.6) and drainage density maps, ten categories were created for each of the analysis. The drainage density map was obtained by using the digitized drainage layer made by the Survey of Japan (1984, 1985 and 1996) and has been divided into six classes. In the TWI (1.84–33.02) map, ten categories were created.

NDVI, namely the normalized difference vegetation index, is a measure of surface reflectance and gives a quantitative estimate of the vegetation growth and biomass (Yilmaz 2009; Pourghasemi et al. 2013b). In this study, the normalized difference vegetation index (NDVI) map was derived from the satellite images, and the NDVI was also considered in preparing landslide susceptibility maps. The NDVI value is calculated as follows:

$$\mathrm{NDVI} = \frac{IR - R}{IR + R} \tag{6-1}$$

where IR is the infrared portion of the electromagnetic spectrum and R is the red portion of the electromagnetic spectrum. The NDVI values vary from −0.27 to 0.62,

and a map of NDVI was classified into five classes.

Lithology is also frequently used in landslide stability studies and plays a very important role in landslide susceptibility analyses, because different lithological units have different susceptibility degrees (Dai et al. 2001; Yalcin et al. 2011). The lithology map of the study area was derived from geological maps and field surveys. Table 1 shows the description of geological units of the study area. The study area is covered by six lithological units such as deposits and terrace; sedimentary; metamorphic; ultramafic; volcanic and plutonic.

The peak ground acceleration (PGA) map of Padang Pariaman District was derived from the measured ground motion maps published by the United States Geology Survey (USGS). It showed the PGA value of the main shock of the Kumamoto earthquake with a magnitude of Mw7.0 on April 16th, 2016. The PGA map was divided into the following five subclasses as: <=0.3g, 0.3-0.4g; 0.4-0.6g; 0.6-0.8g; >0.8g, where g is the gradational acceleration.

6.5.2 Application of the Bivariate Methods (IV and WoE)

The information value method and the Weight of evidence method was produced using the weights for each class of each conditioning factor. Through analysing the relationship between 14 conditioning factors and landslide occurrence, the information value was calculated (Table 6.1).

Table 6.1 represents the relationship between landslide event and the classes of each conditioning factor. Results of the information value method showed that in the case of the relationship between landslide occurrence and elevation, landslide mostly occurred in the elevation range of 200–400 m. It showed that the probability of landslide occurrence is very low in low elevation areas. It also can be seen that, the higher the slope gradient is, the more favourable the slope is to landslide occurrence. In the case of the aspect, the ratio was high for the class of south and southeast facing slopes, having ratios of 0.518 and 0.478 respectively. For the profile and plan curvature, higher curvature values were more favourable in

predicting landslides. The most effective class of lithology group was the volcanic rocks. For SPI, the information value was highest (1.54) for the class of 8.32–29.60, and it was lowest (-0.753) for the class of -0.97-0.56. The highest value for PGA classes as main contributors of landslide belonged to the category of 0.6-0.8 g with a value of 1.002. In the case of s normalized difference vegetation index, the highest IV value (68.03) was related to the low vegetation cover. As for the factor of distance to stream and fault, it shows that, the further the distance is, the low effects of the stream and fault on landslide occurrence is. Also, as the terrain become rougher, it becomes more favourable to landslide occurrence.

Table 6-1 Landslide predictive factors used for statistical LHM

Factor	Class	IV	Wcontrast	Factor	Class	IV	Wcontrast
Elevation (m)	<200	-1.507	-1.612	Stream power index (SPI)	-36.0 - -5.1	1.520	1.571
	200-400	0.942	1.093		-5.1 - -2.77	0.480	0.514
	400-600	0.283	0.388		-2.77 - -0.97	-0.455	-0.504
	600-800	0.014	0.021		-0.97 - 0.56	-0.753	-1.035
	800-1000	-0.510	-0.615		0.56 - 1.34	-0.025	-0.040
	1000-1200	-0.693	-0.711		1.34 - 29.6	1.540	1.763
	1200-1400	-1.756	-1.766	Terrain wetness index (TWI)	1.84-4.0	1.349	1.433
	>1400	0.000	0.000		4.0-6.0	0.221	0.419
Slope gradient (°)	<5	-2.408	-2.725		6.0-8.0	-0.367	-0.501
	5-10	-0.651	-0.750		8.0-10.0	-0.410	-0.464
	10-15	-0.276	-0.316		10.0-12.0	-0.214	-0.227
	15-20	-0.137	-0.154		>12.0	-0.709	-0.731
	20-25	0.108	0.120	Drainage density	<4	-0.376	-0.434
	25-30	0.470	0.516		4-8	0.332	0.581
	30-35	0.806	0.875		8-12	-0.009	-0.014
	35-40	1.219	1.313		12-16	-1.154	-1.234
	40-45	1.555	1.646		16-20	-3.355	-3.373

	45-50	1.951	2.032		20-24	0.000	0.000
	>50	2.301	2.389	Distance to fault (m)	1000	0.721	0.807
Aspect	Flat	0.000	0.000		2000	1.370	1.562
	North	-0.253	-0.290		3000	0.859	0.932
	NorthEast	-0.278	-0.304		4000	0.667	0.705
	East	0.518	0.594		5000	0.122	0.127
	SouthEast	0.478	0.554		10000	0.304	0.393
	South	-0.002	-0.002		15000	-0.408	-0.494
	SouthWest	-0.069	-0.079		20000	-2.140	-2.341
	West	-0.156	-0.181		25000	-4.604	-4.765
	NorthWest	-0.297	-0.341		30000	0.000	0.000
Profile Curvature	<-5	0.936	0.990	Lithology	Deposits and terrace	-1.517	-1.693
	-5 - -2	0.258	0.288		Sedimentary	-0.601	-0.617
	-2 - 2	-0.335	-0.981		Metamorphic	-2.353	-2.370
	2 - 5	0.556	0.632		Ultramafic	0.000	0.000
	>5	1.223	1.313		Volcanic	0.219	1.603
Plan Curvature	<-5	1.230	1.287		Plutonic	0.000	0.000
	-5 - -2	0.643	0.721		Water	0.000	0.000
	-2 - 2	-0.236	-0.875	Normalized difference vegetation index (NDVI)	<0.15	0.822	0.888
	2 - 5	0.314	0.347		0.15-0.30	-0.376	-0.475
	>5	0.864	0.894		0.30-0.45	0.196	0.268
Distance to sream(m)	50	0.218	0.254		0.46-0.60	-0.120	-0.152
	100	-0.195	-0.218		>0.60	-0.032	-0.042
	150	-0.525	-0.574	PGA (g)	<=0.3	-3.378	-3.595
	200	-0.507	-0.550		0.3-0.4	-1.728	-2.012
	250	-0.280	-0.303		0.4-0.6	0.208	0.321
	300	-0.432	-0.461		0.6-0.8	1.002	1.592
	350	-0.240	-0.256		>0.8	0.000	0.000
	400	0.139	0.148	Terrain	<4	-1.787	-2.175

	450	0.232	0.246	roughness	4-8	-0.390	-0.509
	500	0.222	0.233		8-12	0.033	0.042
	1000	0.472	0.607		12-16	0.939	1.151
	1500	-0.287	-0.289		16-20	1.830	2.058
	2000	0.000	0.000		>20	2.262	2.315

As for the weight of evidence method (WoE), generally, it showed the same trends with the information value method. The highest value of weights occurred in the class of 200-400 meters in elevation, greater than 50° and east facing slopes. The lithology map is one of the predictive factors that have direct impacts on landslide occurrence. For the lithology group, the highest weights of 1.603 was obtained in the class of volcanic rocks. In terms of the triggering factors, the class of 0.6-0.8g gave the highest weights of 1.592. The result showed that for a terrain with higher roughness, it is more susceptible to landslides. For the stream power index and terrain wetness index, the high weights occurred in the area with higher values, both in negative and positive. The results also indicated that areas where it is more curved both in profile and plan were more susceptible to landslides. For the factors produced from buffering of distance to the fault, it also a decreasing tendency of possibilities of landslide occurring with the increase of the distances. As a comparison, the highest weights was produced by the class of 500-1000m.

6.5.3 APPLICATION OF THE MULTIVARIATE METHODS (LR AND SVM)

After analysis of effects of each subclasses within each factor, the next step to perform the landslide hazard mapping using the proposed combined methods is the perform the multivariate analysis using the logistic regression and support vector machine method. As stated in chapter 3, in the combined method, the value of the independent landslide predictive factors was replaced by the obtained weights (information values) according to the classes it belongs to (Figure 6-6).

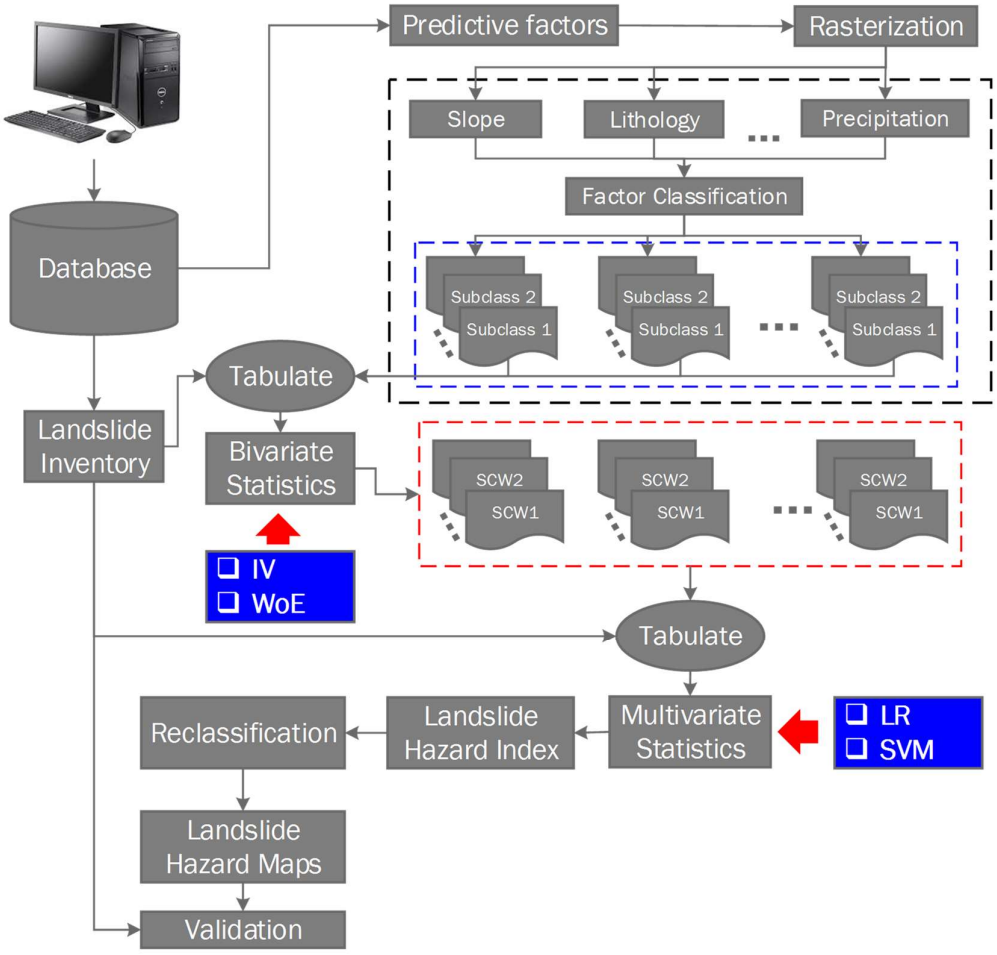

Figure 6-6 Flow chart of the proposed combined methods

The LR coefficients for the three methods are listed in Table 6-2. One is for the LR single method, in which the categorical factors of aspect and lithology were excluded. For the combined method of LR-IV and LR-WoE. The calculated information value or the weight were used to replace the factor values. As can be seen in Table Table 6-2, PGA and slope gradient showed the high and positive correlation with landslide occurrence as it could acquire the highest LR coefficient of 0.122 and 0.022. Similarly, TWI, terrain roughness and drainage density are the other effective conditioning factors, by the LR coefficient of 0.018,0.016 and 0.013 respectively.

Table 6-2 LR Coefficients for different models

No.	Factor	LR Coefficient		
		LR Single	LR-IV	LR-WoE
1	Slope gradient	0.022	0.055	0.087
2	Aspect	--	-0.006	0.001
3	Elevation	0.003	0.012	0.010
4	Plan curvature	-0.103	0.113	0.098
5	Profile curvature	-0.098	0.109	0.087
6	Terrain roughness	0.016	0.009	0.110
7	Lithology unit	--	0.014	0.016
8	Distance to seismic fault	-0.035	-0.021	-0.018
9	SPI	-0.05	0.010	0.009
10	TWI	0.018	0.019	0.016
11	Drainage density	0.013	0.008	0.013
12	Distance to stream	-0.011	-0.008	-0.010
13	NDVI	-0.014	-0.011	-0.015
14	PGA	0.122	0.214	0.131
15	Constant	-19.742	-8.764	-6.954

As for the combined method of LR-IV, PGA and plan curvature also showed the high and positive correlation with landslide occurrence as it could acquire the highest LR coefficient of 0.214 and 0.113. And the factor of profile curvature, elevation, terrain roughness and drainage density are the other effective conditioning factors, by the LR coefficient of 0.109, 0.012, 0.009 and 0.008 respectively. As for the method of LR-WoE, the factor of PGA and terrain roughness showed that highest positive correlation with landslide occurrence with the coefficient of 0.131 and 0.110, other factors with positive correlation of landslide are slope gradient and plan curvature. Finally, the landslide probability map can be calculated using Eq. (3-6) and Eq. (3-7). Similarities, by combining the methods of IV and WoE with the SVM method, we can also obtain the probability maps of landslide occurrence. As stated previous in chapter3, the SVM gives the implicit expressions of the correlations between landslide occurrence and its predictive factors, it is impossible to tell which predictive factor is more important in landslide occurrence.

6.5.4 RESULTS AND VALIDATION

Finally, the probability indexes for the three methods were calculated which range from 0 to 0.971 for LR single method, 0.002 to 0.998 for LR-IV method and

0 to 0.99 for LR-WoE method. While the probability indexes' range for the SVM single, SVM-IV and SVM-WoE were 0 to 0.993, 0 to 0.972 and 0-0.981, respectively. In order to perform LHM, the probability map should be divided into different categories. In the chapter, it is possible to see different types of classification schemes such as standard deviation, quantile, natural break and equal interval. In the current study, in order to compare the different maps with a same scale, the breaks were manually-divided into five classes of landslide hazard levels as: very low (0–0.10), low (0.10–0.30), medium (0.30–0.50), high (0.50–0.70) and very high (0.70–1). The validation has been done by comparing the landslide data with the produced landslide probability map and the validation results were given in Table 6-3.

Table 6-3 Validation and comparison of the obtained landslide hazard maps.

No.	Method	Success Rate	False-Alarm Rate	Miss- Alarm-Rate
1	IV	65%	33%	30%
2	WoE	69%	28%	24%
3	LR	64%	42%	35%
4	SVM	71%	29%	32%
5	LR-IV	79%	23%	22%
6	LR-WoE	74%	31%	19%
7	SVM-IV	84%	26%	21%
8	SVM- WoE	81%	28%	31%

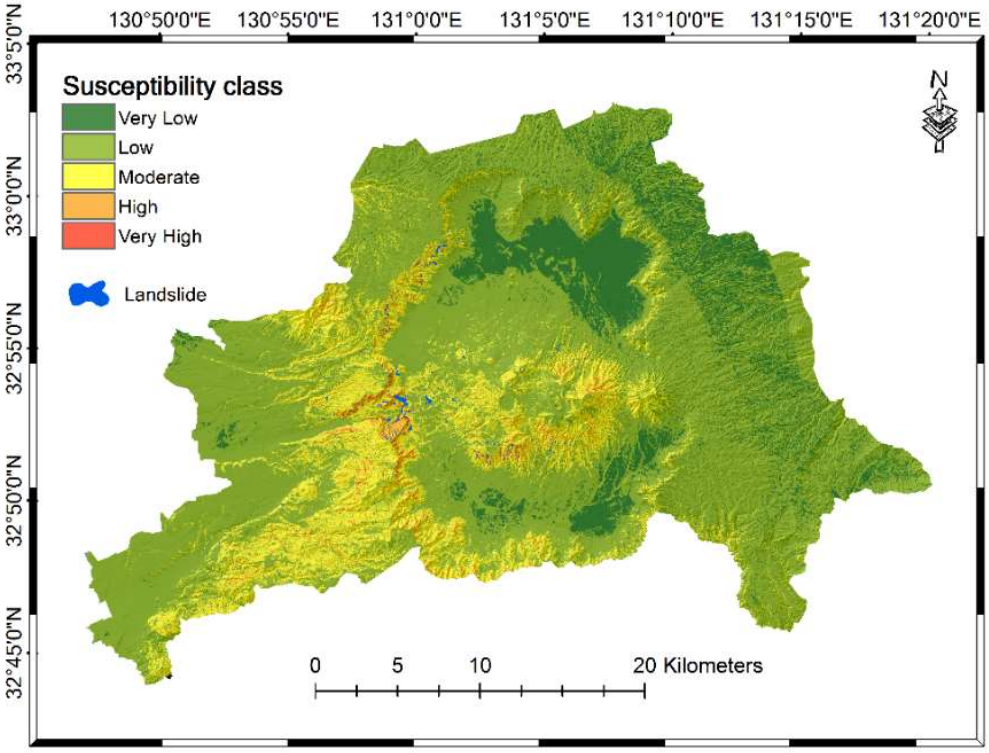

Figure 6-7 LHM using the LR-IV method

Based on the validation results, the combined method of LR-IV gives the lowest false-alarm rate of 23%, followed by the combined SVM-IV and WoE methods of 26%, and 28%, respectively. As for the Miss-alarm rate, lowest 19% of the landslides occurrences were not successfully predicted in the SVM-IV method, followed by the methods of LR-WoE and LR-IV of 21% and 22%, respectively. Therefore, based on a general consideration of the comparison results of false-alarm rate and miss-alarm rate. The combine methods of LR-IV and LR-WoE gives the best results, showing in Figure 6-7 and Figure 6-8.

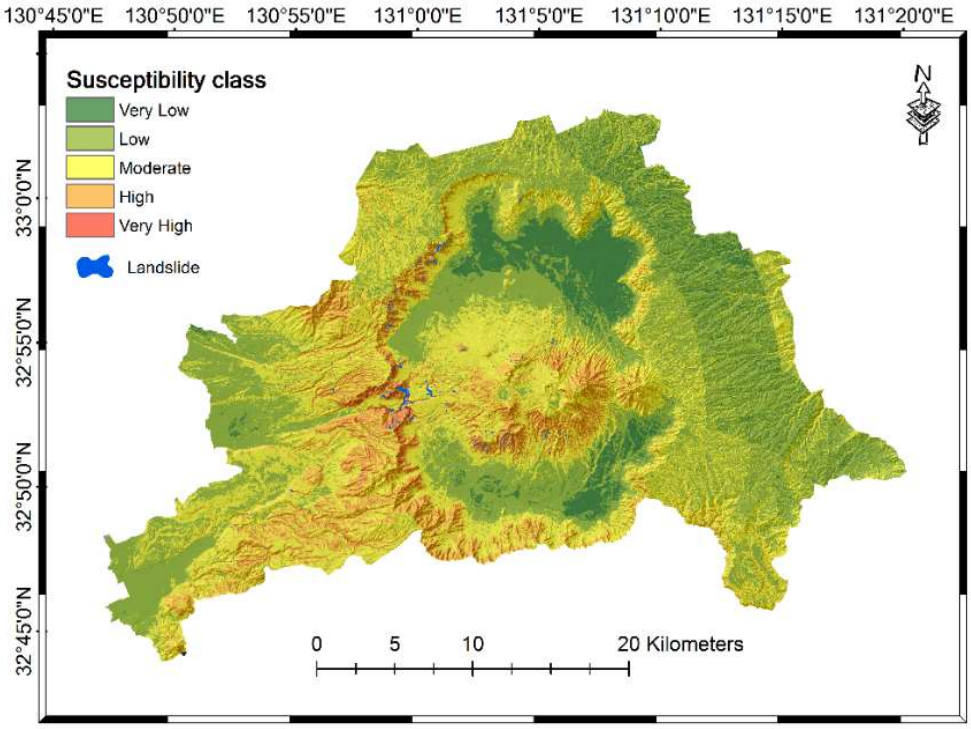

Figure 6-8 LHM using the LR-WoE method

Based on the landslide hazard maps, most parts of the study area are located in very low and low hazard zones. The high and very high landslide hazard areas acquired from the maps covered 6.4% in LR-IV method and 9.8% in LR- WoE of the area and mostly it is located in the central parts of the study area, especially around the Aso volcano. The area which contained volcanic ash, very high elevation and steep slopes was classified as the high and very high hazard zones. The acquired landslide probability map showed that the probability of landslide occurrence is large in high slope and high elevated areas.

6.6 LANDSLIDE HAZARD MAPPING USING GEOLHM-P

6.6.1 PGA ESTIMATION OF THE STUDY AREA

At 16:25 on April 15, 2016 (UCT), a large shallow crustal earthquake (M_w 7.1) occurred beneath Kumamoto city in the Kyushu region, Japan. A moderate

foreshock (M_w 6.1) at 21:26 on April 14, 2016 (UTC) stroke the same region. According to F-net moment sensor solution, the hypocenters of the mainshock and foreshock located at the Futagawa and Hinagu fault zones, two active right-lateral strike-slip faults in the Kyushu region, respectively. There are more than one thousand aftershocks with the intensity above one occurred at the Kumamoto prefecture and its vicinity. The aftershocks with the moment magnitude more than 5.0 are shown in Figure 6-9. Peak ground acceleration (PGA) is recorded as much as 1362cm/s^2 at station KMM16 with the epicenter distance of 2km. Strong ground motions of the 2016 Kumamoto earthquake sequence caused at least 49 fatalities and about 1700 injuries. Numerous structures were damaged seriously or even collapsed during the earthquake sequence. In particular, Kumamoto Castle, one of the most popular tourist destinations in Kumamoto prefecture, suffered destructive damage to roofs and stone walls. Besides, numerous landslides were induced around the mountain area in the Kyushu region. For example, the Great Aso Bridge in Minami Aso village were swept out by a landslide and collapsed into the river. Although two dense strong-motion seismograph network (K-NET and KiK-net) are installed and operated in Japan, there are no strong-motion instruments in some regions suffered heavy damage. Ground-motion simulations for the 2016 Kumamoto earthquake have important implications, not only for seismic hazard assessment, such as the slope stability analysis and landslide run-out estimation, but for response spectrum analysis of structures in the damaged regions.

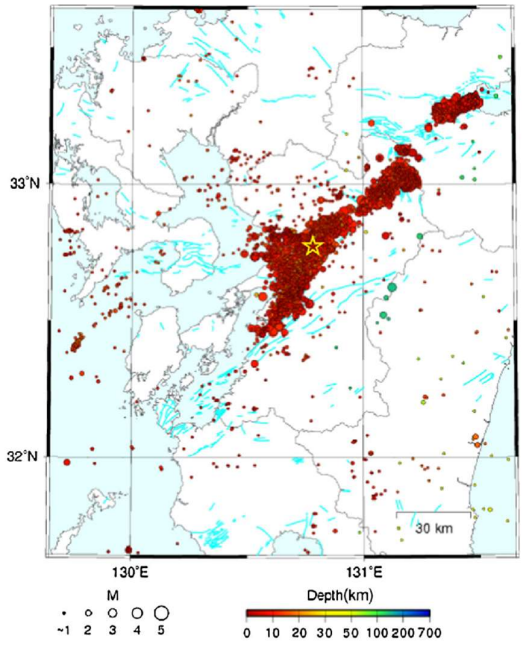

Figure 6-9 Seismicity in and around Kumamoto Prefecture, Kyushu during 26 March to 25 April, 2016 located by the High-sensitivity seismic network (Hi-net) operated by the National Research Institute for Earth Science and Disaster Resilience, Japan (http://www.hinet.bosai.go.jp/). (Zhao, et al, 2016)

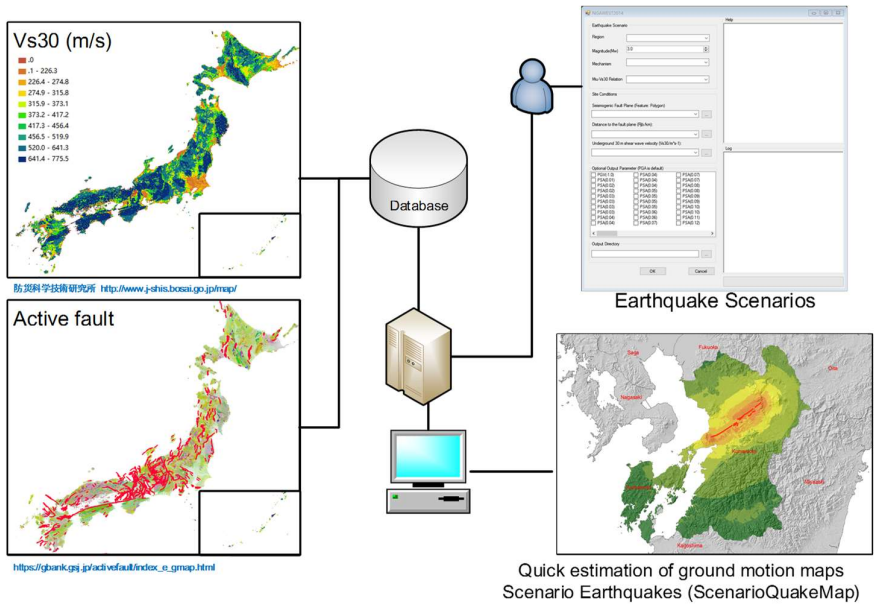

Figure 6-10 Flowchart of PGA estimation

Because of the Active subduction, seismic and volcanic activities are very

Table 6-4 Parameters used in the GeoLHM-P to predict the PGA values

Input Parameter	**Value or code**
Region	Italy and Japan
Magnitude	Mw5.0-Mw7.5
Mechanism	Strike-Slip
Miu-Vs30	Japan
Vs30 data	From JSHIS
Fault Plane	Futagawa fault Hinagu fault

In this chapter, we take the Futagawa and Hinagu fault as the active fault and assumed the different earthquakes on these two fault to estimate the PGA values (Table 6.2). for the Vs30 data, it was downloaded from the Japan seismic hazard information station(JSHIS) (http://www.j-shis.bosai.go.jp/). The general flowchart of the PGA estimation is illustrated in Fig.6.9.

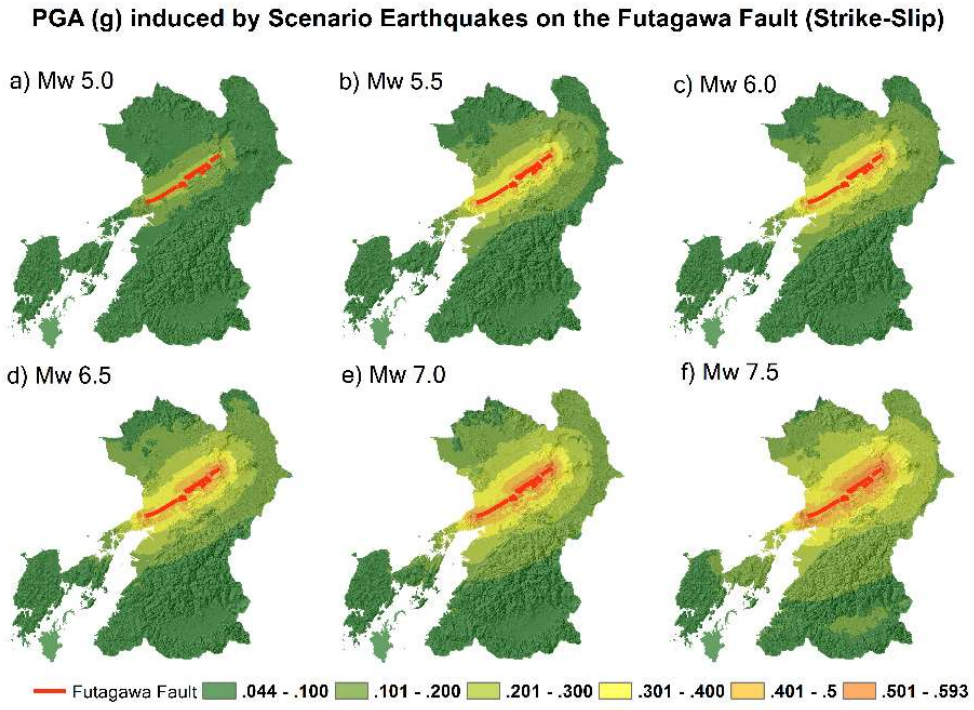

Figure 6-11 PGA values estimated from earthquakes happened on the Futagawa fault

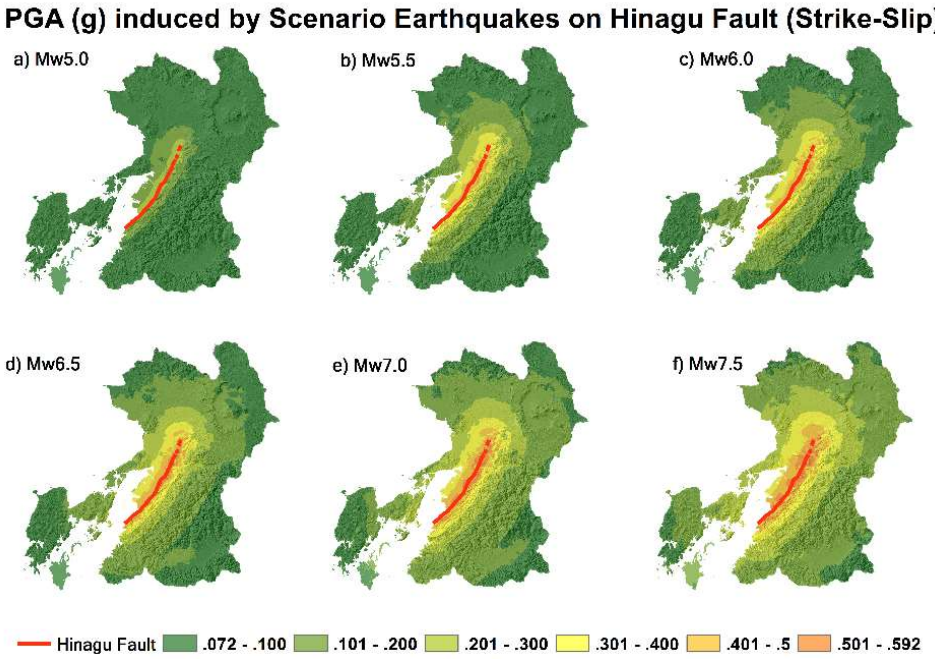

Figure 6-12 PGA values estimated from earthquakes happened on the Hinagu fault

6.6.2 DATA PROCESSING

The biggest challenges for the pseudostatic procedure are the selections of appropriate seismic coefficient and acceptable factor of safety. According to the report published by the International Commission of Large Dams (ICOLD) the horizontal seismic coefficients range from 0.1 to 0.15 and the minimum factors of safety range from 1.0 to 1.5. The same report also shows that in the United States, seismic coefficients have ranged from 0.05 to 0.15, whereas in Japan the coefficients have been less than about 0.2 (Seed 1979). The Corps of Engineers Manual (EM-1110-2-1902) published in 1982 recommended a seismic coefficient value of 0.1 or 0.15 where earthquake threat is major and great, respectively, together with a minimum safety factor of 1.0 for all earthquakes. At issue with all of these values of seismic coefficient is that they were arbitrarily selected and do not rigorously account for the level of expected shaking. Marcuson and Franklin (1983) and Hynes-Griffin and Franklin (1984) related the seismic coefficient value for a dam to the expected peak ground acceleration (PGA) at a site. Marcuson and

Franklin (1983) recommended a seismic coefficient of 1/3 to 1/2 of the PGA at the crest of a dam, whereas Hynes-Griffin and Franklin (1984) recommended a seismic coefficient of 1/2 of the PGA of bedrock (PGArock) with a minimum FS of 1.0 and a 20% reduction in shear strength. Bray et al. (1998) also related the seismic coefficient to the PGA on the bedrock (0.75 × PGArock). This value is appropriate for seismic stability evaluations of solid-waste landfills, where the allowable levels of deformation are relatively small. Stewart et al. (2003) used the data of Bray and Rathje (1998) to develop an expression for the seismic coefficient in terms of ground motion parameters (PGA and duration) and earthquake magnitude (Mw). These seismic coefficient values generally range from 0.25 × PGArock to 0.75 × PGArock. In this study, we set the seismic coefficient as 0.50 × PGArock. In this chapter, 0.25 × PGArock was chosen as the seismic coefficient and factor of safety.

Table 6-5 Distribution patterns of input parameters used in the probabilistic analysis

Geology Unit	C (kPa)	Phi (°)	Gamma (kN/m^3)	Soil Thickness (m)
Deposits and Terrace	0-5	8-15	15-18	10
Sedimentary	5-15	15-25	18-20	10
Volcanic	5-15	20-35	18-20	10

A summary of the geotechnical parameters describing shear strength of the various soils found from in-situ analysis in the is given in Table 6.3 (Picarelli and Vinale 2007). The unit weight of the soil was selected as 18 kN/m3 and the fraction of slab thickness saturated was taken as 0.3. This parameter combination ensures that all statically stable slopes have yield acceleration values greater than zero.

6.6.3 RESULTS AND VALIDATION

In the GeoLHM-P modules, random numbers were generated to obtain the variables, mainly being geotechnical parameters; these variables were entered in the calculation of dynamic factor of safety (DFS). In the method proposed, random numbers were generated to obtain the variables, mainly being geotechnical

parameters; these variables were entered in the calculation of displacement. The simulations ran 2000 times and calculated 2000 DFS values for each grid cell. The DFS mean and standard deviation were calculated, and its probabilistic distribution can be obtained. Given a certain threshold value of DFS, estimated probabilities of DFS exceeding a threshold value were then shown as a map of seismic landslide hazard.

For the threshold value of DFS, according to the report published by the International Commission of Large Dams (ICOLD), the minimum factors of safety range from 1.0 to 1.5. The Corps of Engineers Manual (EM-1110-2-1902) published in 1982 recommended a minimum safety factor of 1.0 for all earthquakes. Hence, as a DFS of 1.2, corresponding to a failed rate of 32.4%, was determined for the threshold value of DFS, and the probability of DFS less than 1.2 was then mapped in Fig. 6.9. This resulting seismic landslide hazard was classified into five categories: very low (0–0.10), low (0.10–0.30), moderate (0.30-0.50) high (0.50-0.70) and very high (0.70–1.0).

By inputting the measured PGA map, we can obtain the landslide hazard maps from the real earthquake scenario of the 2016 Kumamoto earthquake. Here, we assumed that all the landslides were triggered by the main shock of Mw7.0 and don't consider the cumulative effects of the following aftershocks (Figure 6-12).

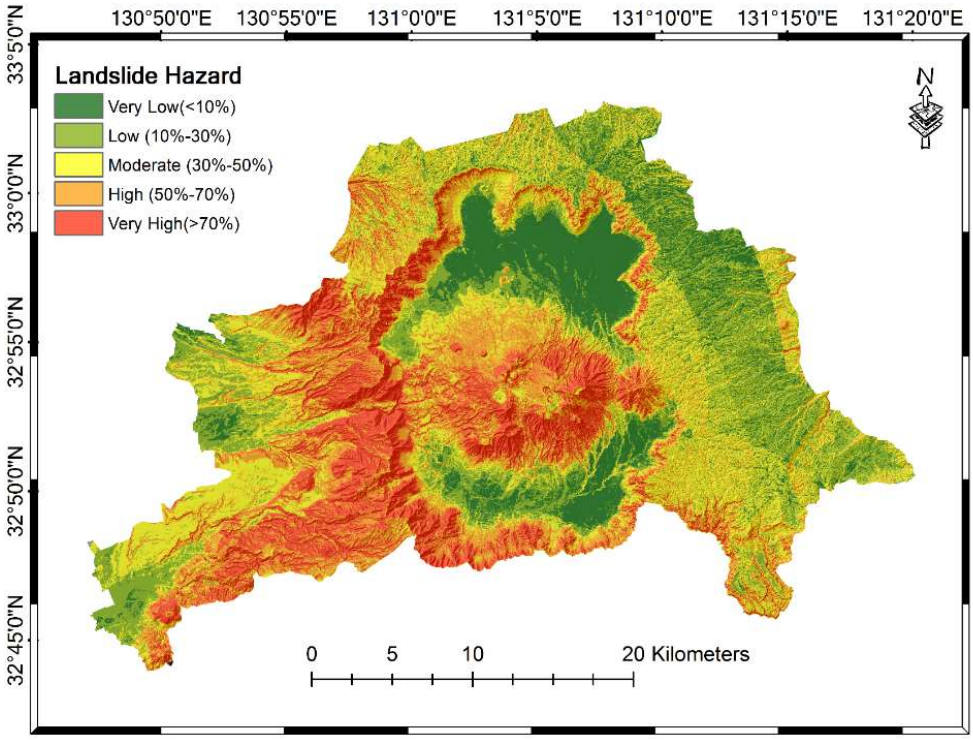

Figure 6-13 Landslide hazard maps by considering the real earthquake scenario of the main shock of the 2016 Kumamoto Earthquake (Mw7.0)

Table 6-6 Validation result of landslide hazard map produced using GeoLHM-P with the real earthquake scenarios of the 2016 Kumamoto Event

No.	Method	Success Rate	False-Alarm Rate	Miss- Alarm-Rate
1	Physically-Based	68%	38%	22%

It can be seen that 22 % of the total area was classified as having very high hazard, and the high-hazard zones were predicted to include 18% of the area. In the resulting map, it was also shown that about 38% of areas with landslide occurrence were classified as medium levels of landslide hazards.

Comparing with the results obtained from the statistical methods, the physically-based methods doesn't give a better result. Also the miss-alarm rate of this method is 22%, the false-alarm rate of 38% was higher than all the statistical methods. Compared with the actual landslides, moreover, it was demonstrated that

the result seems to be over conservative since several locations were mistakenly classified to be areas not prone to landsliding after the earthquake occurrence. Nevertheless, the biggest advantage of the physically-based methods over the statistical methods is that, no historical landslide information is needed and fewer data such as the predictive factors are used in this method. Also, by considering the triggering force of seismic directly, this method can be used to produce landslide hazard maps from future assumed earthquakes. By considering the different PGA maps estimated from different assumed earthquakes, a series of landslide hazard maps were produced as shown in Figure 6.14 and Figure 6.15.

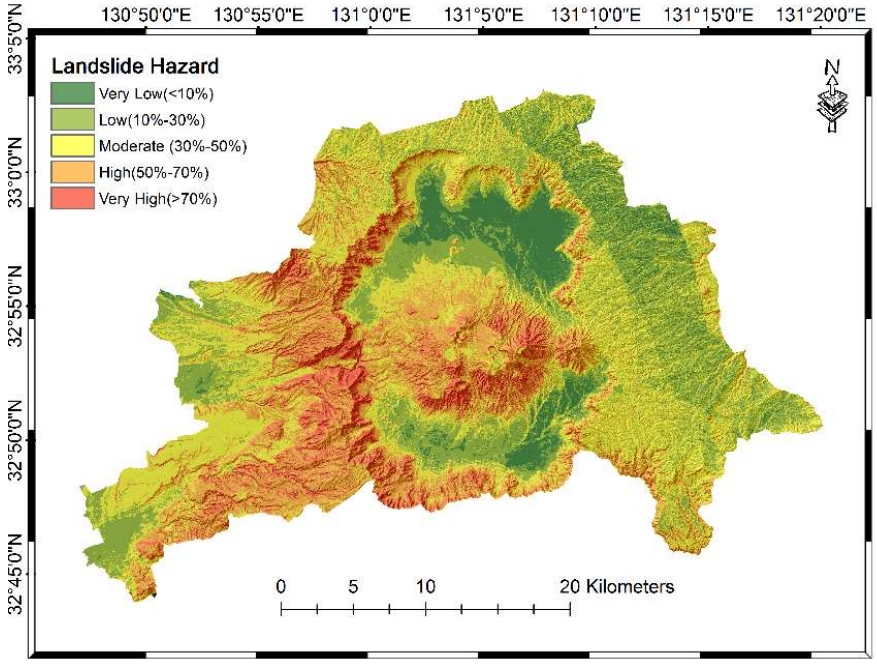

(a) Landslide hazard maps with PGA estimated from an earthquake from Mw5.0 on the Futagawa fault

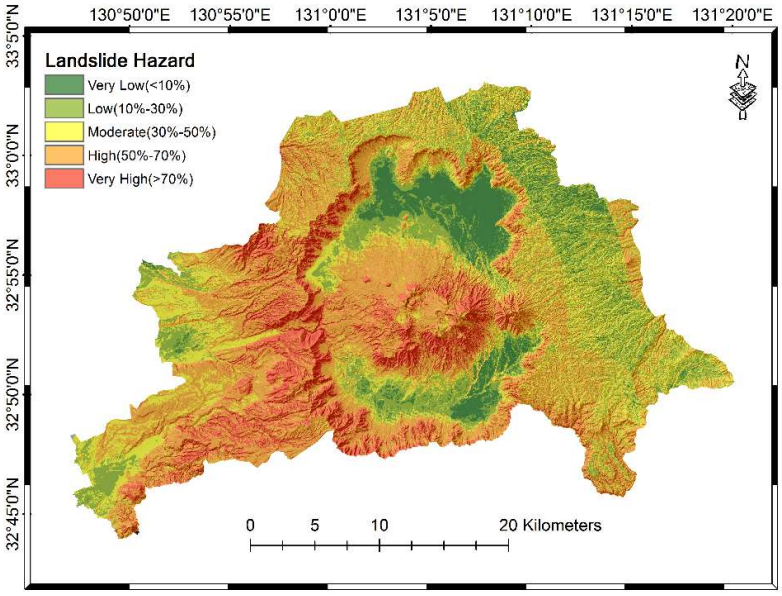

(b) Landslide hazard maps with PGA estimated from an earthquake from Mw6.0 on the Futagawa fault

Figure 6-14 Landslide hazard maps with different PGA inputs estimated from the Futagawa fault

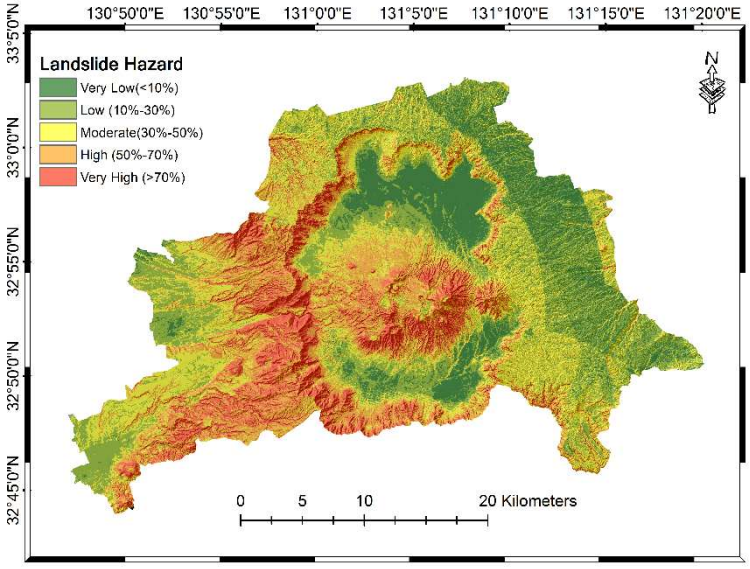

(a) Landslide hazard maps with PGA estimated from an earthquake from Mw5.0 on the Hinagu fault

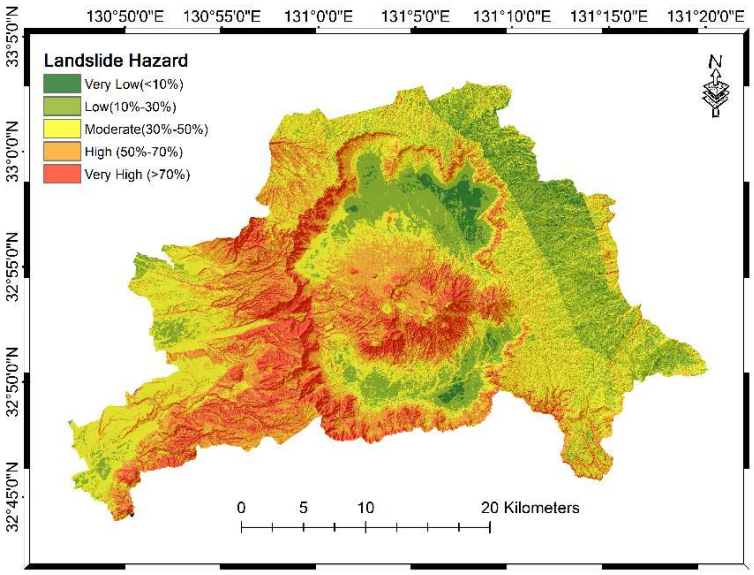

(b) Landslide hazard maps with PGA estimated from an earthquake from Mw6.0 on the Hinagu fault

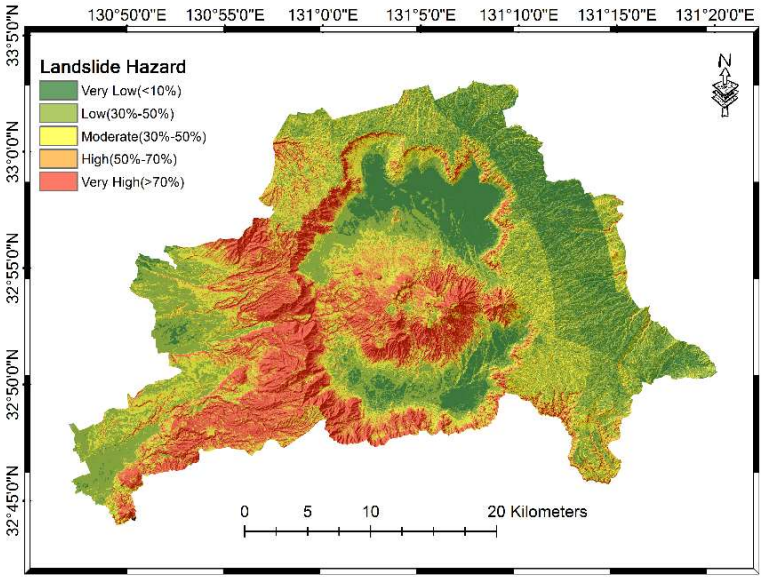

(c) Landslide hazard maps with PGA estimated from an earthquake from Mw7.0 on the Hinagu fault

Figure 6-15 Landslide hazard maps with different PGA inputs estimated from the Hinagu fault

6.7 LANDSLIDE HAZARD MAPPING CONSIDERING THE AFFECTED AREA

In the previous sections, although all the methods were capable to identify the landslide-prone slopes, the landslide affected area were not included. In this section, we use the GeoLHM-R to estimate the affected area of landslides. Generally, three data are required in the developed module. One is the landslide source area, the second is the frictional coefficient and the third is the terrain surface. In this section, the landslide source area was rasterized from the landslide polygons in the landslide inventory in GIS. For the post-earthquake terrain surface, it was derived from the Alos-2 InSAR satellite image provided by Li (2016), which covers the Minami Aso City of the study area. Therefore, we choose the Minami Aso City as the study area.

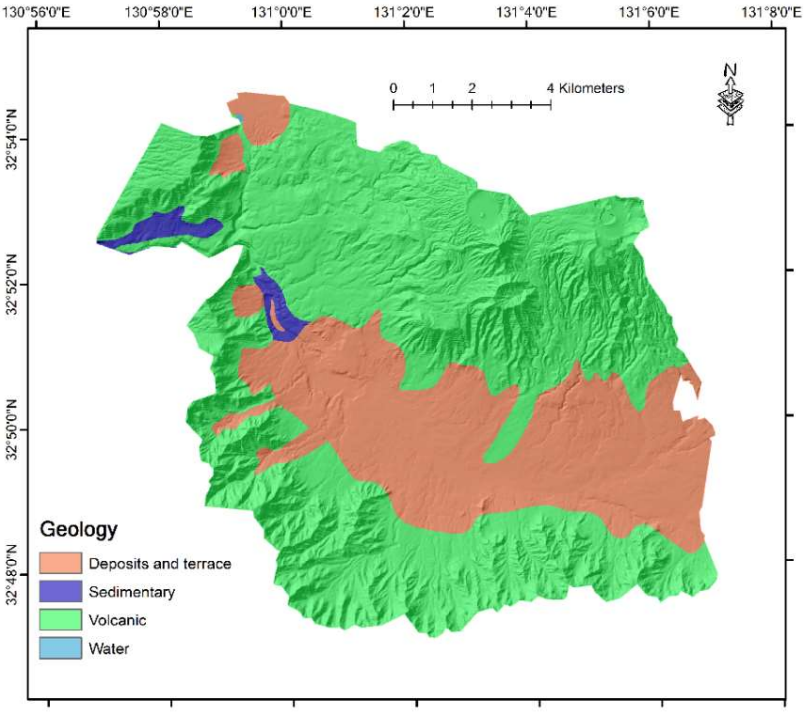

Figure 6-16 General lithological maps of the Minami Aso Mura

6.7.1 DETERMINATION OF THE FRICTIONAL COEFFICIENT

As previously stated in section 5.3 and section 5.4, we estimate the surface

frictional coefficient from the frictional angle of the lithology. Since it is impossible to estimate the frictional coefficient of landslides one by one at a large region, one of the possible method is to estimate the friction coefficient according to the lithology of the landslide. In this study, the study area into three groups as: Deposits and Terrace, Sedimentary and volcanic rocks. And by detailed analysing of three landslide cases triggered during the Kumamoto earthquake, we first back analyzed the frictional coefficient, then by using the back analysis result, we performed the regional landslide hazard mapping by considering the affected area.

Table 6-7 Three cases used for back analysis of the friction coefficient

Case	Location	Lithology	Friction angle(°)	Friction coefficient	Reference
A	32° 52′ 40″ N 130 ° 56 ′ 38″ E	Weathered Marine and non-marine sediments and soils	10-18	0.18-0.26	Wartman et al. (2013)
B	32° 51′ 15″ N 131° 1′ 8″ E	Deposits and Terrace	8-15	0. 14−0. 27	Hansen (1984)
C#	32° 53′ 8″ N 130 ° 59 ′ 10″ E	Volcanic ashes, weathered volcanic rocks and deposits	14-20	0.25-0.36	Sassa et al. (2005)

For case C, please refer to chapter 5

(a) (b)

Figure 6-17 (a) Pre- and (b) Post-Earthquake image of the landslide case A. Red boundary shows the runout extent of the landslide. The blue line shows the

landslide prone areas according to the Act on Sediment Disaster Countermeasures for Sediment Disaster Prone Areas

Figure 6-18 Landslide source area showing in red polygon

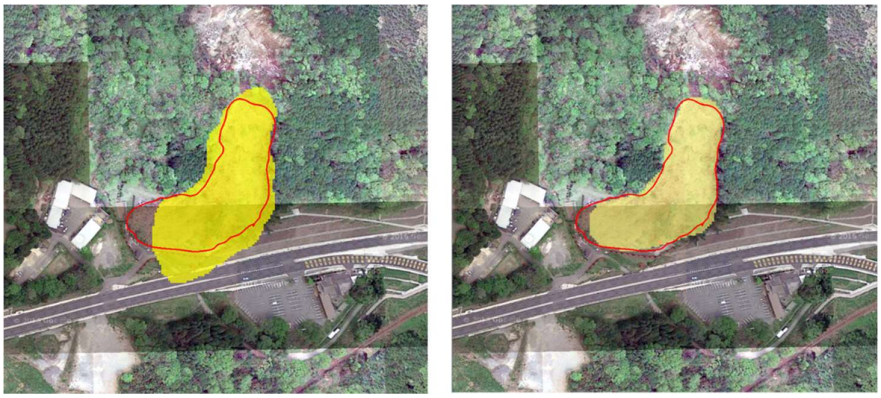

(a) $\mu = 0.20$ (b) $\mu = 0.22$

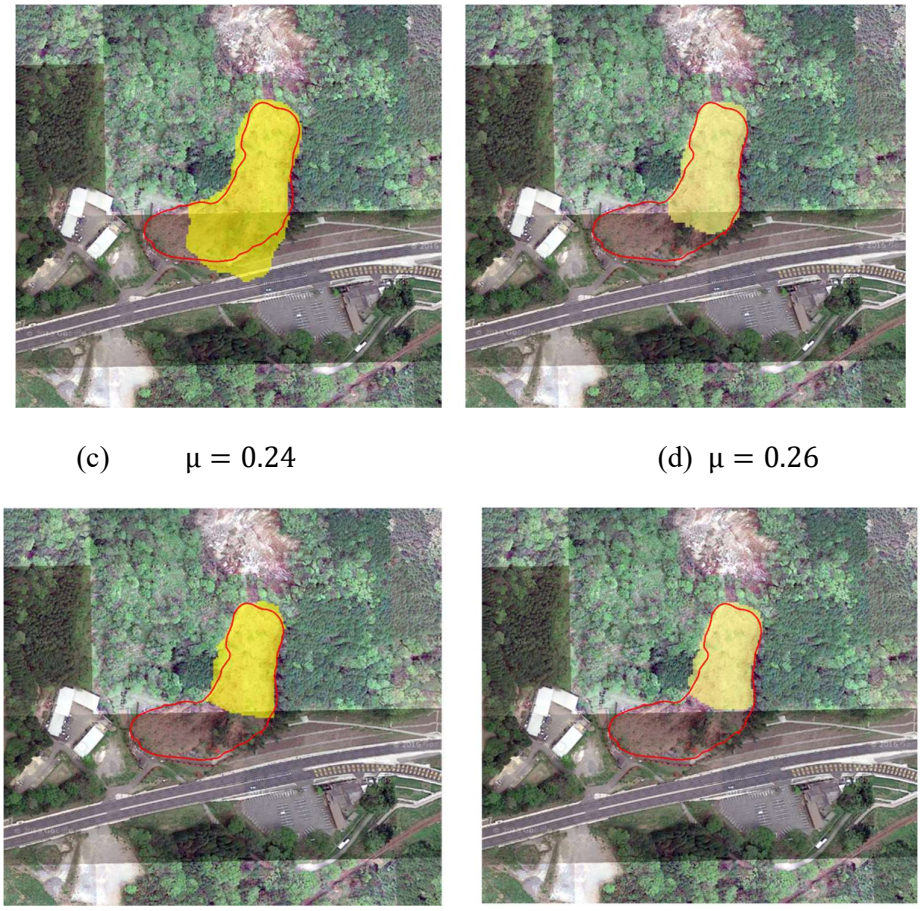

(c) $\mu = 0.24$ (d) $\mu = 0.26$

(e) $\mu = 0.28$ (f) $\mu = 0.30$

Figure 6-19 Back analysis of the friction coefficient of landslide case A. Red boundary shows the runout extent of the landslide. The yellow region show the result of landslide affected area

Based on the back analysis results indicated in Figure 6-19. A best fir friction coefficient of 0.22 was adopted for the Weathered Marine and non-marine sediments and soils.

Figure 6-20 (a) Pre- and (b) Post-Earthquake image of the landslide case B. Red boundary shows the runout extent of the landslide. The blue line shows the landslide prone areas according to the Act on Sediment Disaster Countermeasures for Sediment Disaster Prone Areas

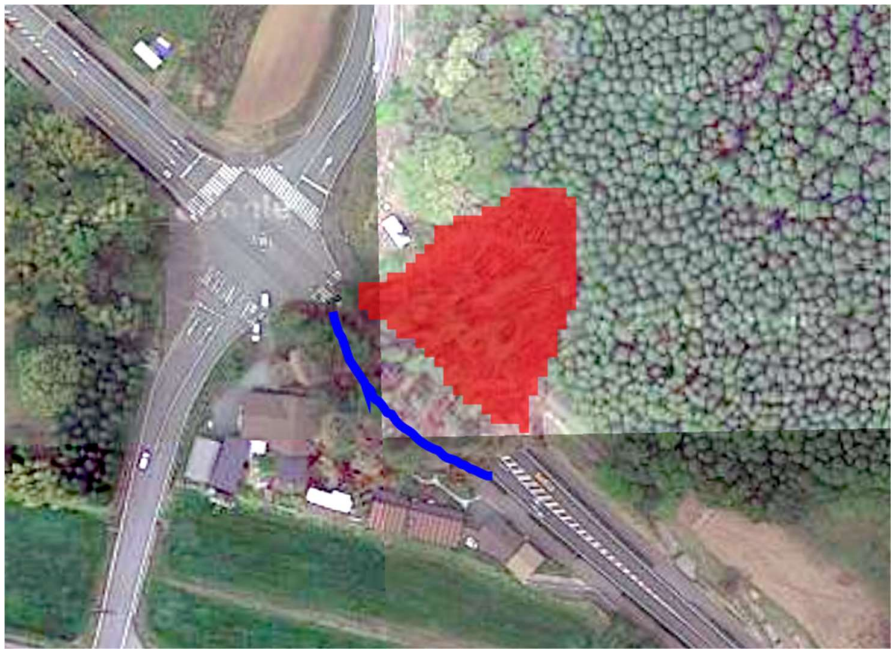

Figure 6-21 Landslide source area showing in red polygon

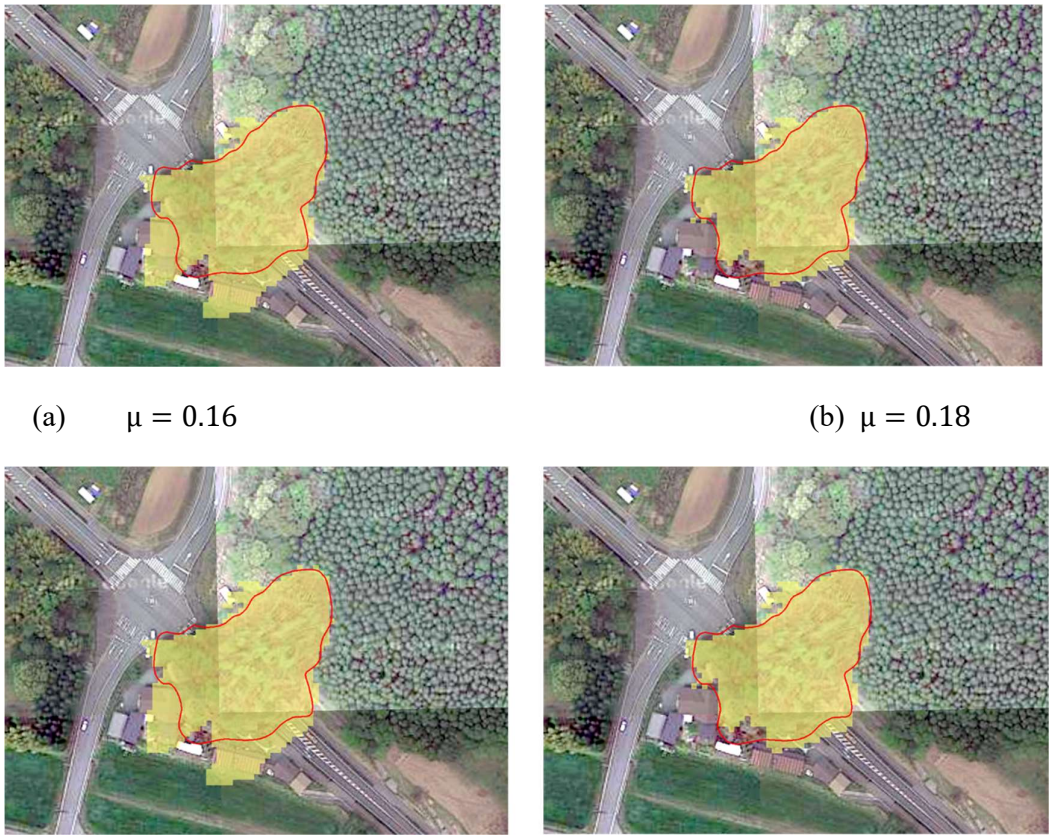

(a) $\mu = 0.16$ (b) $\mu = 0.18$

(c)$\mu = 0.20$ (d) $\mu = 0.22$

Figure 6-22 Back analysis of the friction coefficient of landslide case B. Red boundary shows the runout extent of the landslide. The yellow region show the result of landslide affected area

Similarity, based on the back analysis results indicated in Figure 6-20. A best fir friction coefficient of 0.18 was adopted for deposits and terrace.

6.7.2 REGIONAL LANDSLIDE AFFECTED AREA SIMULATION

Theoretically, in the landslide runout simulation of the landslide affected area, it need to investigate the frictional coefficient case by case. However, for regional simulation, in which, a large number of cases should be simulated at the same time. It is impossible to carry out such detail in-site investigations. Therefore, for the regional simulation, one of the possible way to determine the friction coefficient is to estimate it according to its lithological compositions. One of the biggest

shortcoming of such estimation is the big uncertainties lie in the lithological compositions and the geological and hydrological conditions, such as the weather degree, the water content and so on.

Table 6-8 Friction coefficients used in the simulation

Geology Unit	Frictional coefficient
Deposits and Terrace	0.18
Sedimentary	0.22
Volcanic	0.30

By back analysis of existing landslides to infer the frictional coefficient is one of the possible way suggested in the GeoLHM-R to estimate the frictional coefficient. In the practical case, the landslide source area was rasterized from the landslide polygons in the landslide inventory in GIS. For the post-earthquake terrain surface, it was derived from the Alos-2 InSAR satellite image provided by Li (2016), which covers the Minami Aso City of the study area. The frictional coefficient of the study area was adopted from the back analysis results in the last section (Table 6-5).

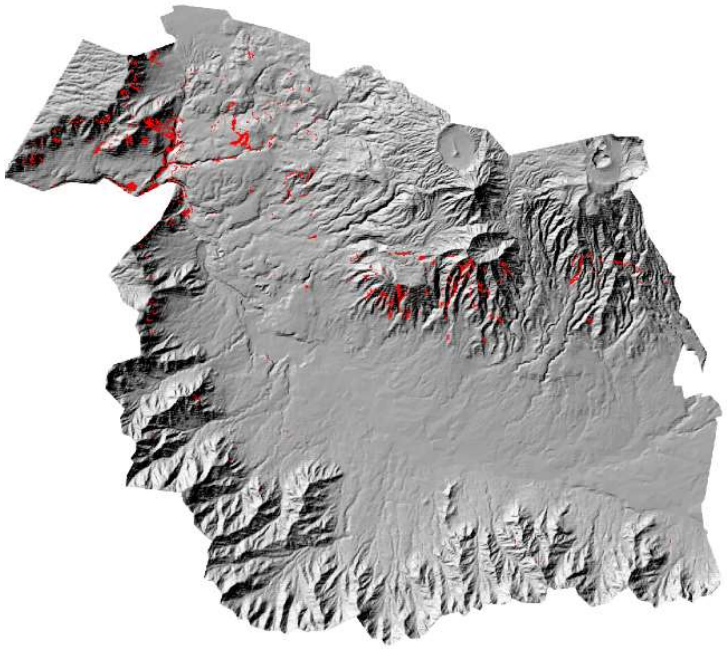

(a) Landslide sources

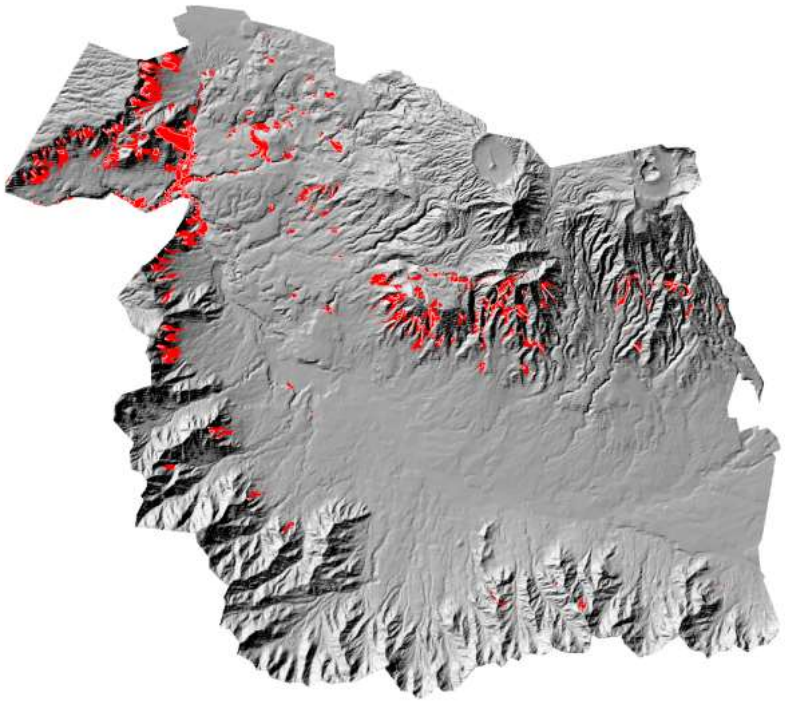

(b) Affected area

Figure 6-23 Landslide hazard maps considering the landslide affected area at the Minani Aso City

Firstly, the landslide source area was rasterized from the landslide polygons in the landslide inventory generated in the section 6.4. Then, a raster map of frictional coefficient was generated by rasterizing the geological map of the area, in which each cell had been assigned a frictional coefficient according to its lithological group. Finally, by loading the post-earthquake terrain raster, the potential landslide affected area was simulated in the GeoLHM-R module.

6.7.3 RESULTS AND DISCUSSIONS

The results of the landslide affected area simulated using the GeoLHM-R was shown in Figure 6-23b. The total plane area (defined as the projected area of the landslides on the horizontal surface) of the landslide source was 823,462 m^2. But considering the landslide affected area, the total area of the landslide extent

increases up to 1,515,417 m^2.

Landslide hazard mapping considering both the landslide-prone slope identification and runout simulation have long been the key issues in Japan. In order to mitigate the landslide disaster, a low with the name of *Act on Sediment Disaster Countermeasures for Sediment Disaster Prone Areas* was enacted in Japan, 2001. In this law, the dangerous zone or particular dangerous zone are specified in order to take countermeasures for these zones. Here is the dangerous zone from the toe of the slope. It is identified as 2 times of the height of the potential landslide slope but less than 50 meters.

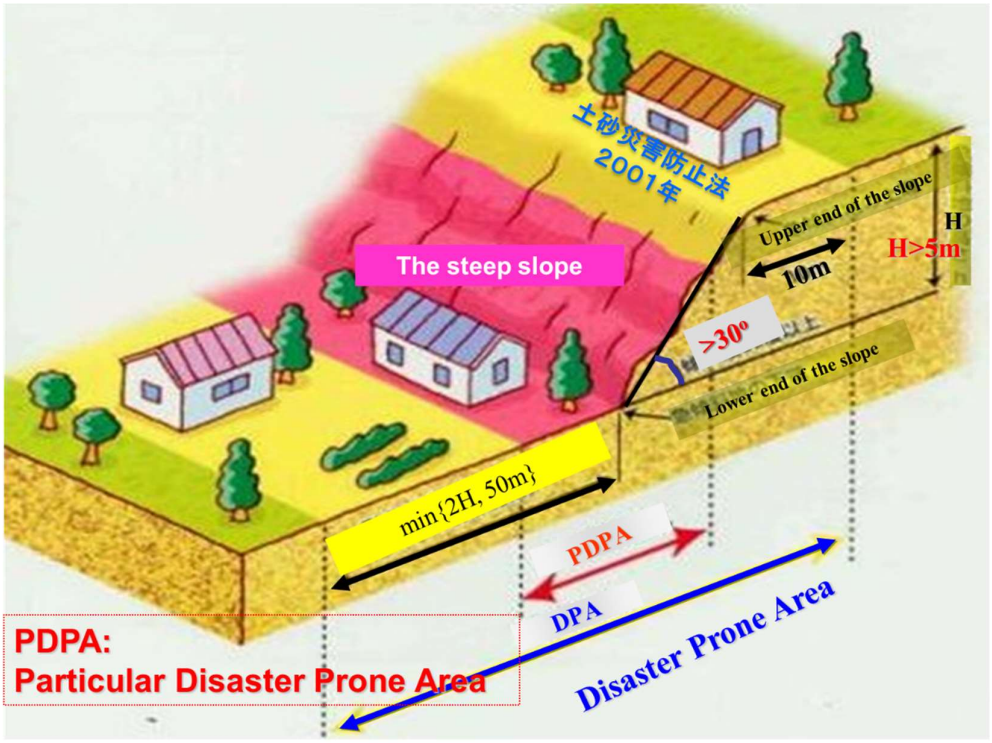

Figure 6-24 Commonly used landslide hazard mapping methods in Japan

The method suggested in this law was empirical and based on the previous statistical results of landslides happened in Japan. Obviously, this method has some limitations in practical use. As indicated in Figure 6-18 and Figure 6-20, the estimated runout zones according the suggested method in the law were obviously less than the real situations. Another limitation of this method in practical use of

large region is that it is impossible to identify a slope unit in GIS and the real terrain topography was ignored, which is very important in landslide affected area estimation.

6.8 CONCLUSIONS`

Earthquake is one of the main contributors in landslide occurrence which results in severe human casualties, property losses and environmental degradation. Earthquake induced landslides can cause extensive and significant damages to both lives and properties. The geographical condition of Kumamoto prefecture, Japan is formed by mountains that easily fall down especially after earthquake. A series of strong earthquakes with maximum magnitude of Mw 7.0 struck this region and its surrounding areas on April 14, 2016. Due to this earthquake a huge number of landslides happened in the Aso region of this area. Therefore, there is a great need for the local governments to investigate an appropriate and rapid solution to detect the landslide hazards in this region. We proposed a practical application of the developed system GeoILHMS to facilitate such a need. Some conclusions can be drawn as follows:

(1) An inventory of 665 landslides triggered by the 2016 Kumamoto earthquake was visually mapped using the online high-resolution images and developed tools.

(2) Landslide hazard maps are produced by using each of statistical methods available in the GeoLHM-S. Validation result of these methods show that the combined method of LR-WoE show the minimum miss-alarm rate of 19%, but is also shows a false-alarm rate of 31%, followed by the combined method of IV-SVM with a miss-alarm rate and false-alarm rate of 21% and 26% respectively.

(3) From the landslide hazard maps obtained using these statistical models, it can be seen that the region around the Aso volcano and its surroundings have several areas with high hazard ratings. This is likely due to the fact that these regions have abundant steep slopes, weathered volcanic rocks

and steep surface.

(4) Landslide hazard map was also produced using the GeoLHM-P module with different PGA maps. Although the accuracy of this landslide hazard maps was less than the statistical methods with a miss-alarm rate of 22% and a false-alarm rate of 38%. The main advantage of this approach is it can be used for regions without historical landslide inventory.

(5) Landslide hazard maps with expected earthquakes of different magnitudes of Mw 5.0, Mw6.0 and Mw7.0 occurring along the Futagawa fault and the Hinagu fault are produced by using the GeoLHM-P. These landslide hazard maps can be served as a reference for prevention of landslides triggered by assumed earthquakes that may happened in the future.

(6) A landslide hazard map of the Minami Aso Mura showing the affected area of landslides was produced using the GeoLHM-R. Since it is hard to assign friction coefficients to each landslide individually, we grouped the study area into three regions based on the lithological maps. For each region, the friction coefficient was determined by a reduction of the friction angle of the rocks.

(7) The produced landslide hazard provides essential frameworks for the development planning and reconstruction of the study area as they present a spatial division of the study area of different levels of potential landslide threat, including the landslide prone areas and the potential affected areas.

REFERENCE

AKKAR, S. & BOMMER, J.J. 2007. Empirical prediction equations for peak ground velocity derived from strong-motion records from Europe and the Middle East. Bulletin of the Seismological Society of America, 97, 511–530, doi: 10.1785/0120060141.

ATKINSON, G.M. 2010. Ground-motion prediction equations for Hawaii from a referenced empirical approach. Bulletin of the Seismological Society of America, 100, 751–761, doi: 10.1785/0120090098.

ATKINSON, G.M. & BOORE, D.M. 1997. Stochastic Point-Source Modeling of Ground Motions in the Cascadia Region. Seismological Research Letters, 68, 74–85, doi: 10.1785/gssrl.68.1.74.

ATKINSON, G.M. & BOORE, D.M. 2006. Earthquake ground-motion prediction equations for eastern North America. Bulletin of the Seismological Society of America, 96, 2181–2205, doi: 10.1785/0120050245.

ATKINSON, G.M. & SILVA, W. 2000. Stochastic modeling of California ground motions. Bulletin of the Seismological Society of America, 90, 255–274, doi: 10.1785/0119990064.

BAKER, R., SHUKHA, R., OPERSTEIN, V. & FRYDMAN, S. 2006. Stability charts for pseudo-static slope stability analysis. Soil Dynamics and Earthquake Engineering, 26, 813–823, doi: 10.1016/j.soildyn.2006.01.023.

BERTI, M., MARTINA, M.L. V, FRANCESCHINI, S., PIGNONE, S., SIMONI, A. & PIZZIOLO, M. 2012. Probabilistic rainfall thresholds for landslide occurrence using a Bayesian approach. Journal of Geophysical Research: Earth Surface, 117, doi: 10.1029/2012JF002367.

BINDI, D., PAROLAI, S., GROSSER, H., MILKEREIT, C. & DURUKAL, E. 2007. Empirical ground-motion prediction equations for northwestern Turkey using the aftershocks of the 1999 Kocaeli earthquake. Geophysical Research Letters, 34, doi: 10.1029/2007GL029222.

BOMMER, J.J., STAFFORD, P.J. & ALARCÓN, J.E. 2009. Empirical equations for the prediction of the significant, bracketed, and uniform duration of earthquake ground motion. Bulletin of the Seismological Society of America, 99, 3217–3233, doi: 10.1785/0120080298.

BOORE, D.M. 2003. Simulation of Ground Motion Using the Stochastic Method. Pure and Applied Geophysics, 160, 635–676, doi: 10.1007/PL00012553.

BOORE, D.M. 2009. Comparing stochastic point-source and finite-source ground-motion simulations: SMSIM and EXSIM. Bulletin of the Seismological Society of America, 99, 3202–3216, doi: 10.1785/0120090056.

BOORE, D.M. & ATKINSON, G.M. 2008. Ground-motion prediction equations for the average horizontal component of PGA, PGV, and 5%-damped

PSA at spectral periods between 0.01 s and 10.0 s. Earthquake Spectra, 24, 99–138, doi: 10.1193/1.2830434.

Caflisch RE (1998) Monte Carlo and quasi-Monte Carlo methods. Acta Numer. 7:1.

CAMPBELL, K.W. 2003. Prediction of Strong Ground Motion Using the Hybrid Empirical Method and Its Use in the Development of Ground-Motion (Attenuation) Relations in Eastern North America. Bulletin of the Seismological Society of America, 93, 1012–1033, doi: 10.1785/0120020002.

CHEN, X.-L., LIU, C.-G., YU, L. & LIN, C.-X. 2014. Critical acceleration as a criterion in seismic landslide susceptibility assessment. Geomorphology, 217, 15–22, doi: 10.1016/j.geomorph.2014.04.011.

CHOUDHURY, D. & SAVOIKAR, P. 2011. Seismic stability analysis of expanded MSW landfills using pseudo-static limit equilibrium method. Waste management & research : the journal of the International Solid Wastes and Public Cleansing Association, ISWA, 29, 135–145, doi: 10.1177/0734242X10375333.

CHOUSIANITIS, K., DEL GAUDIO, V., KALOGERAS, I. & GANAS, A. 2014. Predictive model of Arias intensity and Newmark displacement for regional scale evaluation of earthquake-induced landslide hazard in Greece. Soil Dynamics and Earthquake Engineering, 65, 11–29, doi: 10.1016/j.soildyn.2014.05.009.

Chang, K.-J., Taboada, A. and Chan, Y.-C. (2005) Geological and morphological study of the Jiufengershan landslide triggered by the Chi-Chi Taiwan earthquake. Geomorphology 71(3), 293-309.

Dhakal, A.S., Amada, T. and Aniya, M. (2000) Landslide hazard mapping and its evaluation using GIS: an investigation of sampling schemes for a grid-cell based quantitative method. Photogrammetric Engineering and Remote Sensing 66(8), 981-989.

CROZIER, M.J. & GLADE, T. 2012. Landslide Hazard and Risk: Issues, Concepts and Approach. In: Landslide Hazard and Risk. 1–39., doi: 10.1002/9780470012659.ch1.

GUZZETTI, F., CARRARA, A., CARDINALI, M. & REICHENBACH, P.

1999. Landslide hazard evaluation: A review of current techniques and their application in a multi-scale study, Central Italy. In: Geomorphology. 181–216., doi: 10.1016/S0169-555X(99)00078-1.

Harrison RL (2010) Introduction To Monte Carlo Simulation. AIP Conf Proc 1204:17–21. doi: 10.1063/1.3295638

HUTCHINGS, L. & WU, F. 1990. Empirical Green's Functions from small earthquakes: A waveform study of locally recorded aftershocks of the 1971 San Fernando Earthquake. Journal of Geophysical Research, 95, 1187, doi: 10.1029/JB095iB02p01187.

JIBSON, R.W., HARP, E.L. & MICHAEL, J.A. 2000. A method for producing digital probabilistic seismic landslide hazard maps. Engineering Geology, 58, 271–289, doi: 10.1016/S0013-7952(00)00039-9.

KAYASTHA, P., DHITAL, M.R. & DE SMEDT, F. 2013. Application of the analytical hierarchy process (AHP) for landslide susceptibility mapping: A case study from the Tinau watershed, west Nepal. Computers & Geosciences, 52, 398–408, doi: 10.1016/j.cageo.2012.11.003.

Guzzetti, F., Mondini, A.C., Cardinali, M., Fiorucci, F., Santangelo, M. and Chang, K.-T. (2012) Landslide inventory maps: New tools for an old problem. Earth-Science Reviews 112(1), 42-66.

Ghosh, S., van Westen, C.J., Carranza, E.J.M., Jetten, V.G., Cardinali, M., Rossi, M. and Guzzetti, F. (2012) Generating event-based landslide maps in a data-scarce Himalayan environment for estimating temporal and magnitude probabilities. Engineering geology 128, 49-62.

Hansen, A. (1984) Landslide hazard analysis. Slope instability. Wiley, New York, 523-602.

Martha, T.R., van Westen, C.J., Kerle, N., Jetten, V. and Vinod Kumar, K. (2013) Landslide hazard and risk assessment using semi-automatically created landslide inventories. Geomorphology 184, 139-150.

Ouimet, W.B. (2010) Landslides associated with the May 12, 2008 Wenchuan earthquake: Implications for the erosion and tectonic evolution of the Longmen

Shan. Tectonophysics 491(1), 244-252.

Owen, L.A., Kamp, U., Khattak, G.A., Harp, E.L., Keefer, D.K. and Bauer, M.A. (2008) Landslides triggered by the 8 October 2005 Kashmir earthquake. Geomorphology 94(1), 1-9.

Sassa, K. (2005) Landslide disasters triggered by the 2004 Mid-Niigata Prefecture earthquake in Japan. Landslides 2(2), 135-142.

Sato, H.P., Hasegawa, H., Fujiwara, S., Tobita, M., Koarai, M., Une, H. and Iwahashi, J. (2007) Interpretation of landslide distribution triggered by the 2005 Northern Pakistan earthquake using SPOT 5 imagery. Landslides 4(2), 113-122.

Wartman, J., Dunham, L., Tiwari, B. and Pradel, D. (2013) Landslides in eastern Honshu induced by the 2011 Tohoku earthquake. Bulletin of the Seismological Society of America 103(2B), 1503-1521.

Xu, C., Xu, X.W., Zheng, W.J., Wei, Z.Y., Tan, X.B., Han, Z.J., Li, C.Y., Liang, M.J., Li, Z.Q. and Wang, H. (2013b) Landslides triggered by the April 20, 2013 Lushan, Sichuan Province Ms 7.0 strong earthquake of China. Seismology and geology 35(3), 641-660.

Xu, C., Xu, X., Shyu, J.B.H., Zheng, W. and Min, W. (2014) Landslides triggered by the 22 July 2013 Minxian–Zhangxian, China, Mw 5.9 earthquake: Inventory compiling and spatial distribution analysis. Journal of Asian Earth Sciences 92, 125-142.

Zhou S, Fang L (2015) Support vector machine modeling of earthquake-induced landslides susceptibility in central part of Sichuan province, China. Geoenvironmental Disasters 2:1–12. doi: 10.1186/s40677-014-0006-1

Zhou S, Fang L, Liu B (2015) Slope unit-based distribution analysis of landslides triggered by the April 20, 2013, Ms 7.0 Lushan earthquake. Arab J Geosci 8:7855–7868. doi: 10.1007/s12517-015-1835-2

Zhou, S., Chen, G., & Fang, L. (2016). Distribution Pattern of Landslides Triggered by the 2014 Ludian Earthquake of China: Implications for Regional Threshold Topography and the Seismogenic Fault Identification. ISPRS

International Journal of Geo-Information, 5(4), 46.

Zhou, S., Chen, G., Fang, L., & Nie, Y. (2016). GIS-Based Integration of Subjective and Objective Weighting Methods for Regional Landslides Susceptibility Mapping. Sustainability, 8(4), 334.

Zhou, S., Chen, G., Liu B., & Fang, L. (2016). A Combined Weight of Evidence and Logistic Regression Method for Susceptibility Mapping of Earthquake‐induced Landslides: A Case Study of the April 20, 2013 Lushan Earthquake, China. Acta Geologica Sinica (English Edition), 90(2), 511-524.

CHAPTER 7

7 CONCLUSIONS AND FUTURE STUDIES

7.1 CONCLUSIONS

Landslide is one of the serous natural hazards around the world. As one of the most important and effective disaster prevention measures, landslide hazard maps plays an important role in regional landuse planning and

The following major conclusions can be drawn:

(1) A method for effectively mapping of landslide inventory is proposed by using on-line high-resolution online images. In the proposed method, some Criteria were also defined for visual interpretation of landslides;

(2) Four widely-used statistical landslide hazard mapping methods Information Value (IV), Weight of Evidence (WoE), Logistic Regression (LR), and Support Vector Machine (SVM) are used to produce the landslide hazard maps, the merits, demerits and limitations of each method are clarifed based on a close comparison between the four methods. Generally, all of the four methods shows an acceptable accuracy according to the test results on the landslides triggered by the 2013 Lushan earthquake in China.

(3) Although several validation methods exist, in this chapter, a validation method based on the cross-table of the landslide inventory and its predicted status was employed, since it can give a clear engineering sense. To compare different landslide hazard maps, the miss-alarm rate and false-alarm rate are suggested as the main index to evaluate the performance or

he landslide hazard maps.

(4) Accurate determination of the landslide cells in statistical LHM is very important, a sensitive analysis was carried out to test the effects of threshold landslide coverage on the landslide hazard maps. The result shows that, as the threshold values increase, no obvious effect found on the success rate, however both the miss-alarm rate and miss-alarm rate will increase. Generally, a 10% of the threshold percentage is recommended in this study.

(5) Four new methods are proposed by combining one of IV and WoE methods with one of the LR and SVM methods to improve the accuracy of the model. The validation results show that the combined method could improve the accuracy of the landside hazard maps.

(6) A method for estimate PGA values of each cell a specified fault or the target fault at a region scale is propose based on the on the Next Generation of Ground-Motion Attenuation Models for the western United States (NGA-West2).

(7) Landslide hazard maps considering different assumed earthquakes are produced by using the pseudo-static method based on an infinite slope stability model and the PGA values.

(8) A run-out simulation technique is developed based on modified multiple flow algorithm and the law of conservation of energy. In the proposed technique, the elevation difference between cells is taken into account for determining the possible directions towards which the landslide can move with a certain probability. The law of conservation of energy is used to determine the distance of sediment movement.

(9) One of its main advantages of the proposed module lies in its low data requirement, only the DEM data and potential source are needed for runout prediction. This makes is possible to be applied to predict the landslide affected area at the regional scale. The proposed technique and the developed module had provided a solution to fill the gap exists in landslide prone slope identification and affected area estimation.

(10) The practical example of the GeoLHM-R shows that the maximum runout distance and extent were largely depended on the surface friction coefficient. It is suggested that frictional coefficient can be obtained either by inferred from the lithology map or by back-analysis of existing landslide cases. However, once the potential landslide source is identified and proper frictional coefficient values is determined, reliable landslide effected area can be mapped.

(11) A practical case of developed system was carried out to analysing landslide triggered by the 2016 Kumamoto earthquake. The produced landslide hazard provides essential frameworks for the development planning and reconstruction of the study area as they present a spatial division of the study area of different levels of potential landslide threat, including the landslide prone areas and the potential affected areas.

7.2 FUTURE STUDIES

(1) An effort of landslide inventory mapping should be encouraged in the future study both in the same place and different places. The fully documented landslide database will enable scientists to more accurately establish the relationship between landslides events and both its triggering factor and controlling factor which will be very useful to understand the physical behavior of landslides

(2) Currently, most of the landslide hazard maps are relative static, Therefor, with the development of GIS technologies, the real time warning of landslide hazard through Web-GIS and mobile-GIS technologies should be greatly encouraged.

(3) Future research should also place an emphasis on rock slope stability investigations. This would include geological and discontinuity mapping to provide the necessary input data for stability analyses. The collection of data would ideally involve rock mass characterization and the sampling of rock materials for laboratory analysis (i.e. Strength and constitutive behavior determination), field observations and in situ measurements. In situ monitoring of spatial and temporal variations in pore pressures, slope displacements,

stresses and subsurface rock mass deformations can also provide valuable data for constraining and validating the stability analyses undertaken.

(4) Robust, less time consuming, less computational cost simulation technique which employ the shape of the landslide masses and contact between landslide masses and ground surface is encouraged in order to produce “more physically sound” landslide affected area prediction.

(5) Further studies should also employ the high accuracy of DEM, i.e. LIDAR data to obtain better accuracy of simulation and zoning.